Characterisation of Metal-Amyloid β Peptide Interactions and the Effect of Metals on the Gene Expression of Amyloid Precursor Protein

Gayani Petersingham

Primary Supervisor: Dr Ming Wu

Co-Supervisors: Dr Narsimha Reddy & Dr Allan Torres

A thesis presented to Western Sydney University in

fulfilment of the requirements for the degree of

Doctor of Philosophy (Science)

November 2019

Dedicated to my parents,

Peter and Ruby

Acknowledgements

I would first and foremost, like to express my sincere gratitude to Dr. Ming J Wu, for giving me his invaluable time, direction, motivation, guidance, support, patience and seeing me through to the completion of my research. I am beyond blessed to have the best supervisor anyone could ever ask for. My apologies for all the stress and loss of sleep I have caused you over the years. Words cannot express how thankful I am to you and will forever be indebted. I truly believe you have superpowers. You routinely go above and beyond your academic duties for your students. I am honoured to have had this opportunity to study as your student and hope to provide the same patience and generosity to others, as you have shown me, in my future science career.

A very special thank you to my amazing co-supervisors, Dr. Narsimha Reddy and Dr. Allan Torres for their exquisite collaboration and guidance. Narsimha, you are the kindest academic I have ever known. You inspire me more than you know. My meetings with you were instrumental to my research. I cannot thank you enough for your willingness to help and everything you have done for me. To Allan, you have made me love and appreciate NMR so much. You have taught me so much for which I am so grateful. Your help and encouragement since my honours is greatly appreciated.

I would be amiss if I did not thank my retired, and hopefully well rested, supervisory panel. Dr. Trevor Bailey, you sparked my interest in inorganic chemistry. I will always be grateful for our "quick" meetings which well and truly answered all current and possible future questions I had. Dr. Cindy Kersaitis, thank you for your support and being so understanding.

I would also like to thank all the members of the Ming lab group, for making this experience so enlightening. A special thanks goes to Mohammad, who keeps us sane and willing read my thesis, you are truly amazing! Thank you so much. Your support and friendship have been invaluable to me, the debt I owe you is more than a million Mad Mex trips can repay, but I will start by no longer making fun of your cars. It has been an absolute pleasure working alongside you. I cannot go without thanking my favourite facility manager, Dr Scott Willis, who are always so begrudgingly helpful and nice. Thank you to everyone I had been blessed to know academically.

Thank you to my uni girls and the 'Ladies Who Lunch' Amber, Anita, Ash, Caiti, Christine, Diksha, Kristen, Leah, Pauline, Reika, Ruvi, Serene and Su Su. One of the most amazing things this PhD has given me, is my friendship with such inspirational, strong, intellectual and beautiful women. I have too many fond memories from- couch venting, food adventures, epic road trips, rofling email exchanges, the BTS rabbit hole, make up unboxings and baby visits, which I will cherish for all my days. Thank you for being my uni family.

To my non-uni friends, thank you for your constant amazement, this gave me more confidence than I perhaps deserved. To Dan, Hayley, Mohana, Sam and Steph, I am grateful for you guys always pushing me. You guys helped keep my sanity and always made me laugh. You do not understand the strength you all give me. To Logan, Jack and Mila your smiles, cuddles and mere existence has brightened my darkest days. You might not be able to read this yet, but Gayani promises to always be there and attempt to make you even happier than you have made me.

To my amazing siblings Loashini, Veno and Luxshan, words cannot express how grateful I am for you. Thank you for inspiring me with your greatness. You push me to finish, even when I

desperately wanted to run away. Thank you for always being there and for being my cathartic venting machine.

Finally, to my wonderful Dad and Mum, whose blessings, love and support have given me the confidence to overcome any challenges. You have "patiently" waited a long time for me to finish this. Thank you for all the selfless sacrifices you have made for me. Dad, my love of science comes from you, as does my stubbornness, persistence and inability to accept failure. Mum, you have taught me the importance of hard work, self-respect and a soft heart. You inspire me to be a better person every day. All my achievements are attributed to you both, including this thesis it is as much yours as it is mine. I am forever grateful for your love, strength and motivation. I am so blessed to be your daughter and will always endeavour to make you proud. From the bottom of my heart, I love you and thank you!!

Statement of Authentication

This thesis is submitted in fulfilment of the requirements for the degree of Doctor of Philosophy at Western Sydney University, School of Science. The work presented in this thesis is, to the best of my knowledge and belief, original except as acknowledged in the text. I hereby declare that I have not submitted this material, either in full or in part, for a degree at this or any other institution.

[redacted] .....

Gayani Petersingham

November 2019

Thesis Abstract

Metal ions are present in foods, water and the environment surrounding us. Some of them are essential to the human body, participating in numerous biological functions, whilst others are toxic to living life and have no physiological function. Even the metal ions which are essential for life, such as copper (Cu^{2+}), iron (Fe^{3+}) and zinc (Zn^{2+}), are tightly regulated in the cell. Their excess or dysregulation is detrimental to human health. It is therefore no wonder that metal ions are associated with a variety of human diseases such as neurodegenerative disorders. A wealth of literatures links metal ions (Cu^{2+}, $Fe^{2+/3+}$, Zn^{2+}) to Alzheimer's disease (AD). A non-essential metal ion, i.e. aluminium (Al^{3+}), is the third most abundant metal in the Earth's crust and is becoming more and more bioavailable via foods and water due to environmental contamination and pollution. Consequently, the chronical accumulation of Al^{3+} is insidious to human health. Numerous publications have linked Al^{3+} to AD. However, molecular evidence underlying such claim is still lacking.

AD is a devastating neurodegenerative condition that poses major challenges to human health, with a prevalence of around 35 million patients worldwide. One of the neuropathological hallmarks in AD patients is extracellular amyloid plaques which are composed of amyloid β peptide (Aβ) aggregates. The amyloid cascade hypothesis suggests that aggregation of the Aβ peptide into soluble oligomers and senile plaques is the main driver of AD. Metal ions are found to be present in amyloid plaques, including Cu^{2+}, $Fe^{2+/3+}$, Zn^{2+} and Al^{3+}. The experimental evidence from the literatures thus far points to a role of metal ions in Aβ aggregation and pathogenesis of AD. To this end, the metal ion hypothesis for AD is proposed, which suggests that disruption of metal ion homeostasis promotes Aβ aggregation and onset of AD. However, such a link is still premature, clinical, epidemiological and molecular studies are needed.

Therefore, this thesis takes a molecular approach by NMR (nuclear magnetic resonance) spectroscopy to investigate the interaction of metal ions with Aβ peptide, $A\beta_{1-28}$, and to analyse potential metal chelators for future therapeutic application, and to unravel the effect of metal ions on the expression of APP gene (the gene encoding amyloid precursor protein) as well as the antagonising effect of metal chelators against metal ions in APP gene expression.

In this thesis, I have firstly reviewed the literatures on the metal ions, their interactions with Aβ peptides, their role in Aβ aggregation, and their potential involvement in AD pathogenesis. AD and the current hypotheses for AD pathogenesis have also been reviewed, including amyloid cascade hypothesis, metal ion hypothesis and oxidative stress hypothesis. I have then reviewed a panel of natural metal ligands that might have therapeutic potential to chelate AD related metals and prevent metal related oxidative stress.

By the means of NMR, the interactions of metal ions with $A\beta_{1-28}$ peptide as well as the $A\beta_{1-28}$ analogues were analysed (Chapter 3). The key binding site of Al^{3+} were determined. NMR data showed Al^{3+} interacts with $A\beta_{1-28}$ by the NH and αH of numerous residues experiencing upfield shifts. Using Aβ analogues where His6, His13 and His14 were individually replaced by alanine residue(s) including $A\beta_{1-28}$ His6A (His6 was replaced by alanine), $A\beta_{1-28}$ His13A (His13 was replaced by alanine), $A\beta_{1-28}$ His14A (His14 was replaced by alanine), and $A\beta_{1-28}$ His6,13,14A (all His6, His13 and His14 residues were replaced by three alanine residues), I have demonstrated that the histidine residues (His6, His13 and His14) and N-terminal Asp1 were involved in the Al^{3+} coordination. By comparing Al^{3+} to Zn^{2+}, a relatively well-studied metal ion for its interaction with Aβ, this study found that Al^{3+} has a similar affinity to $A\beta_{1-28}$. Additionally, the change of chemical shift index (CSI) values caused by Al^{3+} coordination indicated the subsequent change of secondary structure of $A\beta_{1-28}$ upon the metal coordination.

The above findings are reported for the first time, because there are no available details for the molecular interaction between Al^{3+} and Aβ. The results provide significant evidence for the potential role of Al^{3+} in Aβ aggregation, hence in AD aetiology.

The ability of metal ions interacting with Aβ *in vitro* means such interaction is potentially existent *in vivo*. Therefore, reducing the metal availability by metal chelation would minimise metal ions' interaction with Aβ. Therefore, the metal coordination of a panel of chelating ligands was characterised in Chapter 4. These ligands are histidine, glutathione (GSH), maltol, citric acid and malic acid. They are naturally occurring, easily metabolised and nontoxic to humans.

The panel of ligands were characterised by NMR and molecular mechanics to explore their ability in metal coordination. The findings demonstrated that they can coordinate Al^{3+}, Cu^{2+} and Zn^{2+}. GSH and histidine in particular exhibited much higher affinity to Al^{3+}, Zn^{2+} and Cu^{2+}. Considering the previously proven antioxidant property for both GSH and histidine, their ability to chelate metal ions could be of significance to treatment of metal-related disorders such as AD.

Following the NMR and molecular mechanics analysis, MTT (3-(4,5-dimethylthiazol-2-yl)-2,5-diphenyltetrazolium bromide) toxicity assays (Chapter 5) were used to determine the potential of the metal ligands in cellular context. Citric acid, was effective at reducing the metal toxicity of 1 mM Al^{3+}, however significantly decreased the cell viability in cells exposed to Zn^{2+}. The ligands, GSH and histidine were overall more effective at ameliorating the metal toxicity of Al^{3+}, Zn^{2+} and Cu^{2+} as well as nonrelated AD metal ion As^{3+} and Cr^{6+}. Moving on to the effect of metal ions on APP gene expression, the findings demonstrated that the relative expression of APP gene in human neuronal cells (SH-SY5Y) is upregulated in the presence of

Al^{3+} and Zn^{2+}, suggesting that these two metal ions are likely to induce higher level of amyloid precursor protein and consequently more Aβ. The upregulation of APP gene expression by metal ions is a novel finding for human neuronal cells, although similar result was found in animal models. It is significant, since such modulation of APP gene expression by metal ions could happen *in vivo*, therefore supporting the current hypothesis that metal ions are involved in AD pathogenesis.

Moreover, the findings demonstrate that chelating ligands such as histidine and GSH reduced the expression of APP gene. Whilst the mechanism of histidine and GSH in reducing APP gene expression is not clear, the finding is of significance in that metal chelation could be at least a strategy to be considered for AD treatment. Future studies on this front is definitely warranted.

In conclusion, the findings of this study provide significant evidence for the interaction of metal ions with Aβ. The molecular details of Al^{3+} and Zn^{2+} with Aβ and its role in upregulating APP gene expression are novel. Therefore, the findings support the unification of the amyloid cascade and metal ion hypotheses. That the metal chelating ligands histidine and GSH can antagonise the effect of metal ions on APP gene upregulation provides a significant avenue for AD treatment strategy.

Publications

Zaman, M., Johnson, A., **Petersingham, G.,** Muench, G., Dong, Q and Wu, M. (2019), 'Protein kinase CK2 is involved in zinc homeostasis in Breast and Prostate Cancer Cells', *BioMetals*, vol 32, no 6, pp 861-873.

Johnson, A., Zaman, M., Veljanoski, F., Phrakaysone, A., Li, S., O'Doherty, P., **Petersingham, G.,** Perrone, G., Molloy, M. and Wu, M. (2017), 'Unravelling the role of protein kinase CK2 in metal toxicity using gene deletion mutants', *Metallomics*, vol 9, no 3, pp 301 - 308.

Johnson, A., Veljanoski, F., O'Doherty, P., Zaman, M., **Petersingham, G.,** Bailey, T., Muench, G., Kersaitis, C. and Wu, M. (2016), 'Molecular insight into arsenic toxicity via the genome-wide deletion mutant screening of Saccharomces cerevisiae', *Metallomics*, vol 8, no 2, pp 228 - 235.

Johnson, A., Veljanoski, F., O'Doherty, P., Zaman, M., **Petersingham, G.,** Bailey, T., Muench, G., Kersaitis, C. and Wu, M. (2016), 'Revelation of molecular basis for chromium toxicity by phenotypes of Saccharomyces cerevisiae gene deletion mutants', *Metallomics*, vol 8, no 5, pp 542 - 550.

Tun, N., Lennon, B., O'Doherty, P., Johnson, A., **Petersingham, G.,** Bailey, T., Kersaitis, C. and Wu, M. (2014), 'Effects of metal ions and hydrogen peroxide on the phenotype of yeast hom6 mutant', *Letters in Applied Microbiology*, vol 60, no 1, pp 20 - 26.

Conference presentations

Petersingham, G., Reddy, N., Torres, A., Wu, M. J. NMR Characterisation of metal-ligand interactions and the effect of these interactions on the gene expression of amyloid precursor protein. Lecture delivered at *Industry Workshop and NMR, MRI & Diffusion Symposium,* Western Sydney University, **2018,** Campbelltown, Australia.

Petersingham, G., Reddy, N., Torres, A., Wu, M. J. Characterisation of metal-ligand interactions and the effect of metal ions on the gene expression of amyloid precursor protein. Poster presented at the *NMR, MRI & Diffusion Symposium,* Western Sydney University, **2018,** Campbelltown, Australia.

Petersingham, G., Zaman, M., Reddy, N., Torres, A., Wu, M. J. Characterisation of metal-amyloid β interactions and the effect of metal ions on the gene expression of amyloid precursor protein. Lecture delivered at the *Bioinorganic Chemistry Gordon Research Seminar (GRS*), **2018,** Ventura, California, USA.

Petersingham, G., Reddy, N., Torres, A., Wu, M. J. Characterisation of metal-amyloid β interactions and the effect of metal ions on the gene expression of amyloid precursor protein. Poster presented at the *42nd Lorne Conference on Protein Structure and Function*, **2017**, Lorne, Victoria, Australia

Table of contents

DEDICATION ..... **I**
ACKNOWLEDGEMENTS ..... **II**
STATEMENT OF AUTHENTICATION ..... **V**
THESIS ABSTRACT ..... **VI**
PUBLICATIONS ..... **X**
CONFERENCE PRESENTATIONS ..... **XI**
TABLE OF CONTENTS ..... **XII**
LIST OF FIGURES ..... **XVII**
LIST OF TABLES ..... **XX**
1 LITERATURE REVIEW **1**
1.1 General introduction 1
1.2 Metal ions 4
1.3 Metal ions and biology 4
1.4 Alzheimer's disease 7
1.5 Amyloid precursor protein (APP) 9
1.6 Amyloid β (Aβ) peptide 12
1.7 Oxidative stress and Alzheimer's disease 16
1.8 AD pathogenesis hypotheses 18
1.8.1 Amyloid cascade hypothesis 19
1.8.2 Metal ion hypothesis 20
1.8.3 Oxidative stress hypothesis 21
1.8.4 Alzheimer's disease multifactorial nature 22
1.9 Metal ions associated with Alzheimer's disease 24
1.9.1 Copper 24
1.9.2 Zinc 26
1.9.3 Aluminium 28
1.10 Toxic metal exposure 32
1.10.1 Arsenic 32
1.10.2 Chromium 33
1.11 Alzheimer's disease therapeutic rational 34

1.12 Metal chelation therapy 35
1.13 Chelating ligands 38
1.13.1 Histidine 38
1.13.2 Glutathione 39
1.13.3 Maltol 41
1.13.4 Citric acid 42
1.13.5 Malic acid 43
1.14 Nuclear Magnetic Resonance (NMR) spectroscopy 44
1.14.1 Structural studies employing NMR spectroscopy 44
1.14.2 General NMR theory 44
1.14.3 Two-dimensional NMR spectroscopy 46
1.14.4 Correlated Spectroscopy (COSY) 47
1.14.5 Total Correlation Spectroscopy (TOSCY) 47
1.14.6 Nuclear Overhauser Effect Spectroscopy (NOESY) 48
1.14.7 NMR assignments in peptides 49
1.15 Experimental approach 51
1.16 Aims 52

2 MATERIALS AND METHODS 53
2.1 General materials, reagents and treatments 53
2.1.1 Metal solutions 53
2.1.2 Ligand solutions 53
2.1.3 Phosphate buffer 53
2.1.4 Synthesis of pyridoxal amino methyl phosphonic acid (PYRAMPA) 54
2.1.5 Synthesis of metal-maltol complexes 54
2.2 Peptide synthesis and purification 55
2.2.1 Design of peptides and peptide sequences 55
2.3 Procedures for NMR acquisition and analysis 56
2.3.1 1D NMR experiments 56
2.3.2 2D Total Correlation Spectroscopy (TOCSY) experiments 56
2.3.3 2D Nuclear Overhauser Effect Spectroscopy (NOESY) experiments 56
2.4 NMR titration of $A\beta_{1-28}$ against metal ions 57

2.5 2D NMR titration of $A\beta_{1-28}$ against metal ions 58
2.6 Binding affinity 59
2.7 NMR titration of ligands against metal ions 59
2.8 General practices for using mammalian neuronal cells 60
2.8.1 Cell line 60
2.8.2 Sterilisation 61
2.8.3 Growth medium 61
2.8.4 Establishment of cell line 62
2.8.5 Cryogenic storage 63
2.9 Cell viability studies of SH-SH5Y cells under metal-ligand treatment 63
2.9.1 Determination of IC_{50} of metal ions 63
2.9.2 MTT cell viability Assay 64
2.10 Quantification of APP Gene Expression 66
2.10.1 Harvesting and purification of RNA for quantitative qRT-PCR 66
2.10.2 cDNA synthesis 67
2.10.3 Quantitative qRT-PCR 68
2.11 Software packages 70

3 THE NMR STRUCTURAL ANALYSIS OF AMYLOID B PEPTIDE AND ITS INTERACTION WITH METAL IONS 71
3.1 Introduction 71
3.2 Results 73
3.2.1 Structural analysis and determination of binding sites in the metal-$A\beta_{1-28}$ complex 73
3.2.1.1 Proton NMR assignments for $A\beta_{1-28}$ residues 73
3.2.1.2 NMR titration of $A\beta_{1-28}$ against Al^{3+} 75
3.2.2 Aluminium titration of $A\beta_{1-28}$ analogues 79
3.2.3 Determination of binding affinity of Al^{3+} to $A\beta_{1-28}$ monitored by NMR spectroscopy 82
3.2.4 Comparison of Al^{3+} and Zn^{2+} binding to $A\beta_{1-28}$ 84
3.2.5 Structure of Al^{3+}-Aβ complex 85
3.3 Discussion 94

3.4 Conclusion 96

4 CHARACTERISATION, AND ASSESSMENT OF METAL COORDINATING ABILITY OF LIGANDS FOR DEVELOPING POTENTIAL THERAPEUTIC AGENTS 97

4.1 Introduction 97

4.2 Results 100

4.2.1 NMR analysis for the coordination of metal ions by individual ligands 100

4.2.2 Histidine 100

4.2.3 Glutathione (GSH) 106

4.2.4 Maltol 113

4.2.5 Citric acid 116

4.2.6 Malic acid 122

4.3 Discussion 127

4.4 Conclusion 130

5 THE IMPACT OF METALS AND LIGANDS ON THE GENE EXPRESSION OF APP IN NEURONAL CELLS 131

5.1 Introduction 131

5.2 Results 132

5.2.1 Determination of IC_{50} of metal ions on SH-SY5Y cells 132

5.2.2 The effect of metal chelating ligands on the cytotoxicity of metal ion in SH-SY5Y cells 137

5.2.3 Gene expression of APP under metal ion exposure and the impact of chelating ligands 143

5.3 Discussion 146

5.3.1 Ligands ameliorated the metal toxicity 146

5.3.2 The effect of Al^{3+} and Zn^{2+}on APP gene expression in SH-SY5Y cells 149

5.3.3 Chelating ligand treatment decreases metal-induced APP gene expression. 150

5.4 Conclusion 152

6 CONCLUDING DISCUSSION 153

6.1 Al^{3+} coordinates to Aβ triggering structural modifications and aggregation..... 153
6.2 Metal chelating ligands antagonise the role of metal ions in APP gene expression..... 157
6.3 The significance and prospective directions..... 159
REFERENCES..... 161
APPENDICES..... 186
Appendix A HPLC chromatogram and MS analysis of $A\beta_{1-28}$ peptides and Aβ analogues.. 186
Appendix B 2D NMR spectra for proton assignment of $A\beta_{1-28}$ peptide..... 191
Appendix C 2D NMR spectra for NMR titration of $A\beta_{1-28}$ against Al^{3+}..... 193
Appendix D 1D NMR titration curve of α amino acid against Al^{3+} and Zn^{2+}..... 196

List of Figures

Figure 1.1 Schematic description of APP proteolytic cleavage.. 10

Figure 1.2 Full amino acid sequence of $A\beta_{42}$ 13

Figure 1.3 Schematic description of the hypotheses of Alzheimer's disease 23

Figure 1.4 Proposed coordination modes of Cu^{2+} to Aβ 25

Figure 1.5 Proposed coordination mode of Zn^{2+} to Aβ 27

Figure 1.6 Proposed therapeutic intervention by multifunctional metal chelators on Aβ aggregation 37

Figure 1.7 Structure of histidine..... 38

Figure 1.8 Structure of glutathione 40

Figure 1.9 Structure of maltol 41

Figure 1.10 Structure of citric acid..... 42

Figure 1.11 Structure of malic acid 43

Figure 1.12 Energy levels for a nucleus with spin 45

Figure 2.1. Schematic explanation of the principle underlying TaqMan technology 69

Figure 3.1 ^{1}H NMR spectra of Al^{3+} titration of $A\beta_{1-28}$ 75

Figure 3.2 2D $^{1}H/^{1}H$ TOCSY NMR spectra of Al^{3+} titrated wild-type $A\beta_{1-28}$ 77

Figure 3.3 ^{1}H chemical shift variations for $A\beta_{1-28}$ induced by 1.0 mole equivalent of Al^{3+} 78

Figure 3.4 ^{1}H NMR titrated spectra of $A\beta_{1-28}$ and analogues 80

Figure 3.5 2D ^{1}H TOCSY spectrum of $A\beta_{1-28}$ H6,13,14A with Al^{3+} 81

Figure 3.6 Binding curve of aluminium to $A\beta_{1-28}$ 83

Figure 3.7 ^{1}H NMR spectra of Zn^{2+} and Al^{3+} titrated $A\beta_{1-28}$ 84

Figure 3.8 The secondary structure of $A\beta_{1-28}$ predictions from CSI values 87

Figure 3.9 The secondary structure of Al^{3+}-$A\beta_{1-28}$ predicted from CSI values..... 89

Figure 3.10 ^{1}H NMR titration of $A\beta_{1-28}$ with Al^{3+} 90

Figure 3.11 Molar ratio vs Δδ plot for the incremental addition of Al^{3+} to $A\beta_{1-28}$ 91

Figure 3.12 Schematic representation of the most affected residues in $A\beta_{1-28}$ by Al^{3+}..... 92

Figure 3.13. The proposed structure of $A\beta_{1-28}$ complexed with Al^{3+} 93

Figure 4.1 The panel of ligands used in this study..... 99

Figure 4.2 ^{1}H NMR spectra of metal ions with histidine 101

Figure 4.3 ^{1}H NMR titration of histidine with Ni^{2+} 102

Figure 4.4 Two proposed structures of the copper-histidine complex.. 103

Figure 4.5 Molar ratio vs Δδ plots for the metal ions to histidine..... 104

Figure 4.6. 2D ^{1}H-^{1}H COSY NMR spectrum of GSH 106

Figure 4.7 ^{1}H NMR titration of metal ion with GSH 108

Figure 4.8 Molar ratio vs Δδ plots for the incremental addition of metal ions to GSH. 110

Figure 4.9 ^{1}H NMR titration of metal ion with maltol..... 113

Figure 4.10 ^{1}H NMR spectra for metal ions and citric acid. 117

Figure 4.11 ^{1}H NMR Al^{3+} titration of citric acid. 118

Figure 4.12 Molar ratio vs Δδ plots for metal ion and citric acid 119

Figure 4.13 ^{1}H NMR metal ion titration of malic acid..... 123

Figure 4.14 Molar ratio vs Δδ plots of metal ions to malic acid. 124

Figure 5.1 Dose-response curve of zinc sulphate in SH-SY5Y cells..... 133

Figure 5.2 Dose-response curves of copper sulphate in SH-SY5Y cells 134

Figure 5.3 Dose-response curve of aluminium maltol in SH-SY5Y cells 135

Figure 5.4 Dose-response curves of chromium trioxide in SH-SY5Y cells 136

Figure 5.5 Dose-response curves of sodium arsenite in SH-SY5Y cells 137

Figure 5.6 Comparative cytotoxic response curves of copper treated with ligands..... 138

Figure 5.7 Comparative cytotoxic response curves of zinc treated with ligands..... 139

Figure 5.8 Comparative cytotoxic response curves of aluminium treated with ligands 140

Figure 5.9 Comparative cytotoxic response curves chromium treated with ligands 141

Figure 5.10 Comparative cytotoxic response curves of arsenic treated with ligands 142

Figure 5.11 Relative expression of APP gene under aluminium or zinc exposure..... 144

Figure 5.12 Relative expression of APP gene in cells treated by ligands with and without Al^{3+} 145

List of Tables

Table 1.1 Various Aβ sequences utilised previously for structural analysis studies..... 15

Table 1.2 ^{1}H Chemical shifts of amino acid residues of random coil peptides and proteins... 50

Table 2.1. Design of peptides used this in this study 55

Table 2.2 sample preparation for NMR titrations of metals to Aβ. 57

Table 2.3 Sample preparation for NMR titrations of metals to ligands. 60

Table 2.4 Details of the SH-SY5Y mammalian cell line used in this project..... 61

Table 2.5. The concentration of metal salts used to determine the IC_{50} of the respective metal ion..... 64

Table 2.6 Treatments used for each plate in ligand toxicity assay..... 65

Table 2.7 Thermal cycler settings for cDNA synthesis 67

Table 2.8. Parameters for the qRT-PCR thermal cycler 68

Table 3.1 Assignments of the chemical shifts of $A\beta_{1-28}$..... 74

Table 3.2 Sequences of the synthetic amyloid β and its analogues..... 79

Table 3.3 Chemical shift index (CSI) values of $A\beta_{1-28}$ 86

Table 3.4 Chemical shift index (CSI) values and sequence correction factors of $A\beta_{1-28}$ in the presence of Al^{3+}..... 88

Table 4.1 The optimized binding structures and energies of metal-histidine complexes. 105

Table 4.2 ^{1}H NMR resonance assignments of GSH..... 107

Table 4.3 The optimized binding structures and energies of metal-GSH complexes. 112

Table 4.4 Analytical data of metal-maltol complexes..... 114

Table 4.5 The optimized binding structures and energies of metal-maltol complexes..... 115

Table 4.6 Analytical data of copper-citrate complex 120

Table 4.7 Molecular modelling studies of metal-citric acid complexes. 121

Table 4.8 Analytical data of copper-malic acid complex..... 125

Table 4.9 The optimized binding structures of metal-MA complexes..... 126

1 LITERATURE REVIEW

1.1 General introduction

Metal ions such as aluminium (Al^{3+}), zinc (Zn^{2+}), ferrous (Fe^{2+}) and cupric (Cu^{2+}) are implicated in the formation of amyloid β (Aβ) peptide aggregates. Aβ aggregation is a hallmark of Alzheimer's disease (AD) (Adlard and Bush, 2006; Nair et al., 2010). The outset this thesis aims to investigate the interaction of metal ions with Aβ, therefore the findings have bearing on the understanding of AD, a progressive neurodegenerative condition with yet to be defined mechanism (Arispe et al., 2010; Ballard et al., 2011). Various factors such as genetic mutations, amyloid precursor protein (APP) processing, Aβ and metal ions have been identified to play a role in AD (Barber, 2012; Lanoiselée et al., 2017). Majority of AD cases are sporadic, not genetically related, with no defined causal mechanisms (Huat et al., 2019). One school of thoughts proposed by a body of experimental findings is that the Aβ peptide serves as a ligand for metal ions and their interactions can eventuate into Aβ aggregation accompanied with oxidative stress in brain (Pearson and Peers, 2006; Bush and Tanzi, 2008; Duce et al., 2011). As metals are natural constituents of the earth's crust, they are inextricably relevant to living organisms, whether they are biologically essential or non-essential. Human exposure to metals constantly increases because of their exponential applications in a variety of industries. Consequently, this study will firstly characterise the interaction of $A\beta_{1-28}$ with metal ions, I will then investigate variety of organic chemical ligands for their interaction with a range of metal ions. The aims are to develop suitable ligands for therapeutic application as metal ion chelators, and to examine the effect of metal ions on APP level in neuronal cells.

The interaction of metal ions with Aβ will be analysed in this project, using $A\beta_{1-28}$, by nuclear magnetic resonance (NMR) spectroscopy, primarily focusing on the highly neurotoxic Al^{3+}, as neither its coordination to Aβ peptide nor its implication in AD have yet been established (Tomljenovic, 2011; Walton, 2012). Characterisation of the interactions of metal ion and Aβ will be conducted by ^{1}H (proton), NOESY (Nuclear Overhauser Effect SpectroscopY) and TOCSY (TOtal Correlated SpectroscopY) NMR. Previous studies have demonstrated that the N-terminal Asp1 and all the three histidine (His6, His13 and His14) residues of Aβ coordinate with metal ions (Danielsson et al., 2007). Aβ peptide analogues were synthesised chemically in this study by substitution of individual histidine residues with alanine which has a short and uncharged side chain in order to dissect the role of histidine residues of Aβ in metal ion coordination. Furthermore, this study will likely reveal other potential coordinating sites such as the arginine residue (Arg5), serine (Ser8), glutamic acid (Glu11) and tyrosine (Tyr10).

The characterisation of a panel of ligands, including histidine, glutathione (GSH), 3-hydroxy-2-methyl-4H-pyran-4-one (maltol), citric acid and malic acid for their interactions with biometals (Zn^{2+} and Cu^{2+}) and non-biological metal ion (Al^{3+}) has been conducted to uncover potential natural metal chelators. The interaction of metal ions and the ligands was analysed using ^{1}H NMR titration experiments, to demonstrate where the metals coordinate to the complexes. The coordination strength and stability of the complexes of the metals to ligands was determined by molecular mechanics (MM2 calculations and HOMO values). Mammalian neuronal cell culture system was also employed for measuring the effect of ligand on metal toxicity in the cells by the colorimetric cell-proliferation assay called MTT assay which uses the tetrazolium salt MTT (3-(4,5-dimethylthiazol-2-yl)-2,5-diphenyltetrazolium bromide) (Mosmann, 1983), in order to determine the ability of the ligands in lowering metal toxicity under biological conditions. The use of the highly toxic heavy metals As^{3+} and Cr^{6+}

demonstrated whether the ligands can chelate highly toxic metals although they are not related to AD, and the findings could lead to application of potential metal chelators for alleviating the toxic metal related health problems.

On the basis of the published evidence (Lin et al., 2008), albeit very limited, it is hypothesised that metal ions could also affect the expression of APP gene. Quantitative RT-PCR (Reverse Transcription Polymerase Chain Reaction) was used to test whether the expression of APP gene in human SH-SY5Y neuronal cells is affected by metal ions such as Al^{3+} and the extensively studied Zn^{2+}. To explore the antagonistic effect the ligands have on metal ions, qRT-PCR was used to measure APP gene expression level in the presence of the ligands and Al^{3+}.

My thesis is of significance on a number of fronts. The molecular details gained from characterising the interaction of metal ions with Aβ should provide support to the notion that metals ions interact with Aβ. The effect of metals on APP gene expression has been scarcely studied until the present, findings on this front should aid our understanding of AD in terms of the potential role for metal ions in AD pathogenesis. By screening a spectrum of potential ligands for metal chelation, findings should benefit the development of therapeutic drugs for metal-related health problems such as AD and acute metal poisoning.

To summarise simply, the aims of this study are firstly to characterise the interactions between metal ions and amyloid β peptide (Aβ); then to analyse the interactions between metal ions and metal-chelating ligands; finally, to uncover the effect of metal ions on the expression of APP gene and the antagonistic effect of ligands against the metal ions.

1.2 Metal ions

Metals ions are constituents of the Earth's crust. Around 95 of the 118 elements in the periodic table are metals. Metal ions are central to protein structure and function. Many metal-binding proteins are enzymes which are present in the early forms of life, prokaryotes, and continued in eukaryotes (Wiiliams, 2012). Roughly 40% of all proteins crystallized to date have a metal bound within the structure and thought to be relevant to function (Waldron et al., 2009). The most abundant metal ion in living organisms is iron, followed by zinc. Metal ions and life have been evolving together (Hong Enriquez and Do, 2012). The complexity of organisms, especially in three steps, prokaryotes, single-cell and then multi-cell eukaryotes, coincides with oxygen-related environmental changes in the evolution of life. For example, the rise of oxygen caused a rise of zinc in the sea as estimated from the analysis of sediments (Hong Enriquez and Do, 2012). During the long evolution process, organisms learned to use or to avoid certain metal ions. Hence, there are essential or non-essential metal ions to living organisms.

1.3 Metal ions and biology

The essential metal ions can be further divided into two camps, including one group which is needed in larger quantity by the organisms (e.g. Ca^{2+}, Mg^{2+}), and the other group which are in much lower abundance such as the trace metal ions such as $Fe^{2+/3+}$, $Cu^{+/2+}$ and Zn^{2+}. A tenet of the cell biology of metals is that some metals tend to bind organic molecules more avidly than others. The natural order of stability for divalent metals, often called the Irving–Williams series (Irving and Williams, 1948), sets out a resulting trend with copper and zinc forming the tightest complexes, then nickel and cobalt, followed by ferrous iron and manganese and finally, forming

the weakest complexes, calcium and magnesium. Zinc is a quintessential metal in metal biology. Going back chronologically, zinc was first found essential to living organism in 1869, by Jules Raulin, a student of Louis Pasteur (Raulin, 1869). It is involved in enzymatic catalysis as a cofactor, structural component in proteins and signal transduction as a second messenger (Hershfinkel et al., 2001; Laity et al., 2001; Maret, 2001; Taylor et al., 2012). The first zinc binding enzyme discovered is carbonic anhydrase (Keilin and Mann, 1940). It is estimated that, in human proteome, there are at least 3000 zinc-binding proteins (Maret, 2012). Many of these proteins are transcription factors for DNA binding and gene regulation (Ebert and Altman, 2008). For non-essential metals, their presence in living organisms is deleterious. For example, aluminium (Al^{3+}) has no biological role in organisms. However, Al^{3+} ions are taken up by humans via drinking water and diet. With climate change and environmental pollution, the acidity of soil is increasing, which leads to the increased solubility of aluminium minerals and increased abundance of Al^{3+} ion in drinking water, plants and foods, and in turn more Al^{3+} ions are accumulated in people. Therefore, aluminium is associated with AD (Huat et al., 2019), although more evidence is required for such a link.

The excess of essential metal ions such as $Fe^{2+/3+}$, $Cu^{1+/2+}$ and Zn^{2+} is harmful to humans. Their optimal physiological concentration range between deficiency and toxicity is relatively small and needs to be tightly controlled. The cellular process to maintain the metal level at optimum is termed as homeostasis. Metal dyshomeostasis results from the disruption of metal homeostasis, which can lead to health disorders. For non-essential metals such as cadmium and hexavalent chromium, tiny amounts of them could promote severe toxicity to the cell (Permenter et al., 2011).

The omnipresence of metals in our quotidian lives presents innumerable hazards and health risks, albeit many of them are essential to human health. It is well known that metals are associated with many chronic health conditions as well as acute toxicity. World Health Organization (WHO) (2010) approximates metals are accountable for a significant mortality and morbidity, with 25% of total burden of disease linked to metal exposure. Metal ions have been found to interact with cell components such as DNA and nuclear proteins, causing DNA damage and conformational changes that may lead to cell cycle modulation, carcinogenesis or apoptosis (Wang and Shi, 2001; Beyersmann and Hartwig, 2008). Their toxicity depends on several factors including the dose, route of exposure, and chemical species, as well as the age, gender, genetics, and nutritional status of exposed individuals (Touchette et al., 2010).

Essential metals are inextricably involved in numerous essential biological processes and enzymatic reactions of the cell. For examples, iron (Fe^{2+} or Fe^{3+}) is a crucial part of haemoglobin for oxygen or carbon dioxide transport (Gupta, 2014). Many enzymes require copper (Cu^{+} or Cu^{2+}) and zinc (Zn^{2+}) to serve as cofactors or prosthetic groups (Tchounwou et al., 2012). Their import into the cell, intracellular trafficking, and export out of the cell must be tightly regulated at the cellular level, in order to maintain homeostasis. Metal dyshomeostasis can result in serious diseases such as cancers and neurodegenerative disorders like AD (Akatsu et al., 2012; Masaldan et al., 2018; Trist et al., 2018).

1.4 Alzheimer's disease

Alzheimer's disease (AD) was firstly reported on November 3, 1906 by a clinical psychiatrist and neuroanatomist - Alois Alzheimer, as a progressive neurodegenerative condition (Hippius and Neundörfer, 2003). AD is the most common form of dementia, by 2020 it is estimated to affect 50 million people worldwide, of which more than 400 000 reside in Australia (Macaulay and O'Meara, 2011; Hebert et al., 2013). Such a high global prevalence leads to serious socioeconomic burden and poses major challenges for human health in the 21st century. The clinical symptoms of AD are progressive cognitive deterioration and decline in memory. Initially the decline in memory occurs via the loss of episodic memory, which is a declarative memory subcategory, leading to a reduction in the ability to recollect recent events (Chopra et al., 2011). The molecular mechanism that causes the cognitive deterioration and decline in memory seen in AD remains an open question, albeit a considerable quantity of studies has been carried out until the present.

The disease is characterised by neuronal and synaptic loss resulting in gliosis and tissue atrophy. The histopathological hallmarks of AD, known as senile plaques and neurofibrillary tangles (Lau et al., 2002), are primarily found in the temporal and frontal cortices (Serrano-Pozo et al., 2011). The extracellular senile plaques were described as a "peculiar substance" by Alzheimer (Hippius and Neundörfer, 2003). In 1984, Glenner and Wong found senile plaques consisted of fibrils, which are made up of an aggregated Aβ peptide (Glenner and Wong, 1984). The intraneuronal neurofibrillary tangles are composed of paired helical filaments of hyperphosphorylated Tau protein (Zatta et al., 2009). The intraneuronal aggregates of hyperphosphorylated and misfolded Tau become extraneuronal ("ghost" tangles) when tangle-bearing neurons die (Serrano-Pozo et al., 2011). Neurofibrillary tangles have a stereotypical

spatiotemporal progression that correlates with the severity of the cognitive decline (Serrano-Pozo et al., 2011).

There are two forms of AD, the familial and sporadic AD. The familial AD is also called early-onset AD, accounts for only 5% of cases (Perrone et al., 2012). It occurs from the gene mutations in the presenilins (PS1& PS2), the APP genes of chromosome 1, 14 and 21 respectively and apolipoprotein isoform gene (ApoE4) (Tanzi et al., 1996; Mattson, 2004; Lanoiselée et al., 2017). However, the majority of cases are sporadic AD which is not due to genetic mutations. Sporadic AD has consistent pathological and clinical characteristics similar to familial AD but has a later age of onset (Kern and Behl, 2009; Pimplikar et al., 2010). Although the senile plaques and neurofibrillary tangles are characteristic lesions for both forms of AD, the molecular mechanism that initiates the pathogenesis in sporadic AD is not fully understood. Recent advances of research activities demonstrated that the Aβ is associated to the AD pathology and considered a critical factor in the pathogenesis of sporadic AD (Hardy and Selkoe, 2002). However, that the very existence of Aβ aggregation in the disease is a cause or a by-product of AD still remains debatable (Hardy, 2006; Lee et al., 2007; Korczyn et al., 2008). Experimental findings supporting the role of Aβ in AD pathogenesis are numerous, only a few examples are described in the following. Transgenic mice containing the APP gene mutation of $Lys^{670} \rightarrow Asn$, $Met^{671} \rightarrow Leu$, lead to increased production of human Aβ resulted in behavioural and memory deficits characteristic of AD (Hsiao et al., 1996). The conformational transition of the secondary structure of Aβ from random coil to β sheet increased the neurotoxicity of the peptide (Ueda et al., 1994). Aggregation of Aβ into amyloidogenic fibrils was found to produce neurotoxic compact plaques, in primary rat hippocampal cultures (Lorenzo and Yankner, 1994). Although these findings illustrate that the aggregation of Aβ is likely a crucial event in the pathogenesis of AD, the specific aspects of the plaque assembly process still requires to be

elucidated. This study will seek to reveal some details on how metal ions interact with Aβ, which could play a role in Aβ aggregation and consequently AD.

1.5 Amyloid precursor protein (APP)

The Aβ peptide is generated after two consecutive cleavage events by β- and γ-secretases of APP encoded by APP gene, a type-1 transmembrane protein with a single transmembrane span and an extracellular N-terminus. APP can also be cleaved by α-secretase within the Aβ domain to release soluble APP derivative and preclude Aβ generation (Zhang et al., 2011). As previously mentioned, genetic mutations in APP, as well as in presenilins (PS1 and PS2), are the cause for familial AD. Also mentioned is that Aβ could play a role in the pathogenesis of sporadic AD. Therefore, it is significant to recognise that APP is a critical protein for AD.

APP is expressed in various tissues, especially in the central nervous system (CNS). It is synthesised in the endoplasmic reticulum and then transported to the Golgi apparatus, where it completes maturation and is finally transported to the plasma membrane. Although its physiological function is still unclear, APP could play an important role in brain development, memory and synaptic plasticity (Breen et al., 1991). It is suggested that APP is involved in neurite outgrowth and synaptogenesis, neuronal protein trafficking along the axon, transmembrane signal transduction, cell adhesion and calcium metabolism (Zheng and Koo, 2006). The metabolism of APP can follow two different pathways shown in Figure 1.1.

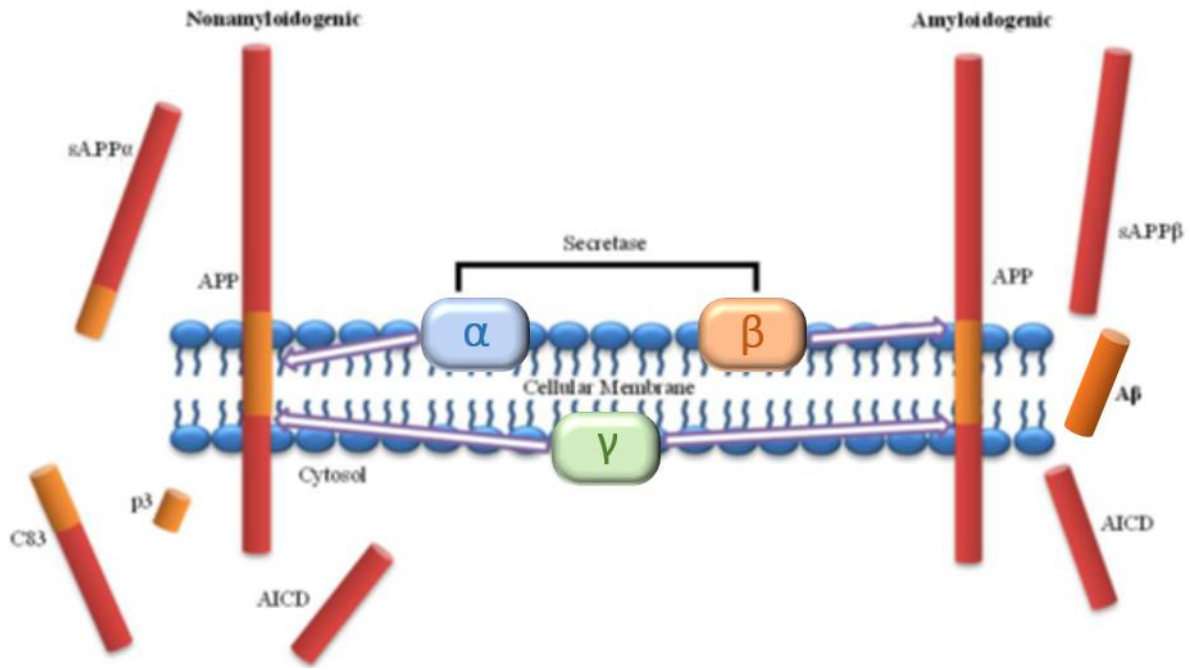

Figure 1.1 Schematic of APP proteolytic cleavage. In the non-amyloidogenic pathway, APP is cleaved by α-secretase and then γ-secretase or β-secretase to form truncated $A\beta_{17–40/42}$ or $A\beta_{1–16}$ peptides respectively. In the amyloidogenic pathway, APP undergoes consecutive cleavage by the β- and γ-secretases, producing $A\beta_{40/42}$ peptide.

Physiological APP undergoes non-amyloidogenic cleavage, predominantly in post-Golgi secretory and endocytic compartments, by α-secretase and γ-secretase, producing soluble APP. The amyloidogenic pathway occurs at the plasma membrane where the APP cleavage is sequentially conducted by β-secretase and γ-secretase. This pathway releases Aβ. As shown in Figure 1.1, both cleavage pathways for APP lead to the formation of carboxyterminal fragments (C83) and amino-terminal fragments secreted APP (sAPPα and sAPPβ). Then followed by the formation of amino-terminal APP intracellular domain (AICD), this fragment is involved in nuclear signalling (Chow et al., 2010). Both non-amyloidogenic and amyloidogenic pathway occur under normal conditions in all cells (Haass et al., 1992). During neuronal activity, Aβ is formed intracellularly in vesicles such as endosomes, then released into the extracellular space of the brain, this process does not necessarily result in AD pathology, as AD pathogenesis is

multifactorial and involves the disruption of multiple mechanisms. However, the soluble form of Aβ is found in healthy brain but the aggregated form is in the brain of AD patients (Glenner and Wong, 1984). Hence numerous hypotheses have been postulated to elucidate the mechanism responsible for the development of senile plaques. In this thesis, the interaction of metal ions with Aβ peptide is investigated, and the effect of metal ions on APP gene expression is also investigated.

Thus far there is scant evidence on the effect of metal ions on APP gene expression. It was demonstrated that cupric and manganese (Mn^{2+}) ions potently increased the expression of APP gene in a time- and concentration-dependent manner (Lin et al., 2008; Kim et al., 2018). As metal ions such as Al^{3+} are implicated in AD (Exley, 2014; Exley and Vickers, 2014), their effect on Aβ aggregation as well as APP gene expression needs to be studied. Therefore, investigation into the effect of metal ions on APP gene expression is part of this project.

1.6 Amyloid β (Aβ) peptide

Aβ was firstly characterised in 1984 by Glenner and Wong (1984). It is a soluble cellular metabolite found in cerebrospinal fluid (CSF) and plasma (Yang et al., 2000). As described previously, Aβ is produced by a variety of cells, from the sequential proteolytic processing of the APP by secretases β and γ (Glenner, 1985; Lahiri and Maloney, 2010).

Aβ encompasses a group of peptides ranging in size from 12 to 42 amino acid residues. The primary amino acid sequence of the 42-residue Aβ isoform $A\beta_{42}$ is shown in Figure 1.2. The C-terminal amino acid sequence of Aβ is mainly composed of hydrophobic residues, which performs an important part in its insolubility and in the initial steps of aggregation. The N-terminal region of Aβ is amphipathic and participates in the binding of Aβ to apoE (Strittmatter et al., 1993), cholesterol (Yao and Papadopoulos, 2002), glycosaminoglycans (Narindrasorasak et al., 1991; Buée et al., 1993), and metal ions (Adlard and Bush, 2006).

DAEFRHDSGYEVHHQKLVFFAEDVGSNKGAIIGLMVGGVVIA

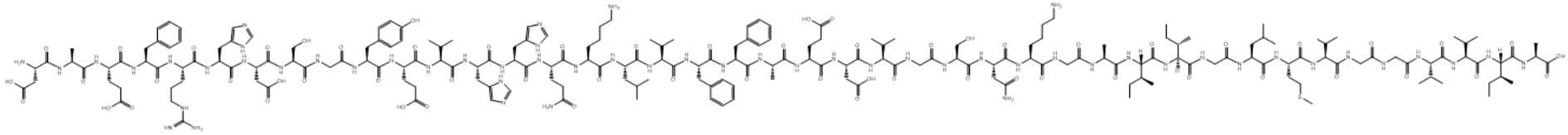

Figure 1.2 Full amino acid sequence of Aβ$_{42}$

Aβ is thought to be an intrinsically unstructured peptide. The secondary and tertiary structure is extensively influenced by environmental milieu, for example, in membrane-like media, the truncated 28 residue long Aβ peptide ($A\beta_{1-28}$) folds into a predominately α-helical structure with a bend centred at residue Val12 (Talafous et al., 1994). Without a defined tertiary structure, studies of its physiological functions are difficult. Emerging data suggests Aβ plays important physiological roles, such as controlling synaptic plasticity (Kamenetz et al., 2003) involved in regulatory neurogenesis, metal ion homeostasis or sequestration, oxidative stress protection, calcium regulation (Cardenas-Aguayo Mdel et al., 2014), immune response and signaling pathways (Ramanathan et al., 2015). Brain disruptions, for example a stroke and trauma, results in an irregular up regulation of APP and accumulation of Aβ (Pierce et al., 1996; van Groen et al., 2005). While the primary function of Aβ still remains to be established, in the brain of AD patient it is in the aggregated form, and in healthy brain tissue it is in the soluble form.

Although decades have passed since Aβ was characterised and associated with AD, how it forms aggregates in the brains of AD patients is still unknown. Multiple factors such as pH, temperature, peptide concentration, and ionic strength have been implicated in the formation of Aβ aggregates (Meisl et al., 2016). However, the extracellular increase of Aβ concentration in the brain has been found to result in Aβ aggregation, forming β-sheet rich structures which are characteristic of AD (Ding and Keller, 2003). Aggregation begins with the formation of oligomers species, these are then re-arranged into protofibrils and fibrils which are found in senile plaques. As the oligomer species in AD patient brains can permeabilize cellular membranes, which consequently initiate a series of events resulting in cell dysfunction and death, it is considered more toxic for cells (Pham et al., 2010; Forloni et al., 2016).

Physiologically, Aβ can vary in length, ranging from 37 to 42 residues depending on the location the γ-secretase cleavage process occurs on APP (Small, 2001; Karran et al., 2011). The chemical properties of Aβ are an important factor in AD pathogenesis. As seen in the Table 1.1, Aβ with various lengths and sequences have been used previously to analyse the different properties of Aβ. While $A\beta_{42}$ is the most toxic form but not as prevalent, compared to its smaller counterparts (Jarrett et al., 1993). $A\beta_{42}$ is enriched in Aβ deposits and it is more prone to fibril formation (Masters et al., 1985; Kang et al., 1987; Vigo-Pelfrey et al., 1993). Studies *in vitro* found that $A\beta_{42}$ peptide also readily aggregates more than the $A\beta_{40}$ peptide, and $A\beta_{42}$ peptide was also found to seed the aggregation of $A\beta_{40}$ peptide (Hilbich et al., 1991; Jarrett et al., 1993).

Table 1.1 Various Aβ sequences utilised previously for structural analysis studies

Aβ Peptide	Sequence	Reference
$A\beta_{42}$	DAEFRHDSGYLEIVHHQKLVFFAEDVGSNGAIIGLMVGGVVI	(Halverson et al., 1990)
$A\beta_{40}$	DAEFRHDSGYEVHHQKLVFFAEDVGSNKGAIIGLMVGGVV	(Touchette et al., 2010)
$A\beta_{1\text{-}28}$	- hAβ28 DAEFRHDSGYEVHHQKLVFFAEDVGSNK-NH2 - rAβ28 DAEFGHDSGFEVRHQKLVFFAEDVGSNK-NH2 - Ac- rAβ28 Ac- DAEFRHDSGYEVHHQKLVFFAEDVGSNK-NH2 - Ac- hAβ28 Ac- DAEFGHDSGFEVRHQKLVFFAEDVGSNK-NH2	(Gaggelli et al., 2007)
$A\beta_{1\text{–}16}$	DAEFRHDSGYEVHHQK	(Kowalik-Jankowska et al., 2003)
$A\beta_{1\text{–}12}$	DAEFRHDSGYEV	(Narayan et al., 2013)

Notes: h- human, r- rat and Ac- acetylation of the N-terminus

To ensure this study is relevant to the biological reality, it will be conducted at the biological pH of 7.4. In terms of studying the peptides by ^{1}H NMR analysis, previous studies have illustrated the tendency for $A\beta_{40}$ to undergo rapid conformational changes, causing large up field shifts. This property would cause the characterisations of the resulting metal-ligand complex difficult, thus the use of larger peptides would not be feasible in this project. Also, the longer peptides, such as $A\beta_{42}$, can rapidly aggregate and suddenly form fibrils. Therefore, when compared to the larger counterparts, the truncated 28 residues long Aβ peptide ($A\beta_{1-28}$) is practically more manageable, in regard to its propensity to precipitate or aggregate out of a solution. Shorter Aβ peptides cannot be used as under biological conditions pH of 7.4, it will not undergo aggregation (Mekmouche et al., 2005), thus rendering secondary structural studies less relevant to the disease development. Furthermore, $A\beta_{1-28}$ contains three histidine residues which are possibly involved in metal coordination. Hence this study will use the $A\beta_{1-28}$, with the sequence of DAEFRHDSGYEVHHQKLVFFAEDVGSNK. Since the precise mechanism of Aβ aggregation is yet to be identified, it is expected that the outcome of this study can enhance our understanding of Aβ aggregation in terms of the role of metal ions in the process.

1.7 Oxidative stress and Alzheimer's disease

Another feature of AD is its association with oxidative stress. Oxidative stress occurs with the increased production of reactive oxygen species (ROS), caused by the inadequate detoxification of cellular antioxidant defence system. ROS is a collective term for oxygen radicals (superoxide and hydroxyl) and non-radical derivatives (hydrogen peroxide), they bear unpaired electrons (Kim et al., 2015). ROS are very unstable and readily cause damages in macromolecules such as proteins, lipids and nucleic acids (Bhattacharya, 2015).

The brain is susceptible to oxidative stress as a result of relatively low concentrations of antioxidants, higher levels of polyunsaturated fatty acids and the elevated oxygen requirements (Evans, 1993; Huang et al., 2016). In particular, the mitochondria is a major source of oxidative stress, as it requires high levels of oxygen for the energy production (Bhat et al., 2015). A characteristic pathological feature of AD is oxidative stress and mitochondrial dysfunction. In AD patients, in the neocortex exhibits metabolic markers of oxidative stress include free radical induced damage of brain proteins, lipids and DNA. Increased concentration of redox active metals ions, Cu^{2+} and Fe^{2+} result in the production of ROS via the involvement in Fenton reactions and Haber-Weiss reaction. These reactions are shown below in Equations 1.1 to 1.3-

Fenton reactions:

$$M^{n+} + H_2O_2 \rightarrow MI^{(n+1)+} + HO^{\bullet} + OH^{-} \quad (1.1)$$

$$M^{(n+1)+} + H_2O_2 \rightarrow MI^{n+} + HOO^{\bullet} + H^{+} \quad (1.2)$$

Haber-Weiss reaction:

$$O_2^{\bullet -} + H_2O_2 \rightarrow O_2 + HO^{\bullet} + OH^{-} \quad (1.3)$$

The biochemical relationships amongst Aβ, metal ions, plaques, oxidative stress and AD is multifaceted and intriguing. *In vitro* evidence suggests Aβ plays a role in oxidative stress in AD brain, such as synthesised Aβ can cause lipid peroxidation of synaptosomes (Butterfield et al., 1994). The coordination of Cu^{2+} and Fe^{3+} to Aβ has been found to catalyse the production of ROS, in particular the highly reactive hydroxyl radical (Nakamura et al., 2007). Aβ is also able to reduce Cu^{2+} to Cu^{+} and Fe^{3+} to Fe^{2+}, simultaneously generating ROS, hydrogen peroxide and hydroxyl radical (Huang et al., 1999). The mechanistic reaction of this is detailed by Huang et al. (2004) in Equations 1.4 to 1.6.

$$2A\beta + M^{(n+1)+} \rightarrow (A\beta - A\beta^{\bullet})^{+} + M^{n+} \quad (1.4)$$

$$M^{n+} + O_2 \rightarrow MI^{(n+1)+} + O_2{}^{-} \quad (1.5)$$

$$O_2{}^{-} + O_2{}^{-} + 2H^{+} \rightarrow H_2O_2 + O_2{}^{\bullet} \quad (1.6)$$

This subsequently demonstrates a relationship between Aβ, metal ion and oxidative stress. On one hand, Aβ production and metal ions can play an important role in the oxidative process and subsequent mitochondrial dysfunction seen in AD (Sayre et al., 2005; Murakami et al., 2012; Trist et al., 2018). On the other hand, metal dyshomeostasis and oxidative stress are major factors that trigger the production and oligomerization of Aβ in AD (Butterfield, 2002; Drago et al., 2008; Tabner et al., 2011; Murakami et al., 2012). Therefore, the interactions between oxidative stress, metal ions and Aβ may be the multifaceted culprits which trigger and accelerate AD pathogenesis.

1.8 AD pathogenesis hypotheses

In the past decades, many different hypotheses for AD pathogenesis have been proposed. Some, such as the cholinergic hypothesis of AD state cognitive impairment comes from dysfunction of acetylcholine (Francis et al., 1999). However, trials to inhibit this pathway with symptom-treating receptor antagonists, had limited efficiency (Weinstock, 1995). Hence the quest for more causative pathogenic targets continues until the present. Stemming from the different features of the disease, the three main hypotheses have emerged, i.e., amyloid cascade hypothesis, metal ion hypothesis and oxidative stress hypothesis. A major theme of my study is the interaction between Aβ and metal ions as well as the oxidative process surrounding this interaction, thus this section will discuss these competing hypotheses.

1.8.1 Amyloid cascade hypothesis

Although multiple risk factors have been associated with the sporadic AD, it is not clear what factors can cause the disease. However, one thing is almost certain, that is, Aβ is linked to AD, albeit whether it is the cause or effect is still debatable. The 'amyloid cascade hypothesis' is the most influential model for the pathology of AD proposed over the last 25 years (Karran and De Strooper, 2016). It suggests the deposits of Aβ aggregates in the brain is imperative step in the development of AD (Hardy and Higgins, 1992). The abnormal processing of APP, as well as its aberrant metabolism, causes excessive Aβ in the brain, therefore, resulting in Aβ aggregation, neurodegeneration and neuronal call death accompanied with AD (Budimir, 2011).

This hypothesis is supported firstly by the discovery of the APP gene which exists on chromosome 21. APP gene is mutated in both familial AD and Down syndrome (Barber, 2012). Secondly, observations of individuals with Down syndrome are affected by neuropathological features indistinguishable from AD patients (Olson and Shaw, 1969; Glenner and Wong, 1984). Studies showed that in Down syndrome the temporal sequence of events initiated with the formation of plaques, followed by the development of neurofibrillary tangles and the subsequent neuronal cell damage also seen in AD (Rumble et al., 1989).

As the amyloid cascade hypothesis suggests that Aβ deposition in the brain is the cause of AD (Hardy and Higgins, 1992), thus implying that if Aβ deposition is eliminated, AD would be cured or ameliorated in human subjects. However, the data accumulated in the years after the hypothesis proposed, even Hardy himself (Hardy, 2009) asked the provocative question, "Has the amyloid cascade hypothesis for Alzheimer's disease been proved?". Clinical trials with Aβ-related immunotherapy provided inconclusive answers. Aβ immunotherapy with synthetic Aβ

peptide (AN-1792) and adjuvant QS-21 was the first active immunotherapy for AD (Robinson et al., 2004; Lee et al., 2005). The therapy was based on AN-1792 provoking the immune response in order to eliminate amyloid deposits in brain (Nicoll et al., 2003). Preclinical evidence demonstrated the therapy prevented Aβ deposition. However, Phase IIA trials were suspended in early 2002 when 6% of patients, who received the vaccine, developed meningoencephalitis (Robinson et al., 2004; Gilman et al., 2005). Despite the trials being abandoned, studies found Aβ immunotherapy can be beneficial in AD, as post mortem analysis demonstrated the clearance of senile plaques in the immunised group (Holmes et al., 2008). The amyloid cascade hypothesis has continued to gain support in the past two decades, with genetic studies and many current treatment strategies intending to reduce Aβ production or increase Aβ metabolic rate (Barage and Sonawane, 2015).

1.8.2 Metal ion hypothesis

With what specifically initiates the excessive Aβ and the variation in its metabolism still unknown, and the incomplete success for therapeutic anti-amyloid drugs, numerous studies point to the other factor, i.e. metal ions. This is triggered by the fact that metal ions were found in amyloid plaques and that Aβ accumulation and aggregation can be markedly affected by metal ions in the brain (Bolognin et al., 2011; Kim et al., 2018). The 'metal ion hypothesis', also known as the 'neurotoxic trace element hypothesis', suggests that the aggregation of Aβ and its neurotoxicity is mediated by metallochemical reactions, as well as impaired metal homeostasis (Bush and Tanzi, 2008). The metal ion hypothesis indicates that the interaction of Aβ with metal ions is the causative factor of neuronal cell loss and AD (Blessed et al., 1968; Mann and Esiri, 1989; Selkoe, 1991; Kim et al., 2018). In support of the metal hypothesis, it has been shown that AD patients have elevations in brain iron (Fe^{2+}) level and accumulation of

copper (Cu^{2+}), zinc (Zn^{2+}) and aluminium (Al^{3+}) in cerebral Aβ deposits such as senile plaques (Cherny et al., 2001; Bush et al., 2003; Miller et al., 2006). An important breakthrough for the metal ion hypothesis, was numerous observations that Al^{3+}, Zn^{2+}, Fe^{2+} and Cu^{2+} are essential for formation and structural integrity of Aβ aggregates, oligomers, and fibrils (Atwood et al., 1998; Lovell et al., 1998; Dong et al., 2003; House et al., 2004; Huang et al., 2004; Miller et al., 2006; Talmard et al., 2009). Metal ions can also bind to the location of the γ-secretase cleavage, which subsequently limits the cleaving by β-secretase (Bush et al., 1993). This results in the increased production of Aβ.

1.8.3 Oxidative stress hypothesis

The third hypothesis of AD pathogenesis asserts that age, environmental or genetically enhanced oxidative stress results in the gene defects and declining mitochondrial function and triggers the pathogenesis of AD (Markesbery, 1997; Bhat et al., 2015; Cheignon et al., 2018). The oxidative stress leads to neurological disorders, by initiating apoptosis in neurons (Nakamura et al., 2007; Dumont and Beal, 2011). The neurological apoptosis occurs by triggering a range of pathways from lesions, misfolded proteins, excitotoxicity or Ca^{2+} dyshomeostasis (Beal, 1995). Numerous post mortem human studies support that oxidative stress is a constant feature of the AD brain pathology, with the increased oxidative stress biomarkers and ROS-oxidized proteins detected in the frontal and parietal lobes and in the hippocampus of AD (Subbarao et al., 1990; Hensley et al., 1995; Smith et al., 1997; Markesbery and Carney, 1999; Lauderback et al., 2001; Butterfield et al., 2006). Mice models demonstrate oxidative stress features of lipid and protein oxidation is present in the early development of their phenotype (Matsuoka et al., 2001; Anantharaman et al., 2006). As

indicated in section 1.7, Aβ aggregates have the potential to form ROS. Hence the neurodegeneration around the amyloid plaques are also associated to oxidative stress.

1.8.4 Alzheimer's disease multifactorial nature

The amyloid cascade hypothesis, metal ion hypothesis and oxidative stress hypothesis reveal the multifactorial nature of AD, with several pathological factors such as oxidation, inflammatory response, disruption of metal ion homeostasis considered as both the triggers and subsequent events of Aβ aggregation (Mantyh et al., 1993; Hou et al., 2004; Huang et al., 2004; Kurganov et al., 2004; Boyd-Kimball et al., 2005; Hung et al., 2008; Bolognin et al., 2011; Meisl et al., 2016). While the etiological mechanism of AD remains unclear, evidence supports the notion that metals are critically involved as factors or cofactors in AD etiopathogenesis. Many features of the three hypotheses are inextricably linked via metal ions, as shown in Figure 1.3. Metal ions are related to both Aβ aggregates and oxidative stress, indicating a consequential involvement in AD.

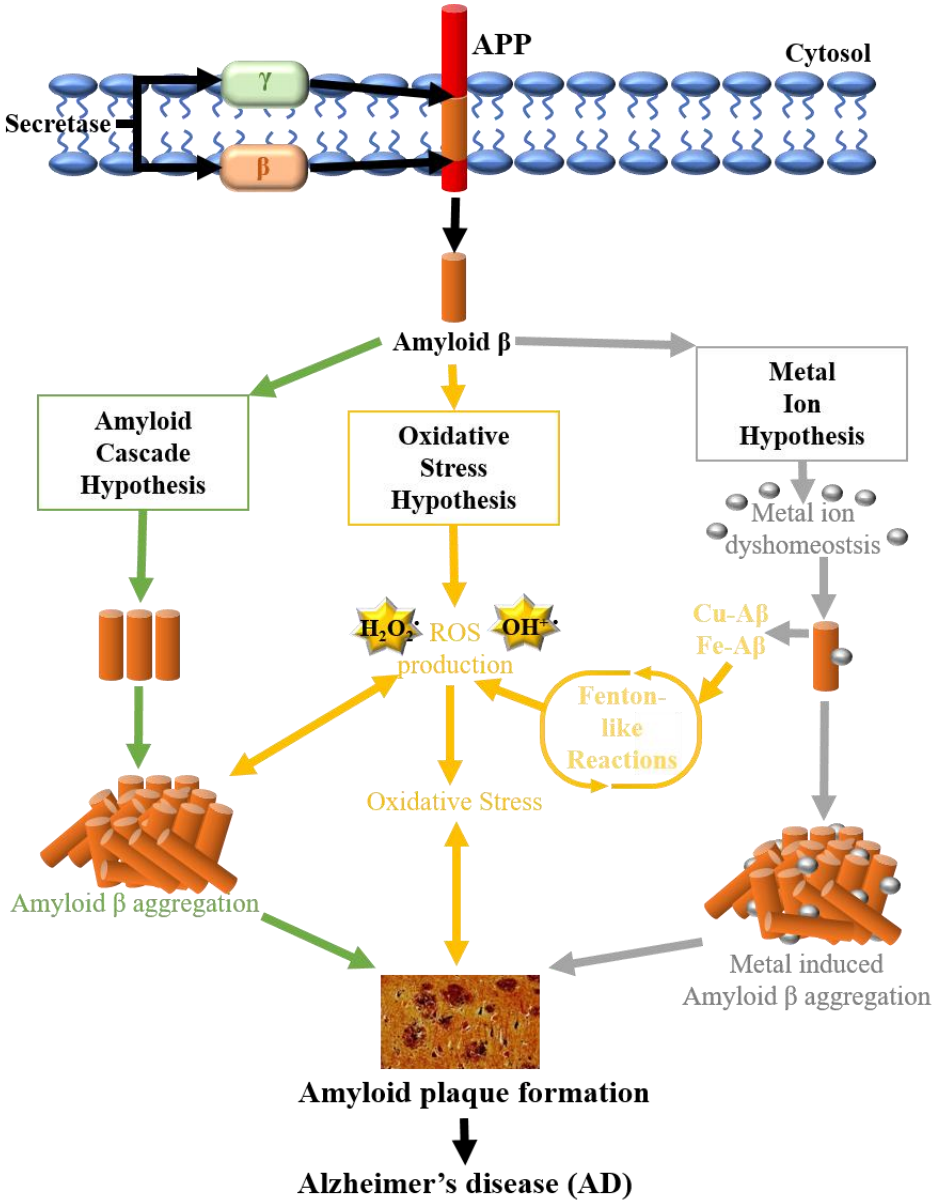

Figure 1.3 Schematic description of the hypotheses for Alzheimer's disease. Amyloid β (Aβ) monomers produced via the cleavage of APP (amyloid precursor protein) by β- and γ- secretase. In the amyloid cascade hypothesis Aβ monomers aggregate, resulting in the formation of amyloid plaques (image sourced from Tschanz, 2011)which in turns cause AD. The production of ROS plays a major role in the oxidative stress hypothesis. ROS are believed to be either the cause or a by-product of Aβ aggregation and amyloid plaques. ROS can also be formed by Fenton-like reactions through the binding of Aβ monomers to $Cu^{+/2+}$ or $Fe^{2+/3+}$, leading to Aβ aggregation and amyloid plaques. The metal ion hypothesis highlights metal dyshomeostasis which leads to Aβ aggregation and AD. These three hypotheses are connected, as metal ions can be involved in the ROS generation, Aβ aggregation, and the formation of amyloid plaques.

1.9 Metal ions associated with Alzheimer's disease

The dyshomeostasis of the brain's metal ions promotes Aβ aggregation. In the case of copper and iron, they can generate reactive oxygen species, which may involve in AD development (Bush and Tanzi, 2008; Drew, 2017). Donnelly et al (2007) referred to Aβ as metal sinks due to the high concentration of metals in Aβ plaque. Metals Al^{3+}, Zn^{2+}, Cu^{+}/Cu^{2+} and Fe^{2+}/Fe^{3+} have been found in amyloid plaque of AD patients at concentration of 0.5-1 mmol L^{-1} (Faller and Hureau, 2009). Along with the global warming and elevated environmental pollution, our exposure to metal ions increases and this in turn adversely affects human health. The role of metal ions (targeted in this study i.e. copper, zinc, aluminium, arsenic and chromium) in Aβ coordination and aggregation has been investigated in the past years, the findings are reviewed below.

1.9.1 Copper

Copper has a major role in brain metabolism, it is essential for Cu/Zn superoxide dismutase (SOD1) for antioxidant defence, electron transport, mitochondrial respiratory chain, dopamine β-hydroxylase, biosynthesis, and ceruloplasmin for iron homeostasis (Waggoner et al., 1999; Donnelly et al., 2007). Cu^{2+} homeostasis is particularly important, as concentrations of free Cu^{2+} exceeding 10^{-18} M can cause oxidative damage (Rae et al., 1999). Numerous studies have indicated Cu^{2+} homeostasis is severely impaired in AD (Brown and Kozlowski, 2004; Gaggelli et al., 2006). Elevated concentrations of Cu^{2+} have been found in AD brains (Zheng et al., 2010). The Cu^{2+} levels in the serum of AD patients is 54% higher than controls (Squitti et al., 2002). The Cu^{2+} concentrations of 19.3 ± 6.3 μg/g are found in AD neuropil and up to 30.1 ± 11.0 μg/g in amyloid plaques (Lovell et al., 1998). Aβ has a high affinity for Cu^{2+} and coordination is found to alter the morphology of aggregated Aβ fibrils (Cherny et al., 1999). In primary cortical

neurons, the binuclear Cu-Aβ_{1-42} complex is neurotoxic. The Cu-Aβ_{1-42} complex exhibits indicators of oxidative stress, inducing higher levels of lipid peroxidation and dityrosine (Smith et al., 2006). ROS production is frequently attributed to Cu^{2+}, in comparison to AD related Fe^{2+}, as Cu^{2+} has a higher redox activity (Nakamura et al., 2007 ; Cheignon et al., 2018).

In vitro studies have found that Aβ has a high affinity to Cu^{2+} and that the morphology of the Cu^{2+} bound Aβ aggregates are distinguishable from the other metals tested (Zn^{2+}, Ca^{2+} and Mg^{3+}) (Cherny et al., 1999). Cu^{2+} normally binds Aβ in a 1:1 stoichiometry (Syme et al., 2004). Hou and Zagorski (2006) found a weak detection of the signal for the ^{1}H atoms bonded to ^{15}N atoms of the histidine residues, thus confirming findings that imidazole nitrogen of histidine are metal binding sites for Cu^{2+} (Watt et al., 2011), with the possible existence of a second, low-affinity binding site situated around the N-terminus (Asp1 and Ala2). The coordination of Cu^{2+} to Aβ has been comprehensively studied with a few techniques (Beauchemin and Kisilevsky, 1998; Syme et al., 2004; Streltsov et al., 2008). The most accepted coordination modes (Hureau, 2012) are illustrated in Figure 1.4, with the corresponding binding affinity (K_D) of 10^{10} M^{-1}(Alies et al., 2013).

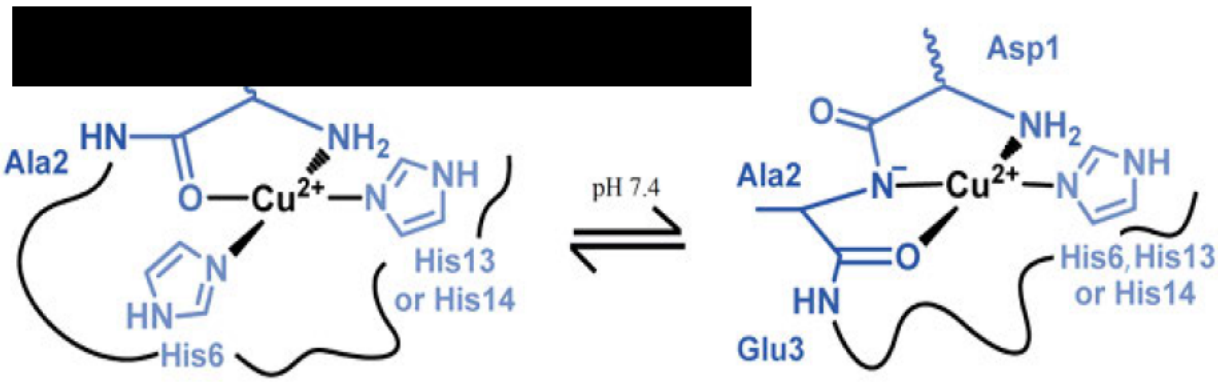

Figure 1.4 Proposed coordination modes of Cu^{2+} to Aβ. Structure is based on bibliographic data (Hureau, 2012) the corresponding binding affinity constant values (K_D) at pH 7.4 are found to be 10^{10} M^{-1} (Alies et al., 2013).

At physiological pH, Cu^{2+} binding modes are found with the distorted square planar geometry, which is preferred by the d^9 metal ion. The slight fluctuation around physiological pH results in the structural interconversions between Figure 1.4A and B. The coordination mode of Figure 1.4A is adopted at slightly lower pH, where Cu^{2+} binds via the histidine residues, N-terminal amine and carbonyl of the amide bond between Asp1-Ala2. At a higher pH, the binding mode of Figure 1.4B is found, in which the Cu^{2+} coordination through a histidine residue, N-terminal amine, the carbonyl of the amide bond between Ala2-Glu3 and the deprotonated nitrogen of the amide bond between Asp1-Ala2. As the interaction of Cu^{2+} and Aβ has been previously established, it will not be the main metal of focus in my study.

1.9.2 Zinc

Zinc (Zn^{2+}) is a *d* block metal with a d^{10} configuration and an atomic number of 30. It is one of the essential trace metal ions in living organisms - the second most abundant transition metal after iron ($Fe^{2+/3+}$). In the recent decades, Zn^{2+} has been found to be involved in multitudes of biological functions. In the central nervous system (CNS), Zn^{2+} plays a central role in processes such as apoptosis, oxidative stress, immune defence, neurogenesis, motor coordination, memory, and synaptic plasticity (Lu et al., 2000; Smart et al., 2004; Kepp, 2012). The majority of Zn^{2+} is in the testes, muscle, liver, and brain (Chen et al., 2016). However, zinc dyshomeostasis has been associated with AD, and vascular-type dementia (Watt et al., 2011; Kawahara et al., 2014). Burnet (1981) was the first to suggest the role of zinc in AD pathogenesis. The genetic risk factor in familial AD, the ApoE4 gene is related to higher serum levels of Zn^{2+} (Mattson, 2004).

Evidence indicates Zn^{2+} affect Aβ in numerous ways, via transcription factor zinc-fingers, as bound Zn^{2+} in active sites of proteases (Lovell, 2009), and direct coordination to $A\beta_{40/42}$ (Yang et al., 2000; Danielsson et al., 2007). Zn^{2+} can also coordinate to APP, at the α secretase site

(Bush et al., 1993). Consequently cleavage of APP is left to β and γ secretase which increases production of $A\beta_{40/42}$ (Bush et al., 1994). Zinc-dependent amyloidosis is indicated to be a result from zinc-amyloid interaction (Mantyh et al., 1993). Under physiological condition *in vitro*, rapid Aβ aggregation mediated by Zn^{2+} have been observed (Huang et al., 2000).

Similar to Cu^{2+}, the interactions of Zn^{2+} and Aβ have been well documented (Yang et al., 2000; Danielsson et al., 2007; Faller and Hureau, 2009; Nair et al., 2010; Watt et al., 2011). Previous findings indicate that Zn^{2+} binds to Aβ in a 1:1 stoichiometry with a mononuclear binding site (Danielsson et al., 2007). The study found the majority of Zn^{2+} binding sites are located within the first 16 residues in the hydrophilic section of the N-terminal, as only two sites are present on the carboxyl terminal (Atrián-Blasco et al., 2017). The three histidine residues in the N-terminus of $A\beta_{42}$ peptide, are involved in zinc binding (Danielsson et al., 2007; Watt et al., 2011) with an equilibrium between His13 and His14 for one binding position anticipated (Alies et al., 2016). Studies using Aβ analogues supported this equilibrium, finding that all three histidine residues (His 6, His 13 and His 14) are zinc binding sites (Liu et al., 1999; Yang et al., 2000).

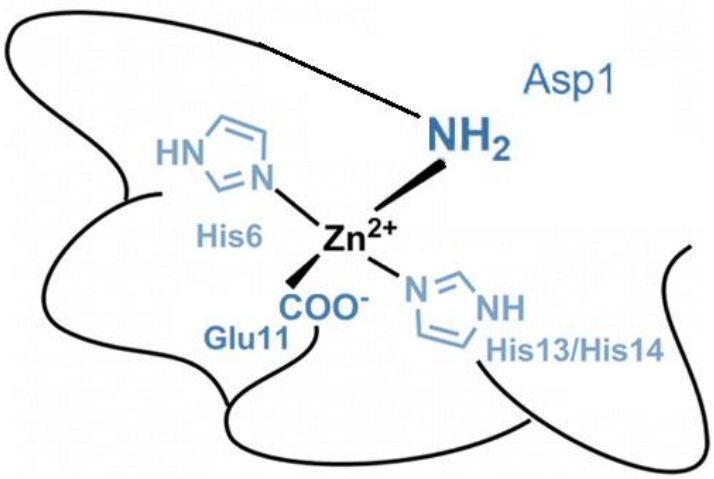

Figure 1.5 Proposed coordination mode of Zn^{2+} to Aβ. Structure is based on bibliographic data (Danielsson et al., 2007; Watt et al., 2011) with an binding affinity constant values (Ka) at pH 7.4 are found to be 10^5 M^{-1} (Alies et al., 2016).

Based on these studies the most plausible first-coordination sphere structure of Zn^{2+}–Aβ is illustrate in Figure 1.5. The coordination mode of Zn^{2+} to Aβ, maintains the Zn^{2+} preferred tetrahedral geometry, binding through two histidine residues (His6 andHis13 or His14), as well as the N-terminus of Asp1 and the carboxylic acid R group of Glu11 (Gaggelli et al., 2007) Zn^{2+} along with Al^{3+} will be investigated in this study.

1.9.3 Aluminium

Aluminium is the third most abundant metallic element found on earth (Exley, 2004). Due to its abundance Al^{3+} is readily found in water, airborne dust and foods. It is also used in antiperspirants sprays and medicines such as adjuvant in vaccines and antacids. The main contributor for the intake of Al^{3+} in humans is via food and drink. Al^{3+} is insidious as it accumulates over time. Since the kidneys are the key organ for detoxification, neurotoxic effects of Al^{3+} have been described in dialysis patients (Parkinson et al., 1981), who exhibited elevated aluminium concentrations in plasma and brain tissue. Such patients showed disorientation, memory impairments, and, at advanced stages, dementia (Parkinson et al., 1981). Al^{3+} exhibits a high affinity to proteins, which it is able to cross-link.

Despite aluminium being defined as redox inactive, Al^{3+} can become redox-active with the use of a very harsh reducing agent (Myers et al., 2011). It also has potent pro-oxidant abilities demonstrated by the formation of an aluminium superoxide semi-reduced radical cation $^{\bullet}AlO_2^{2+}$, which is more powerful oxidant than either $O_2^{-\bullet}$ or $HO_2^{-\bullet}$(Exley, 2004). The ability of Al^{3+} to be a neurotoxin was established over 100 years ago (Yokel, 2012). Al^{3+}plays a role in dialysis encephalopathy (Alfrey et al., 1976) and increases proinflammatory cytokines in the CNS (Campbell, 2004). In human breast MCF-7 cancer cells, the presence of Al^{3+} was found to

increase the processes of metastasis (Darbre et al., 2013). Understandably the safety of Al^{3+} in humans has been controversial for a century.

One of the major sources of Al^{3+} exposure is food preservatives or contamination from food, cooking and cookware, which accounts for an intake of about 20 mg/day (Greger and Sutherland, 1997). Hence Al^{3+} is commonly absorbed through the gastrointestinal tract. The inhalation of Al^{3+} in antiperspirant aerosol or as air-borne particulates allows the absorption of Al^{3+} through across the respiratory tract into systemic circulation (Yokel, 2012). Aluminium adjuvants are also present in vaccines (Hem, 2002).

Various Al^{3+} chemical species can occur *in vivo,* which possess various physical, chemical and biological properties. The presence of Al^{3+} have been detected in numerous biological fluids including urine (Davenward et al., 2013), CSF (Roos et al., 2013), sweat (Genuis et al., 2011) and seminal fluids (Hovatta et al., 1998). Aluminium is excreted from the body by a number of different modes of excretion, for non-systemic aluminium faeces is the major route and urine eliminates systemic aluminium (Ruipérez et al., 2012).

According to UV spectroscopy and thermodynamic modelling two primary aluminium species exists in blood extracellular fluid (ECF) (Harris et al., 2003). In plasma, Al transferrin (Tf) accounts for approximately 93% and Al citrate accounts for about 5.5% of Al^{3+} species (Yokel, 2012). Al^{3+} has no known biological role, however, it is present in human brain tissue in concentrations of 1.02 to 2.01 µg/g dry weight across the four main lobes (House et al., 2012). Al^{3+} has two potential routes to enter the brain from blood, firstly through the blood brain barrier (BBB) and secondly through the choroid plexus (CP) into the CSF (Xu et al., 1992; Allen et al., 1995). Concentrations of aluminium is higher in plasma, but the metal ions can rapidly enter brain ECF and CSF (Yokel, 2012).

Al^{3+} is the first exogenous metal to be identified as a risk factor in AD, as reviewed by multiple authors (Neri and Hewitt, 1991; Bondy, 2010; Frisardi et al., 2010; Tomljenovic, 2011). Recent reports have indicated that the exposure to Al^{3+} contributes to the development of AD (Exley, 2014). Studies found that in post mortem studies of familial AD patients the mean Al^{3+} concentration of the occipital, frontal, temporal and parietal lobes was 3.89, 3.66, 2.03 and 1.61 µg/g dry weight respectively (Mirza et al., 2017). Oxidative stress is accelerated by Al^{3+} *in vivo* and *in vitro* (Khan et al., 2006). The reaction of Al^{3+} with superoxide (O_2^-) produces radical ions ($^{\bullet}AlO_2^{2+}$) which increase the Fenton and Haber-Weiss reactions (Exley, 2004).

Unlike Cu^{2+} and Zn^{2+}, Al^{3+} is not considered as an AD related metal and the metal ions association to AD is still controversial, because of insufficient evidence. However, numerous studies provide possible mechanisms for the involvement of Al^{3+} in amyloid plaque formation (Neri and Hewitt, 1991; House et al., 2004; Drago et al., 2008; Chen et al., 2011). Similar to other metal ions, Al^{3+} is found directly bond to Aβ in senile plaques (Yumoto et al., 2009). A study aimed to determine the different effects of Cu^{2+}, Fe^{2+}, Fe^{3+}, Zn^{2+} and Al^{3+} on the aggregation and toxicity of Aβ showed that metal binding to Aβ significantly altered the chemical properties of Aβ, and that Al^{3+} was found to induce one of the most irregular aggregation behaviour, leading to the formation of highly toxic amyloid fibrils (Bolognin et al., 2011). Aggregation caused by the presence of aluminium was greater compared to zinc, copper and iron (Kuroda and Kawahara, 1994). Aβ bound to Al^{3+} was revealed to show the largest radius of 30 nm for the resulting aggregates. Studies suggest trivalent metal ions such as Al^{3+} are significant to the formation of plaques, whereas Cu^{2+} and Zn^{2+} are deposited adventitiously (House et al., 2004; Exley, 2006). Along with the effect of Al^{3+} on Aβ aggregation the use of enzyme-linked immunosorbent assay (ELISA) indicated Al^{3+} was the only metal ion bound Aβ species which induced the production of excessive APP (Bolognin et al., 2011). Walton and Wang (2009)

demonstrated APP is upregulated *in vivo,* under Al^{3+} exposure in rat models. However, a contradicting study indicated that it did not increase the expression of APP compared to other AD related metal ions (Lin et al., 2008).

The trivalent aluminium ion has an effective radius of 0.51 Å (Aghav et al., 2011). As it has a positive charge, the aluminium ion will readily accept electron pair donors and function as a Lewis acid. The high charge and small ionic radius of Al^{3+} gives it a strong polarizing effect on the adjacent atoms and can be classified as a hard Lewis acid (McCafferty, 2003). It can form complexes of higher stability with ligands containing hard donor groups. As a hard Lewis acid it has an affinity for bases. Ligands with the most effective donor atoms possess a strongly basic negative charge. In complexes Al^{3+} prefers binding to oxygen atoms due to the smaller size however, nitrogen binding also occurs (Djurdjevic et al., 2005). A coordination numbers of four, five and six are most commonly reported for Al^{3+}, allowing the preferred geometry of tetrahedral and octahedral (Jennison et al., 1999; Streitz and Mintmire, 1999). Too many ligands coordinating to Al^{3+} would be less stable as a result of crowding a relatively small metal ion radius, however an insufficient amount of ligands would cause Al^{3+} into an unfavourable geometry (Urwin et al., 2016).

The interaction of Al^{3+} and Aβ is the major theme of this thesis. Although the coordination of Al^{3+} to Aβ is implicated in the pathogenesis of AD, the molecular details of aluminium binding with Aβ is lacking until the present. This thesis will aim to determine the coordination of Al^{3+} in Aβ and determine the binding affinity, as well as study the effect of Al^{3+} on the expression of APP gene.

1.10 Toxic metal exposure

Since the early 20th century the industrial production and emissions of toxic metals have dramatically increased. This enhances the risk of exposure to human beings. Two highly toxic metal ions which are associated to our aging population are discussed below.

1.10.1 Arsenic

Arsenic is naturally present in ground and drinking water, air and foods. Its mining and industrial usage leads to the increased contamination of water and crops. Rice, the staple food of Asia, often contains an elevated level of arsenic, due to pollution and its natural prevalence in ground waters originating from the river systems of the Himalayas (Sohn, 2014). The metalloid ion exists in multiple oxidation states, but mainly trivalent As^{3+} or pentavalent As^{5+}. Both As^{3+} and As^{5+} are toxic. Particularly, As^{3+} is becoming increasingly abundant in our environment. This study uses sodium arsenite ($NaAsO_2$), therefore, focusing on As^{3+}. In arsenic pathogenesis the reactive oxygen species-induced oxidative damage is a common characteristic, and arsenic also alters the integrity of mitochondria (Jomova et al., 2011). Chronic arsenic toxicity is a global environmental health problem affecting millions of people in the Unites States, Germany, Bangladesh and Taiwan. For example, an epidemiology study conducted by Lin et al (2013) evaluated the arsenic levels in drinking water and mortality of liver cancer in Taiwan, finding that within the analysed 20-year period, there were 1130 cases of liver cancer (802 males and 301 females). The study found that villages exposed to arsenic concentrations of 0.64 mg/L and above from the water supply, showed an increase in the liver cancer cases.

Furthermore, arsenic has also been linked to AD (Gong and O'Bryant, 2010). Arsenic toxicity induces hyperphosphorylation of protein Tau and up-regulated transcription of the amyloid

precursor protein (APP), which are involved in the formation of neurofibrillary tangles and brain amyloid plaques (Dewji et al., 1995; Giasson et al., 2002). Compared to the research intensity on the other metals such as Cu^{2+}, Zn^{2+} and Al^{3+}, there is a limited amount of data about the effect of Ar^{3+} on neurons and Aβ aggregation. Anyhow, the association of Ar^{3+} with AD may have illustrated at least one aspect of AD, that is, there are many factors involved in AD development in humans. If the ligands used in this study could coordinate strongly to Ar^{3+}, the therapeutic aspect of the ligand would be quite useful in ameliorating arsenic toxicity and its related health problems.

1.10.2 Chromium

Chromium is the sixth most abundant element in the earth's crust (De Flora, 2000). The benefits of chromium have been exploited in many areas such as leather tanning, electroplating, stainless steel production and clinical orthopaedics. It is predominantly found in the stable trivalent state or Cr^{3+} form, and the strong oxidizing hexavalent state (VI) or Cr^{6+} form (Barceloux, 1999). The hexavalent Cr^{6+} ion is highly toxic and has carcinogenesis effects in humans (Zhitkovich, 2011). The Birmingham hip resurfacing arthroplasty resulted in the significant increase in serum chromium levels (Weinstock, 1995). The body is able to reduce Cr^{6+} to Cr^{3+}, which is imperative as Cr^{3+} is essential in the metabolism of cholesterol, fat and glucose, with required concentrations of 50 to 200 µg/day (Jones, 1990). However higher concentrations of Cr^{6+} can lower the body's reduction capability, consequently the hexavalent ions will accumulate and damage DNA (Jones, 1990; Nigam et al., 2014). Research has shown presence of Cr^{6+} increase the development of DNA adducts, DNA-protein cross links, breaking of DNA strands, the aberrations and instability of chromosomes (Hu et al., 2011). Nigam et al. (2014) found that a large group of genes had a significant dysregulation of expression from exposure to Cr^{6+}. Thus, chromium homeostasis is

critical to health, either excess amount or deficiency can adversely affect human's health. So far, there is no evidence of chromium's involvement in Aβ aggregation. However, if the ligands in my study prevent Cr^{6+} toxicity, the therapeutic aspect of the ligand would address various metal related health problems.

In summary, mounting evidence demonstrates the role of metal ions in human metabolism and diseases. In recent years, a new view has emerged, which focuses on a more general picture of metal ion homeostasis (White et al., 2006; Singh et al., 2013). This view details interaction of metal ions with Aβ as just a part of the overall metal homeostasis process. This new thinking is in fact an extension of the metals hypothesis of AD, again accentuating the possible role of metals in Aβ aggregation and oxidation.

1.11 Alzheimer's disease therapeutic rational

The multifactorial nature of AD demonstrated by several pathological factors from, oxidation, inflammatory response, disruption of metal ion homeostasis, thought as the both the triggers and subsequent events of Aβ aggregation (Mantyh et al., 1993; Hou et al., 2004; Huang et al., 2004; Kurganov et al., 2004; Boyd-Kimball et al., 2005; Hung et al., 2008; Bolognin et al., 2011; Meisl et al., 2016). This in turn supports the development of multifunctional therapeutic compounds in association to AD. Drug development for AD primarily focuses on Tau based and amyloid based strategies (Kepp, 2012). Considering the multiple factors are involved in the pathogenesis of AD, drugs targeting single causes are inefficient to prevent the progression of the neurodegeneration. The crucial role metal ions play in multiple pathways of AD supports that metal chelation therapy is a significant therapeutic approach. An effective drug for AD should have more than one or two of the

following properties, restrict ROS production, metal chelating ability, high cellular uptake, ability to cross the BBB, antioxidant capabilities, reduce Aβ aggregation or inhibit Aβ production. However, designing metal chelators with selective and specific properties is highly challenging. As in the case of lipophilic metal chelator clioquinol (5-chloro-7-iodo-8-hydroxyquinoline, CQ), it significantly lowered amyloid plaques, resulting in improved cognitive behaviour in phase II clinical trials. However long term use of CQ, resulted in subacute myelo-optic neuropathy (SMON) (Cahoon, 2009 ; Mancino et al., 2009). CQ did demonstrate a close association between metal dyshomeostasis and the onset and/or progression of AD, although the underlying biochemical mechanisms for some conditions remain unclear. Nevertheless, there is a beneficial aspect for BBB penetrable antioxidant and metal-chelating compounds (DeWeerdt, 2011).

1.12 Metal chelation therapy

Chelation therapy is increasingly acknowledged as a worthwhile strategy for decreasing the abnormal accumulation of the metals such as copper, iron and zinc, as well as nonessential and toxic metals such as aluminium, cadmium, lead, mercury, chromium and arsenic (Yokel et al., 1996; Andersen, 2004). Chelation therapy becomes an alternative treatment for AD albeit still controversial, in spite of the undesirable clinical results of the chelators such as CQ and EDTA (Bush and Masters, 2001; Treiber et al., 2004; Hegde et al., 2009).

The underlying mechanism for metal chelation therapy is that coordination of chelating agent to a metal ion results in the formation of a stable complex, thus preventing the metal ion from interacting with other biological molecules such as Aβ. Developing an effective therapeutic chelating agent requires desirable physical and chemical characteristics such as high affinity for

the toxic metal, bioavailability, ability to penetrate cell membrane, high solubility, rapid elimination of metal ions, natural metabolism and excretion (Andersen, 2004).

Many chelating compounds are found in natural products or well-known drugs for other purposes (Park, 2010; B Pocernich et al., 2011). This natural metal chelators approach could be adapted to AD therapies, due to the multifunction capabilities. As shown in Figure 1.6 a natural multifunctional metal chelator (MMC) could address all pathogenic factors of the amyloid cascade, metal ion and oxidative stress hypothesis previously illustrated in Figure 1.3. In addition to being antioxidant and metal-chelating, those compounds should also be capable of crossing the BBB and must be of reasonable small molecular weight. The panel of ligands I have used were selected for their known metal sequestering properties, namely, histidine, glutathione (GSH), maltol, citric acid and malic acid. These ligands are naturally occurring, easily metabolised and not toxic to humans. By screening of these potential ligands, desirable metal ligands can be discovered. The following section will discuss the selected ligands as chelating compounds.

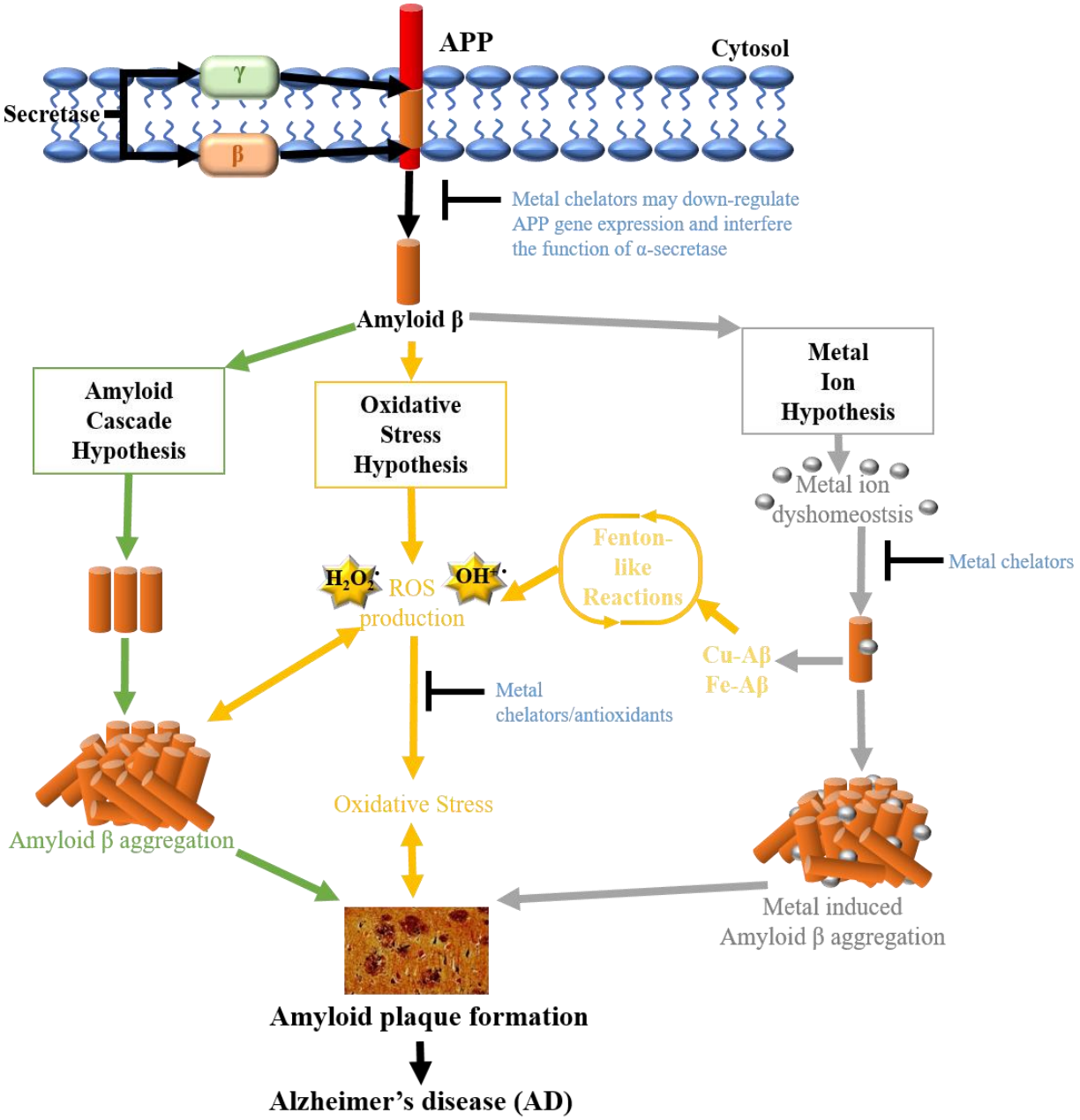

Figure 1.6 Proposed therapeutic intervention by multifunctional metal chelators on Aβ aggregation. The multifunctional metal chelators (MMC) can lower the function of β-secretase by preventing metal ions from binding to APP at the α-secretase cleavage site, therefore allowing the formation of sAPPα, which is nontoxic. MMC can prevent the over-production of APP and hence reducing Aβ accumulation in the amyloid cascade hypothesis. Certain MMC have antioxidant capabilities which can reduce oxidative stress and scavenge ROS in the oxidative stress hypothesis. Excess metal ions, from the metal ion hypothesis, can be removed by MMC before their interactions with Aβ, preventing the formation of ROS and Aβ aggregation. Image sourced from Tschanz, 2011.

1.13 Chelating ligands

1.13.1 Histidine

Among the 20 naturally occurring amino acids, histidine (Figure 1.7) is the most active and versatile member that plays the multiple roles in protein interactions, often the key residue in enzyme catalytic reactions. This in turn accentuates the significance of histidine for Aβ which contains three histidine residues in its N-terminus. It is, in this regard, an almost perfect metal binding peptide. A vast body of literature demonstrates that the metal coordinating role of histidine is of no surprise (Van Campen and Gross, 1969; Djurdjevic et al., 2001; Arispe et al., 2008; Shin and Saxena, 2008; Nair et al., 2010; Matsui et al., 2017). The imidazole side chain of histidine, shown in Figure 1.7, is a common coordinating site in metalloproteins and is a part of catalytic sites in many enzymes (Strange et al., 1987; Housecroft and Sharpe, 2008). The coordination role of histidine has also been applied in genetic engineering for protein expression and purification. Polyhistidine tag is widely used in design of gene constructs, so that the expressed proteins can be easily purified via nickel (Ni^{2+}) affinity chromatography (Hochuli et al., 1988).

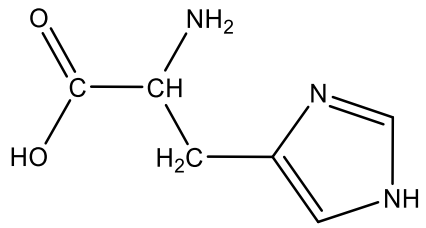

Figure 1.7 Structure of histidine.

Unlike the histidine residues in Aβ, as a free amino acid, histidine has four potential coordination sites, through the carboxylate group, the amino group, and the two nitrogens of

the imidazole. This study explores the role of histidine as a chelating ligand. Histidine may be able to form metal-ligand complexes with some of the metals of interest. This study will determine the binding affinity of histidine and metal ions, in comparison to the other ligands. The relative binding affinities of the ligands could determine the best coordinating ligands and can lead to future therapeutic agents. Smaller ligands like histidine have less steric hindrance, hence would readily bind to metal ions, prevent their accumulation and the subsequent aggregation of Aβ.

1.13.2 Glutathione

GSH is a tripeptide (Figure 1.8) and is a prevalent endogenous antioxidant in the cell. GSH plays a fundamental role in detoxification of ROS and nucleophilic compounds, thus regulating the intracellular redox environment (Dringen, 2000). The concentration of GSH is decreased with age and in diseases with oxidative stress including AD (Liu and Choi, 2000). Neuronal cells are also protected against Aβ42 induced protein oxidation with the upregulation of GSH (Boyd-Kimball et al., 2005), and GSH was found to provide protection against $A\beta_{42}$ induced apoptosis in cortical neurons (Medina et al., 2002; Barber and Griffiths, 2003). Hence GSH has potential as a therapeutic strategy in AD treatment.

In regards to the characteristic metal dyshomeostasis observed in AD, GSH is also one of the most versatile metal binding ligand, playing an essential role in metal storage, transport and metabolism (Hammond et al., 2001). The metal-related functions of GSH include the mobilization and delivery of metals to ligands, the cross transport of metal along cell membranes and finally, a cofactor in redox reactions involving metals (Ballatori et al., 2009).

GSH is a tripeptide made up of three amino acid residues, namely glutamate, cysteine and glycine.

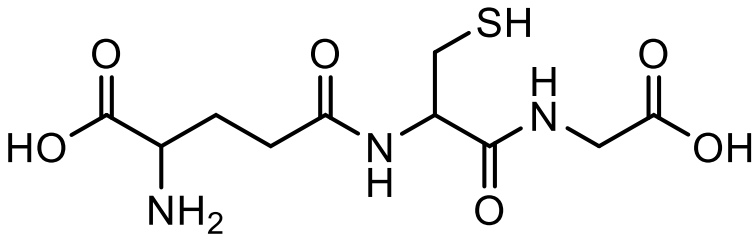

Figure 1.8 Structure of glutathione

GSH is a multidentate ligand, with the presence of eight potential metal binding sites, though simultaneously coordinated to a single metal ion is not possible. Hence the coordination chemistry of GSH to metals allow the formation of polynuclear complexes (Krezel and Bal, 1999). The eight donor atom of GSH are classed as the amine donors, carboxylate donors, the thiol group and the peptide bonds. Due to the variety of donor atom types it is of no surprise that GSH is a versatile metal binding ligand. GSH has a high affinity for metals forming thermodynamically stable complexes with numerous metals including Cr^{6+}, Mn^{2+}, Fe^{2+}, Co^{2+}, Au^{+}, Ag^{+}, Pb^{2+}, Ni^{2+}, Cu^{2+}, Zn^{2+}, Cd^{2+} and Hg^{2+} (Krężel and Bal, 1999; Wang et al., 2009; Liu et al., 2014; Ngamchuea et al., 2016). Hence this thesis will determine the molecular details of GSH in metal ion coordination, and its binding affinity with metal ions, in comparison to the other ligands. The comparison of GSH, an established metal chelator, to the other ligands could aid the determination of the strongest metal coordinating ligands. Multifunctional ligands such as GSH would readily coordinate metal ions and reduce the formation of reactive oxygen species.

1.13.3 Maltol

The study of 3-hydroxy-2-methyl-4H-pyran-4-one or maltol (Figure 1.9) in this thesis stems from its ability to bind readily to metal ions. Maltol belongs to a family of hydroxypyrones, and it is a naturally occurring organic compound, often used primarily as a flavour enhancer (Liboiron et al., 2005). It is present in roasted malt (from which it gets its eponymous name). Humans have increased consumptions of malt foods. The maltol-metal complex, gallium maltolate, is an anticancer drug which is orally bioavailable (Bernstein et al., 2000; Chua et al., 2006). Maltol is known to form extremely stable and neutrally charged complexes with a variety of metal ions, including the trivalent cations Fe^{3+}, Al^{3+}, Ga^{3+}, and In^{3+} (Santos et al., 2005). Maltol has been found to increase the transport of Al^{3+} (Langui et al., 1990; Liboiron et al., 2005). It can act as a strong bidentate ligand, coordinating through the carbonyl group and the α-OH group as seen in Figure 1.9.

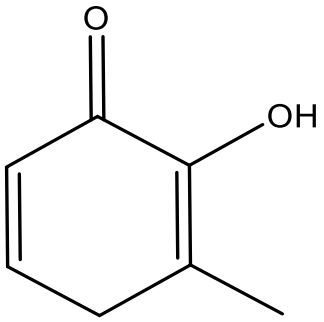

Figure 1.9 Structure of maltol

Interestingly, the study conducted by Antipova et al. (2005) on the structure and stability of maltol–Al^{3+} complexes found maltol to be a suitable chelate ligand. With the $AlMal_3$ complexes being electrically neutral, water soluble and relatively stable at the pH 4-8, the study concluded it fulfilled the requirements of a substance aimed to remove excess Al^{3+} ions within humans (Antipova et al., 2005). The potential of maltol being a therapeutic ligand is explored in this thesis for its ability to coordinate and form stable complexes with a range of metal ions. Maltol

is a strong metal chelating ligand with little to no antioxidant ability. Hence the comparison of maltol to multifunctional ligands (GSH and histidine) would be worthwhile.

1.13.4 Citric acid

Citric acid (2-hydroxy-1,2,3-propanetricarboxylic acid, Figure 1.10) plays a crucial role in the Krebs cycle, hence has a great biological significance and many roles in the human body, one of which is the ability of its conjugate base, citrate, to chelate metals (Silva et al., 2009). Due to this ability to form thermodynamically stable complexes with a variety of metal ions, it has found widespread use in food and pharmaceutical industries as well as in medicine (Wyrzykowski and Chmurzyński, 2010). The capability of citrate coordinating to Fe^{2+} has long been used by plants and microbes. For example, iron deficient *Bradyrhizobium japonicum* are known to secrete citric acid in order to enhance iron-absorption (Guerinot et al., 1990). The study carried out by Silva et al. (2009) on Fe^{3+} citrate speciation in aqueous solutions used spectrophotometric titration to determine the affinity constant for iron and citrate. The study found the following complexes were formed M_2L_2 - $[Fe_2(CA)_2]^{2-}$, M_3L_3 - $[Fe_3(CA)_3]^{3-}$, ML_2 - $[Fe\ (CA)_3]^{5-}$, MLH - [Fe (HCA)] (Silva et al., 2009), where M denotes metal, L denotes ligand.

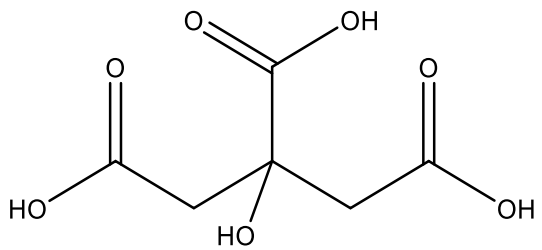

Figure 1.10 Structure of citric acid

The study by Silva et al. (2009) describes citric acid as a multidentate ligand. The structure of citric acid (Figure 1.10) corresponds to an asymmetric ligand, containing at least seven potential

donor sites capable of metal ion coordination such as an α-position hydroxyl group, one α-position carboxyl group and two β-position carboxyl groups. Citric acid can assemble metal ions in diverse arrangements as both chelator and bridging spacer. Therefore, citric acid is a very appealing chelator, as monomeric, binuclear and polymeric metal complexes. Hence citric acid is explored for its metal chelating potential in this study.

1.13.5 Malic acid

Malic acid (Figure 1.11) is a dicarboxylic acid. This organic acid is present in living organisms. It is non-toxic and used as a food additive. To reduce Al^{3+} toxicity, plants would release organic acids such as malic acid, citric acid and oxalic acid, from the root's apex to stop Al^{3+} from entering the cell. The ability of malic acid to chelate metal ions has been previously investigated (Ma, 2000). The internal detoxification of Al^{3+} was accomplished by the formation of an Al^{3+}-malic acid complex (Ma, 2000). While malic acid cannot directly prevent the formation of reactive oxygen species, it is capable of detoxifying redox metals Cu^{2+} and Fe^{3+} (Salovaara et al., 2002; Brajenović and Tonković, 2003; Radalla, 2015).

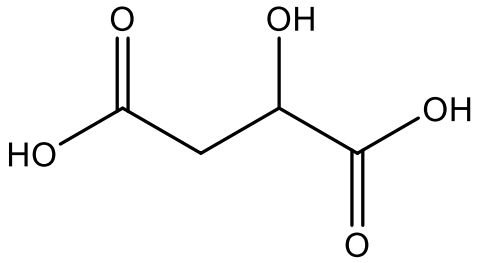

Figure 1.11 Structure of malic acid

The five oxygen donor atoms of malic acid seen in Figure 1.11 allows the acid to act as a multidentate metal ligand. Despite the predominately acidic donor atoms of malic acid, it has been found to coordinate to various metals including Ce^{3+}, W^{6+}, Pr^{3+}, Nd^{2+}, Cu^{2+}, Ni^{2+}, Co^{2+} and

Zn^{2+}, Sm^{3+}, Al^{3+}, Ca^{2+}, U^{6+} and In^{3+} (Markovits et al., 1972; Delhaize et al., 1993; Senthil Raja et al., 2013; Radalla, 2015). The metal chelating potential of malic acid is explored in this study.

1.14 Nuclear Magnetic Resonance (NMR) spectroscopy

1.14.1 Structural studies employing NMR spectroscopy

Nuclear Magnetic Resonance (NMR) spectroscopy is used in the determination of structure and interactions between both Aβ peptide and ligands with metal ions at the molecular level. NMR is used to study the resonance frequency that results from the interaction of magnetic field with nuclei that posse magnetic dipole, such as ^{1}H, ^{2}H, ^{13}C, ^{14}C, ^{15}N, ^{17}O, ^{19}F, and ^{31}P. In the determination of protein/peptide's secondary and tertiary structures, NMR spectroscopy is an important technique. The advantage of NMR compared to other techniques in structural biology and chemistry is its ability to analyse the samples in physiological conditions and is non-destructive. This section will outline the general theory and principles of NMR spectroscopy.

1.14.2 General NMR theory

NMR is based on the interactions between the magnetic moments of atomic nuclei and magnetic fields which can yield structural information. The subatomic particles such as electrons, protons and neutrons have four basic properties which include mass, charge, magnetism and spin. As measuring nuclear magnetism and spin have basically no effect on a substance's physical and chemical behaviours, these properties can therefore be used to determine a compound's structure without chemical composition disturbance. The nucleus has spin angular momentum, and may be considered as spinning about an axis, which is important in yielding NMR signals. Individual unpaired electrons, protons and neutrons have a positive or negative spin of

magnitude 1/2, hence as a result the nucleus has a magnetic moment and generates its own magnetic field. Therefore, a sample that contains atomic nuclei with spin, has a magnetic field. When an external magnetic field (B_0) is applied to the sample, the magnetic moments on the spins are either aligned with or against the magnetic field. Hence two spin states exist, the lower-energy, α spin state (+1/2) or higher-energy, β spin state (-1/2). The energy difference (ΔE) between the two spin states depends on the strength of B_0.

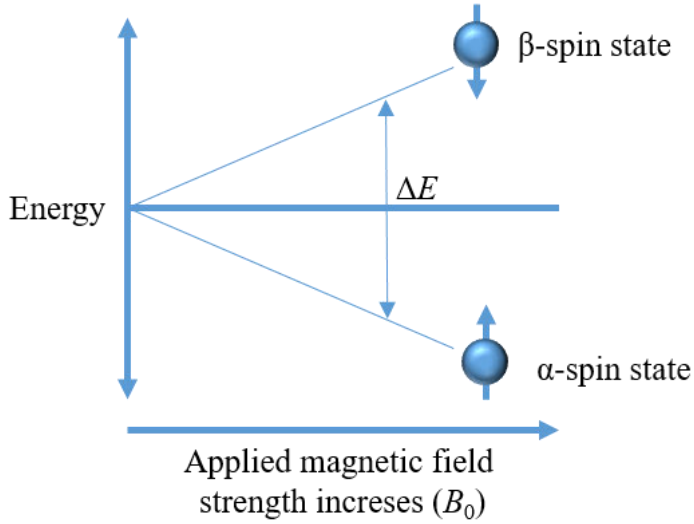

Figure 1.12 Energy levels for a nucleus with spin. In the presence of an applied magnetic field, the magnetic moments of the nuclei line up with or against the field.

Net magnetisation (M) is produced by the alignment of the spins with the B_0. During NMR experiments, short radio frequency (RF) pulses are applied, which excite all proton simultaneously and flip the direction of the nuclear spin alignment. This allows protons to absorb energy at a specific frequency known as Larmor frequency. Relaxation occurs when the atomic nuclei return to the original state, which generates induced magnetic signals. The RF signals recorded by receiver coils, are referred to as free induction decay (FID). The FID is mathematically processed by Fourier transformation which converts the signal into frequency domain signal projected as an NMR spectrum. The resulting resonance signal are specific to

the proton or ^{1}H (hydrogen atom isotope), present in the molecules. As different protons in a peptide or molecule will have different chemical and magnetic environment, structural information from each proton can be extracted by NMR indirectly from the position of signals. Hence the ability to assign groups of resonances to a specific proton type within a protein. This includes the backbone ^{1}H, side chain amide ^{1}H, aromatic side chain ^{1}H, aliphatic side chain ^{1}H and αH in regions of β sheet structures (Reid et al., 1997). The NMR spectroscopy described thus far is known as one dimensional (1D) NMR spectroscopy. The technique is valuable in the analysis of small molecules. 1D NMR experiments can provide different kinds of information about a protein or peptide, which can be performed in physiological condition, allowing the structural configurations to be similar as those present *in vivo*.

1.14.3 Two-dimensional NMR spectroscopy

Larger molecules such as peptides and proteins contain numerous magnetically non-equivalent nuclei, resulting in signal overlap. Hence the extension of 1D NMR into multiple dimensions is essential in the study of peptides. Two-dimension (2D) NMR spectroscopy plots the signal intensity of a 1D NMR along two frequency axes. Consequently, the peak in a 2D NMR spectra has an intensity and two frequency co-ordinates (Rubin, 2017). The homonuclear 2D NMR methods utilised in this thesis transfer magnetization between the same nuclei connected by bonds or through space.

1.14.4 Correlated Spectroscopy (COSY)

Correlated spectroscopy (COSY) yields signals from homonuclear through bond interactions (*J*-coupling). The bond connectivity of a molecule is determined through protons that are *J*-coupled by two or three bonds (Arseniev et al., 1982). Simple COSY experiments, consists of 90° pulses, involves an initial RF pulse (p1), an evolution time (t_1), followed by the second RF pulse (p2), and then measurement time (t_2). The initial RF pulse results in the magnetisation of the transverse plane which evolves over the time interval of t_1. During the second RF pulse transfer magnetisation from one proton to the other proton. A COSY spectrum has two types of peaks, cross peaks and diagonal peaks. A COSY peak occurs at a frequency $\omega 1 = \Omega A$, $\omega 2 = \Omega B$ which indicates the spin at the offset chemical shift (ΩA) is coupled to another spin at offset chemical shift (ΩB) (Keeler, 2005). COSY is a standard experiment for the analysis of scalar spin-spin through bond coupling connectivities. This method provides information for the identification of chemical shifts of spins that are coupled to one another, hence allowing determination of the *J*-coupling network in the molecule.

1.14.5 Total Correlation Spectroscopy (TOSCY)

Total correlated spectroscopy (TOSCY) is another form of homonuclear ^{1}H 2D-correlation NMR method, in which two ^{1}H coupled spins indicate the existence of a cross-peak multiplet. TOCSY spectra provide correlations between all the protons of a coupled spin system or network. For TOCSY, the quintessential period is during the pulse sequence (mixing period) in which only scalar coupling is acting while the chemical shift is suppressed. During the mixing period, there is magnetisation exchange among *J*-coupling networks (Keeler, 2005). TOCSY is a useful method for the identification of coupled spins which belong to a network of spins, which is essential for overlapping spectra of a complex which would otherwise have

unambiguous spectra. These features are essential in the assignment of proton signals in a protein spectrum. TOCSY experiments are applicable to peptide studies as correlation cross peaks allows the identification of protons belonging to individual amino acid residues (Reid et al., 1997).

1.14.6 Nuclear Overhauser Effect Spectroscopy (NOESY)

Nuclear Overhauser Effect SpectroscopY (NOESY) method identifies the spins undergoing cross relaxation and measures the cross relaxation rates. The NOESY results from direct dipolar couplings providing means of cross-relaxation, and only spins close to one another in space will undergo cross-relaxation (Wüthrich, 1986). In NOESY, experiments identify the Nuclear Overhauser Effects (NOEs) within a molecule, which enables the identification of protons within close proximity in space (Neuhaus and Williamson, 1989). NOESY experiments the pulse sequence involve three 90° RF pulses. The initial pulse results in the magnetization into the x-y plane which precesses in the evolution time t_1. The following pulse rotates this magnetisation to the z axis which allows dipolar coupling with other spins during the subsequent mixing period. The third and final pulse forms a transverse magnetization from the remaining longitudinal magnetization. Following the third pulse, acquisition begins, and the transverse magnetization is expressed as a function of the time t_2. NOESY spectra consist of cross peaks generated from the transverse magnetization. The non-equilibrium z component magnetisation is exchanged between the spin systems within close proximity via intra- or intermolecular dipolar relaxation during the mixing period (Wüthrich, 1986). NOESY is used in the sequential assignment of resonances and determination of the three dimensional structure investigation of peptides and proteins.

1.14.7 NMR assignments in peptides

NMR provides essential structural data of peptide in solution. NMR assignments of the proton resonances are determined from 2D NMR experiments (Wüthrich, 1986). The signals from individual spin system are correlated to other spins through bond (*J*-coupling) or space (dipolar coupling) thus allowing the signal of every amino acid residue to be assigned. The identification of the amino acids in a sequence is performed by sequence-specific assignment method. Signals of individual spin systems are assigned through TOCSY experiments which provide through bond correlations of the resonances in same spin systems. Therefore, the cross-sections of the TOCSY spectra of Aβ peptide will illustrate cross-peaks from the NH to αH, βH, γH, δH, and aroH (if appropriate). The spin systems resonances are reference to published chemical shifts of random coil (Wüthrich, 1986; Reid et al., 1997).

Identifying the position of the amino acids in the sequence is conducted by NOESY experiments which identify the protons of neighbouring amino acids that are close in proximity through space. Sequential distances are the distance between protons of two adjacent amino acids. In sequential NMR assignment, a spin system of amino acid residue starts with the proton of the backbone nitrogen (NH), followed by the proton on the α-carbon (αH) and then the side chain (βH, γH, δH, aroH, etc.). The typical chemical shifts proton in random coil peptides and proteins are shown in Table 1.2.

Table 1.2 ^{1}H Chemical shifts of amino acid residues of random coil peptides and proteins.

Residue	NH	αH	βH	other
Ala	8.25	4.35	1.40	
Arg	8.27	4.40	1.80, 1.92	γH 1.72; δH 3.31
Asn	8.75	4.76	2.76, 2.83	
Asp	8.41	4.77	2.75, 2.84	
Cys	8.31	4.69	2.96, 3.28	
Gln	3.41	4.37	2.01, 2.13	γH 2.38
Gly	8.39	3.96		
His	8.41	4.63	3.20, 3.26	4H 7.14; 2H 8.12
Ile	8.19	4.22	1.86	γH 1.19, 1.48, 0.94
Leu	8.42	4.39	1.65	γH 1.65; δH 0.94, 0.90
Lys	8.41	4.36	1.75, 1.87	γH 1.47; δH 1.71; εH 3.02
Met	8.42	4.51	2.00, 2.16	γH 2.63; εH 2.13
Phe	8.23	4.66	2.99, 3.22	aroH 7.34
Pro		4.71	1.98, 2.30	γH 2.30; δH 3.65
Ser	8.38	4.5	3.89	
Thr	8.24	4.35	4.22	γH 1.23
Trp	8.09	4.71	3.20, 3.22	2H 7.24; 4H 7.17, 7.65; 6H 7.24; 7H 7.50
Tyr	8.18	4.6	2.92, 3.13	aroH 7.15, 6.86
Val	8.44	4.18	2.13	γH 0.94, 0.97

Adapted from Wüthrich (1986) and Reid et al. (1997) residues are non-terminal.

A sequence specific assignment of a peptide is achieved by correlating proton in one residue to proton in the next residue in the sequence using NOE interactions. Hence it is estimated that the NOE correlation between αH of the N-terminal residue (i) and the NH of the next residue (i + 1), and occasionally from the Hβ of residue i and the NH of residue i+1 (Jacobsen, 2007).

1.15 Experimental approach

This study utilises the analytical techniques of NMR spectroscopy in acquisition of molecular details of the interactions between metal ions and Aβ peptide. The use of NMR titrations provides information on the interaction of various ligands and metal ions, particularly the stoichiometric ratio, coordination sites and binding affinity. NMR titration of Aβ with metal ions reveals the residues involved in metal coordination. Whilst such titration reveals the effect of metal ions on the primary structure of Aβ, the effect of metal ions on the secondary structure of Aβ will be unravelled by the chemical shift index (CSI). K_D values were obtained from chemical shifts variations ($\Delta\delta$) in the titration of Al^{3+} and Zn^{2+}. K_D values determined which metal ion has the strongest binding affinity to the peptide. Furthermore, with the NMR titration of ligands with metal ions, their potential in metal chelation will be explored, which should aid future development of therapeutic agents for AD treatment. Molecular mechanics was used to determine the relative strength and stability of the metal ligand complexes. Following the NMR analysis for molecular details of metal coordination of Aβ and the metal chelation of ligands, a biological study was carried out using MTT cell viability assays on SH-SY5Y neuronal cells to establish the capacity of the ligands in reducing metal toxicity. The effect of the ligands was also tested against the toxic metal ions, As^{3+} and Cr^{6+}, which are not related to AD. This would expand the therapeutic potential to toxic metal exposure. Finally, the effect of metal ions on the expression of APP gene in the human neuronal cells and the antagonistic effect of the chelation ligands against the metal ions was investigated by quantitative reverse transcription polymerase chain reaction (qRT-PCR).

1.16 Aims

1. To characterise the interactions between metal ions and Aβ by NMR.
2. To determine specific aluminium binding sites in $A\beta_{1-28}$.
3. To analyse the interactions between metal ions and a repertoire of ligands, with NMR analysis and molecular mechanics.
4. To uncover if the chelating ligands can reduce metal toxicity in mammalian neuronal cells using MTT assay.
5. To uncover the effect of metal ions on the expression of amyloid precursor protein (APP) gene and the effect of ligands against metal ions by qRT-PCR.

2 MATERIALS AND METHODS

2.1 General materials, reagents and treatments

The required general materials were purchased from Sigma Aldrich, Sydney, Australia. All the specific chemicals and solvents used were of analytical grade or higher, obtained from commercial suppliers. The MilliQ^{TM} system (Millipore, Australia) was the source of filtered and deionised water, which was used to prepare all stock solutions, media and buffers.

2.1.1 Metal solutions

All metal stocks solutions and treatments were made using zinc(II) nitrate hexahydrate (reagent grade, 98%), copper(II) chloride dihydrate (ACS reagent, ≥99.0%), aluminium(III) chloride hexahydrate (*ReagentPlus*®, 99%), sodium (meta)arsenite (≥90%) or chromium(VI) oxide (ACS reagent, ≥98.0%).

2.1.2 Ligand solutions

All ligand stock solutions and treatments were made using maltol (analytical standard), L-glutathione (reduced, ≥98.0%), L-histidine (*ReagentPlus*®, ≥99%; TLC), citric acid anhydrous (ACS reagent, ≥99.5%), DL-malic acid (*ReagentPlus*®, ≥99%).

2.1.3 Phosphate buffer

The 90% H_2O:10% D_2O 10 mM stock solution of the phosphate buffer was prepared by dissolving the monobasic $NaH_2PO_4.H_2O$ (0.0780 g) and the dibasic $Na_2HPO_4.7H_2O$ (0.5188 g) in 225 mL Milli Q water and 25 mL D_2O. The pH of the buffer solution was adjusted to 7.45 ± 0.01 by titrating with concentrated hydrochloric acid solution. The pH of the solutions was measured using an Accumet excel XL15 pH meter.

2.1.4 Synthesis of pyridoxal amino methyl phosphonic acid (PYRAMPA)

A solution of (2.46 mmoles) 500 mg of pyridoxal hydrochloride salt in methanol was added dropwise to a solution of (2.46 mmoles) 273 mg of aminomethylphosphonic acid (AMPA). The reaction mixture was basified with the addition of (6.90 mmoles) 385 mg solid KOH. The characteristic deep orange-yellow colour of the Schiff base was observed. Methanol was removed under vacuum. Leaving the microcrystalline material of the tripotassium salt of the Schiff base behind. The base was reduced in 25 mL of dry methanol and the addition of 2 equivalents of solid (2.1 mmoles) 81 mg sodium borohydride. Reduced material was concentrated by pumping off most of the methanol under vacuum. The mixture was acidified with the addition of minimum amount of 6.0 M HCl. The white precipitate was recovered by gravity filtration. After 48 hr the filtrate was transferred from room temperature to -4 °C for a further 48 hr for the crystallization of PYRAMPA. Yields of 83% of the theoretical, 0.68 g of product, was obtained. Melting point 263 ± 2 °C.

2.1.5 Synthesis of metal-maltol complexes

Synthesis of each metal complex involved dissolving 3.15 g (0.025 mol) of maltol and 2.5 g (0.01 mol) of $Zn(NO_3)_2.6H_2O$; 3.78 g (0.03 mol) of maltol and 2.71 g (0.01 mol) of $AlCl_3.6H_2O$; 3.15 g (0.025 mol) of maltol and 2.50 g (0.01 mol) of $CuCl_2.2H_2O$ in 160 mL in Milli Q water. Mild heating was used to assist dissolution. Once the maltol was fully dissolved the pH was adjusted to pH 8.3. The solution was further heated to 65 °C with gentle stirring to produce precipitate. When the reaction mixture was cooled and filtered, washed several times with acetone and dried overnight in a vacuum desiccator.

2.2 Peptide synthesis and purification

Peptides representing various fragments and analogues of Aβ were synthesised by employing solid phase Fmoc chemistry and produced by Auspep in Tullamarine, Victoria. After removal from the resin and deprotection, the samples were purified using reverse phase high performance liquid chromatography (HPLC) and characterised using mass spectrometry (MS), for the purity of synthesised Aβ and Aβ analogues see Appendix A. Synthesised peptides were supplied lyophilised and stored in the freezer at –40 °C or –80 °C.

2.2.1 Design of peptides and peptide sequences

Peptides were synthesised according to the human sequence of Aβ in which the N-terminus were left as a free native amino group and C-terminus was truncated to $A\beta_{1\text{-}28}$ fragments. Together with the wild-type $A\beta_{1\text{-}28}$ peptide, three analogues of $A\beta_{1\text{-}28}$ were synthesised in which His6, His13 or His14 residues were individually replaced by alanine and one analogue in which the all three histidine residues (His6, His13 and His14) were all replaced by alanine. Sequences are given Table 2.1 below:

Table 2.1. Design of peptides used this in this study

Peptide	Sequence
$A\beta_{1\text{-}28}$	DAEFR**H**DSGYEV**HH**QKLVFFAEDVGSNK
Aβ H6A	DAEFR**A**DSGYEV**HH**QKLVFFAEDVGSNK
Aβ H13A	DAEFR**H**DSGYEV**A**HQKLVFFAEDVGSNK
Aβ H14A	DAEFR**H**DSGYEV**H**AQKLVFFAEDVGSNK
Aβ H6,13,14A	DAEFR**A**DSGYEV**AA**QKLVFFAEDVGSNK

2.3 Procedures for NMR acquisition and analysis

NMR experiments were performed on either a Bruker Avance 400 MHz (9.4 T) NMR spectrometer equipped with a BBFO probe or the Bruker Avance III 600 MHz (14.1 T) NMR spectrometer equipped with a BBI probe. 1D and 2D NMR spectra were collected at 298 K. Water suppression was achieved using WATER-suppression by GrAdient-Tailored Excitation (WATERGATE) sequence, with "W5" binomial rf pulses.

2.3.1 1D NMR experiments

All 1D ^{1}H experiments were recorded with 128 scans, 4 dummy scans, a spectral width of 12 ppm, and an acquisition time of 1.70 s. Prior to Fourier transformation, the measured FIDs were zero-filled and then multiplied with an exponential window function with a 0.3 Hz line broadening.

2.3.2 2D total correlation spectroscopy (TOCSY) experiments

TOCSY experiment employed a DIPSI2 sequence for isotropic mixing, with a mixing time of 75 ms. The spectra were collected with 256 x 1024 data points. The number of transients collected for each FID were 16, and the FIDs were zero-filled to 1024 points in F1 dimension and to 4096 data points in F_2 dimension before Fourier transformation.

2.3.3 2D Nuclear Overhauser Effect Spectroscopy (NOESY) experiments

The NOESY experiments were acquired with two different mixing times, 250 and 600 ms. Data were zero filled to 2048 points in both F_1 and F_2 without linear prediction and then Fourier transformed with a sine-bell-squared window function shifted between 90° and 45°. A polynomial baseline correction was applied to both sides of the residual water signal.

2.4 NMR titration of $A\beta_{1-28}$ against metal ions

Samples were prepared for NMR measurements by dissolving the freeze dried peptide in 600 µL of 90% H_2O:10%D_2O phosphate buffer. A concentration of $A\beta_{1-28}$ of 1.0 mM was used, the peptide concentrations were confirmed using the extinction coefficient (Gill and Von Hippel, 1989) of 1280 M^{-1} cm^{-1} (due to the single tyrosine residue). Then transferred to 5 mm Norell® NMR tube.

The addition of metal ions to the Aβ peptides was performed using small aliquots from highly concentrated stock Al^{3+} and Zn^{2+} solutions, as indicated in Table 2.2 so that the resulting solutions had M^{n+}/Aβ mole ratio varying from 0:1 to 4:1.

Table 2.2 sample preparation for NMR titrations of metals to Aβ.

Al^{3+}:Aβ	[Aβ] (mM)	Aβ (µL)	[M^{n+}] Stock (mM)	Volume of M^{n+} stock (µL)
0.00	1	600	0	0.0
0.10	1	600	0.1	1.2
0.20	1	600	0.2	2.4
0.30	1	600	0.3	3.6
0.50	1	600	0.5	6.0
1.00	1	600	1.0	9.0
2.00	1	600	2.0	12.0
4.00	1	600	4.0	24.0

The pH of experiments was pH 7.4 to recreate physiological conditions as much as possible. The pH of the samples was determined before and after each of the experiment were carried out. The pH was measured (Accumet excel XL15 pH benchtop meter) and adjusted using small amounts of 10-100 mM NaOH or HCl.

2.5 2D NMR titration of $A\beta_{1-28}$ against metal ions

Samples for the NOESY and TOCSY NMR experiments were prepared by dissolving the freeze dried peptide to give a concentration of approximately 1.0 mM. The peptide concentration was then confirmed using the extinction coefficient (Gill and Von Hippel, 1989) of 1280 M^{-1} cm^{-1} (due to the single tyrosine residue). The pH of the samples was determined before and after. The pH was adjusted using aliquots of 10-100 mM NaOH or HCl. Then transferred to 5 mm Norell® NMR tube. The addition of 1.0 molar equivalent metal ions to the Aβ peptides was performed using 9 µL from a 50 mM stock solution of Al^{3+} and Zn^{2+}. NOESY and TOCSY NMR experiments were conducted on the apo Aβ peptide sample followed by the 1.0 molar equivalent metal ions Aβ peptide sample.

2.6 Binding affinity

A varied Hill Equation was used to determine binding affinity (K_D). In this technique the changes in chemical shift (Δδ) of resonances, caused by the addition of metal ions are measured. Values of K_D were derived from the relationship between metal concentration and the Δδ, expressed in a binding curve by fitting the data to the Hill Equation (2.1) below using Origin 2019 analysis software.

$$y = \Delta\delta_{max} \frac{[m]^n}{K_D{}^n + [m]^n} \tag{2.1}$$

Where:

y =	change in chemical shift corresponding to metal concentration
$\Delta\delta_{max}$ =	the point at which the peptide is saturated by metal ions
[m] =	metal concentration corresponding with the change in chemical shift
K_D =	the binding affinity, computes using x value at half $Vmax$ value.
n =	The Hill coefficient (n = 1)

2.7 NMR titration of ligands against metal ions

The addition of metal ions to the Aβ peptides was performed using aliquots of the concentrated stock solutions for Al^{3+} and Zn^{2+}, as indicated in Table 2.3 so the resulting solutions had MI^{+}/Aβ mole ratio varying from 0:1 to 3:1. Metal ion and ligand solutions were made in 90% H_2O:10% D_2O phosphate buffer.

Table 2.3 Sample preparation for NMR titrations of metals to ligands.

M^{n+}/Ligand	[Ligand] mM	Ligand µL	[M^{n+}] mM	M^{n+} µL	Total µL
0.00	10	500	0	100	600
0.15	10	500	7.5	100	600
0.25	10	500	12.5	100	600
0.50	10	500	25	100	600
0.75	10	500	37.5	100	600
1.00	10	500	50	100	600
2.00	10	500	100	100	600
3.00	10	500	150	100	600

Samples were then transferred into 5 mm NMR tubes. The ^{1}H NMR spectra of these solutions were recorded using the Bruker Avance 400 MHz spectrometer at 298 K. Spectra were processed using standard Bruker TOPSPIN software (version 2.1).

The stoichiometry of the resulting metal-ligand complexes was determined through mole ratio plots of changes in chemical shifts ($\Delta\delta$) versus [M^{n+}]/[Ligand] from the changes in the slope.

2.8 General practices for using mammalian neuronal cells

2.8.1 Cell line

In this project SH-SY5Y mammalian neuronal cell line (CellBank Australia) was used. As shown in Table 2.2 SH-SY5Y cells were isolated from a 4-year female patient with neuroblastoma. The cells are of epithelial morphology and mainly adherent.

Table 2.4 Details of the SH-SY5Y mammalian cell line used in this project

Cell type	SH-SY5Y
Organism	*Homo sapiens,* Human
Tissue	Bone marrow
Morphology	Epithelial
Growth mode	Adherent
Disease	Neuroblastoma
Age	4 years
Gender	Female

2.8.2 Sterilisation

The class II biological safety cabinet (Gelaire AS-2252.2) was used to aseptically culture cells, passage cells and change media. The safety cabinet underwent UV light exposure for 30 min and wiped down with 70% ethanol immediately prior to and post use.

Before all exterior materials are taken into the sterile biological safety cabinet, materials were sterilised with 70% ethanol. Sterilisation of bottles, tubes, pipette tips, and heat-stable solutions was achieved by autoclaving for 30 min at 121 °C (Tuttnauer 3150EL, Australia). Heat-sensitive reagents were filtered through a 0.2 µm filter.

2.8.3 Growth medium

The growth medium used for neuroblastoma cells SH-SY5Y was complete DMEM/F12 Hams (Sigma-Aldrich, Australia) supplemented with 10% foetal bovine serum (FBS) (Lot:1622598, Life Technologies, Australia) and 1% antibiotics (penicillin/streptomycin) (Life Technologies, Australia).

For the cryogenic storage, the freezing medium used was made from DMEM/F12 Hams for SH-SY5Y cells, supplemented with 20% FBS and 10% dimethyl sulfoxide (DMSO, Sigma-Aldrich).

2.8.4 Establishment of cell line

Cell were seeded into 75 cm^2 tissue culture flask (Greiner Bio-One, Germany) at 2.1×10^6 cells in 12 mL complete DMEM/F12 Hams and incubated at 37 °C, 5% CO_2 (Thermo Scientific HERA 150). Cultures were examined under an inverted microscope (Olympus CKX41) daily to monitor the health and confluence. Once cultures reached a confluency of 80%, cells were passaged into three 75 cm^2 flask, or from one 75 cm^2 flask to three 25 cm^2 flasks. To carry out passaging, cells were washed with 5 mL of phosphate-buffered saline (PBS) (137 mM NaCl, 2.7 mM KCl, 10 mM Na_2HPO_4 and 2 mM KH_2PO_4 at pH 7.4). Then trypsinised with 1 mL trypsin (Life Technologies, Australia) and incubated at 37 °C with 5% CO_2 for 2-5 min. Once detached, the cells are resuspended in complete DMEM/F12 Hams medium. The cell suspension was mixed by gentle pipetting to ensure cell suspensions were homogenous. Then using a hemocytometer (Hawksley BS. 748) cells were counted and aliquots of the cell suspensions were pipetted into new 75 cm^2 flasks and brought to a final volume of 12 mL complete medium, with flasks containing 2.1×10^6 cells. The cells were then observed under microscope to ensure consistency cell density and health. The flasks were then returned to the incubator for growth.

Cell cultures for experiments in microtitre plates were produced from the 75 cm^2 flasks with 80% confluency according to culture maintenance procedures stated above. Once cells had reached 80% confluency cells were washed using 5 mL PBS, trypsined and using a

hemocytometer (Hawksley BS. 748) cells were counted. The microtitre plates were seeded with the suspended cells at 7000 cells per well and incubated at 37 °C with 5% CO_2 for 36 hr.

2.8.5 Cryogenic storage

Frozen stocks preparation was accomplished by culturing cells in the 75 cm^2 flasks in complete medium until 80% confluency. The cells were then washed using 5 mL PBS, then trypsined and incubated at 37 °C with 5% CO_2 for 3-5 min. After detachment of cells, 10 mL of complete DMEM/F12 Hams medium was added to the flask and the cells were suspended by multiple aspiration by pipette. Cell suspension was then transferred to 15 mL Falcon tubes (Sigma-Aldrich, Australia) and centrifuged (Allegra X-15R) at 900 g for 5 min. The supernatant was aspirated to resuspend cells in 3 mL of freezing medium. Suspended cell solution was then pipetted 1 mL aliquots into cryovials (Greiner Bio-one, Germany). The cells were slowly brought to -196 °C by being placed in an insulated styrofoam container (Sigma-Aldrich, Australia) at -80 °C (Thermo Scientific -80C ULT) for 12 hr, after which the vials were transferred to liquid nitrogen storage at -196 °C.

2.9 Cell viability studies of SH-SH5Y cells under metal-ligand treatment

2.9.1 Determination of IC_{50} of metal ions

To determine the metal treatment concentrations IC_{50} values were calculated for SH-SY5Y cells, in microtitre plates consisting of 7000 cells in 190 µL of complete media, in each well. Plates were incubated at 37 °C with 5% CO_2 for 36 hr. Following incubation cells were treated with 10 µL stock solutions at 20× the respective metal salts that had been filter sterilised. The SH-SY5Y cells were treated as detailed in Table 2.5 then incubated.

Table 2.5. The concentration of metal salts used to determine the IC_{50} of the respective metal ion.

Metal treatment	Concentrations used (µM)
$ZnSO_4$	0, 25, 50, 100, 150, 175, 200, 225, 250, 275, 300 and 375 µM
$CuSO_4$	0, 5, 10, 20, 50, 100, 125, 150, 175, 200, 225 and 250 µM
$Al(mal)_3$	0, 5, 10, 20, 50, 100, 125, 150, 175, 200, 225 and 250 µM
CrO_3	0, 1, 2.5, 5, 7.5, 10, 12.5, 15, 17.5, 20, 30, 40, 50, 60, 70, 80, 90 and 100 µM
$NaAsO_2$	0, 2.5, 5, 7.5, 10, 12.5, 15, 17.5, 20, 22.5, 25, 30, 40, 50, 60, 70, 80, 90 and 100 µM

To measure cell viability an MTT (3-(4,5-dimethyliazol-2-yl)-2,5-diphenyl-2H-tetrazolium bromide) (Sigma-Aldrich, Australia) colorimetric assay was conducted following a 6 hr incubation period of metal ion treatments. MTT assays were conducted by adding 50 µL of MTT (5 mg/mL in PBS) to each well and incubated for 2 hr at 37 °C with 5% CO_2. Then medium plus the MTT was aspirated and the formazan crystals formations in each well were dissolved in 100 µL DMSO. The optical absorbance at 600 nm (A_{600}) of the microtitre plates was measured using a spectrophotometer (Multiskan EX, Thermo Electron, USA). The IC_{50} values were determined based on the titration curve generated using Excel.

2.9.2 MTT cell viability Assay

To determine the effect of ligands on the metal toxicity of SH-SY5Y cells. Microtitre plates were prepared containing 7000 cells in 200 µl complete media, in each well. SH-SY5Y cells were grown for 36 hr at 37 °C, 5 % CO_2 and then prepared for treatment. The specific treatments of Al^{3+} is given in Table 2.6 for clarity.

Table 2.6 Treatments used for each plate in ligand toxicity assay.

Plates	Treatments
1	$Al(mal)_3$ (0 µM, 175 µM, 500 µM, 800 µM, 1000 µM, 1500 µM, 1750 µM, 2000 µM) in each treatment well.
2	$Al(mal)_3$ (0 µM, 175 µM, 500 µM, 800 µM, 1000 µM, 1500 µM, 1750 µM, 2000 µM) plus 10 µL Histidine (160 µM) in each treatment well.
3	$Al(mal)_3$ (0 µM, 175 µM, 500 µM, 800 µM, 1000 µM, 1500 µM, 1750 µM, 2000 µM) plus 10 µL Glutathione (160 µM) in each treatment well.
4	$Al(mal)_3$ (0 µM, 175 µM, 500 µM, 800 µM, 1000 µM, 1500 µM, 1750 µM, 2000 µM) plus 10 µL Maltol (160 µM) in each treatment well.
5	$Al(mal)_3$ (0 µM, 175 µM, 500 µM, 800 µM, 1000 µM, 1500 µM, 1750 µM, 2000 µM) plus 10 µL Citric Acid (160 µM) in each treatment well.
6	$Al(mal)_3$ (0 µM, 175 µM, 500 µM, 800 µM, 1000 µM, 1500 µM, 1750 µM, 2000 µM) plus 10 µL Malic Acid (160 µM) in each treatment well.

The experimental design was repeated with zinc nitrate hexahydrate, copper chloride dihydrate, sodium (meta)arsenite and chromium (VI) oxide. The concentration ranges for metal treatments are: 0-250 µM zinc nitrate hexahydrate, 0-2000 µM copper chloride dehydrate, 0-2000 µM sodium (meta) arsenite, and 0-100 µM chromium (VI) oxide.

Once treated SH-SY5Y cells were incubated for 8 hr, an MTT (3-(4,5-dimethylthiazol-2-yl)-2,5-diphenyl-2H-tetrazolium bromide) colorimetric assay was used to quantify cell viability on adherent cells. Cells were treated with 50 µl MTT solution (5 mg/ml in PBS) to each well resulting in formazan crystals solubilized in 100 µl DMSO. Culture plates were gently shaken

before optical density was measured using a spectrophotometer (Multiskan EX, Thermo Electron, USA) at 600 nm.

2.10 Quantification of APP Gene Expression

2.10.1 Harvesting and purification of RNA for quantitative qRT-PCR

The SH-SY5Y cells were cultured in 75 cm^2 flasks to 80% confluence at which point 1 mL TRIzol™ reagent (Thermofisher) was added directly into the flask. The solution was aspirated several times to homogenise the lysate, then transferred to 2 mL Eppendorf tubes. To ensure complete dissociation of the nucleoprotein complexes, the resulting lysate was allowed to stand for 5 mins at room temperature before the addition of 200 µL of chloroform, subsequently followed by another incubation at room temperature for a further 3 min. Samples were then centrifuged for 15 min, 12000 g, 4 °C to separate the solution into three distinct phases. The RNA containing upper organic phase was transferred, without touching the white layer in the middle, into a new tube by careful pipetting. The addition of 0.5 mL isopropanol resulted in the precipitation of the RNA. Following the 10 min incubation the sample was centrifuged for 10 min at 12000 g at 4 °C. Consequently, total RNA precipitated forming a white gel-like pellet at the bottom of the Eppendorf tube. The supernatant was discarded and 1 mL of 75% ethanol was added. The sample was vortexed for 5 sec then centrifuged for 5 min, 7500 g, 4 °C. The supernatant was removed and the pellet allowed to air dry. The dried pellet was resuspended in 30 µL RNase-free water by aspirating numerous times. The resulting RNA sample was stored at -80 °C. The purity and recovery were determined by NanoDrop based on the A260/A280 ratio and the peak shapes at 260 and 280 nm. The RNA pellet was dissolved in 50 µL of DEPC water. Nano drop reading with ratio set to 260/280 used to test RNA purity.

2.10.2 cDNA synthesis

cDNA synthesis was carried out with the high-capacity cDNA reverse transcription kits (Thermo Fisher Scientific). The reagents and RNA samples were firstly thawed over ice. The RNA samples were then diluted to 0.1 µg/µL. The master mix for the reverse transcription consisted of 2 µL 10X reverse transcription buffer, 0.8 µL 25X dNTP mix, 2 µL 10X reverse transcription random primers, 1 µL Multiscribe™ reverse transcriptase, and 4.2 µL DEPC-treated water. Each reaction required 10 µL of master mix combined with 10 µL of 0.1 µg/µL RNA sample.

Reaction tubes were mixed and aspirated by pipette and brief vortex to push the solution to the bottom and to eliminate air bubbles. Reaction mixtures were run on a Veriti 96 well thermal cycler (Applied Biosystems) according to the protocol in Table 2.7.

Table 2.7 Thermal cycler settings for cDNA synthesis

Step	Temperature (°C)	Time
1	25	10 min
2	37	120 min
3	85	5 min
4	4	Until collection

Once cycling was finished, validation for cDNA samples was achieved by measuring the UV absorbance as optical density at A260/A280 ratio.

2.10.3 Quantitative qRT-PCR

Real time quantitative reverse transcription polymerase chain reaction (qRT-PCR) was carried out using TaqMan PCR assays (Thermo Fisher Scientific). The samples and reagents were thawed on ice. cDNA samples were diluted to a concentration of 500 ng/µL cDNA. Every 20 µL reaction assay comprised of 1 µL 20X TaqMan assay (primers and probe), 10 µL TaqMan gene expression master mix, 1 µL of template and 8 µL DEPC treated water or 9 µL for the control with no template. Each sample was run in triplicate for every assay. Assays contained specific primer probe combinations targeted to APP and GAPDH (endogenous control) which encodes Glyceraldehyde 3-phosphate dehydrogenase. The thermal cycler settings used are shown in Table 2.8 and Figure 2.1 illustrates how the reaction works.

Table 2.8. Parameters for the qRT-PCR thermal cycler

Stage	Temperature (°C)	Duration (mm:ss)
Hold	50	2:00
Hold	95	10:00
Cycle (40 cycles)	95	0:15
	60	1:00

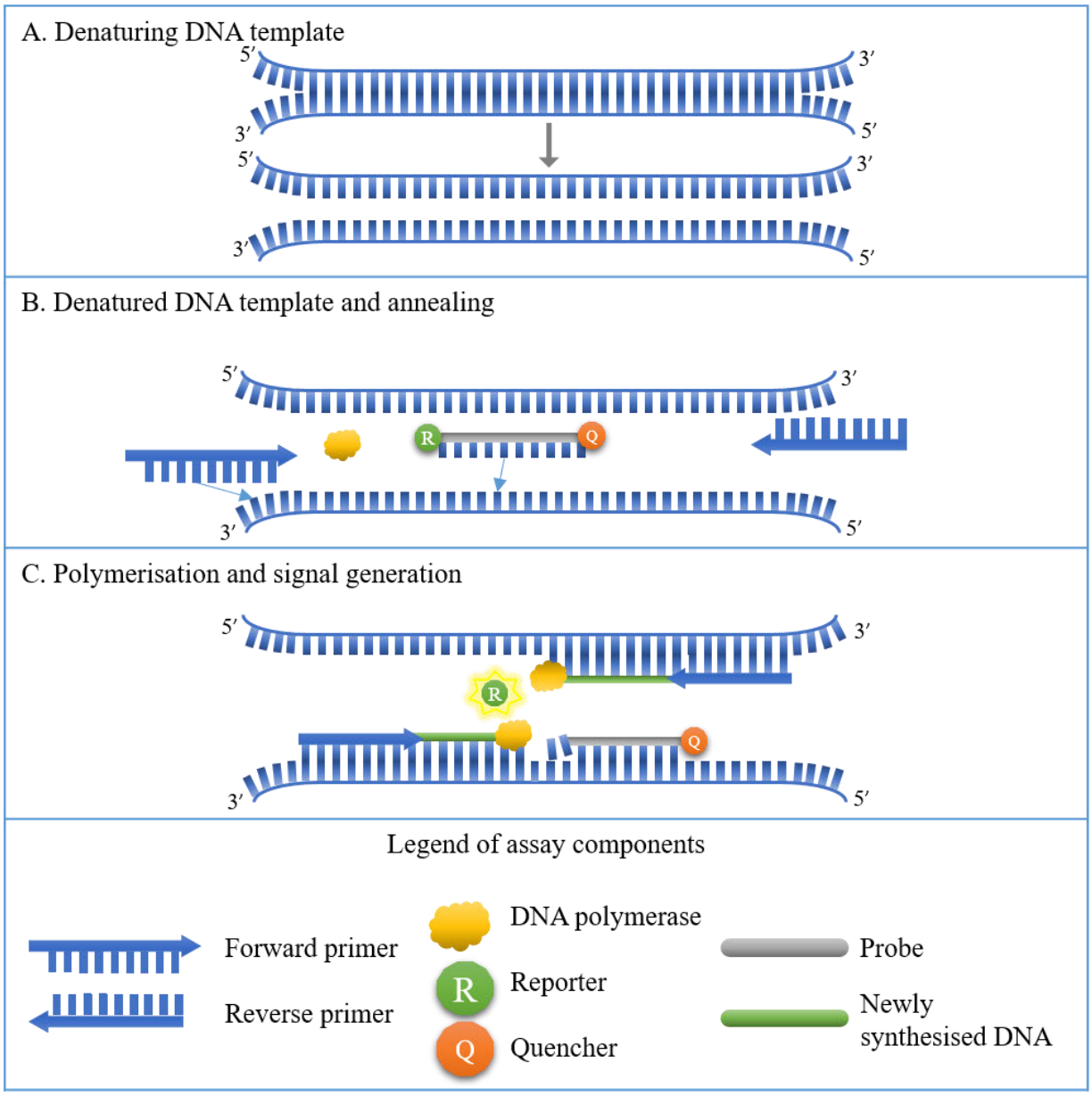

Figure 2.1. Schematic explanation of the principle underlying TaqMan technology. A) At the start of qRT-PCR, double stranded DNA melts due to the increased temperature. B) Temperature is lowered to an annealing temperature to allow the primers and probe bind to their specific target sequences. C) *Taq* DNA polymerase catalyses the extension of a new strand with the use of unlabelled primers and the cDNA template strand. When the polymerase reaches the TaqMan probe the reporter is displaced away from the quencher, causing fluorescence. With each cycle more reporter molecules are released, resulting in the increased intensity of fluorescence, in proportion to the amount of amplicon synthesized. Therefore, each cycle represents the doubling of DNA template, this multiplication follows an exponential trajectory.

The generated data was analysed using the $2^{-\Delta\Delta CT}$ method (Schmittgen & Livak, 2008) where the cycle threshold of the gene of interest in the control is normalised to the cycle threshold of the endogenous control in control conditions, giving ΔCTc. The cycle threshold of the gene of interest under the experimental conditions is normalised to the cycle threshold of the endogenous control under experimental conditions giving you a value for ΔCTe. Then ΔCTe is normalised to ΔCTc to give ΔΔCT. The expression fold change is given by raising 2 to negative ΔΔCT (exponent).

2.11 Software packages

Icon 3.1 was used to process and analyse NMR data. Assignment of proton resonances was done using SPARKY with published assignments for Aβ as a guide. Origin 9 software was used for determination of binding affinity. MNOVA used to format and display 1D NMR data. Molecular mechanics was conducted using HyperChem 8.0 and Chem3D 15.1. Statistical analysis was conducted with one-way ANOVA in SPSS statistical software.

3 THE NMR STRUCTURAL ANALYSIS OF AMYLOID β PEPTIDE AND ITS INTERACTION WITH METAL IONS

3.1 Introduction

This chapter aims to define the interaction of metal ions with the $A\beta_{1-28}$ peptide. As described in Chapter 1.9, the interactions of biometals Cu^{2+} and Zn^{2+} with Aβ have been studied in the past years. The Aβ fragments, ranging from 12- 42 residues in length can bind metal ions. Danielsson et al. (2007) and Syme et al. (2004) determined the coordination geometry of, Zn^{2+} and Cu^{2+}. The metal binding of Aβ indicates that the dyshomeostasis of $Fe^{2+/3+}$, Cu^{2+} and Zn^{2+} could induce senile plaque accumulation (Lovell et al., 1998; Bolognin et al., 2011; Oshiro et al., 2011; Craddock et al., 2012; Singh et al., 2013). In contrast to these biometals which have biological functions in the brain, aluminium (Al^{3+}) has no biological role, and is present in human brain tissue in concentrations of 1.02 to 2.01µg/g dry wt across the four main lobes (House et al., 2012).

Aluminium association to AD has been previously documented (Crapper et al., 1973; Perl and Brody, 1980). The exposure to aluminium has been indicated to contribute to the development of AD (Exley and Vickers, 2014). Aggregation of Aβ caused by the presence of aluminium was greater compared to iron, copper and zinc (Kuroda and Kawahara, 1994). However, the details of interaction between aluminium and Aβ has not yet been established.

This chapter will determine, by NMR analysis, the specific coordination geometry and the residues involved in the coordination of Al^{3+} to Aβ, and the structural variations of Aβ as a consequence of the metal coordination. The $A\beta_{1-28}$ peptide and $A\beta_{1-28}$ analogues (H6A, H13A,

H14A and H6,13,14A) are used to determine whether all histidine residues play an equal role in coordinating to the metal ion.

Chemical shift perturbation (CSP) in a ligand follows changes in its chemical shifts when an interacting metal ion is added. Measuring CSP makes quantitative use of the chemical shift changes to probe the geometry and strength of the interactions. CSP is an extremely reliable method to determine interaction sites, provided that the crystal structure or peptide sequence is kno1wn and the spectrum is assigned. It is proposed that the examination of CSP of Aβ when metal ions are added will determine the location of the binding site, the affinity of the metal ion, effect of aluminium on the secondary structure of Aβ, and potential structure of a Aβ-Al^{3+} complex. Chemical shift changes are sensitive to structural changes and can be accurately measured. Therefore, genuine binding interactions will produce CSP. The analysis involves NMR titrations, measuring the chemical shifts at each point following the peak's movement, and measuring how each peak moves throughout the titration. Resonances affected by the metal additions are the possible binding sites for Aβ. The comparison of Al^{3+} and Aβ titrations to the previously published Zn^{2+} and Aβ titrations will indicate if the binding sites for the two metal ions are different or not. The titration of Aβ with Zn^{2+} will also indicate similarities or differences in binding sites and modes of the metal-Aβ complexes. Once saturated by metal ions, the chemical shift perturbation as a function of Δδ vs $[Al^{3+}]/[A\beta_{1-28}]$ can reveal the stoichiometric ratio of the Al^{3+}-Aβ complex. Moreover, the shape of the titration curve can often be fitted to obtain a value for the dissociation constant (K_D) of the metal-peptide complex, which is a measure of affinity of Al^{3+} to Aβ. Measuring CSP makes quantitative use of the chemical shift changes to probe the binding sites, geometry and interactions. This would in turn provide valuable structural insight into the nature of the binding of metal ion to Aβ.

3.2 Results

3.2.1 Structural analysis and determination of binding sites in the metal-Aβ_{1-28} complex

3.2.1.1 Proton NMR assignments for Aβ_{1-28} residues

In order to delineate the key binding sites of Al^{3+} in Aβ_{1-28}, the resonance assignments of all protons in apo Aβ_{1-28} peptide alone were performed firstly by examining the TOCSY and NOESY cross-peaks, see Appendix B. TOCSY provided total correlation of proton spin system in each amino acid residue. NOESY provided sequential NOE correlations between the protons of neighbouring spin systems. NOEs occur due to dipolar couplings resulting from interactions of spins via space. Table 3.1 shows the chemical shifts of all protons in Aβ_{1-28} peptide. From the known assignments of HN protons, it is straight forward to assign αH and other side chain protons of individual amino acid residues.

Table 3.1 Assignments of the chemical shifts of Aβ$_{1-28}$

Residues	Experimental chemical shifts (*δ*ppm) of amino acid residues of Aβ$_{1-28}$ *			
	NH	αH	βH	Others
Asp1	nv	4.09	2.64, 2.77	
Ala2	8.16	4.28	1.37	
Glu3	8.44	4.17	1.87	γH 2.10, 2.19
Phe4	8.23	4.54	2.98	aroH 7.15, 7.25
Arg5	nv	4.27	1.60, 1.72	γH 1.47, δH 2.98
His6	nv	4.51	3.03, 3.10	aroH 6.99, 7.80
Asp7	8.31	4.60	2.64	
Ser8	8.13	4.45	3.87	
Gly9	7.94	3.88, 3.94		
Tyr10	7.93	4.52	2.93, 3.04	aroH 7.05, 6.78
Glu11	8.38	4.20	1.84, 1.90	γH 2.18
Val12	8.04	3.94	1.93	γH 0.72, 0.84
His13	nv	4.57	2.99	aroH 6.91, 7.77
His14	nv	4.52	3.01, 3.08	aroH 6.92, 7.78
Gln15	8.31	4.24	2.03, 2.24	γH 2.31; εNH 6.84, 7.52
Lys16	nv	4.26	1.64, 1.78	γH 1.36, 1.41; εH 2.95
Leu17	8.19	4.31	1.43, 1.58	γH 1.60; δH 0.83, 0.90
Val18	7.93	4.01	1.9	γH 0.73, 0.81
Phe19	8.19	4.56	2.92, 2.98	aroH 7.16, 7.30
Phe20	8.18	4.55	2.94, 3.10	aroH 7.23, 7.32
Ala21	8.19	4.22	1.36	
Glu22	8.33	4.19	1.99, 2.03	γH 2.24
Asp23	8.4	4.64	2.63, 2.72	
Val24	8.09	4.13	2.17	γH 0.93, 0.95
Gly25	8.50	3.88, 3.96		
Ser26	8.34	4.37	3.87	
Asn27	nv	4.74	2.76, 2.84	δNH 6.89,7.59
Lys28	7.88	4.15	1.80	γH1.64, 1.69; δH 1.36; εH 2.98

nv- resonances not observed due to the fast exchange with solvent.

*obtained from the TOCSY and NOESY experiments in in 90% H_2O:10% D_2O (δ in ppm) at 298K.

3.2.1.2 NMR titration of $A\beta_{1-28}$ against Al^{3+}

In 2D experiments of $A\beta_{1-28}$, the prolonged run times resulted in the line broadening due to peptide aggregation. Thus, despite the good resolution, not all resonances were visible in the TOCSY and NOESY spectra. In contrast, ^{1}H NMR has less signal dispersion which could be caused by an exchange process and peptide aggregation. ^{1}H NMR allows characterisation of residues effected by metal coordination. Therefore, the combination of these two sets of data provides a detailed characterisation of aluminium binding to $A\beta_{1-28}$. To characterise Al^{3+} coordination to $A\beta_{1-28}$, ^{1}H NMR titration was used. Figure 3.1 shows the 1D proton NMR spectrum in the aromatic region of $A\beta_{1-28}$ titrated with increasing amounts of Al^{3+}.

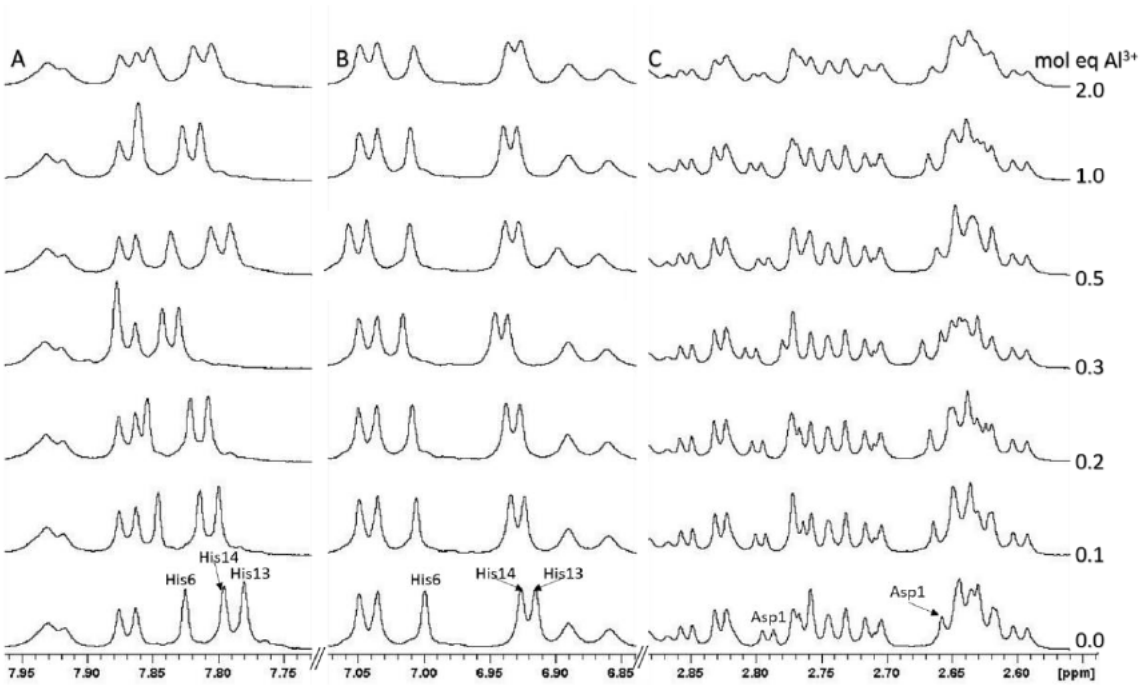

Figure 3.1 ^{1}H NMR spectra of Al^{3+} titration of $A\beta_{1-28}$. [1 mM] $A\beta_{1-28}$ in 10% H_2O:90% D_2O, pH 7.4 at 289K. The titration was carried out as described in Section 2.4 of Chapter 2. The three spectra sections (A, B and C) show perturbed resonances of respective protons. A) NH region, B) aromatic region, C) βH region.

The incremental additions of Al^{3+} caused the perturbation of numerous NMR resonances, by means of broadening or chemical shifts variations. 1D ^{1}H NMR spectra show that Al^{3+} affected signals from all the three histidine residues (His6, 13 and 14) by exhibiting up field shifts of the 2H (Figure 3.1A) and 4H (Figure 3.1B) resonances of the imidazole side chain.

This observation suggests the involvement of the histidine residues as the metal binding sites. The αH and two diastereotopic βH protons of Asp1 at 2.64 and 2.77 ppm in Figure 3.1C are also perturbed with the addition of Al^{3+}. Therefore, the coordination of Al^{3+} to $A\beta_{1-28}$ may also involve the N-terminus. Based on the 1D proton NMR spectrum other residues were unaffected by the addition of Al^{3+}. Hence the binding sites of Aβ for Al^{3+} are limited to the His6, His13, His14 and Asp1.

To confirm these binding sites in Aβ, 2D TOCSY of Aβ containing 1.0 mole equivalent of Al^{3+} was conducted (Figure 3.2, full spectra in Appendix C) in order to determine which residue-specific spin systems were affected by the metal ion. The addition of Al^{3+} caused perturbation of the cross peaks of Aβ.

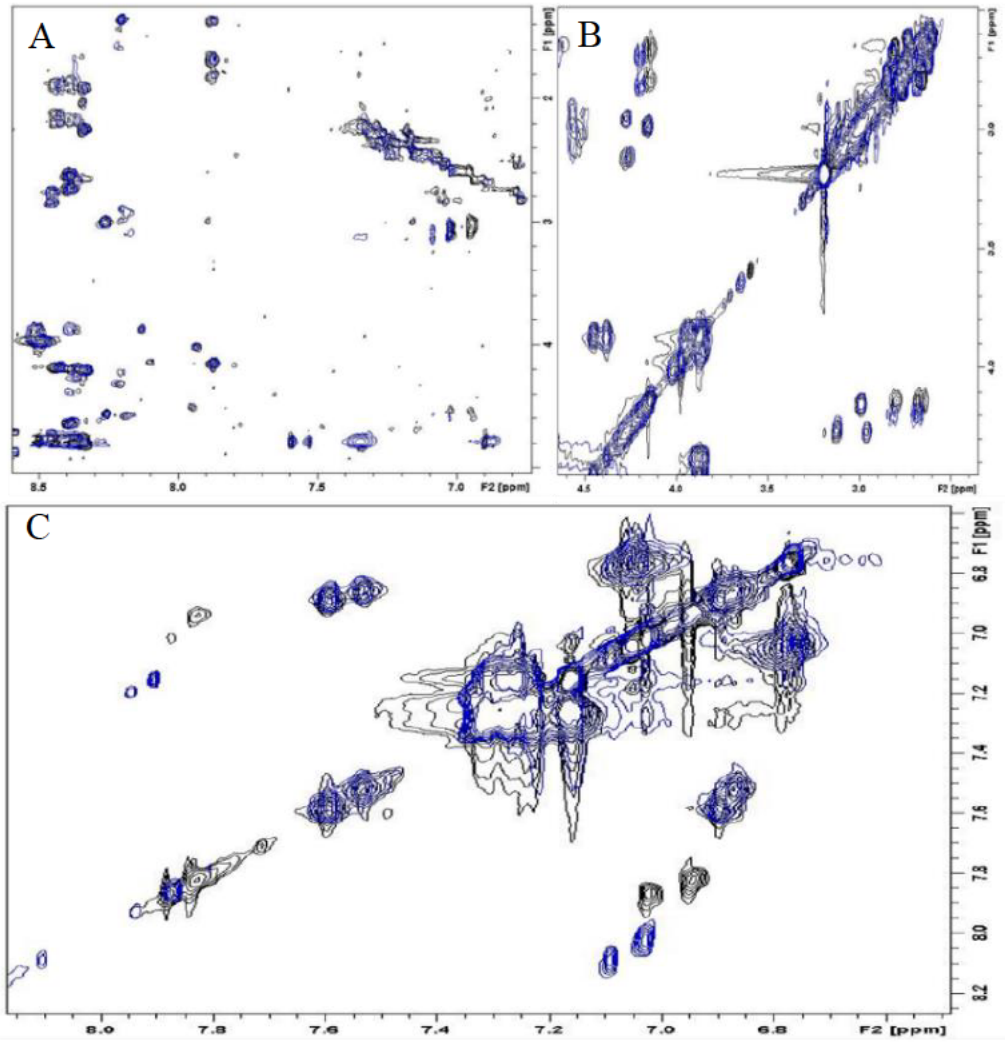

Figure 3.2 2D $^{1}H/^{1}H$ TOCSY NMR spectra of Al^{3+} titrated wild-type Aβ$_{1-28}$. (A) The HN-αH region (B) aromatic region (C) The βH-αH region. Wild-type Aβ$_{1-28}$ in10% H_2O:90% D_2O pH 7.4 at 298K, apo (black) and one equimolar Al^{3+} (blue).

From the addition of equimolar of Al^{3+} to Aβ$_{1-28,}$ the chemical shift variations experienced by the individual residues are summarised in Figure 3.3.

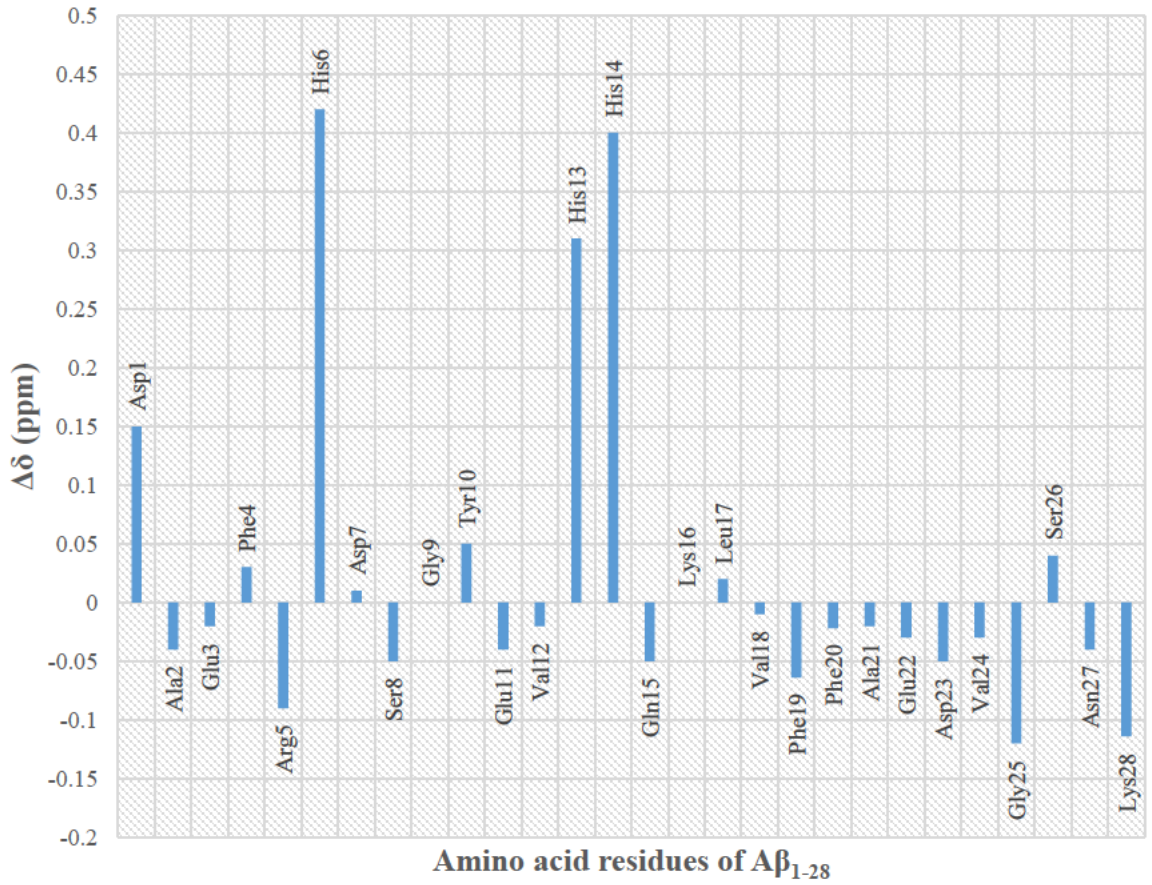

Figure 3.3 ^{1}H chemical shift variations for Aβ$_{1-28}$ induced by 1.0 mole equivalent of Al^{3+}. Aβ$_{1-28}$ 1 mM was in 10% H_2O:90% D_2O pH 7.4 at 298K. The sum of all the chemical shift variations (Δδ) experienced by the protons of the residues were calculated by using the formula $\Delta\delta = \delta_{holo}-\delta_{apo}$.

As seen from these results, the residues His6, His13 and His14 experienced the largest change in chemical shift, followed by Asp1, Gly25 and Lys28. The residues Arg5, Tyr10 and Phen19 did experience chemical shift variations, to a lesser degree. A weaker coordination may occur via these residues.

In summary, the 2D analysis and 1D titration experiments of Aβ supports the primary binding site of Aβ$_{1-28}$ are His6, His13, His14 and Asp1. This also indicates potential secondary weak

binding sites of Gly25 and Lys28. The residues Arg5, Tyr10 and Phen19 are affected by the addition of Al^{3+}, however this variation in chemical shift may be due the change in structural arrangement caused by the involvement of neighbouring residues in the coordination of Al^{3+}.

3.2.2 Aluminium titration of $A\beta_{1-28}$ analogues

In an attempt to further verify key residues involved in Al^{3+} binding to Aβ, its analogues (H6A, H13A, H14A) were synthesised, in which each of the three histidine residues were replaced by alanine residues individually, and a fourth analogue (H6,13,14A) was synthesised in which all three histidine residues were replaced by alanine residues. The sequence of these $A\beta_{1-28}$ analogues are given in Table 3.2.

Table 3.2 Sequences of the synthetic amyloid β and its analogues

Designation	Sequence
$A\beta_{1-28}$	DAEFR**H**DSGYEV**HH**QKLVFFAEDVGSNK
Aβ H6A	DAEFR**A**DSGYEV**HH**QKLVFFAEDVGSNK
Aβ H13A	DAEFR**H**DSGYEV**A**HQKLVFFAEDVGSNK
Aβ H14A	DAEFR**H**DSGYEV**H**AQKLVFFAEDVGSNK
Aβ H6,13,14A	DAEFR**A**DSGYEV**AA**QKLVFFAEDVGSNK

The Al^{3+} was titrated against each of the analogues and 1D ^{1}H NMR spectra were recorded. Figure 3.4 shows the 1D ^{1}H NMR spectra in the NH, aromatic and βH regions of apo and one mole equivalent Al^{3+} in $A\beta_{1-28}$ as well as the four analogues including H6A, H13A, H14A and H6,13,14A. The separate resonances for the protons of the three His 2H and 4H (centred at ~7.8 ppm and ~6.9 ppm respectively) and the Asp1 βH (at 2.6 ppm and 2.7 ppm) resonances can be distinguished in the spectra.

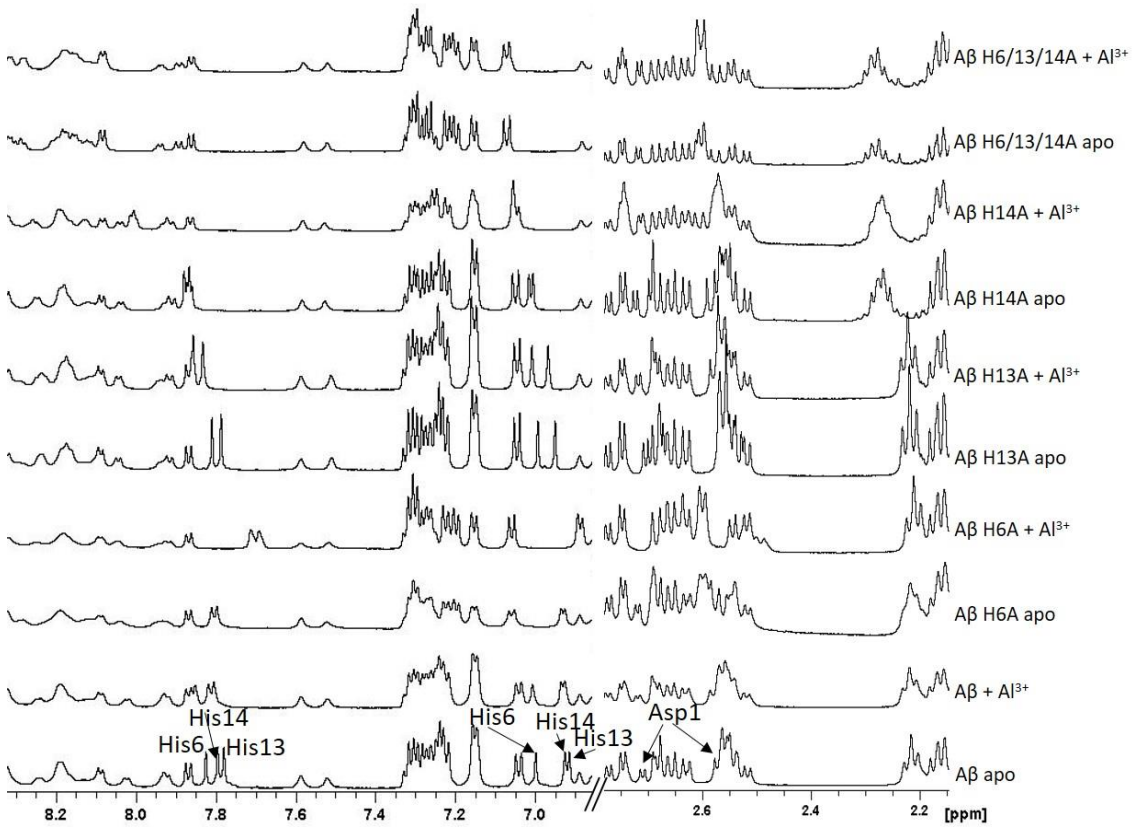

Figure 3.4 ^{1}H NMR titrated spectra of Aβ$_{1–28}$ and analogues. The spectra of Aβ$_{1-28}$ apo as well as its analogues respectively (0 mol eq Al^{3+}) and 1.0 mol eq Al^{3+} are shown in the amide, aromatic and βH regions. All peptides are at 1.0 mM concentration in 10% H_2O:90% D_2O, pH 7.4 at 298K.

The comparison of the spectra (Figure 3.4) of apo Aβ$_{1-28}$ (bottom) and the Al^{3+} additions, indicate that the metal ion causes a significant decrease of His and Asp1 signals, as compared to the rest of the spectrum. The effects of Al^{3+} addition on all four analogues also caused line broadening of His resonances but the observed effects are not the equivalent to the original Aβ$_{1-28}$ spectra. The addition of Al^{3+} to H6A caused significant line broadening of the Asp1 βH resonances. The 4H signals from His13 and His14 residues were not affected by the Al^{3+}. However, Al^{3+} caused the 2H of His13 and His14 to experience a downfield chemical shift with a Δδ greater than the Aβ$_{1-28}$ spectra. In the case of H13A, the His 2H and 4H signals from His6

and His14 residues are still clearly visible, and despite a small shifting upfield, are not significantly broadened upon Al^{3+} addition. However, from Figure 3.4 the signals of His 2H and Asp1 βH protons experiences the largest CSP of H13A. The H14A spectra show broadening of the His signals but remain unshifted relative to their apo spectra. Slight changes where observed in the H6,13,14A peptide analogue for the βH region shown in Figure 3.5 (see Appendix C for full spectrum), line broadening was seen overall but resonance did not experience changes in chemical shift, apart from Asp1.

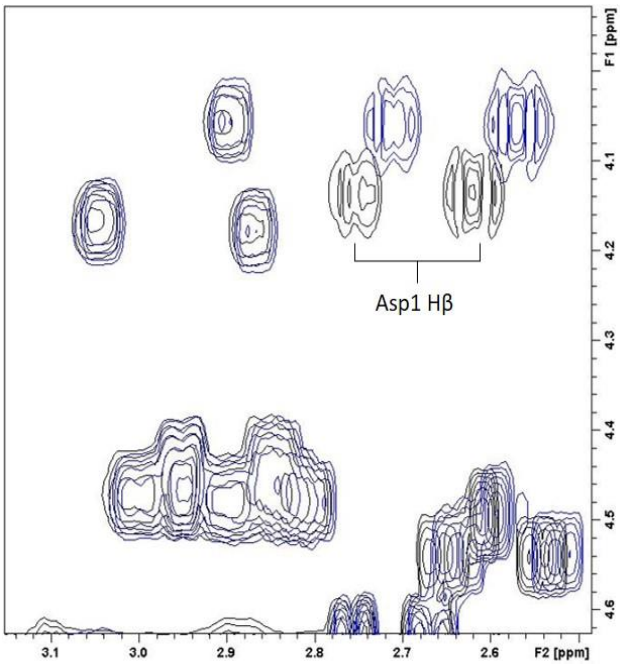

Figure 3.5 2D ^{1}H TOCSY spectrum of Aβ$_{1–28}$ H6,13,14A with Al^{3+}. The βH region of apo Aβ$_{1–28}$ H6,13,14A (black) with 1.0 mol eq Al^{3+}(blue) is shown. The Aβ$_{1–28}$ H6,13,14A peptide is at 1.0 mM concentration in 10% H_2O:90% D_2O, pH 7.4 at 298K. The slow exchange cross peaks observed for Asp1 βH are highlighted.

TOCSY results also indicated the only residue in H6,13,14A affected by Al^{3+} addition was Asp1 as seen in Figure 3.5. As the βH was more affected than the αH and with aluminium's oxygen donor preference, it is suggested Al^{3+} coordinates to the carboxylate group of Asp1. Taken

together, the results with $A\beta_{1-28}$ analogues confirm that the aluminium binding site in Aβ is in the N-terminus and are consistent with the involvement of the three histidine residues in the coordination.

3.2.3 Determination of binding affinity of Al^{3+} to $A\beta_{1-28}$ monitored by NMR spectroscopy

The binding affinity experiments used the ^{1}H NMR titration and a varied Hill Equation to determine binding affinity (K_D). In this technique the CSP of the residues caused by the addition of metal ions are measured as a change in chemical shift (Δδ). Values of K_D were derived from the relationship between metal concentration and the Δδ. The binding curves are constructed as outlined in section 2.6, by fitting the data to the Hill Equation (2.1) shown below and by using Origin 9 software.

$$y = \Delta\delta_{max} \frac{[m]^n}{{K_D}^n + [m]^n} \tag{2.1}$$

This experiment used CSP of the $A\beta_{1-28}$ residues effected by the aluminium titration. The binding curves obtained for the $A\beta_{1-28}$ are given in Figure 3.6 and for each concentration the respective steady state equilibrium values were plotted and fitted to the Hill equation for a 1:1 binding stoichiometry ratio and n=1 in equation 1, to determine the dissociation constant KD.

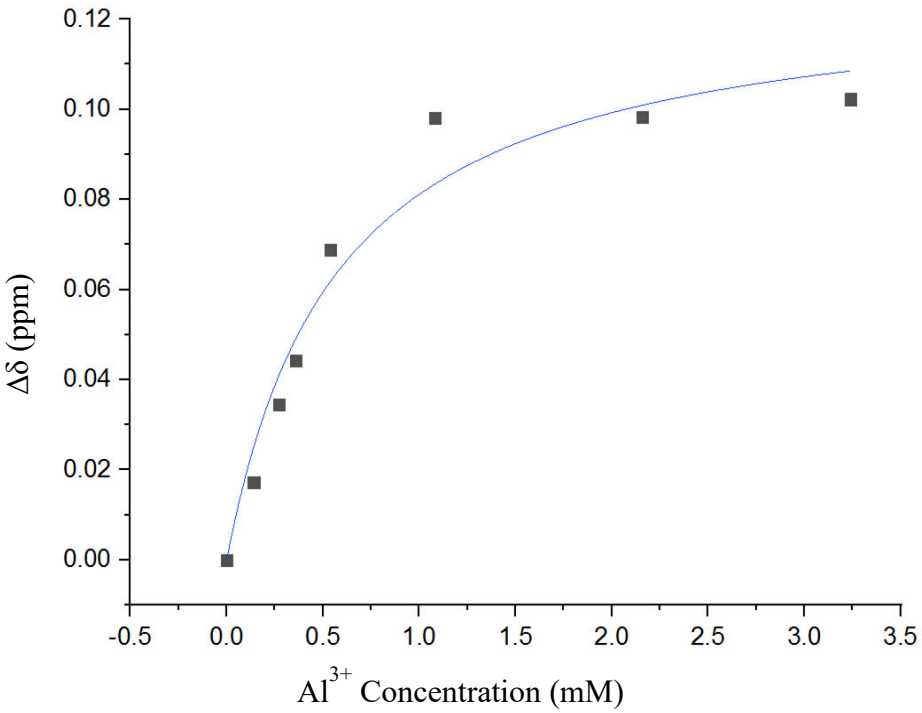

Figure 3.6 Binding curve of aluminium to Aβ$_{1-28}$. The sum of the chemical shift changes (Δδ) for the Aβ resonances as a function of aluminium concentration. The curve represents the best fit of the quadratic equation that describes 1:1 complex formation. The K_D of Aβ$_{1-28}$ and Al^{3+} was 0.35 ± 0.03 mM.

The curve in Figure 3.6 corresponds a binding affinity of (K_D) 0.35 ± 0.03 mM and $\Delta\delta_{max}$ = 0.13 ± 0.01 ppm. This was derived from the average binding affinities of replicated titrations along with the standard error (SEM) for this average.

3.2.4 Comparison of Al^{3+} and Zn^{2+} binding to $A\beta_{1-28}$

In order to compare aluminium to an extensively studied metal ion, Zn^{2+}, the characterisation of Zn^{2+} binding to Aβ was also conducted using ^{1}H NMR. Figure 3.7 shows the 1D proton NMR spectra in the aromatic region of $A\beta_{1-28}$ loaded at one mole equivalent of Zn^{2+}at pH 7.4. The presence of the Zn^{2+} ions caused a number of NMR resonances to be perturbed. The 2H and 4H resonances of the histidine residues shift to a higher field upon addition of Zn^{2+}. Both residues' signals undergo some broadening, in particular the 2H resonance of the Zn^{2+} bound complex which is in fast/intermediate exchange. A lower upfield shift and broadening effect is seen in the Al^{3+} bound complex. The relative difference between deshielded peaks indicates much stronger binding efficiency of Zn^{2+} to Aβ in comparison to Al^{3+}.

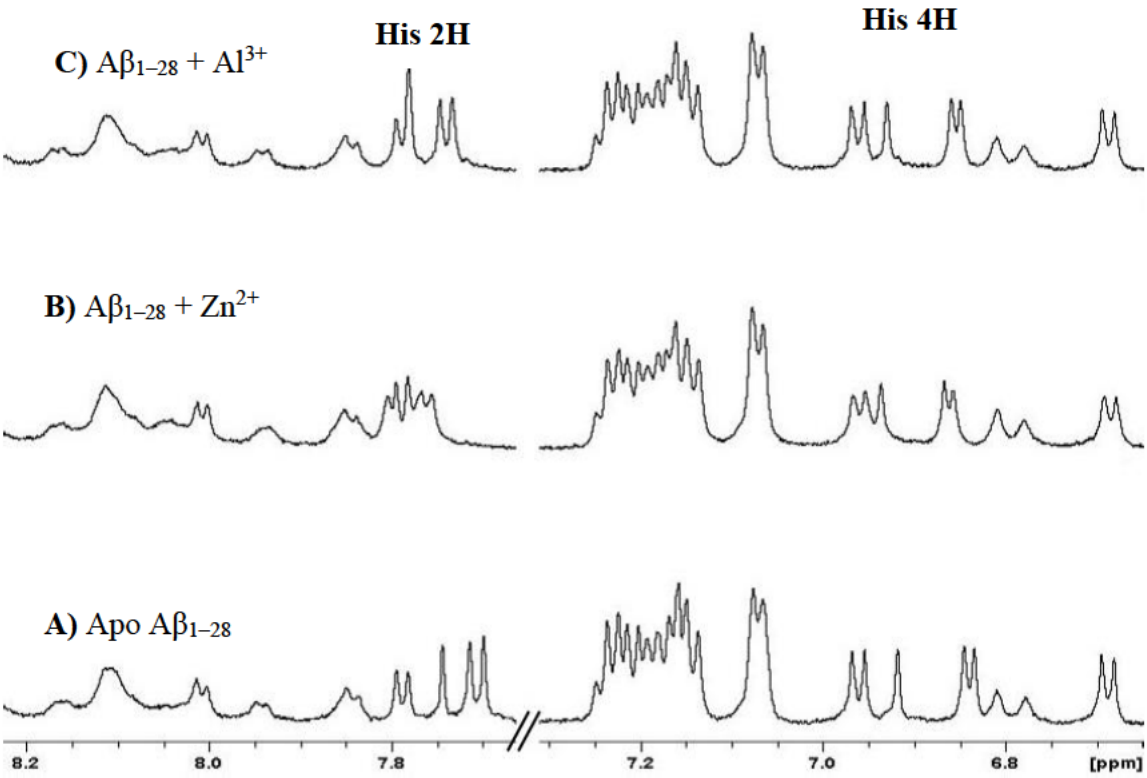

Figure 3.7 ^{1}H NMR spectra of Zn^{2+} and Al^{3+} titrated $A\beta_{1-28}$. 2H and 4H resonances of His6, 13 and 14 are shown. $A\beta_{1-28}$ is in 10% H_2O:90% D_2O, pH 7.4 at 298K. (A) Apo $A\beta_{1-28}$; (B) $A\beta_{1-28}$ with 1.0 mol eq Zn^{2+}; (C) $A\beta_{1-28}$ with 1.0 mol eq Al^{3+}.

The similar changes in chemical shift observed for the resonances of 2H and 4H of His 6, 13 and 14 in Figure 3.7 suggest aluminium and zinc binds to the same binding site of $A\beta_{1–28}$. For zinc, the K_D = 0.28 ± 0.03 mM, indicating Zn^{2+} has only a slightly higher binding affinity compared to Al^{3+} (0.35 ± 0.03 mM) at physiological pH. These results indicate a very similar complexing ability of Zn^{2+} and Al^{3+}.

3.2.5 Structure of Al^{3+}-Aβ complex

3.2.5.1 Chemical shift index (CSI) based secondary structure

The CSP approach provide a means to study the effects of metal ions on the secondary structure of Aβ peptide, using the chemical shift index (CSI) based method developed by Wishart et al. (1992). The structural analysis based on the CSI method was conducted by comparing the chemical shifts of αH in an amino acid residue acquired from the NMR assignments to its random coil chemical shifts reference. This comparison assigns a chemical shift value in the form of a simple three-state (-1, 0, 1) index. A CSI value of '1' is assigned to a residue if the measured chemical shift is greater than 0.1 ppm the CSI reference value; a '-1' is given to residues with a αH smaller than the reference and a '0' value is given if the experimental and reference chemical shifts are within the expected range. The use of these CSI values provides insights of secondary structure. An uninterrupted group of CSI values of three or more '-1' indicates a helix. Any groupings of three or more '1', uninterrupted by a '-1', specify the presence of a β strand. All other regions are designated as random coils. The results of this comparison are provided in Table 3.4 for $A\beta_{1-28}$ without the metal ion.

Table 3.3 Chemical shift index (CSI) values of Aβ1-28

Residues	αH from this experiment	αH coil[a]	αH Difference	CSI values
Asp1	4.09	4.76	-0.67	-1
Ala2	4.28	4.35	-0.07	1
Glu3	4.17	4.29	-0.12	-1
Phe4	4.54	4.66	-0.12	-1
Arg5	4.29	4.38	-0.09	1
His6	4.51	4.63	-0.12	-1
Asp7	4.60	4.76	-0.16	-1
Ser8	4.45	4.50	-0.05	1
Gly9	3.87	3.97	-0.10	-1
Tyr10	4.52	4.60	-0.08	1
Glu11	4.19	4.29	-0.10	-1
Val12	3.94	3.95	-0.01	1
His13	4.57	4.63	-0.06	1
His14	4.52	4.63	-0.11	-1
Gln15	4.24	4.37	-0.13	-1
Lys16	4.26	4.36	-0.10	-1
Leu17	4.31	4.17	0.14	1
Val18	4.01	4.60	-0.59	-1
Phe19	4.56	4.66	-0.10	-1
Phe20	4.55	4.66	-0.11	-1
Ala21	4.22	4.35	-0.13	-1
Glu22	4.19	4.29	-0.10	-1
Asp23	4.64	4.76	-0.12	-1
Val24	4.13	3.95	0.18	1
Gly25	3.87	3.97	-0.10	-1
Ser26	4.37	4.50	-0.13	-1
Asn27	4.74	4.75	-0.01	1
Lys28	4.15	4.36	-0.21	-1

[a] CSI Residue-Specific αH Random Coil Shifts (Wishart et al., 1992; Reid et al., 1997).

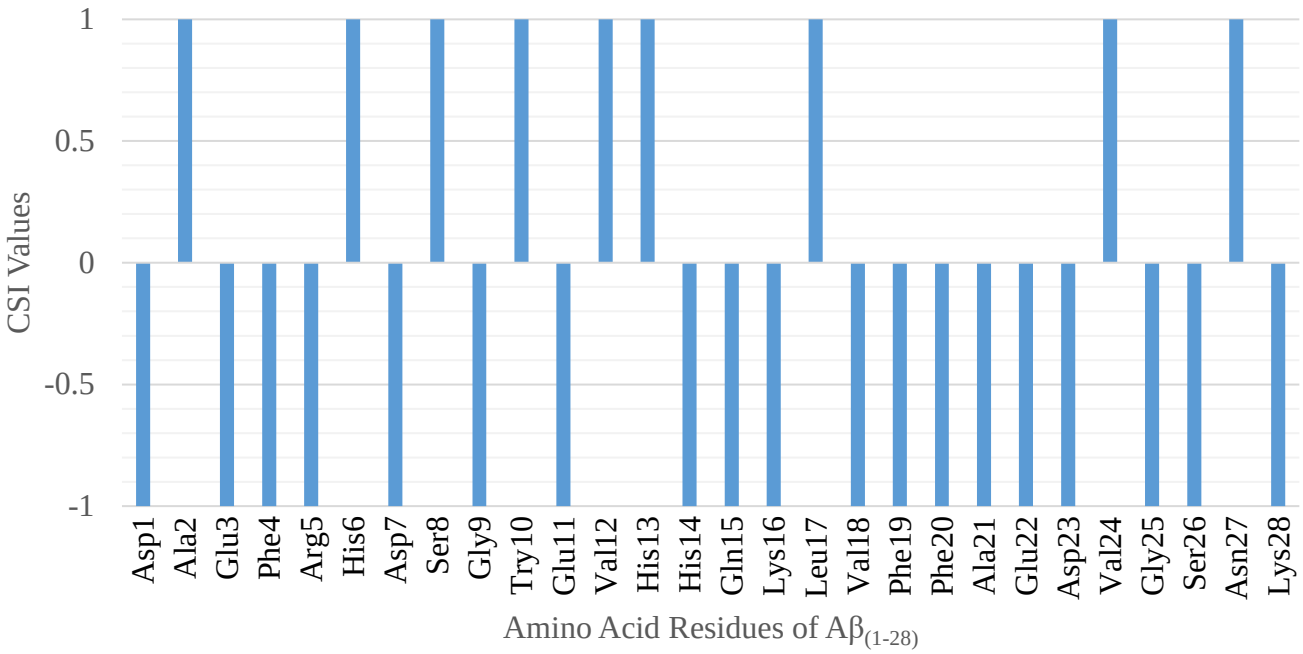

Figure 3.8 The secondary structure of Aβ$_{1-28}$ predictions from CSI values of αH chemical shifts. '+1' and '-1' mean the positive and negative deviation of chemical shifts from random coil values and refer to β strand and α helix structure, respectively.

As indicated in Figure 3.8 the secondary structure of Aβ$_{1-28}$ contains random coil near the N-terminus and the possible α helix from Val18 to Asp23. The binding of metal ions would change the secondary structure of Aβ$_{1-28}$ to allow the coordination geometry required of the metal, due to the rearrangement of binding sites donor atoms around the metal centre. Hence the effect of Al^{3+} on the CSI values and subsequent secondary structure of Aβ$_{1-28}$ was measured and predicted. The secondary structural changes induced by Al^{3+} coordination can be seen in Table 3.4 and Figure 3.9.

Table 3.4 Chemical shift index (CSI) values and sequence correction factors of Aβ$_{1-28}$ in the presence of Al^{3+}

Residues	αH from this experiment	αH coil[a]	αH Difference	titrated CSI values
Asp1	4.18	4.76	-0.58	-1
Ala2	4.28	4.35	-0.07	1
Glu3	4.17	4.29	-0.12	-1
Phe4	4.55	4.66	-0.11	-1
Arg5	4.24	4.38	-0.14	-1
His6	4.55	4.63	-0.08	1
Asp7	4.60	4.76	-0.16	-1
Ser8	4.43	4.50	-0.07	1
Gly9	3.94	3.97	-0.03	1
Try10	4.48	4.60	-0.12	-1
Glu11	4.26	4.29	-0.03	1
Val12	3.92	3.95	-0.03	1
His13	4.59	4.63	-0.04	1
His14	4.56	4.63	-0.07	1
Gln15	4.59	4.37	0.22	-1
Lys16	4.26	4.36	-0.10	-1
Leu17	4.31	4.17	0.14	1
Val18	4.51	4.60	-0.09	1
Phe19	4.56	4.66	-0.10	-1
Phe20	4.56	4.66	-0.10	-1
Ala21	4.26	4.35	-0.09	1
Glu22	4.21	4.29	-0.08	1
Asp23	4.62	4.76	-0.14	-1
Val24	4.12	3.95	0.17	1
Gly25	3.91	3.97	-0.06	1
Ser26	4.37	4.50	-0.13	-1
Asn27	4.71	4.75	-0.04	1
Lys28	4.11	4.36	-0.25	-1

[a] CSI Residue-Specific αH Random Coil Shifts (Wishart et al., 1992; Reid et al., 1997).

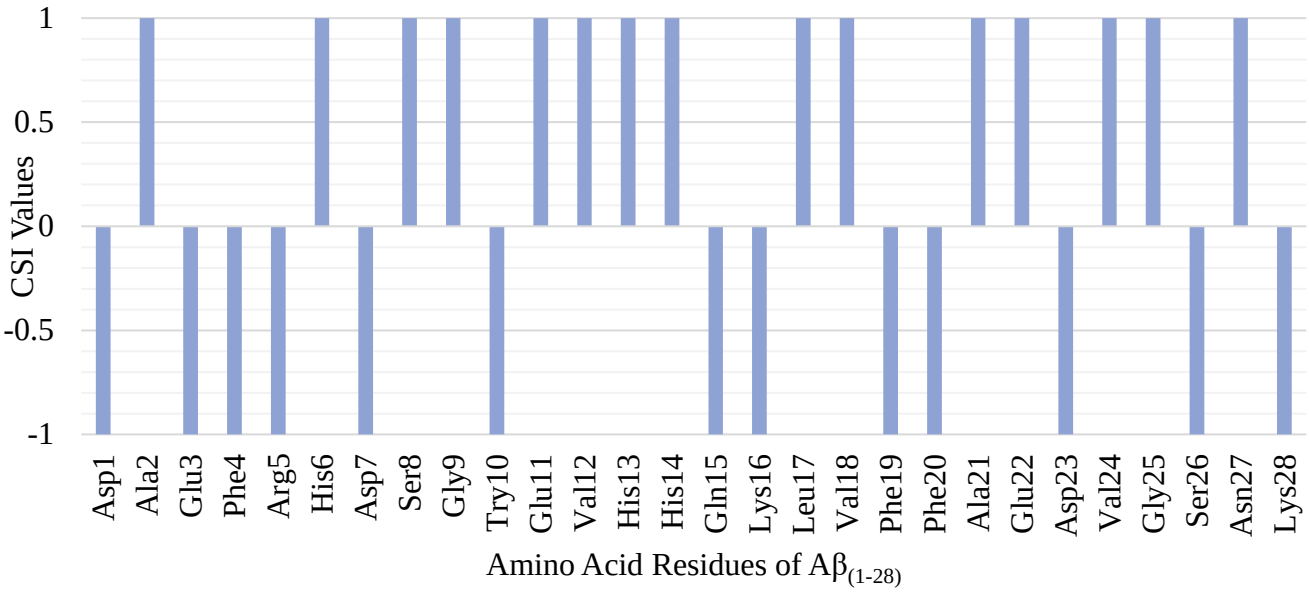

Figure 3.9 The secondary structure of Al^{3+}-$A\beta_{1-28}$ predicted from CSI values of Ha chemical shifts. '+1' and '-1' mean the positive and negative deviation of chemical shifts from random coil values and refer to β strand and α helix structure, respectively.

The addition of Al^{3+} causes the secondary structure of $A\beta_{1-28}$ to convert CSI values (Figure 3.9) from random coil and α helix to random coil and potential β strand from Glu11 to Gln15. The random coil supports the change of $A\beta_{1-28}$ to coordinate to Al^{3+} preferred geometrical arrangement. The β strand also demonstrates the effect of the constricted binding of both His13 and His14 has on peptides backbone. Shortening the bond length is expected from the formation of the His- Al^{3+}-His bridge.

3.2.5.2 Stoichiometry of Al^{3+}-Aβ complex

A 1.0 mM $A\beta_{1-28}$ peptide in 10% H_2O:90% D_2O was used in the titration to determine the stoichiometric ratio of the Al^{3+}-Aβ complex, as shown in Figure 3.10.

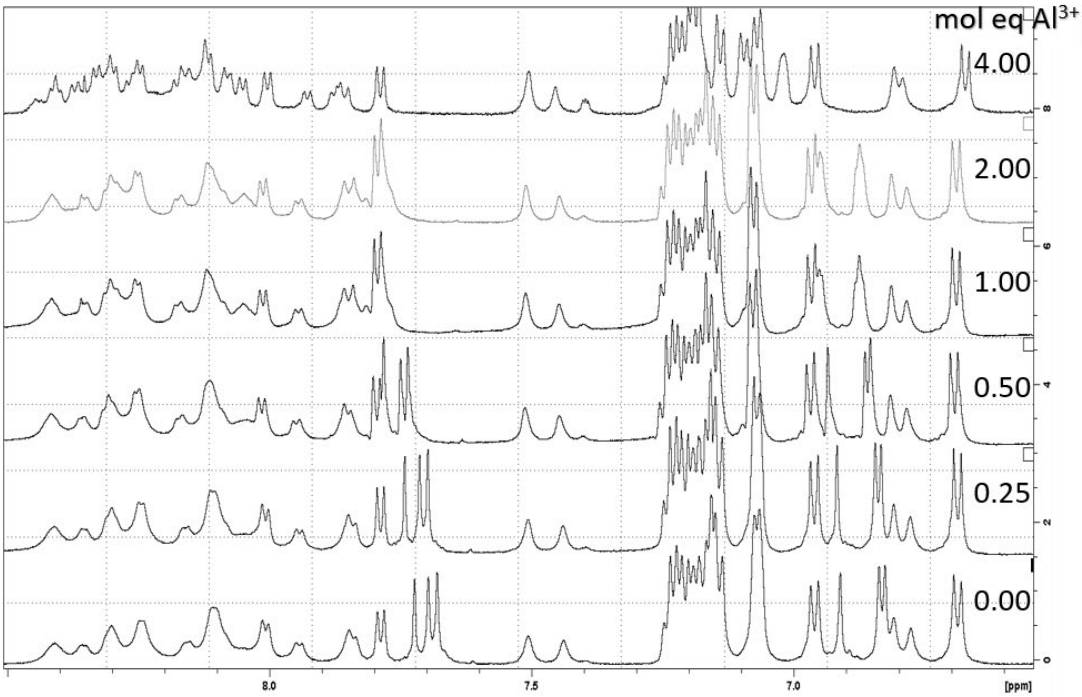

Figure 3.10 ^{1}H NMR titration of $A\beta_{1–28}$ with Al^{3+}. The titration was carried out in D_2O at 298 K and at a pH of 7.45 ± 0.01. Apo spectrum is for 2.4 mg of $A\beta_{1–28}$ dissolved in 10% H_2O:90% D_2O; the spectra are for the Aβ solution with incremental additions of Al^{3+} ranging from 0.0-4.0 molar equivalence (mol eq).

The chemical shift variations seen at 7.60-7.80 ppm and 6.80-6.95 ppm represent the respective protons of 2H and 4H, for the histidine residues (His6, His13 and His14). From Figure 3.10, the complex stoichiometry was observed in the mole ratio plot of Figure 3.11, by using the chemical shifts of perturbed histidine protons whose variations were more significant.

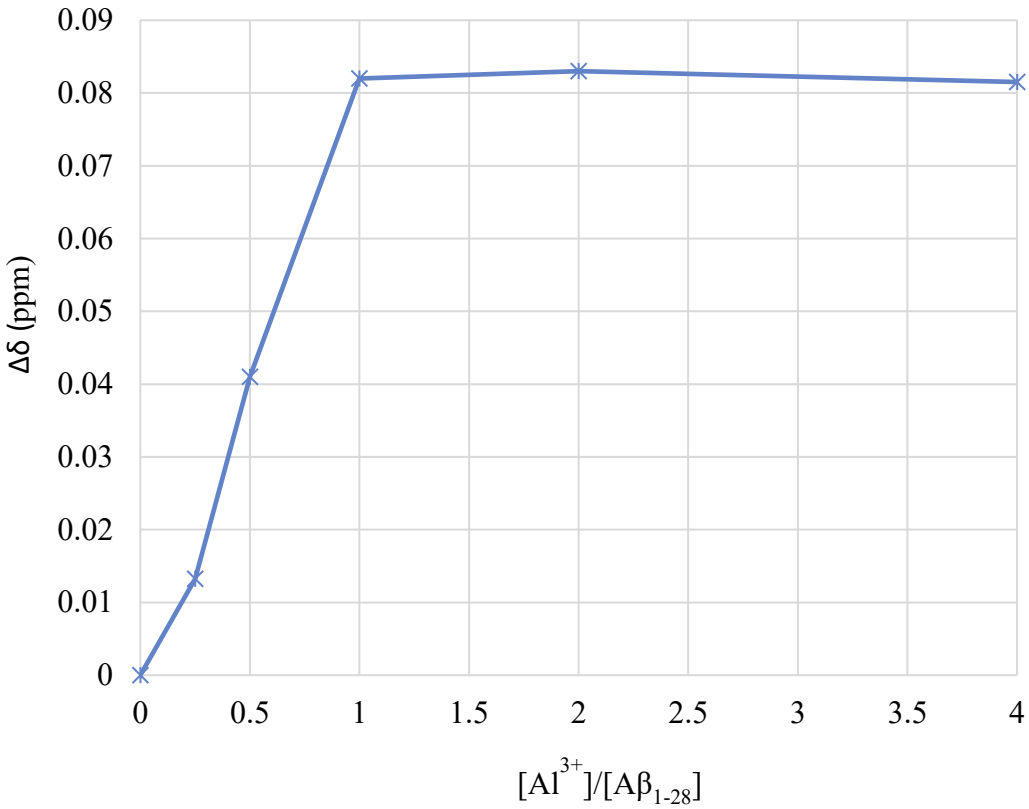

Figure 3.11 Molar ratio vs Δδ plot for the incremental addition of Al^{3+} to $A\beta_{1-28}$. The concentration of $A\beta_{1-28}$ is kept constant at 1.0 mM. The concentration ratio for Al^{3+} to $A\beta_{1-28}$ was varied from 0 to 4 molar equivalents. The stoichiometry Al^{3+} to $A\beta_{1-28}$ was found to be 1:1 as indicated by the abrupt changes in the slope of the curve.

The molar ratio plot in Figure 3.11, demonstrates the sum of the change in chemical shift (Δδ) of histidine protons, caused by the incremental addition of Al^{3+} plotted against the molar equivalence to Al^{3+} ($[Al^{3+}]/[A\beta_{1-28}]$), the stoichiometric ratio of the Al^{3+}: $A\beta_{1-28}$ complex was determined through mole ratio plot as shown in Figure 3.11. The abrupt changes in slope of the curve the stoichiometric ratio of the $Al^{3+}/A\beta_{1-28}$ complex was found to be 1:1.

3.2.5.3 Proposed coordination of Al^{3+} to $A\beta_{1-28}$

The structural data collected thus far from the broadening and chemical shift variation of ^{1}H and 2D NMR data reveal the specific residues involved in Al^{3+} binding. These amino acid residues are recapitulated in Figure 3.12.

Name of residue	Asp1	Arg5	His6	Try10	His13	His14	Phen19	Gly25	Lys28
Δδppm	0.15	0.09	0.42	0.05	0.31	0.40	0.07	0.11	0.12

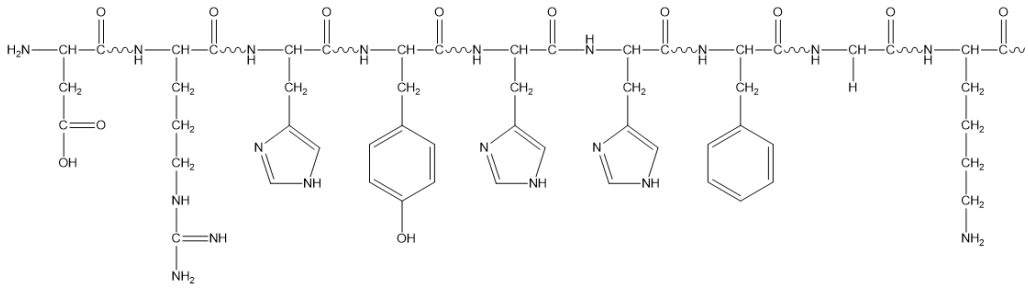

Figure 3.12 Schematic representation of the most affected residues in $A\beta_{1-28}$ by Al^{3+} addition.

At 298 K and pH 7.4, the residues mainly affected by Al^{3+} addition are the Asp1 and the three His. This is followed by Lys28, Gly25, Arg5, Phen19 and Tyr10. These results give rise to the coordination model of Figure 3.13 for the $A\beta_{1-28}$ peptide binding to Al^{3+}.

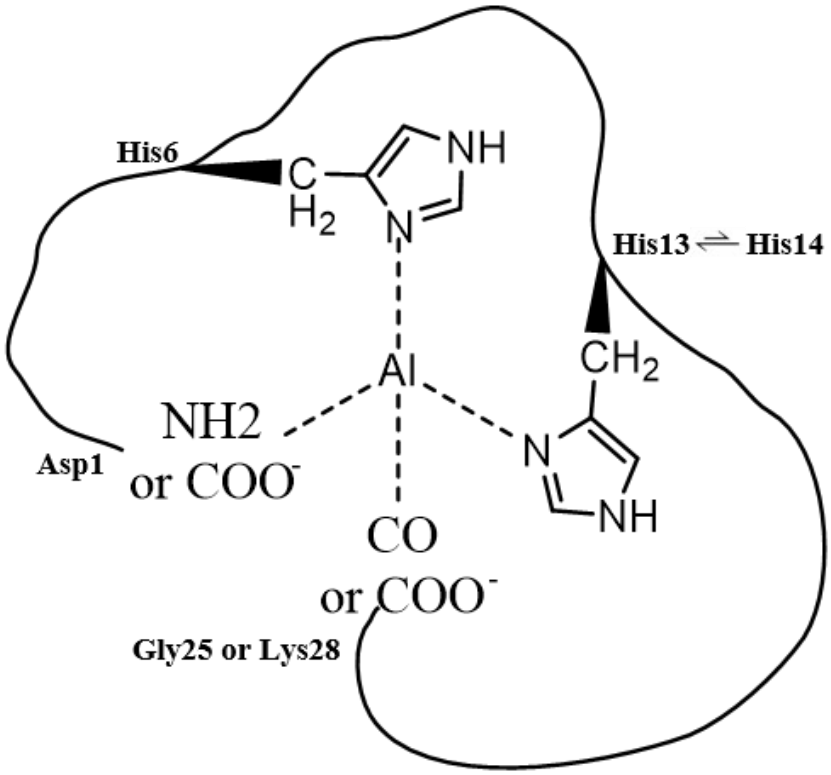

Figure 3.13. The proposed structure of Aβ$_{1–28}$ complexed with Al^{3+}. The Al^{3+} ion is coordinated through the imidazole nitrogens of the three histidine residues, His6, His13, and His14, the N-terminal Asp1 and Gly25/Lys28.

The binding involves the three histidines, the N-terminal Asp1 and Gly25/Lys28. The Arg5, Tyr10 and Phen19 were not significantly affected by Al^{3+} and thus its direct binding was ruled out. The Δδ of Arg5, Tyr10 and Phen19, are expected from residues in a turn to accommodate the Al^{3+} coordination of neighbouring resides. The Δδ of the βH of Lsy28 and Gly25 suggest the respective C-terminus and carbonyl are involved in binding. Due to the proximity of His13 and His14 it is impracticable the coordination for both is simultaneous. Instead it is suggested the imidazole rings of the residues His13 and His14 are in equilibrium for one binding position. With the His13 residue favoured due to the higher affinity.

3.3 Discussion

The amyloid β peptide is a major component of insoluble amyloid deposits in Alzheimer's disease, and the ability of Aβ to exist in different conformations is dependent on residues 1-28, $A\beta_{1-28}$ (Huang et al 2004), which is used in this study. Al^{3+} is likely to induce irregular aggregation behaviour of the Aβ peptide the main constituent of the senile plaques that is the hallmark of AD (Bolognin, 2011). In AD patients, Al^{3+} ions are found in the brain tissue (Mirza et al., 2017). It has been found that Al^{3+} can mediate the formation of amyloid plaques (Zhang et al., 2011). The previous data collected by using UV, Raman microscopy, CD spectroscopy and atomic force microscopy (AFM) techniques *in vitro* have provided quantitative and qualitative insights into the binding of metal ions (Zn^{2+}, Cu^{2+}) to Aβ via the histidine imidazole rings in isolated senile plaque cores of Alzheimer's disease brain (Dong et al., 2003; Syme et al., 2004; Danielsson et al., 2007; Marino et al., 2010; Bousejra-El Garah et al., 2011).

By using ^{1}H NMR my findings demonstrate that Al^{3+} ions interact with the Aβ peptide. The ^{1}H, NOESY and TOCSY NMR spectra of Aβ with the bound Al^{3+} illustrate several exchange phenomena, perturbations in the spectra (Figures 3.1 to 3.3). Using various Aβ analogues the involvement of histidine residues in Al^{3+} binding was verified (Figures 3.4 and 3.5).

Resonances perturbed by metal coordination are characteristically from protons within close proximity to the chelating metal ion. Data from $A\beta_{1-28}$, $A\beta_{1-28}$ H6A, $A\beta_{1-28}$ H13A, $A\beta_{1-28}$ H14A and $A\beta_{1-28}$ H6,13,14A analogues suggest that all three histidine residues and N-terminal amino group are involved in binding Al^{3+} ions. Addition of Al^{3+} to H13A and H6A resulted in the greatest difference in spectra relative to $A\beta_{1-28}$, supporting the observation by Liu et al. (2008) that His13 and His6 are crucial residues for metal binding. Interestingly, His13 is not present

in the Aβ of rats, and Aβ does not exhibit amyloid accumulation in aged rats' brains (Huang et al., 2004). This may indirectly highlight the critical role of His13 in human Aβ aggregation. The involvement of the N-terminus and histidine residues in Al^{3+} coordination to $A\beta_{1-28}$ is supported by Al^{3+} 2D NMR analysis in which only significant chemical shift perturbations of these residues are revealed. Previously identified residues in relation to coordination of metal ions including Ser8, Tyr10 and Val12 (Narayan et al., 2013) has no significant observable chemical shift variations. In summary, residues perturbed by the presence of Al^{3+} are primarily residues Asp1, His6, His13 and His14 while other resonances are relatively unaffected.

The comparison of Zn^{2+} and Al^{3+} coordination to Aβ demonstrates that both metal ions have similar potential to compete and strongly bind to the same His 6, 13 and 14 residues, as Zn^{2+} and Al^{3+} have a strong affinity for histidine imidazole rings.

The pathogenesis of AD involves the structural transition of Aβ from the predominantly random coil structure of soluble Aβ to a conformation of β-sheet in proto-filaments and aggregation of Aβ (L.C. Serpell, 2000). CSI data from NOESY and TOCSY suggest that the apo $A\beta_{1-28}$ produced a typical CSI values of the random coil and possible α-helix conformation. However, in the presence of aluminium the characteristic grouping of '+1' CSI values of titrated Aβ indicates conformational change of the peptide backbone from a random-coil structure to β-sheet. A β-sheet structure appears from Glu11 to Gln15. These observations provide support to the notion that Al^{3+} facilitates the transformation of the Aβ peptides from the initial random coil structure to the β-sheet in AD patients. This is consistent with studies by Zhang et al (2011) which was based on monitoring the Thioflavin T fluorescence and CD conformation curves of aluminium titrated $A\beta_{40}$. Hence, the findings in this chapter on the interaction of Al^{3+} with Aβ is of biological significance. Considering the abundance of non-biological aluminium in

drinking water, food sources and medicinal adjuvants, its uptake and potential interaction with Aβ presents an insidious risk for aging humans.

3.4 Conclusion

The interactions between metal ions Zn^{2+} and Al^{3+} with Aβ were analysed using NMR spectroscopy. The molecular data obtained through NOESY and TOCSY demonstrate, for the first time, that Al^{3+} can coordinate to Aβ strongly via the Asp1 and the three histidine residues. Secondary bind sites of the C-terminus and carbonyl of Lys28 and Gly25 are also indicated. The presence of Al^{3+} also initiates the transformation of Aβ secondary structure from random coil to β sheet, which is characteristic of amyloid oligomerization. The findings provide further evidence for the possible involvement of Al^{3+} in the pathogenesis of AD.

4 CHARACTERISATION, AND ASSESSMENT OF METAL COORDINATING ABILITY OF LIGANDS FOR DEVELOPING POTENTIAL THERAPEUTIC AGENTS

4.1 Introduction

As described in Chapter 1.3, metal ions (M^{n+}) play a wide range of roles such as enzyme cofactors, signalling messengers and redox participants in many physiological and pathological functions (Riordan, 1977; Okafor et al., 2017; Nam et al., 2018). Although biometals are crucial in neurobiological processes, metal ion overload or the presence of toxic metals such as aluminium are insidious to human health. Metal toxicity generally occurs as a result of exposure, dyshomeostasis and chronic accumulation. Molecules that have been designed to sequester excess metals from the brain are being explored as therapeutic agents in many neurodegenerative disorders, such as AD, Parkinson's disease (PD), Creutzfeldt-Jakob disease (CJD), and Amyotrophic Lateral Sclerosis (ALS) (Opazo et al., 2003; Sayre et al., 2005; Slivarichova et al., 2011; Sheykhansari et al., 2018; Portaro et al., 2019). Specifically investigated here are chelating molecules in order to identify lead molecules for the development of potential therapeutic agents.

The interaction of Al^{3+} with the Aβ peptide, shown in Chapter 3, is relevant to the *in vivo* environment, which in turn may play an important role in the aetiology of AD (D'Haese and De Broe, 2001; Bolognin et al., 2011; Exley and Vickers, 2014; Mirza et al., 2017). Increased concentrations of Cu^{2+}, Zn^{2+} and Al^{3+} are thought to be responsible for amyloid β (Aβ) plaque development, due to the presence of these metal ions in the Aβ plaque of post-mortem AD patients (Mirza et al., 2017).

With multitudes of alternative drug developments currently underway, Aβ metal-based therapeutics remains a promising prospect for the treatment of AD. However, the extended use of strong chelators such as CQ and desferrioxamine affects biometals homoeostasis, inhibiting physiological processes of essential metal binding to biomolecules including metalloenzymes. Apart from their cytotoxicity, these chelators rarely coordinate more Al^{3+}. Therefore, to prevent the adverse effects of synthetic chelators and find effective Al^{3+} chelators, natural occurring molecules with chelating abilities would be ideal.

Furthermore, metal-induced redox processes such as Cu^{2+}, induces result in the formation of ROS and subsequently oxidative stress is another feature of AD (Multhaup et al., 1996; Bush et al., 2003; Saporito-Magriñá et al., 2018). Although what initiates the biochemical mechanism for AD is still unclear, it is a logical step to prevent the interaction of excess metals with Aβ, and at the same time address the oxidative imbalance. Current therapeutic interventions are aimed at metal ions clearance in the brain, without targeting the oxidative stress. Antioxidant treatments have been studied alone as palliative options for the alleviation of AD symptoms (Prasad et al., 2000). Therefore, this study aims to evaluate natural ligands, their chelating potentials and antioxidant abilities.

I have used a panel of potential ligands (Figure 4.1) in a search for natural metal chelators. These ligands are naturally occurring, easily metabolised and not toxic to humans, including, histidine, glutathione, maltol, citric acid and malic acid. The amino acid, histidine has four potential coordination sites, through the carboxylate group, the amide group, and the two nitrogens of the imidazole. As presented in Chapter 3 the His6, His13 and His14 residues are the metal binding site within Aβ. The tripeptide, glutathione (GSH) is a potent physiological

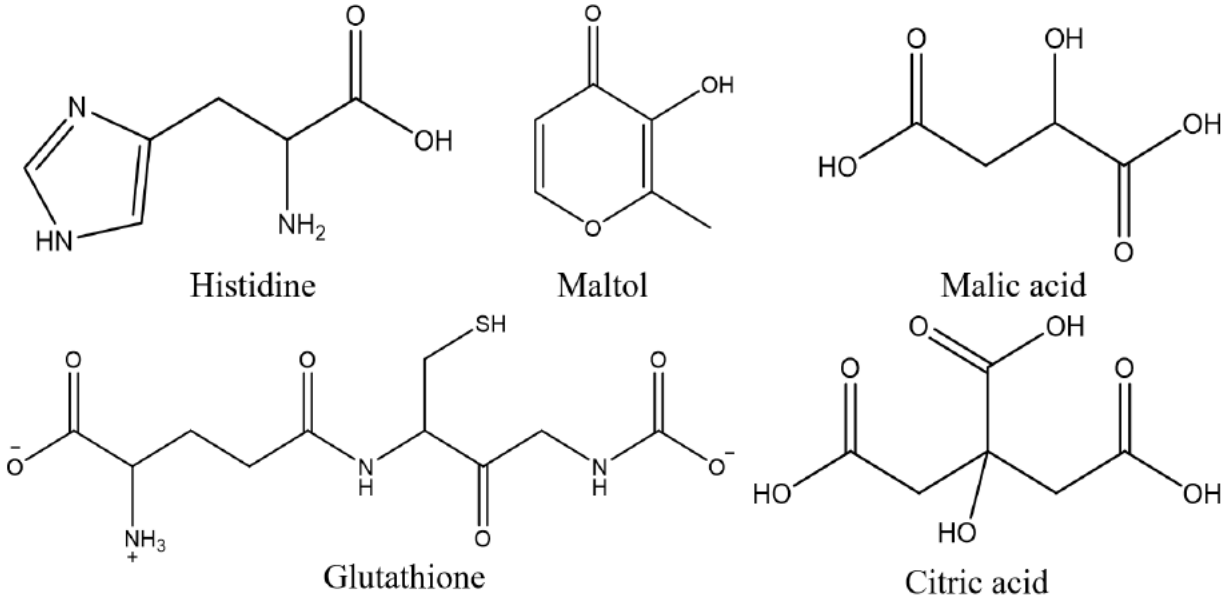

Figure 4.1 The panel of ligands used in this study. The molecules in the panel of metal ligands are explored for their chelation capability with metal ions (Al^{3+}, Cu^{2+} and Zn^{2+}).

chelator responsible for the cellular response, transport, and excretion of metal ions (Forman et al., 2009; Hernandez et al., 2015). It is also used as a biomarker in metal toxicity overload and it prevents cellular oxidative damage from reactive oxygen species formed by heavy metals. Maltol is a natural organic compound, and it is a potential agent for the removal of excess Al^{3+} ions within humans (Antipova et al., 2005). The organic acids, citric acid (2-hydroxypropane-1,2,3-tricarboxylic acid) and malic acid (2-hydroxybutanedioic acid) are biological metabolites in the human body and plants. The ability of citrate coordinating to metal ions has long been used by plants and microbes (Silva et al., 2009). Malic acid and citric acid are released from the roots apex by plants as a response to Al^{3+} accumulation (Ma, 2000).

The main aim of this chapter is therefore to test natural and synthetic ligands for their metal-chelating ability. Using ^{1}H NMR to titrate them with a panel of metal ions to determine their coordination sites and binding modes. The stability and coordination strength of the metal ligand complex were analysed and assessed by molecular modelling. The electronic structure

calculations were performed with the aid of the computer programs, HyperChem 8.0 and Chem3D 15.1. These programs were employed for determination of the optimised structures of metal-ligand complexes, minimum binding energies and HOMO energy values.

4.2 Results

4.2.1 NMR analysis for the coordination of metal ions by individual ligands

4.2.2 Histidine

The details of metal ion binding to histidine revealed by ^{1}H NMR are shown in Figure 4.2, including ^{1}H NMR spectra of histidine only (apo His), and histidine plus 0.5 molar equivalent of metal ion Al^{3+}, Cu^{2+} and Zn^{2+} respectively. The spectrum for apo histidine is labelled with the corresponding resonances ^{1}H δ (ppm) to the structure of histidine (top). The respective protons are, αH, 3.88; βH, 3.07; 4H, 6.95; 2H, 7.63ppm.

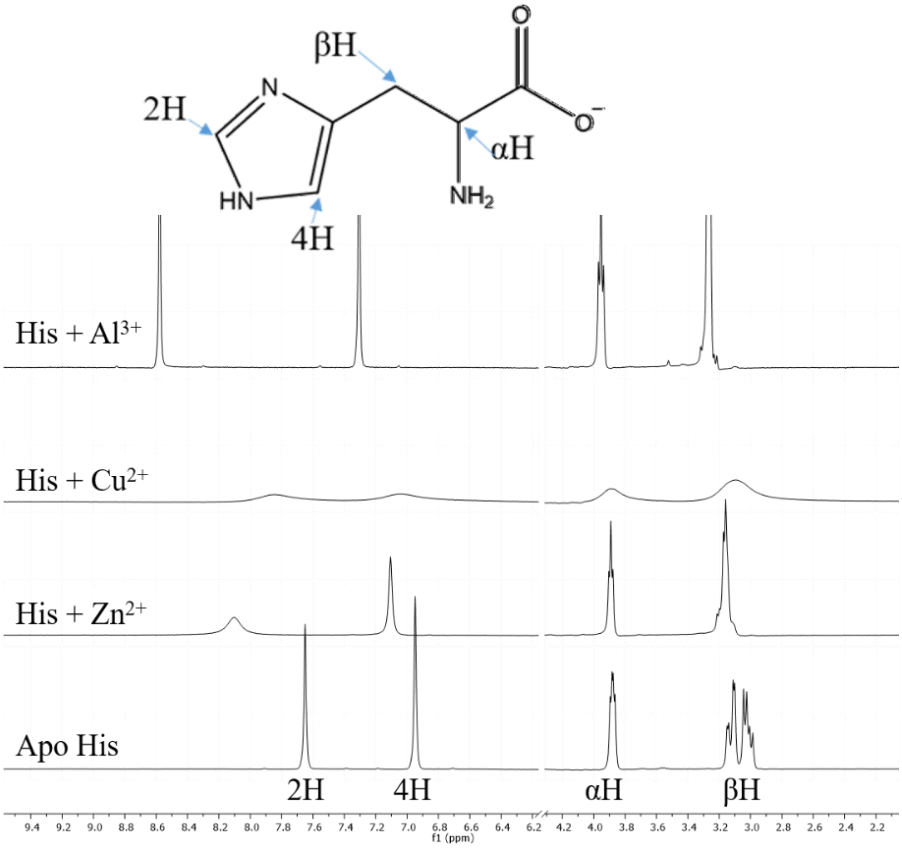

Figure 4.2 ^{1}H NMR spectra of metal ions with histidine. Experimental conditions: 10% H_2O:90% D_2O at pH 7.4 ± 0.05 (adjusted with phosphate buffer, the final phosphate concentration is 10 mM), assay temperature 298K. The chemical structure of histidine is shown (top) with assigned protons labelled for the corresponding resonances. Spectra from bottom to top are apo His, His + Zn^{2+}, His + Cu^{2+} and His + Al^{3+}. In each of the metal ion titrations, the [M^{n+}]/[His] ratios are 0.5.

The resonances at 6.95 and 7.95 ppm, corresponding to imidazole 4H and 2H, were relatively most deshielded with the addition of Al^{3+} and Zn^{2+}, indicating strong coordination of histidine through imidazole. The relatively small extent of deshielding and line broadening of the αH and diastereotopic βH at δ 3.90 and 3.10 ppm suggests the amide and carboxyl groups may also be involved in the coordination with Al^{3+} and Zn^{2+}, albeit to a weaker degree.

Due to the paramagnetic nature of Cu^{2+} significant line broadening occurred and minimum CSP can be measured. Minor upfield shifts of resonance of imidazole 2H, indicating coordination of Cu^{2+} by histidine. However, detailed binding analysis was not possible due to the line broadening. As Ni^{2+} often mimics Cu^{2+} in binding to ligands (Klewpatinond and Viles, 2007), Ni^{2+} was therefore used as a surrogate of copper in the ^{1}H NMR titration with histidine in order to understand binding tendencies of copper without the interference of its paramagnetic property. The NMR titration spectra for Ni^{2+} titration is presented in Figure 4.3.

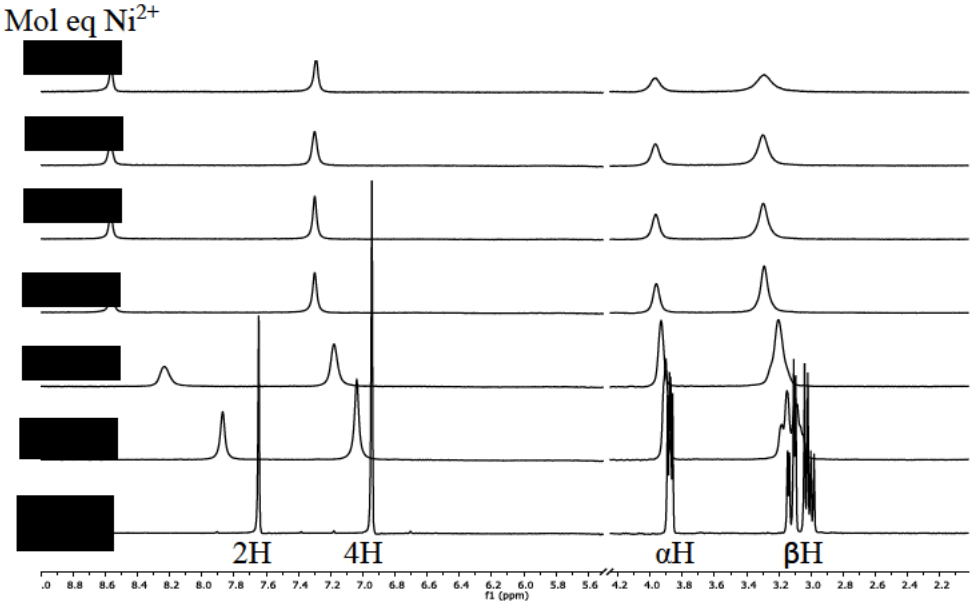

Figure 4.3 ^{1}H NMR titration of histidine with Ni^{2+}. Experimental condition: 10% H_2O:90% D_2O at pH 7.4 ± 0.05 (adjusted with phosphate buffer, the final phosphate concentration is 10 mM), assay temperature 298K. 1st spectrum is 10 mM histidine apo His; spectra 2 to 7 are for incremental additions of the Ni^{2+} solution to the apo histidine. In each of these later solutions the $[Ni^{2+}]$/[His] ratios (from the bottom) are as follows: 2nd 0.1; 3rd, 0.25; 4th, 0.5; 5th, 0.75; 6th, 1.00 and 7th, 2.00. The spectra show the key resonances affected by the addition of Ni^{2+}.

Similar to Al^{3+} and Zn^{2+}, the chemical shift variations from Figure 4.3 indicates Ni^{2+}, and by extension Cu^{2+}, can bind to histidine. The deshielding of histidine's 4H and 2H resonances upon

the addition of Ni^{2+}, seen in Figure 4.3, indicates the involvement of the imidazole NH. The relatively small extent of deshielding of αH and diastereotopic βH suggests the amide and carboxyl groups may also be involved in the weak coordination. The overall line broadening indicates slow exchange, consistent with the formation of two complexes for the copper coordination, as seen in Figure 4.4.

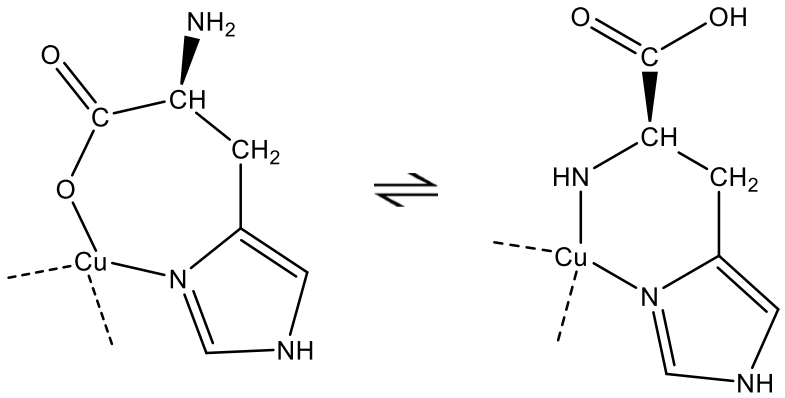

Figure 4.4 Two proposed structures of the copper-histidine complex. Coordination modes of histidine to Cu^{2+} are glycine-like (N-Cu-O) and histamine-like (N-Cu-N).

The changes in chemical shift (Δδ) caused by the incremental additions of metal ions, in the ^{1}H NMR titration of histidine were calculated. The largest deshielding caused by metal titration was observed for 2H of the imidazole group. Figure 4.5 presents the mole ratio plots for the $[M^{n+}]/[His]$ and chemical deshielding of the 2H protons. These plots were used to determine stoichiometry.

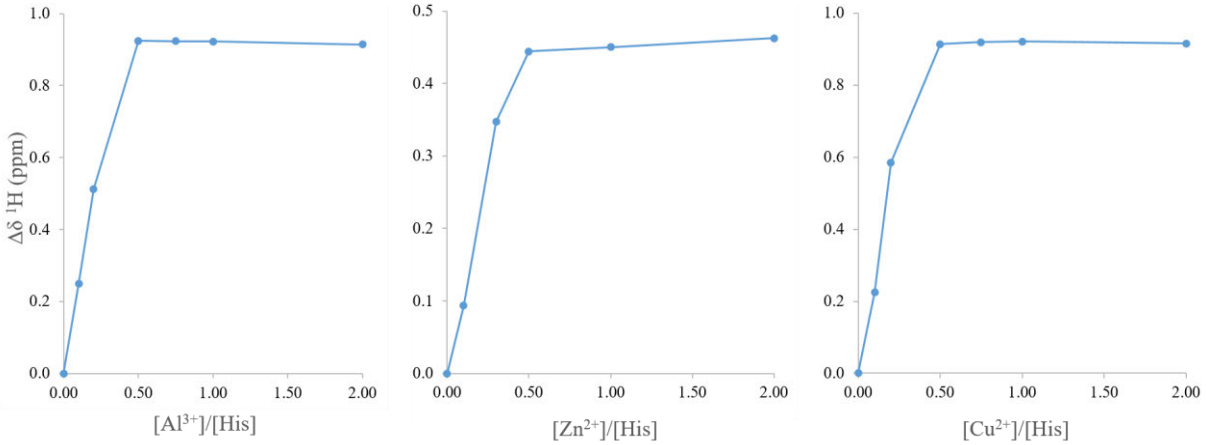

Figure 4.5 Molar ratio vs Δδ plots for the metal ions to histidine. The concentration of histidine is kept constant at 10 mM and the respective metal ion concentration was varied from 0.0 to 2.0 molar equivalents. Each slope represents the respective change in chemical shift (Δδ) for the resonances against the $[M^{n+}]/[His]$ ratio. The stoichiometry of Al^{3+}, Zn^{2+} and Cu^{2+} to histidine was found to be 1:2 as indicated by the abrupt changes in slope.

From the changes in the slope at lower mole ratios followed by the abrupt plateau after the $[M^{n+}]/[His]$ of 0.5 indicates the stoichiometry of 1:2 for histidine complexes with Al^{3+}, Cu^{2+} and Zn^{2+}.

With the determination of binding sites and stoichiometric ratio, molecular modelling was used to obtain structural information on the coordination modes. Molecular mechanic studies provide the energy minimized conformation. While solvent effect is important in the complexes, computational model isolated molecule calculations of the metal-ligand complexes without solvent effect or the coordinated water molecules. The bare system studies allow the analysis of interactions between metal ions and the ligands. The MM2 and Huckel calculations were employed in the determination of the metal-ligand complexes optimized structures, relative minimum binding energies and HOMO energy values (Table 4.1).

Table 4.1 The optimized binding structures and energies of metal-histidine complexes. The proposed structures of metal-histidine complexes, relative energies and HOMO energy values of proposed energy-minimized molecular structures of metal-histidine complexes. The total energies for each complex are relative to the complex with the lowest calculated MM2 (Cu-His). Colour codes: C, grey; H, white; O, red; N, blue; M^{n+}, dark grey.

	Al(His)$_2$	**Zn(His)$_2$**	**Cu(His)$_2$**
General scheme of metal-His complex	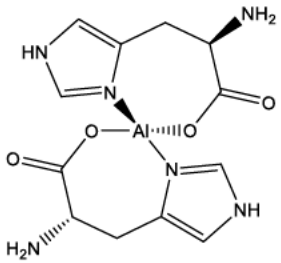	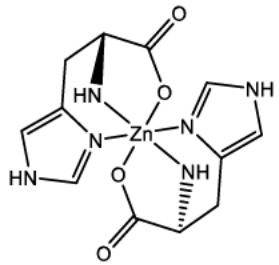	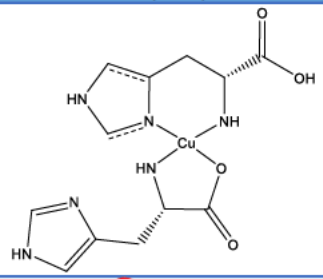
Proposed energy minimized structure of metal-His complex	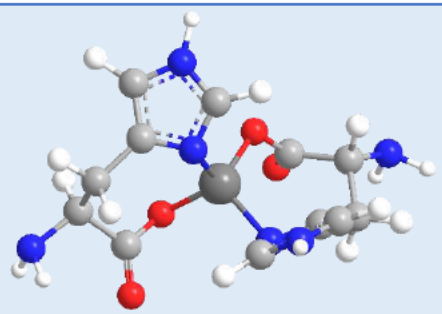	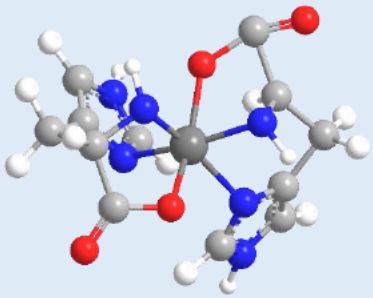	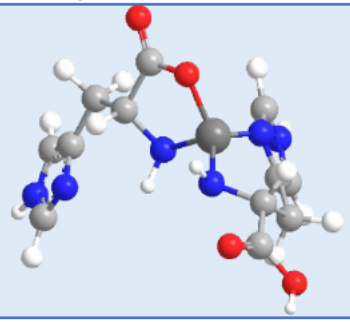
MM2 (total energy) in kcal/mol	61.33	107.62	0
HOMO values (eV)	-6.010	-8.554	-9.513

4.2.3 Glutathione (GSH)

In order to determine the metal ion binding sites in GSH, the ^{1}H resonance assignments of all protons in the tripeptide were first performed employing 2D cosy NMR correlations (Figure 4.6). Assignments are summarised in Table 4.2.

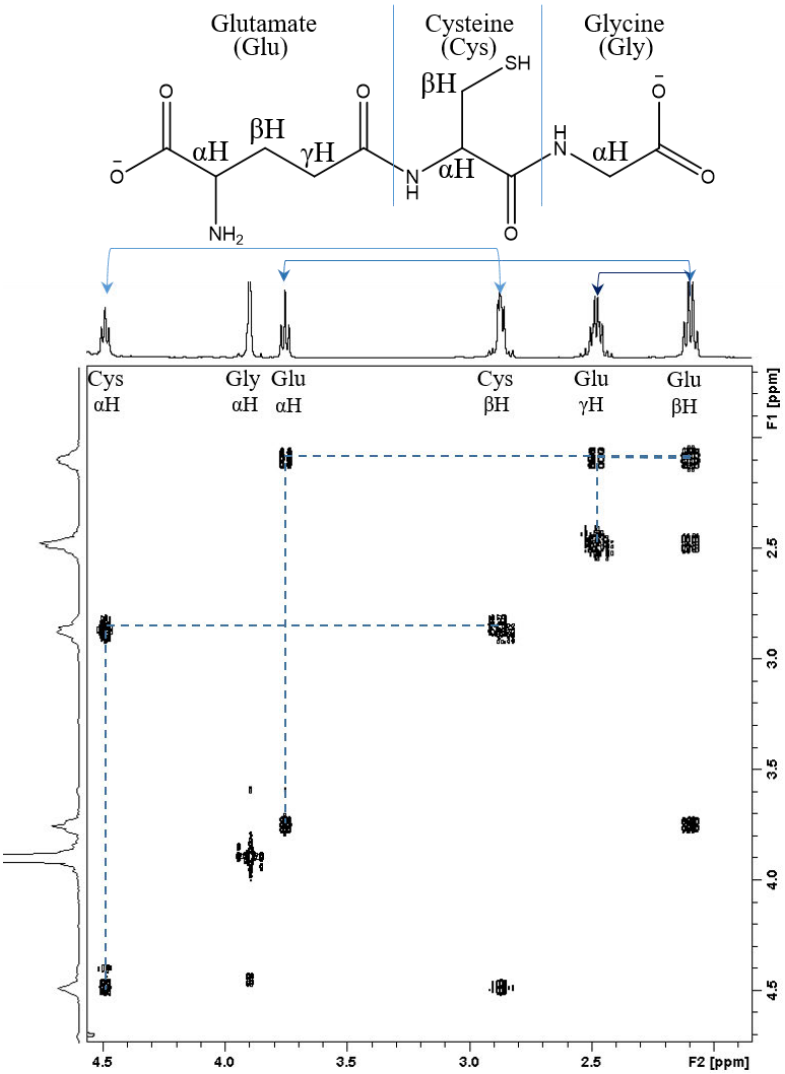

Figure 4.6. 2D ^{1}H-^{1}H COSY NMR spectrum of GSH. Experimental condition: 10 mM GSH in D_2O at pH 7.4 ± 0.05 (adjusted with phosphate buffer, the final phosphate concentration is 10 mM), assay temperature 298K. The labelled GSH structure (top) correspond to the assignment of the protons and cross peaks on the spectra.

Table 4.2 ^{1}H NMR resonance assignments of GSH

Residues	Experimental chemical shifts (ppm) of amino acid residues of GSH*			
	NH	αH	βH	Others
Glutamate (Glu)	7.77	3.71	2.07	γH- 2.47
Cysteine (Cys)	8.28	4.49	2.88	
Glycine (Gly)	8.39	3.78		

*obtained from the ^{1}H NMR and COSY experiments

GSH has numerous potential binding sites including two carboxylate groups, an amino group, and a thiol group. Identifying which of these are involved in the coordination to Al^{3+}, Cu^{2+} and Zn^{2+}, involved carrying out ^{1}H NMR titrations of metal ion in aqueous solutions of GSH at physiological pH and 298 K. Figure 4.7 compares ^{1}H NMR spectra of apo GSH, to GSH in the presence 0.5 molar equivalents, of metal ions. The addition of Al^{3+}, Cu^{2+} and Zn^{2+} results in various changes to the resonances of GSH, such as CSP and line broadening.

^{1}H NMR spectra shown in Figure 4.7 were used to determine the metal binding sites in GSH. The addition of metal ions induced CSP of resonances in GSH. Characteristic CSP patterns of chelated GSH provides indications of a coordination mode.

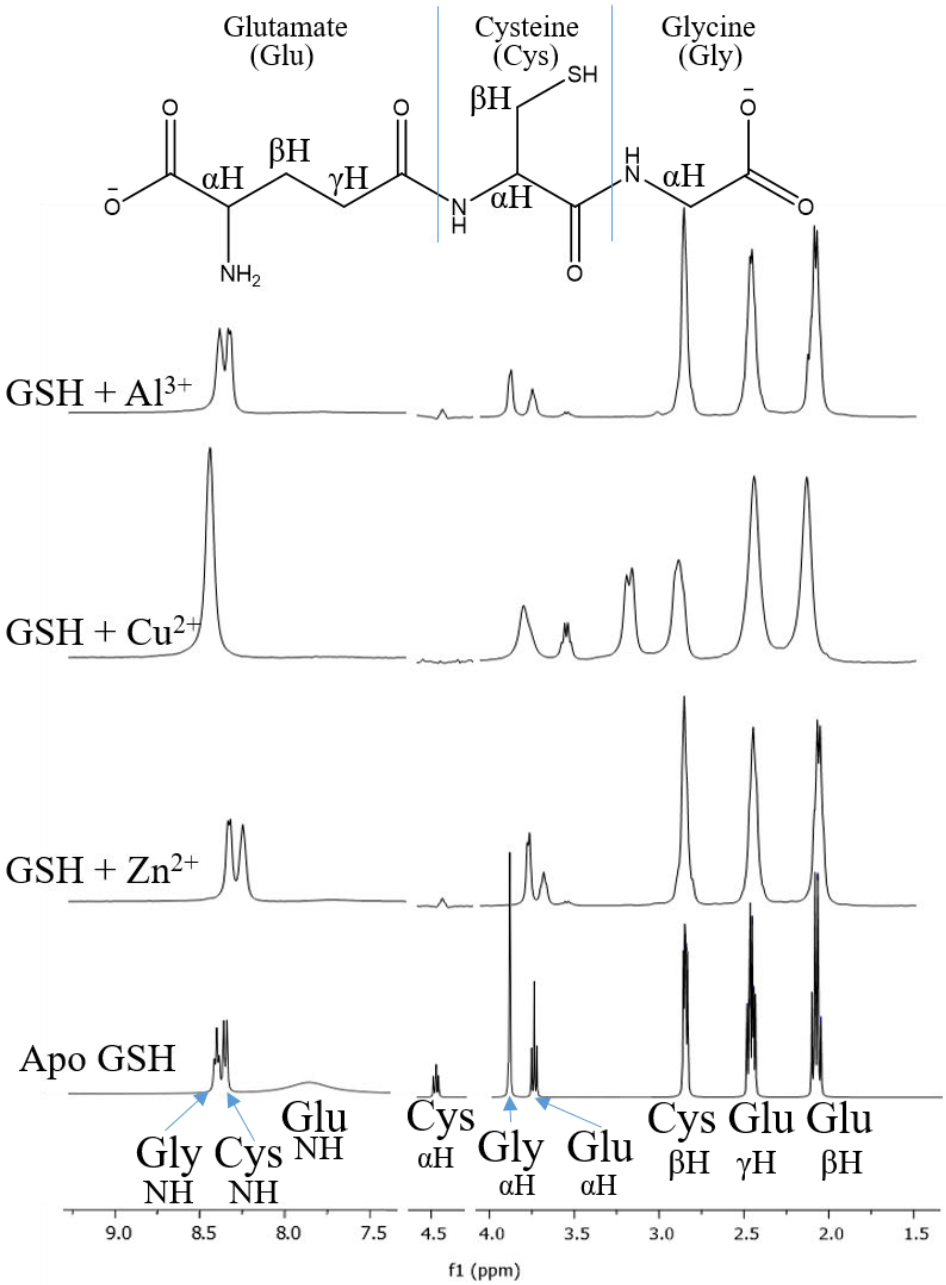

Figure 4.7 ^{1}H NMR titration of metal ion with GSH. Experimental condition: 10% H_2O:90% D_2O at pH 7.4 ± 0.05 (adjusted with phosphate buffer, the final phosphate concentration is 10 mM), assay temperature 298K. The chemical structure of GSH is shown (top) with assigned protons labelled for the corresponding resonances. From bottom to top, apo GSH, GSH + Zn^{2+}, GSH + Cu^{2+} and GSH + Al^{3+}. In each of these later solutions the [M^{n+}]/[GSH] ratios was 0.5. The intensity of the δ ppm of CH was significantly reduced due to the proximity to the suppressed water signal at 4.70 ppm.

The complexation with Al^{3+} resulted in the broadening of the resonance peaks in GSH. The presence of signals of the two NH protons of the glycine and cysteine indicated that they are not directly involved in the coordination to Al^{3+}. The NH signals are shifted upfield, which suggests that the neighbouring groups may be involved in coordination with the metal. The disappearance of the broad NH of glutamate indicates direct coordination at this site. However, as aluminium prefers oxygen donors, the loss of the NH_2 signal may also reveal a strong coordination to the glutamic acid carboxyl group. Hence the binding interactions with Al^{3+} are mainly via two negatively charged carboxylate groups of glycine and glutamate.

The addition of Cu^{2+} results in the βH resonance of the cysteine's slight downfield shift with a considerable line broadening. Because of the Cu^{2+} redox potential, the overall oxidation shown in reaction Equation (4.1) takes place which results in the formation of the oxidised form of GSH, GSSH. The spectral change and lack of line broadening seen in Figure 4.7 can be explained in terms of the formation of Cu^{+}-GS^{-} as indicated in reaction Equation (4.2). Since Cu^{+} is a diamagnetic metal ion, excessive line broadening is not observed. However, with the addition of excess Cu^{2+} the resonances experienced the line broadening effect of the NH of glycine and cysteine, due to the formation of the paramagnetic GSSG-Cu complex corresponding to Equation (4.3). The significant down field shift of the αH of the glutamate residue is consistent with the coordination of Cu^{2+} to the carboxylate and amide groups.

$$2\mathrm{GSH} + \mathrm{Cu}^{2+} \rightleftharpoons (\mathrm{GSSH}) + \mathrm{Cu}^{+} + \mathrm{H}^{+} \tag{4.1}$$

$$\mathrm{GSH} + \mathrm{Cu}^{+} \rightleftharpoons (\mathrm{Cu}^{+} - \mathrm{GS}^{-}) + \mathrm{H}^{+} \tag{4.2}$$

$$\mathrm{GSSH} + \mathrm{Cu}^{2+} \rightleftharpoons (\mathrm{Cu}^{2+} - \mathrm{GSSG}) + \mathrm{H}^{+} \tag{4.3}$$

The addition of Zn^{2+} resulted in the downfield shift of the NH of glycine and cysteine. This suggests the involvement of thiol group of cysteine in the coordination of GSH to Zn^{2+}. The αH

of glycine is also significantly deshielded suggesting the formation of the GSH-Zn^{2+} complexes, where Zn^{2+} is chelated by the NH_2 or CO_2^- of the end amino group of glycine.

The numerical change in chemical shift (Δδ) caused by the incremental additions of metal ions, in the ^1H NMR titration of GSH were calculated. The significantly large deshielding of each metal titration was observed for ^1H resonances of the glutamic acid (E) αCH group. Figure 4.8 presents the mole ratio plots for the $[M^{n+}]/[GSH]$ and chemical deshielding for the Δδ of glutamic acid (E) αCH group.

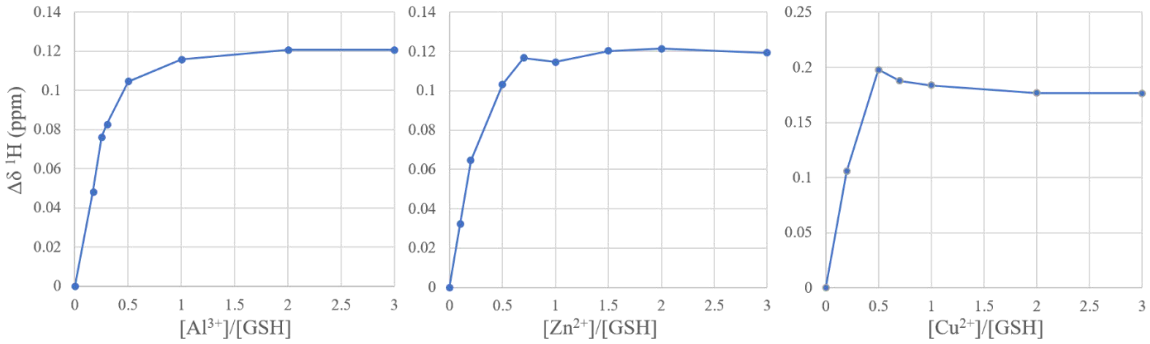

Figure 4.8 Molar ratio vs Δδ plots for the incremental addition of metal ions to GSH. The concentration of GSH is kept constant at 10 mM and the respective metal ion concentration was varied from 0.0 to 3.0 molar equivalents. Each slope represents the respective change in chemical shift (Δδ) for the resonances against the $[M^{n+}]/[GSH]$ ratio. As indicated by the slope, the stoichiometry of Al^{3+}, Zn^{2+} and Cu^{2+} to GSH was found to be 1:2, with potential 1:1 binding mode for Al^{3+} and Zn^{2+}.

From the abrupt change at lower mole ratio followed by the plateau in the slope after the $[M^{n+}]/[GSH]$ of 0.5 indicates a stoichiometry of 1:2 for GSH complexes with Cu^{2+} and Zn^{2+}. The mole ratio plot for Al^{3+} and Zn^{2+} with GSH indicates the possible formation of a 1:1 and 1:2 complex for Al^{3+} and Zn^{2+}.

Due to the multiple binding sites detected for GSH, many configurations were tested. Using the data collected thus far, the electronic structure calculations were performed. Table 4.4 illustrates the GSH and metal complexes with the optimized structures, lowest relative binding energies and the corresponding HOMO values.

Table 4.3 The optimized binding structures and energies of metal-GSH complexes. The proposed structures of metal-GSH complexes, relative energies and HOMO energy values of proposed energy-minimized molecular structures of metal-GSH complexes. The total energies for each complex are relative to the complex with the lowest calculated MM2 (Zn-GSH). Colour codes: C, grey; H, white; O, red; N, blue; S, yellow; M^{n+}, dark grey.

	Al(GSH)2	Zn(GSH)2	Cu-GSSH
General scheme of metal-GSH complex	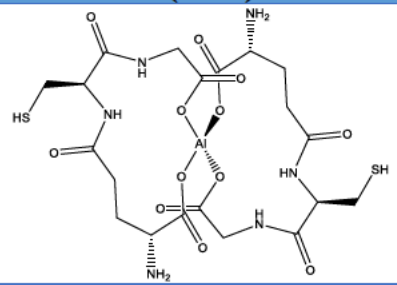	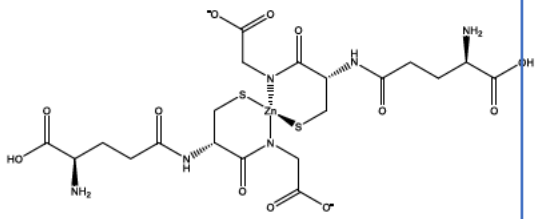	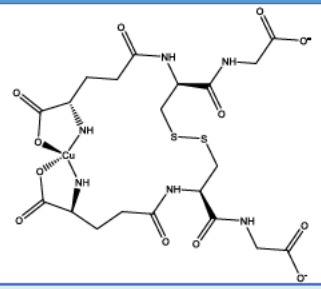
Proposed energy minimized structure of metal-GSH complex	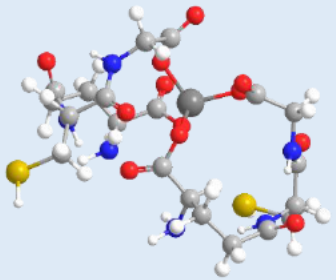	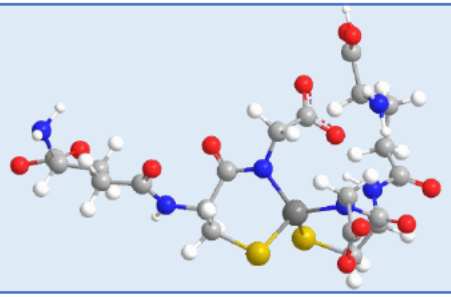	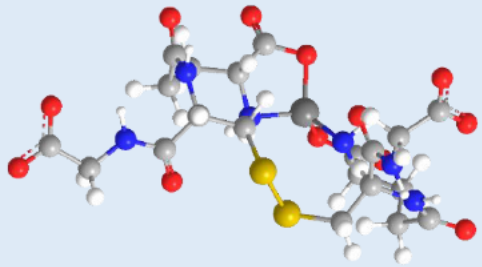
MM2 (total energy) in kcal/mol	110.0638	0	69.8705
HOMO values (eV)	-9.843	-9.315	-9.728

4.2.4 Maltol

The details of metal ion binding to maltol (Mal) by ^{1}H NMR are shown in Figure 4.9, including ^{1}H NMR spectra of maltol only (apo Mal), and maltol plus 0.5 molar equivalent of metal ion Al^{3+}, Cu^{2+} and Zn^{2+} respectively. The spectrum for apo maltol is labelled with the corresponding resonances δ^1H (ppm), and the structure of maltol. The assignments for the respective protons are, 6H, 7.92; 5H, 6.43 and CH_3, 2.30 ppm.

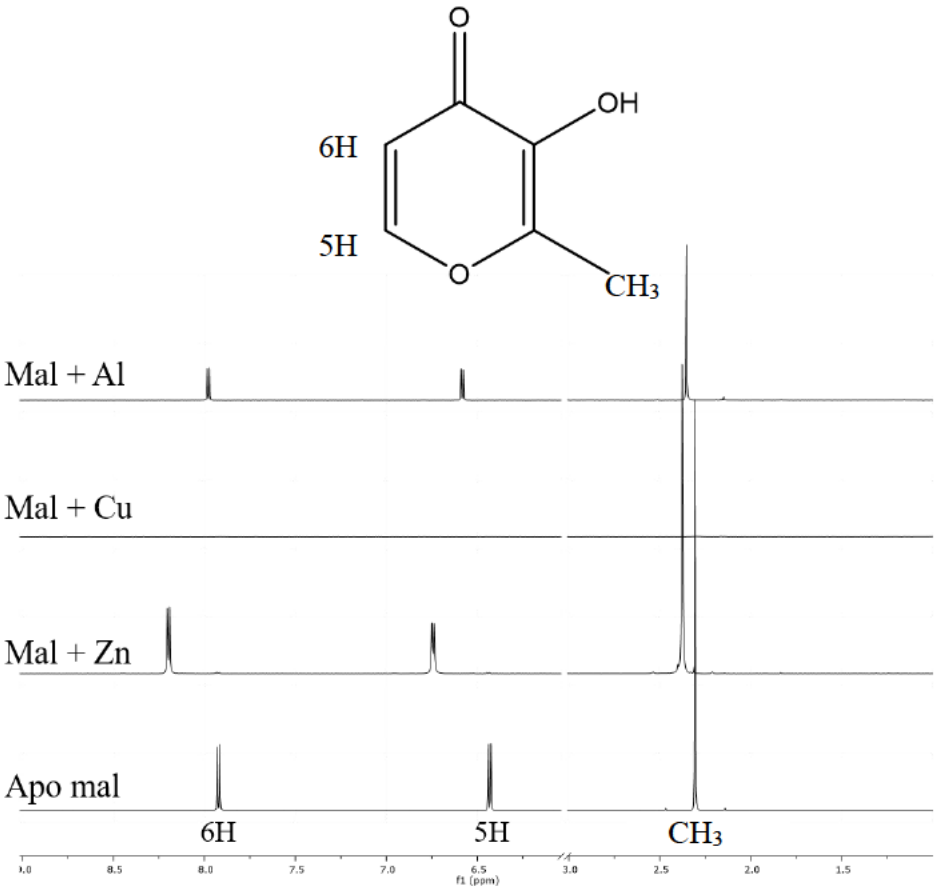

Figure 4.9 ^{1}H NMR titration of metal ion with maltol (mal). Experimental condition: 10% H_2O:90% D_2O at pH 7.4 ± 0.05 (adjusted with phosphate buffer, the final phosphate concentration is 10 mM), assay temperature 298 K. From bottom to top, apo mal, mal + Zn^{2+}, mal + Cu^{2+} and mal + Al^{3+}. In each of these later solutions the $[M^{n+}]/[Mal]$ ratios (from the bottom) is 0.5. The chemical structure of maltol is shown (top) labelled with the corresponding assigned protons and resonances.

Due to the heavy precipitation of apo maltol at the assay temperature 298 K and the line broadening effect of Cu^{2+}, the NMR titration of maltol with metal ions was not used to determine stoichiometry. The metal-maltol complexes were synthesised as per Chapter 2.1.5. The stoichiometric calculations of maltol-metal complexes were based on data of elemental analysis (Table 4.4).

Table 4.4 Analytical data of metal-maltol complexes

Compound	Formula	Yield (%)	Analysis (%) found (Calculated)		
			C	H	M^{n+}
$Al(Mal_3)_3$	$Al(C_6H_5O_3)_3$	78.3	53.75 (53.74)	4.10 (3.76)	6.78 (6.71)
$Zn(Mal)_2$	$Zn(C_6H_5O_3)_2.2H_2O$	77.6	40.65 (40.99)	3.79 (4.01)	18.51 (18.60)
$Cu(Mal)_2$	$Cu(C_6H_5O_3)_2$	73.4	46.15 (45.94)	3.01 (3.21)	20.07 (20.25)

From the data clearly the experimental values shown for each of the complexes are in good agreement with the theoretical values. The calculated ratio of the complexes of Al^{3+} was 1:3, while for the complexes of Cu^{2+} and Zn^{2+} the ratio was 1:2.

With the known stoichiometric ratio and ability of maltol to act as a strong bidentate ligand coordinating through the carbonyl group and the α-OH group, molecular mechanics were carried out. The relative stability and the coordination strength of the metal-maltol complexes from the relative minimum energies and HOMO energy values for all energy minimized conformation of the metal-maltol complexes are presented in Table 4.5.

Table 4.5 The optimized binding structures and energies of metal-maltol complexes. The proposed structures of metal-maltol complexes, relative energies and HOMO energy values of proposed energy-minimized molecular structures of metal-citric acid complexes. The total energies for each complex are relative to the complex with the lowest calculated MM2 (Cu-mal) Colour codes: C, grey; H, white; O, red; M^{n+}, dark grey.

	Al(mal)$_3$	**Zn(mal)$_2$**	**Cu(mal)$_2$**
General scheme of metal-GSH complex	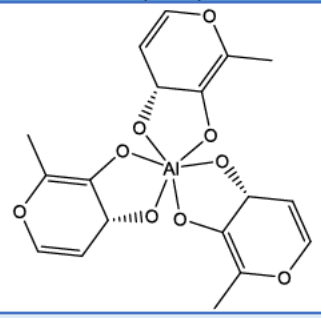	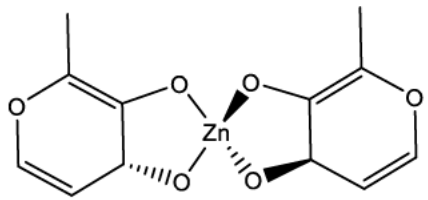	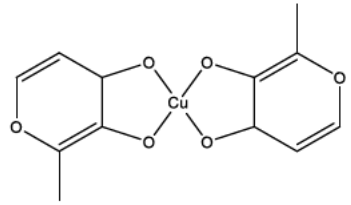
Proposed energy minimized structure of metal-GSH complex	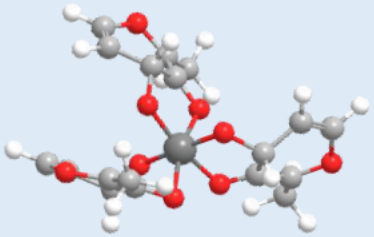	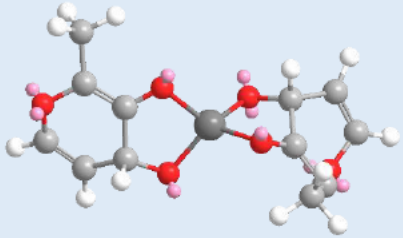	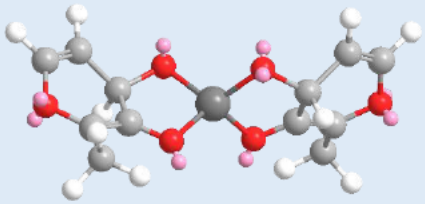
MM2 (total energy) in kcal/mol	78.309	10.081	0
HOMO values (eV)	-8.757	-8.900	-8.921

4.2.5 Citric acid

The structure of citric acid has three ionisable protons; at pH 7.4 these acidic hydrogens would be deprotonated to from citrate as shown in Figure 4.10 (top). The symmetric configuration of citrate yields two enantiotropic CH_2COOH groups, thus citric acid/citrate is classified as prochiral. The equivalent enantiotropic hydrogens of CH_2 in citrate exhibit indistinguishable protons signals in NMR. As such the only proton detected by ^1H NMR is the enantiotropic hydrogens at 2.51 ppm. The hydrogens resonances overlay each other but display splitting due to the prochirality of citrate. The ^1H NMR metal titrations of citrate (CA) and metal ions (Al^{3+}, Cu^{2+} and Zn^{2+}) caused CSP of the enantiotropic hydrogens.

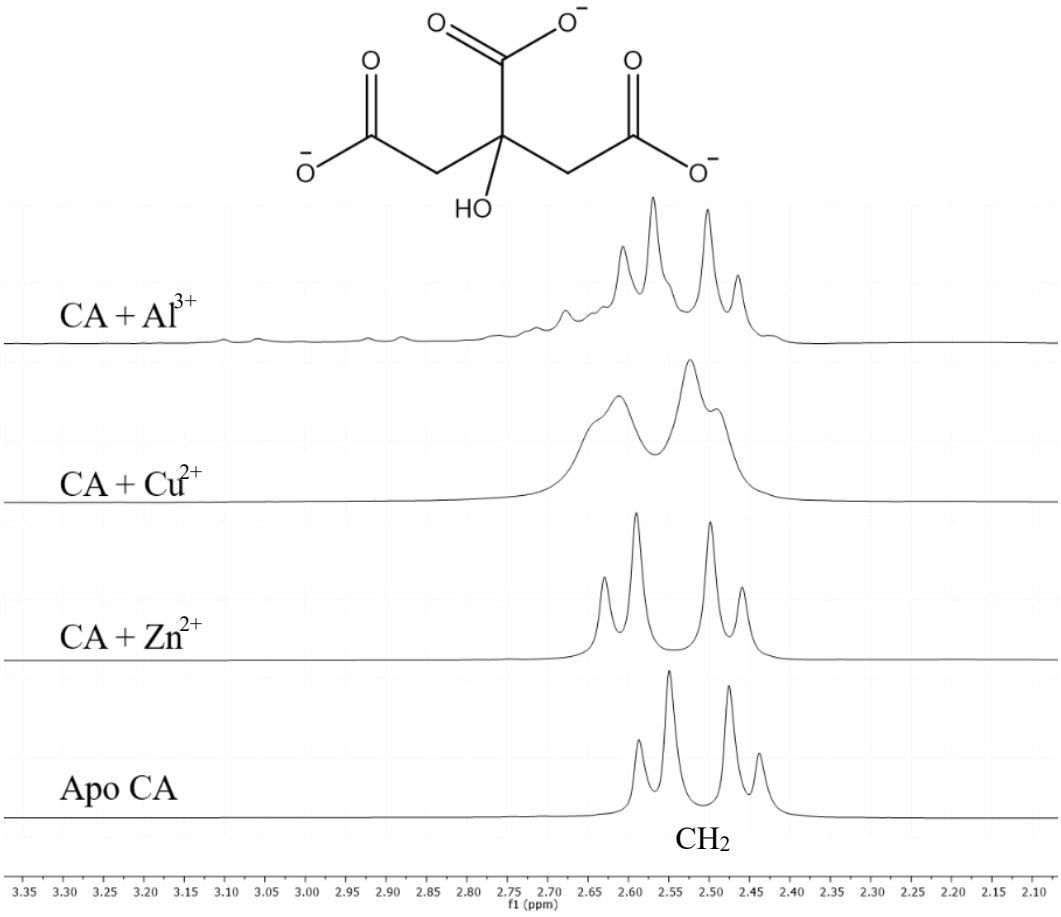

Figure 4.10 ^{1}H NMR spectra for metal ions and citric acid. The chemical structure of citrate (CA) are indicated (top). Experimental condition: 10% H_2O:90% D_2O at pH 7.4 ± 0.05 (adjusted with phosphate buffer, the final phosphate concentration is 10 mM), assay temperature 298 K. From bottom to top, apo CA, CA + Zn^{2+}, CA + Cu^{2+} and CA + Al^{3+}. In each of these later solutions the [M^{n+}]/[CA] ratios (from the bottom) is 0.5. The chemical structure of citrate (top) are indicated. The respective protons assignments of the doublet of doublets at δ 2.51 ppm is the enantiotropic hydrogens of the two CH_2COO^- groups.

Figure 4.10 shows the 1D proton NMR spectra of citric acid with 0.5 mole equivalent of metal ions, Al^{3+}, Cu^{2+} and Zn^{2+}. All resonances of citric acid are affected by the addition of metal ions with three ionisable protons. Citric acid is a tridentate ligand, with all three COO^- groups acting as potential binding sites.

The addition of Cu^{2+} and Zn^{2+} results in the upfield shift of the overlapping signal of the enantiotropic hydrogens, suggesting the coordination of the metal ions occurs via both terminal carboxylic acid groups. However, the addition of Al^{3+} caused significant splitting (Figure 4.11) as the two sets of CH_2 protons are now visibly different. This observation is thought to be a result of Al^{3+} binding to one terminal carboxylic acid group, causing a loss in the molecule's symmetry.

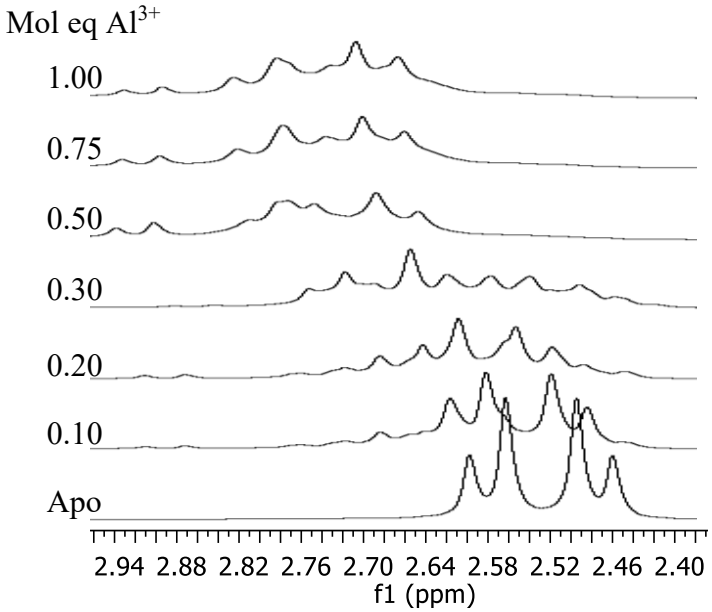

Figure 4.11 ^{1}H NMR Al^{3+} titration of citric acid. 1st spectrum is for apo 10 mM citrate in 10% H_2O:90% D_2O buffered by 10 mM phosphate at a pH of 7.4 ± 0.05 and at 298K; spectra 2 to 7 are for incremental additions of Al^{3+} to the apo CA solution. In each of these later solutions the $[M^{n+}]/[CA]$ ratios (from the bottom) are as follows: 2nd 0.10; 3rd, 0.20; 4th, 0.30; 5th, 0.50; 6th, 0.75 and 7th, 1.00.

The loss of symmetry caused by Al^{3+} coordination was demonstrated more clearly by the NMR titration in Figure 4.11 for the same solutions. The loss of symmetry of the enantiotropic hydrogens seen with the addition of Al^{3+} to citric acid indicates the coordination through the central and a single terminal carboxylic acid group.

The CSP of citric acid caused by the addition of Al^{3+} and Zn^{2+} were calculated and plotted in the mole ratio plots of Figure 4.12 to determine stoichiometry of the metal-citric acid complex.

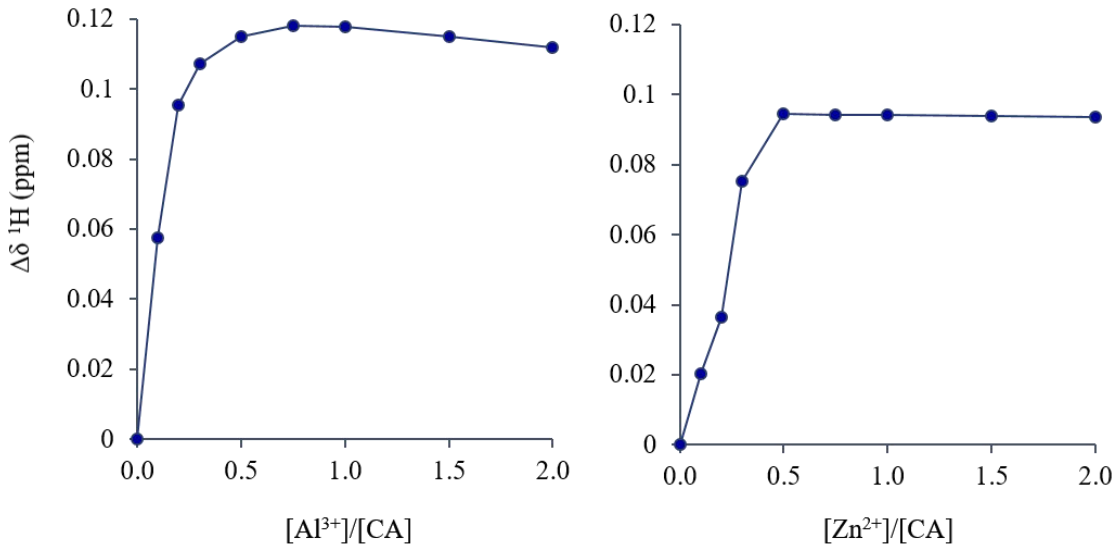

Figure 4.12 Molar ratio vs Δδ plots for metal ion and citric acid. The concentration of citric acid is kept constant at 10 mM and the respective metal ion concentration was varied from 0.0 to 2.0 molar equivalents. Each slope represents the change in chemical shift (Δδ) for the resonances of the enantiotropic hydrogens against the $[M^{n+}]/[CA]$ ratio. The stoichiometry (M^{n+}:CA) of the complex with Zn^{2+} was found to be 1:2 as indicated by the changes in slope. The mole ratio plot for the CA complex with Al^{3+} indicates multiple binding modes.

The mole-ratio plot for the $[Al^{3+}]/[CA]$ indicated the potential stepwise formation of Al(CA), $Al(CA)_2$ and $Al(CA)_3$. This observation is consistent with the results obtained from molecular modelling (Table 4.7) data for this complex. The plateau of the mole ratio plot after the 0.5 mole equivalence point (M^{n+}/CA) reveals the coordination of Zn^{2+} to citric acid, in a 1:2 complex.

The titration of Cu^{2+} resulted in line broadening of the enantiotropic hydrogens. The mole ratio plots also did not reach a clear saturation point. Hence the stoichiometric calculation of the copper-citrate complex was determined from elemental analysis (Table 4.6).

Table 4.6 Analytical data of copper-citrate complex

Formula	Yield %	Analysis (%) found (Calculated)		
		C	H	Cu^{2+}
$Cu_2C_6H_4O_7.2H_2O$	89.0	22. 23 (22.58)	2.33 (2.53)	36.20 (39.81)

The experimental values shown for each of the copper-citrate complex are in good agreement with the theoretical values. The calculated mole ratio of the complex was 2:1.

From these simple observations and the ability of citric acid to act as a tridentate ligand, the coordination modes of the metal ion and citric acid can be deduced. Molecular mechanics were carried out to find the relative minimum energies and HOMO energy values for all energy minimized conformation of the metal-CA complexes and are presented in Table 4.7.

Table 4.7 Molecular modelling studies of metal-citric acid complexes. The proposed structures of metal-citric acid complex, relative energies and HOMO energy values of proposed energy-minimized molecular structures of metal-citric acid complexes. The total energies for each complex are relative to the complex with the lowest calculated MM2 (Cu-CA) Colour codes: C, grey; H, white; O, red; respective M^{n+}, dark grey.

	Al(CA)$_2$	**Zn(CA)$_2$**	**Cu$_2$(CA)**
Proposed structures of metal-CA complex	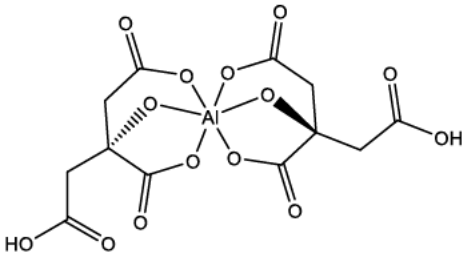	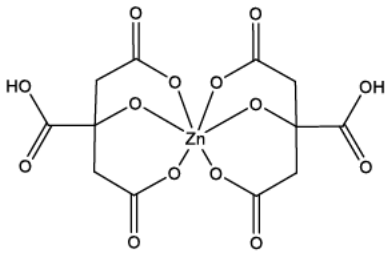	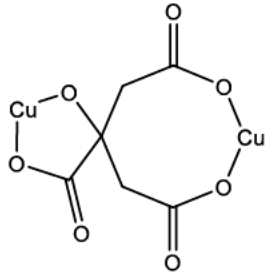
Energy minimized structure of metal-CA complex	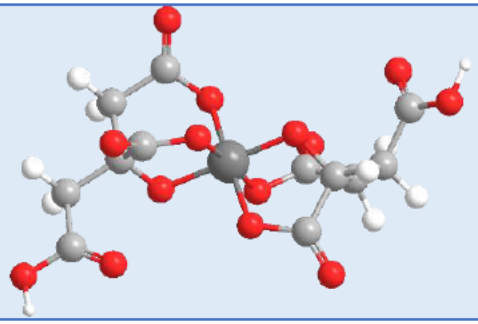	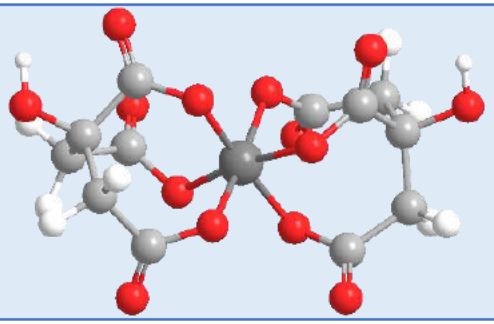	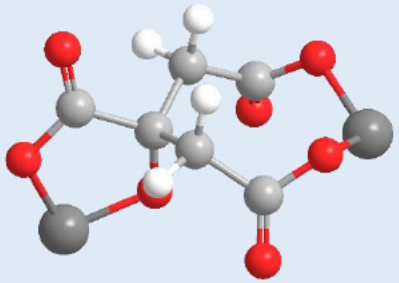
MM2 (total energy) in kcal/mol	34.434	42.190	0
HOMO values (eV)	-10.742	-12.153	-12.879

4.2.6 Malic acid

The details of metal ion (M^{n+}) binding to malic acid (MA) by ^{1}H NMR are shown in Figure 4.13, including ^{1}H NMR spectra of malic acid only (apo MA), and malic acid plus 0.5 molar equivalent of metal ion Al^{3+}, Cu^{2+} and Zn^{2+} respectively. At assay pH 7.4, the deprotonation of both carboxy groups of malic acid results in the formation of the conjugate base, malate. The spectrum for apo malate is labelled with the corresponding resonances and the structure of malic acid is at the top. The respective protons are CH, 4.22; CH_2, 2.59 and 2.24 ppm.

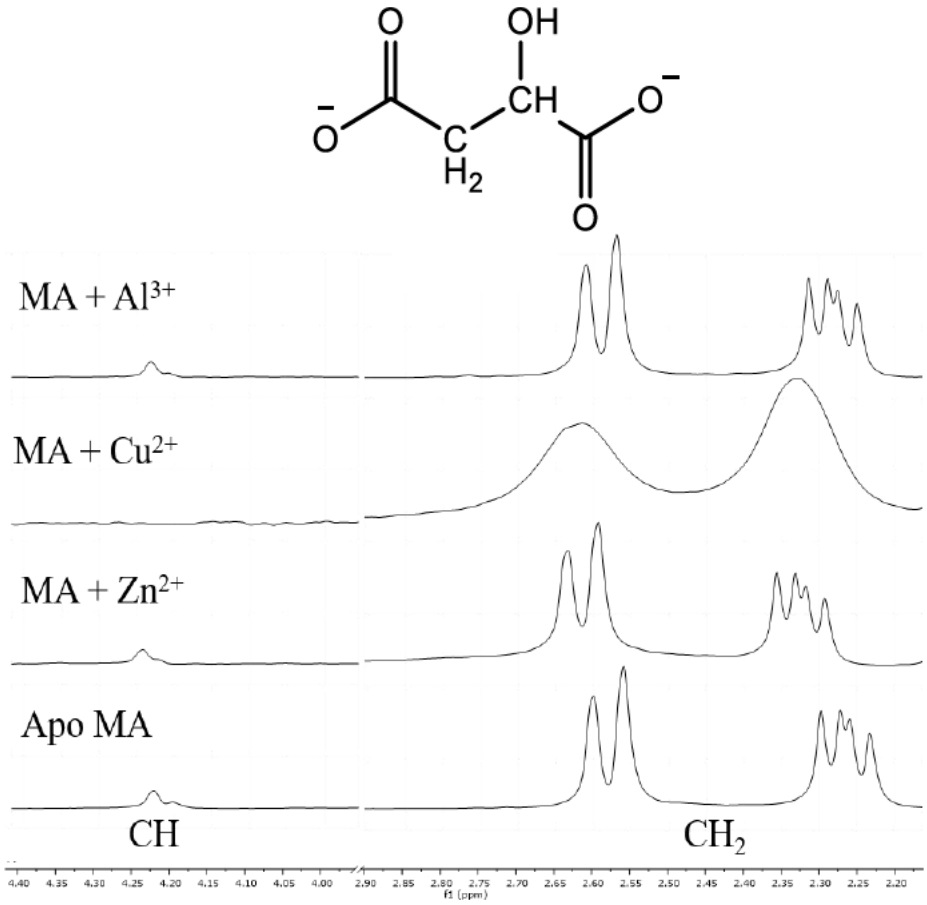

Figure 4.13 ^{1}H NMR metal ion titration of malic acid. Experimental condition: 10% H2O:90% D2O at pH 7.4 ± 0.05 (adjusted with phosphate buffer, the final phosphate concentration is 10 mM), assay temperature 298 K. From bottom to top, apo MA, MA + Zn^{2+}, MA + Cu^{2+} and MA + Al^{3+}. In each of these later solutions the [M^{n+}]/[MA] ratios (from the bottom) is 0.5. The assignments for the respective protons are indicated on the chemical structure of malate (top) CH, 4.22; CH_2, 2.59 and 2.24 ppm. The CH resonance intensity was significantly reduced due to the proximity to the suppressed water signal at 4.70 ppm.

The metal induced CSP of malic acid in Figure 4.13 has characteristic NMR patterns of chelated malic acid and provides indications of a coordination mode. Malic acid has the ability to act as a tridentate ligand with two carboxylates and a hydroxyl group. Figure 4.13 demonstrates which of the binding sites are involved in the coordination to Al^{3+}, Cu^{2+} and Zn^{2+}. The downfield shift caused by the addition of metal ions to the resonances of CH and CH_2 indicate the involvement of the carboxylate groups. The significantly large deshielding of CH at 4.22 ppm caused by the

addition of Al^{3+}, Cu^{2+} and Zn^{2+} implies that the involvement of malic acid's hydroxyl group in metal binding

The numerical change in chemical shifts (Δδ) caused by the incremental additions of metal ions, in the ^{1}H NMR titration of malic acid were calculated. For each metal titration, the significantly deshielded ^{1}H resonance within malic acid was that of CH group. Figure 4.14 presents the mole ratio plots for the $[M^{n+}]/[MA]$ and Δδ of CH, to determine stoichiometry of the metal-malic acid complex.

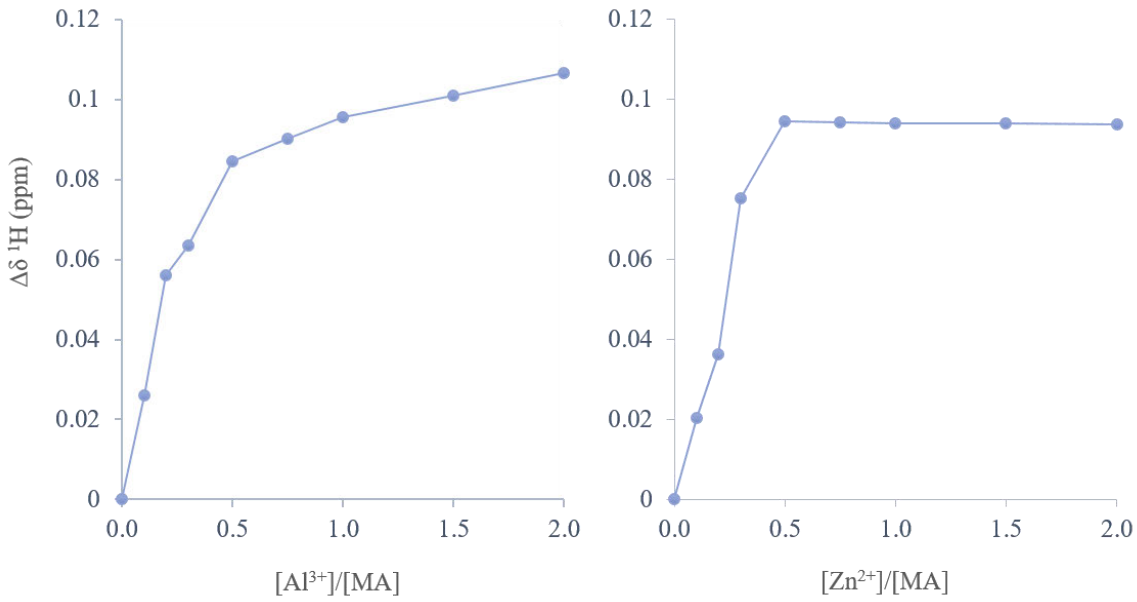

Figure 4.14 Molar ratio vs Δδ plots of metal ions to malic acid. The concentration of malic acid was kept constant at 10 mM and the respective metal ion concentration was varied from 0.0 to 2.0 molar equivalents. Each slope represents the change in chemical shift for the resonances of the enantiotropic hydrogens against the $[M^{n+}]/[MA]$ ratio. The stoichiometry (M^{n+}/MA) of the complex with Al^{3+} and Zn^{2+} was found to be 1:2 as indicated by the changes in slope.

In Figure 4.14, the mole ratio plot for Zn^{2+} plateaus after 0.5 molar equivalents of the metal ion is added. Hence the Zn-malate complex stoichiometry is 1:2. The mole ratio plot for Al^{3+} is typical of mole-ratio plot for a 1:2 complex in which the ligand is in excess.

The titration of Cu^{2+} resulted in line broadening of the CH and CH_2 resonances. Hence the stoichiometric calculation of the copper-malic acid complex was determined from elemental analysis (Table 4.8).

Table 4.8 Analytical data of copper-malic acid complex.

Formula	Yield %	Analysis (%) found (Calculated)		
		C	H	Cu^{2+}
$Cu(C_4H_4O_5)_2$	89.0	29.20 (29.32)	2.37 (2.46)	18.65 (19.39)

The experimental values shown for each of the copper-malic acid complex are in agreement with the theoretical values calculated ratio of the complex in 1:2.

The information obtained from the stoichiometric calculations and the CSP of resonances affected by the addition of metals ions the structural information was used in the molecular modelling studies. The energy minimized conformation and relative minimum energy and HOMO energy values of all the complexes are presented in Table 4.9.

Table 4.9 The optimized binding structures of metal-MA complexes. The proposed structures of metal-malic acid complex, relative energies and HOMO energy values of proposed energy-minimized molecular structures of metal-malic acid complexes. The total energies for each complex are relative to the complex with the lowest calculated MM2 (Cu-MA) Colour codes: C, grey; H, white; O, red; respective M^{n+}, dark grey.

	$Al(MA)_2$	$Zn(MA)_2$	$Cu(MA)_2$
General scheme of metal-MA complex	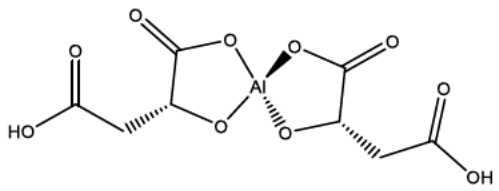	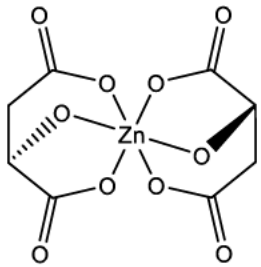	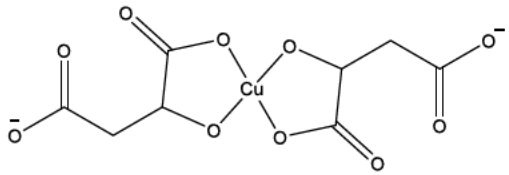
Proposed energy minimized structure of metal-MA complex	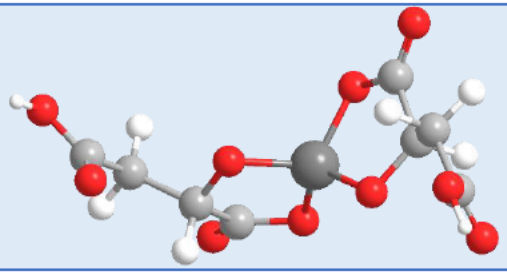	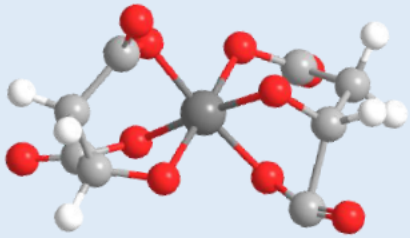	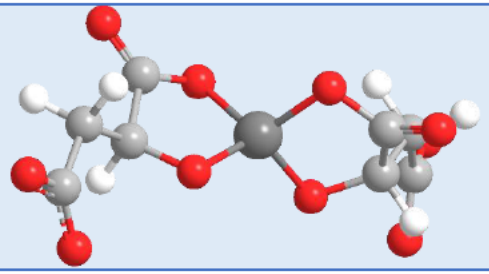
MM2 (total energy) in kcal/mol	10.30	32.003	0
HOMO values (eV)	-11.316	-11.520	-12.618

4.3 Discussion

This chapter is about the ability of individual ligands to bind various metal ions. Naturally occurring metal chelators such as the ones I am reporting here may have therapeutic applications in the treatment and alleviation of age-related health problems like dementia. The panel of ligands in this chapter were selected for their metal-binding proclivity, lack of cytotoxicity, and potential antioxidant activity.

^{1}H NMR titration experiments show histidine binds strongly to Al^{3+}, Zn^{2+} and Cu^{2+}, at a biologically relevant pH 7.4, with a stoichiometry of M^{n+}: histidine of 1:2 (Figure 4.5). Histidine is the main metal binding site in Aβ (Chapter 3), hence its ability to coordinate as a free amino acid to Al^{3+}, Zn^{2+} and Cu^{2+} is not unusual. The proposed binding schemes in Table 4.1 indicate the coordination to metal ions occurs via the N2-imdazole group, the NH and COOH groups. The energy minimization calculations performed by using molecular mechanics (MM2) demonstrated that the minimized energy structure for a bidentate ligand is lower than that of the tridentate. The observed upfield shift of the resonances 2H and 4H of the imidazole group supports the view that Al^{3+} binds to histidine relatively more efficiently compared to Zn^{2+} or Cu^{2+}. This is further demonstrated by the significantly lower HOMO values for the Al^{3+}-His complexes of -0.010 eV, judged by the computational molecular modelling studies. My results conclude that, histidine is a chelating ligand able to coordinate strongly with Al^{3+}. The complexes formed with Al^{3+}, Zn^{2+} and Cu^{2+} demonstrate the potential of histidine as a chelating ligand (with therapeutic value to AD). In addition, I have surveyed all 20 amino acids for their interaction with metal ions, see Appendix D. The findings shed light on the individual amino acid interactions with metal ion. While amino acids can act as ligands to Al^{3+} and Zn^{2+}, histidine

was a significantly strong metal chelator. This is further supported as indicated by Chapter 3 findings that it is mainly the histidine residues in Aβ that confer its metal binding ability.

The interactions between GSH and Al^{3+}, Zn^{2+} or Cu^{2+} (Figure 4.7) show that each of these metal ions bind to the potential coordination sites of glutathione with a high degree of specificity, with the actual sites involved in metal binding being dependent on the type and concentration of the metal ions. At physiological pH, the coordination of the GSH to Al^{3+} occurred via the glycine and glutamate carboxylate groups. The mole ratio plot indicated the stepwise formation of a 1:1 and 1:2 Al-GSH complex consistent with the studies conducted by Wang et al. (2009). The energy minimization of the Al-GSH complex in 1:2 ratio yielded the configuration with the higher stability. GSH showed weaker coordination to Al^{3+}, compared to Zn^{2+} thiol coordination. The titration of GSH with Cu^{2+} supports that the metal ion oxidised GSH in a two-step reaction resulting in the formation of the Cu^{+} and GSSH (Kato et al., 1999), when Cu^{2+} forms complex with GSH and catalyses the reaction (Singh et al., 2014). The rate of GSH oxidisation is decreased with the increased concentration of GSH, and this was found to be the result of the formation of an inactive Cu-GSH complex (Ngamchuea et al., 2016). GSH is a versatile endogenous antioxidant, which is abundant in the body. In this context it is significant that the GSH concentration is found to be significantly lower in hippocampal regions of AD patients (Mandal et al., 2015). The upregulation of endogenous antioxidants is vital in combating oxidative stress, a known characteristic of AD, thus helping to slow the disease advancement (Pocernich and Butterfield, 2012). As demonstrated here, GSH strongly coordinates to AD related metals. Such finding, in combination with its proven antioxidant activity, supports the potential of GSH in combating AD.

The comparison of the steric energy of various conformations of the metal-maltol complexes gives information on the relative coordination strength and stability of those complexes. It was shown that the complexation of maltol with Cu^{2+} yielded the complex with the highest stability. Also, the HOMO values of $Al(mal)_3$, -8.757 eV; $Zn(mal)_2$, -8.900 eV; $Cu(mal)_2$, -8.921 eV indicate great stability of these complexes. Maltol is known for high bioavailability, favourable toxicity profile and significantly high metal ion complex stability (Thompson et al., 2006). The synthetic modifications and extensions of maltol may increase the variety of its potential medicinal applications (Mukha et al., 2007).

Interaction of the metal ions with the citric acid ligand in solution at physiological pH results in the formation of a metal-citrate complex in a 2:1 ratio for Cu^{2+} and 1:2 for Al^{3+} and Zn^{2+}. The complexation of citric acid to Al^{3+} resulted in an asymmetrical complex, with the binding of one terminal carboxylic acid group to Al^{3+}. With four available oxygen donors, citric acid is an ideal chelating ligand for Al^{3+}, as indicated by the lower HOMO values of -10.742 eV for the $Al(CA)_3$ complex compared to the -12.153 eV for $Zn(CA)_2$ and -12.879 eV for Cu_2CA complexes. The presence of Al^{3+} in *Arabidopsis*, Zn^{2+} in wheat, and Cu^{2+} in *Zea mays* cause the exudation of citrate from the root, which actively chelates the metal ions (Gramlich et al., 2013; Dresler et al., 2014; Wang et al., 2018). While the ability to bind and chelate metals from biological systems is established, citric acid has relatively low affinity for metal ions, as evident from the comparison of HOMO values of the other ligands tested. This indicates while the chelating ligand may bind to Al^{3+}, Zn^{2+} and Cu^{2+}, citric acid may not efficiently eliminate the metal ions. Deng et al. (1998) demonstrated that by using rat models, citrate increases the accumulation of $A1^{3+}$.

A similar low affinity is seen in the complexation of malic acid to Al^{3+}, Zn^{2+} and Cu^{2+}. The relative energies of the metal-malate are indicative of the formation of the stable complexes. The HOMO values of -11.316 eV for Al^{3+}MA, -11.520 eV for Zn^{2+}MA and -12.618 eV for Cu^{2+}MA, demonstrating a similar metal affinity as citric acid.

4.4 Conclusion

In conclusion, the metal-binding properties for a panel of ligands were characterised by NMR and molecular mechanics. The relatively high affinity of maltol, GSH and histidine to Al^{3+}, Zn^{2+} and Cu^{2+} suggests their potential in metal chelation, which should be explored in future for drug development against diseases such as AD. The diverse coordinating sites available in the ligands GSH and histidine demonstrate their effectiveness in chelating various metal ions. The fact that they are natural molecules in human cells is a convenient bonus, their usefulness in treatment of metal-related health problems should be definitely considered.

5 THE IMPACT OF METALS AND LIGANDS ON THE GENE EXPRESSION OF APP IN NEURONAL CELLS

5.1 Introduction

Thus far, there is a strong association amongst metal ions, Aβ and AD according to numerous publications (Cherny et al., 1999; Lynch et al., 2000; Adlard and Bush, 2006; Duce et al., 2011), the extent of which is still debateable (Pollard et al., 1995; Drew, 2017). My findings demonstrate a strong interaction of metal ions and Aβ (Chapter 3) supports the argument that both metal ions and Aβ play a role in AD. A complex neurodegenerative disease such as AD has no clear causative aetiology. However, in the past few decades most AD therapeutic studies were focused on targeting one factor at a time varying from preventing metal induced apoptosis to Aβ aggregation, metal-Aβ coordination, Aβ accumulation or oxidative stress. This chapter aims to explore the effect of metal ions on the expression of APP gene, and then to gauge the antagonistic action of ligands on metal ions which may up-regulate APP gene expression. Currently there is a deficiency of data on this front, nor is there any work carried out on chelating ligands which may intervene metal ions' effect on APP gene expression. Therefore, it would be worthwhile to investigate the potential effect of metal ions on APP expression and to subsequently find a natural chelating ligand which can stop such metal ions in the process.

I will now focus on the toxicity of Al^{3+}, $Cu^{2+}$and Zn^{2+}, and additionally arsenic (As^{3+}) and chromium (Cr^{6+}) which might not relate to AD but are detrimental to human health (Kim et al., 2011; Lambrou et al., 2012; Mahajan and Sidhu, 2019). To determine if metal ions, Al^{3+} and Zn^{2+}, play a role in APP gene expression, I treated the human neuronal cells with the metal ions

and then carried out qRT-PCR for analysing the expression of APP gene. In parallel, the effect of ligands on metal-induced APP expression (if any) was also analysed.

5.2 Results

5.2.1 Determination of IC_{50} of metal ions on SH-SY5Y cells

Prior to investigating the effects of the metal ions on APP gene expression, their appropriate dosage was initially established. The experimental details of IC_{50} determination is described in Chapter 2.8.1, the dose response curves for each metal ion studied were acquired and the subsequent IC_{50} of each metal ion was determined. Figures 5.1 to 5.5 are the dose response curves for $ZnSO_4$, $CuSO_4$, $Al(mal)_3$, CrO_3 and $NaAsO_2$, as well as solvent controls in human neuroblastomas cells (SH-SY5Y). The dose-response curves indicated the IC_{50} values for the metal ions was 180 µM for Zn^{2+} (Figure 5.1); 1000 µM for Cu^{2+} (Figure 5.2); 1000 µM for Al^{3+} (Figure 5.3); 18 µM for Cr^{6+} (Figure 5.4); 16 µM for As^{3+} (Figure 5.5). Consequently, the determined IC_{50} values for the individual metal ions were used as a dosage for the ensuing experiments.

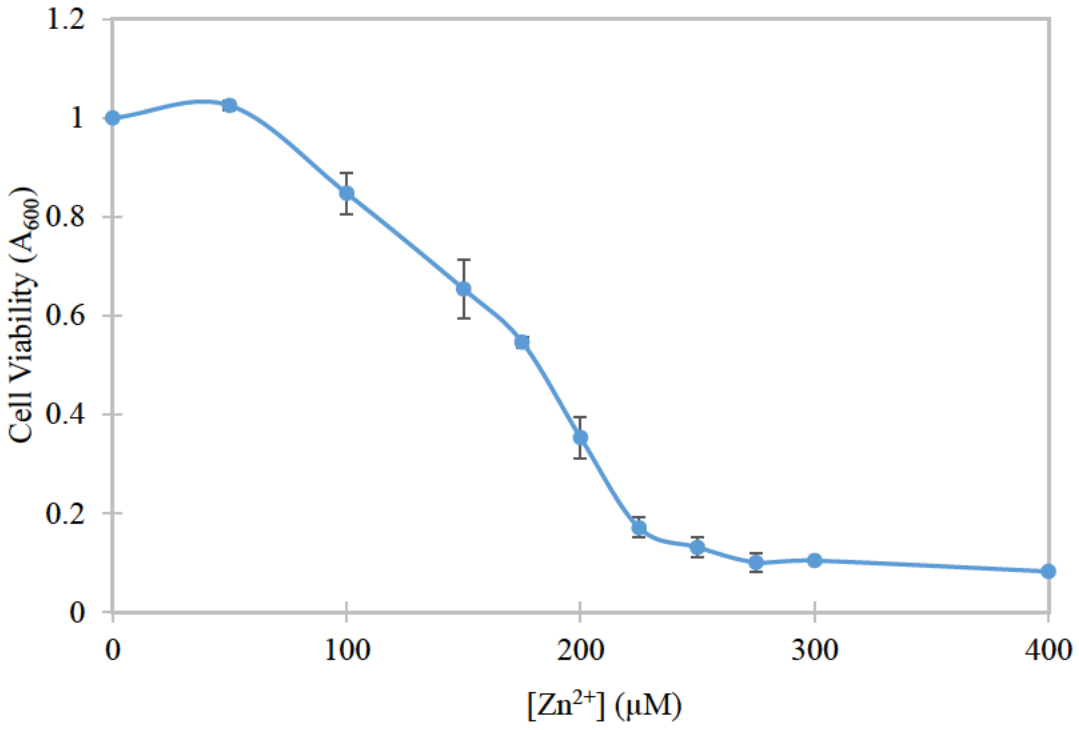

Figure 5.1 Dose-response curve of zinc sulphate in SH-SY5Y cells. The cells were treated with a range of $ZnSO_4$ concentrations 0-400 μM and the MTT assay was carried out to determine the cell viability. The IC_{50} of Zn^{2+} for SH-SY5Y cells was determined to be 180 μM. Experiment consisted of eight replicates. The mean of triplicate experiments was used to obtain each data point and SD values are represented as error bars.

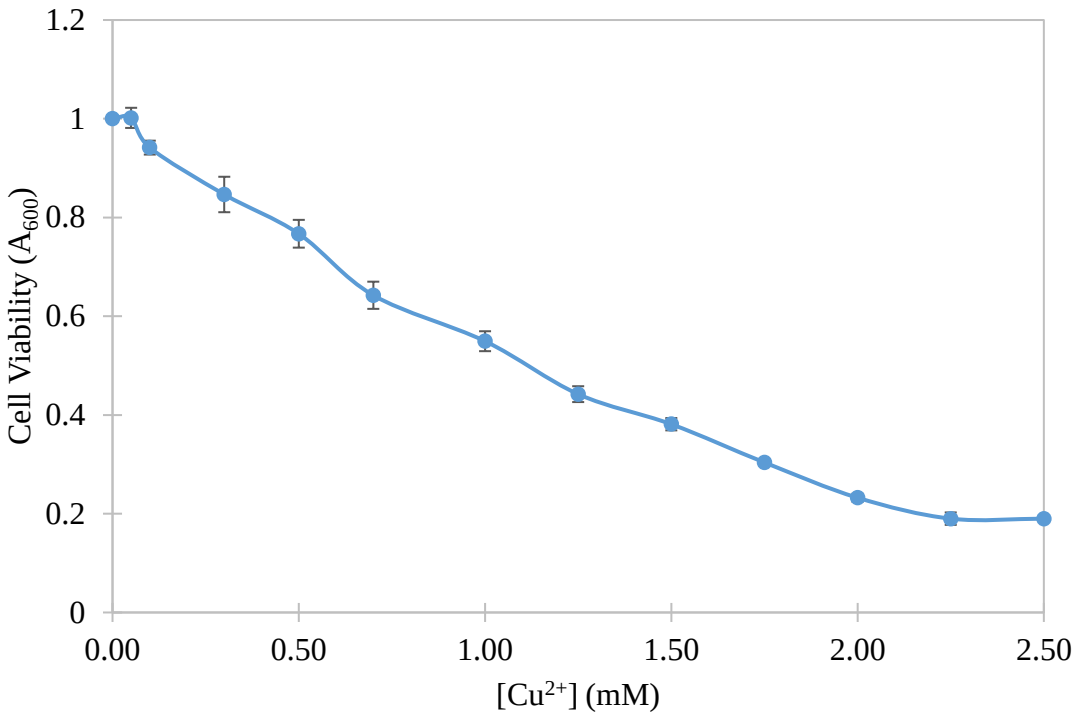

Figure 5.2 Dose-response curves of copper sulphate in SH-SY5Y cells. The cells were treated with a range of $CuSO_4$ concentrations as indicated and the MTT assay was used to determine cell viability. The IC_{50} of Cu^{2+} for SH-SY5Y cells was determined to be 1000 µM. Experiment consisted of eight replicates. The mean of triplicate experiments was used to obtain each data point and SD values are represented as error bars.

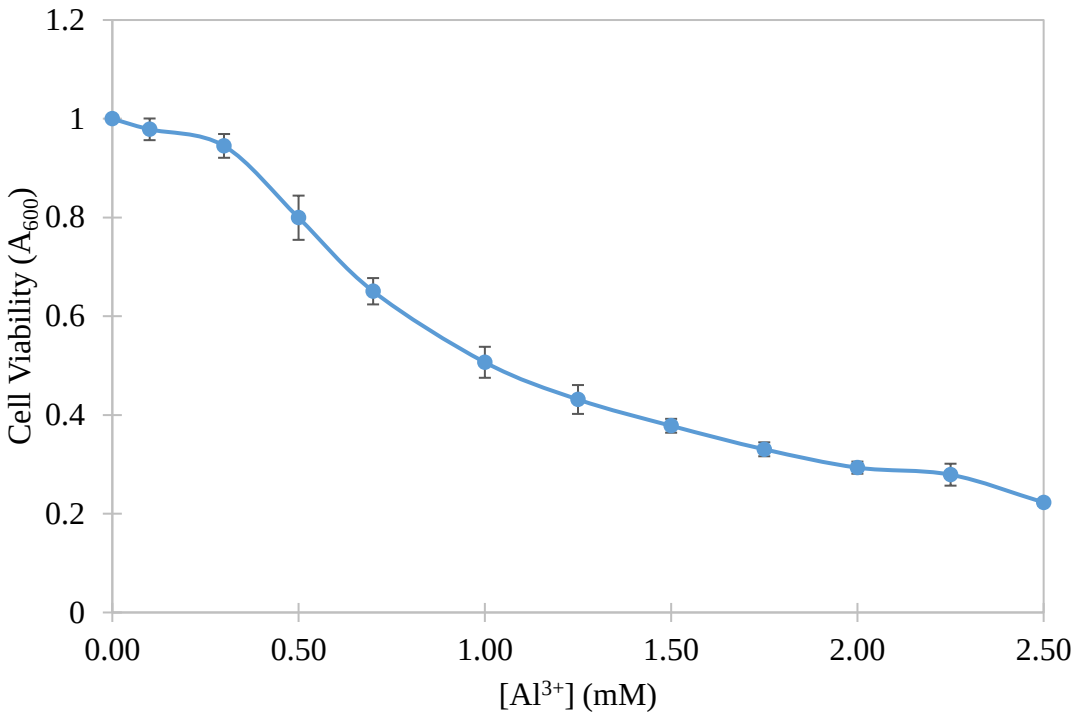

Figure 5.3 Dose-response curve of aluminium maltol in SH-SY5Y cells. The cells were treated with a range of $Al(mal)_3$ concentrations as indicated and the MTT assay was used to determine cell viability. The IC_{50} of Al^{3+} for SH-SY5Y cells was determined to be 1000 µM. Experiment consisted of eight replicates. The mean of triplicate experiments was used to obtain each data point and SD values are represented as error bars.

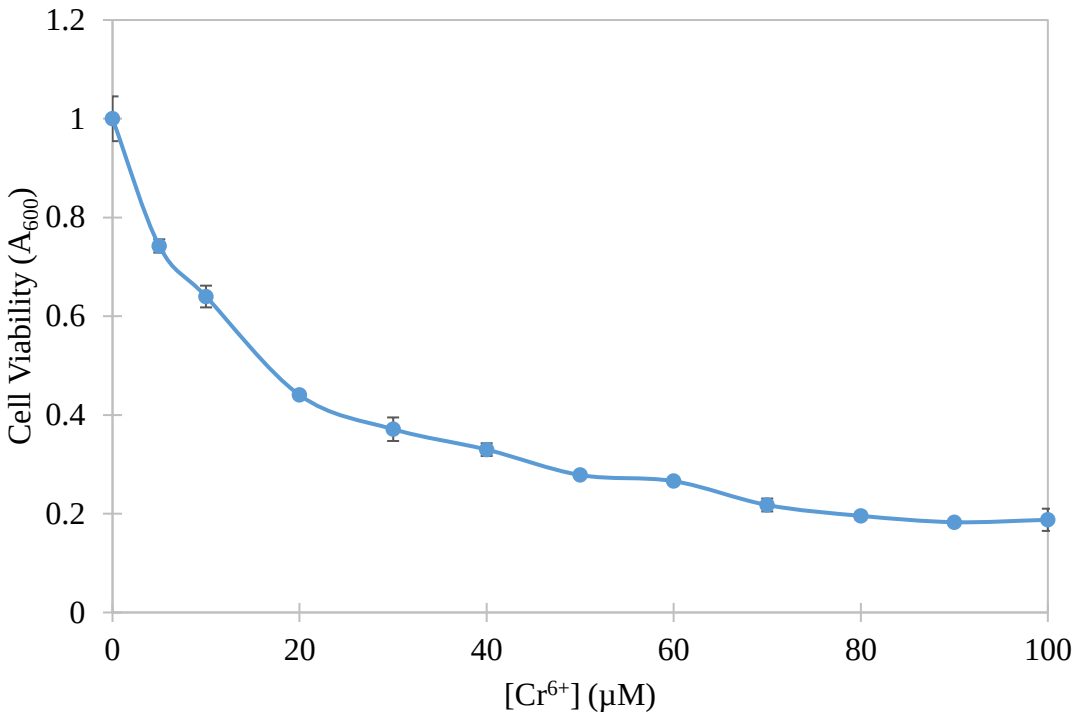

Figure 5.4 Dose-response curves of chromium trioxide in SH-SY5Y cells. The cells were treated with a range of CrO_3 concentrations as indicated and the MTT assay was used to determine cell viability. The IC_{50} of Cr^{6+} for SH-SY5Y cells was determined to be 18 µM. Experiment consisted of eight replicates. The mean of triplicate experiments was used to obtain each data point and SD values are represented as error bars.

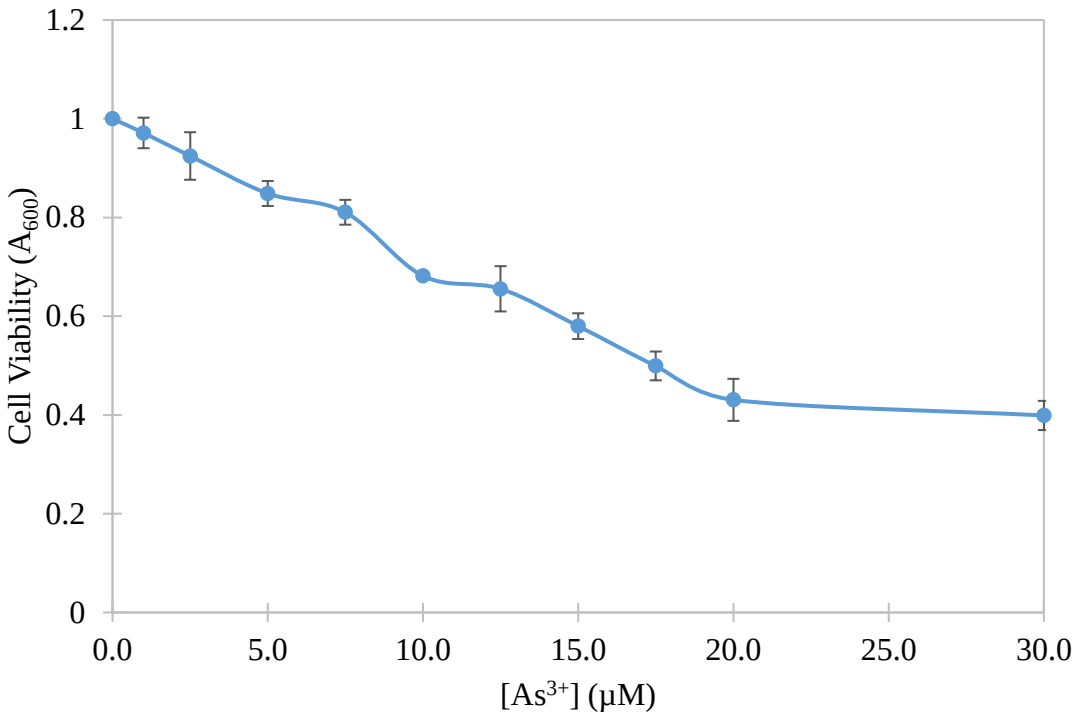

Figure 5.5 Dose-response curves of sodium arsenite in SH-SY5Y cells. The cells were treated with a range of $NaAsO_2$ concentrations as indicated and the MTT assay was used to determine cell viability. The IC_{50} of As^{3+} for SH-SY5Y cells was determined to be 16 µM. Experiment consisted of eight replicates. The mean of triplicate experiments was used to obtain each data point and SD values are represented as error bars.

5.2.2 The effect of metal chelating ligands on the cytotoxicity of metal ion in SH-SY5Y cells

To establish if the ligands can chelate the metals in physiological conditions and reduce metal toxicity, MTT assays were performed. Following the methods as described in Chapter 2.8.2, comparative cytotoxic response curves for each ligand plus each metal ion were obtained (Figures 5.7-5.11). For metal plus ligand, the treatment of the neuronal cells with each metal ion and the ligand resulted in the change of cytotoxicity compared to the metal alone as seen in

Figures 5.7 to 5.11. Metal alone serves as the control for each metal ion treatment ($Al(mal)_3$, $CuSO_4$, $ZnSO_4$, CrO_3 and $NaAsO_2$ respectively).

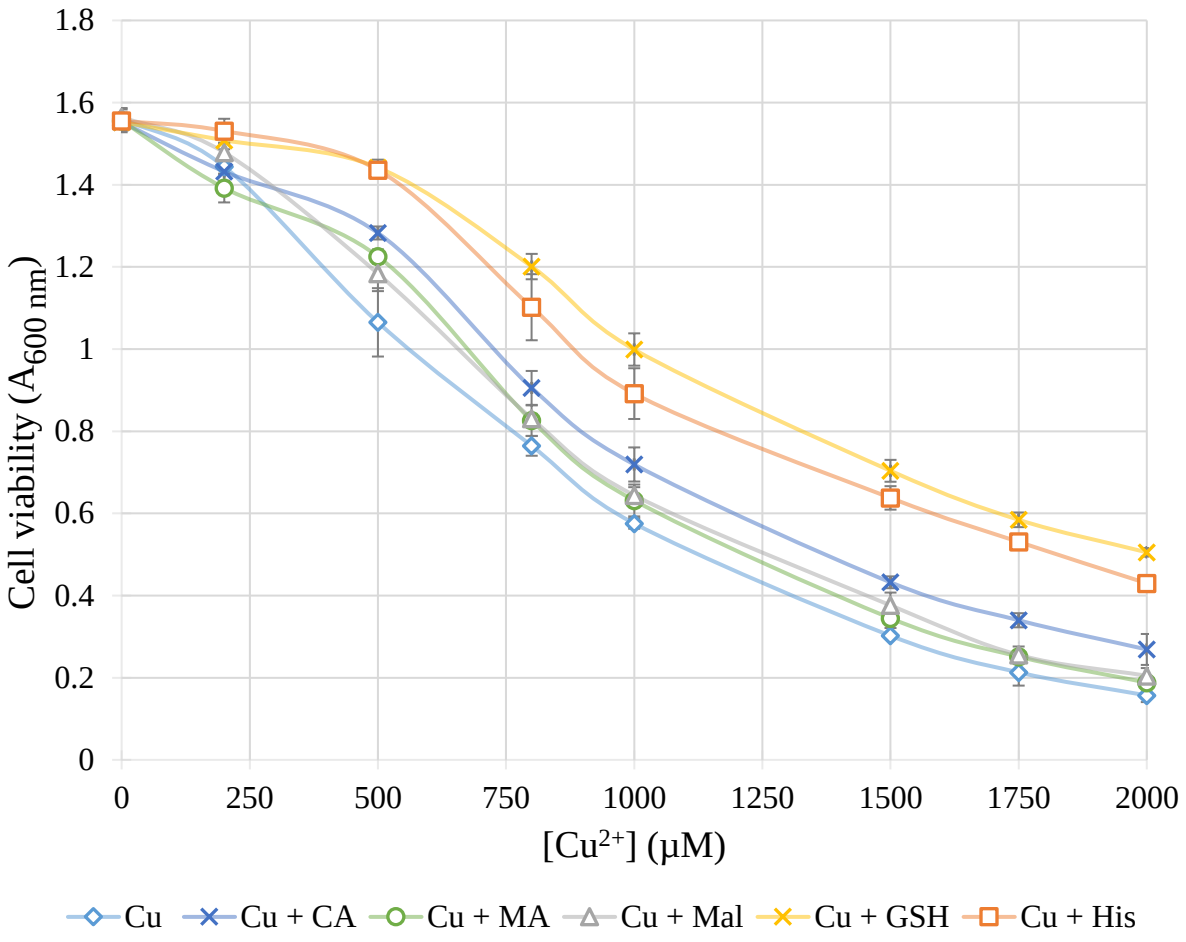

Figure 5.6 Comparative cytotoxic response curves of copper treated with ligands. The SH-SY5Y cells were exposed to increasing concentrations of $CuSO_4$ with each ligand including citric acid (2000 µM), malic acid (2000 µM), maltol (3000 µM), glutathione (2000 µM) or histidine (2000 µM), then incubated for 6 hr. The cell viability was determined by MTT assay. The values are the result of triplicate experiments and SD values are represented as error bars.

The ligands protected SH-SY5Y cells against the cytotoxic effect of Cu^{2+} exposure (Figure 5.6). While the presence of GSH and histidine significantly increased cell viability against Cu^{2+}, a slight increase in cell viability against the metal ion is seen with the treatment of citric acid,

maltol and malic acid. The marked increase of cell viability by GSH and histidine against Cu^{2+} demonstrates the ligands' ability to coordinate Cu^{2+} under the physiological condition for SH-SY5Y cells.

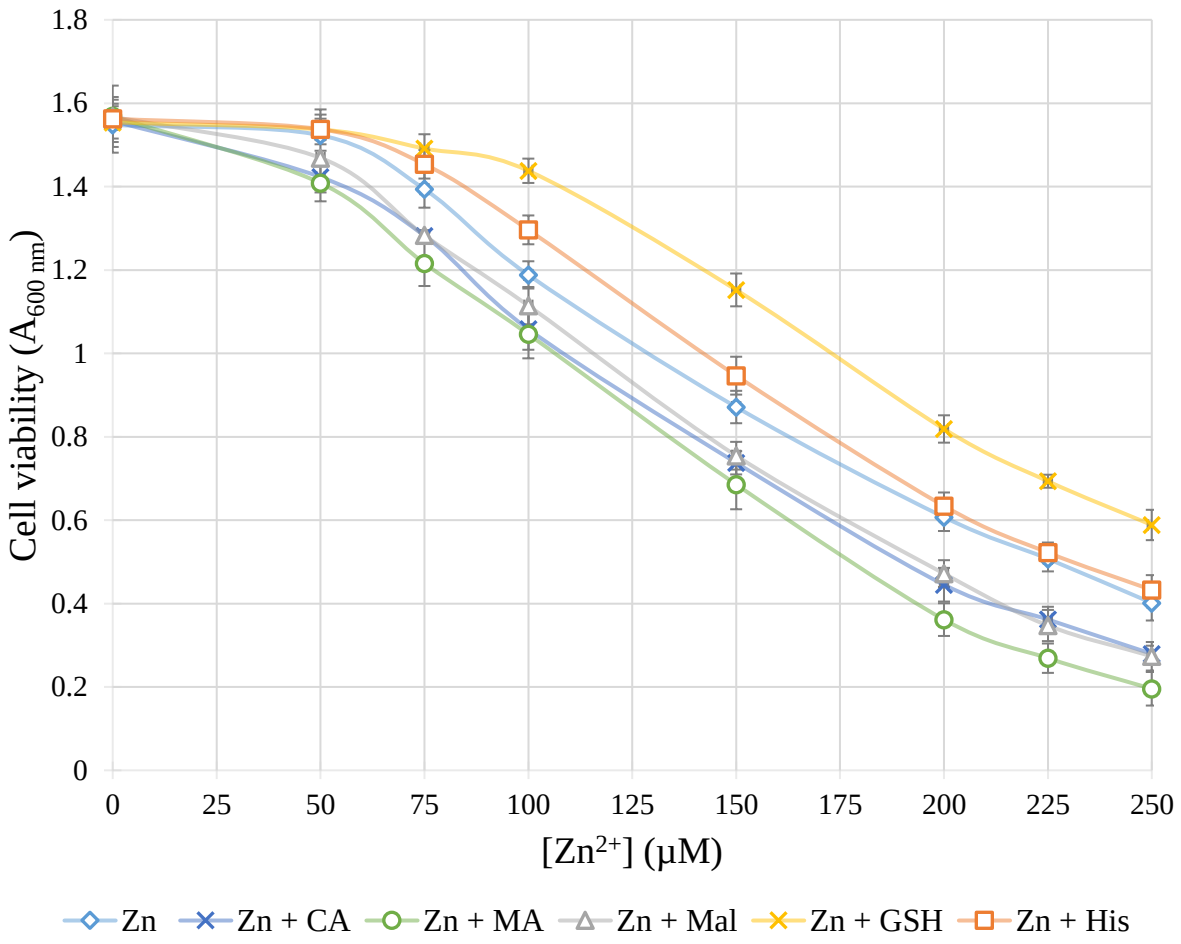

Figure 5.7 Comparative cytotoxic response curves of zinc treated with ligands. The SH-SY5Y cells were exposed to increasing concentrations of $ZnSO_4$ with each ligand including citric acid (2000 μM), malic acid (2000 μM), maltol (3000 μM), glutathione (2000 μM) or histidine (2000 μM), then incubated for 6 hr. The cell viability was determined by MTT assay. The values are the result of triplicate experiments and SD values are represented as error bars.

For zinc, GSH and histidine protected cells from the cytotoxic effects of zinc (Figure 5.7). Citric acid, malic acid and maltol are ineffective on the cytotoxic effect of zinc exposure, and unexpectedly, they increased zinc cytotoxicity.

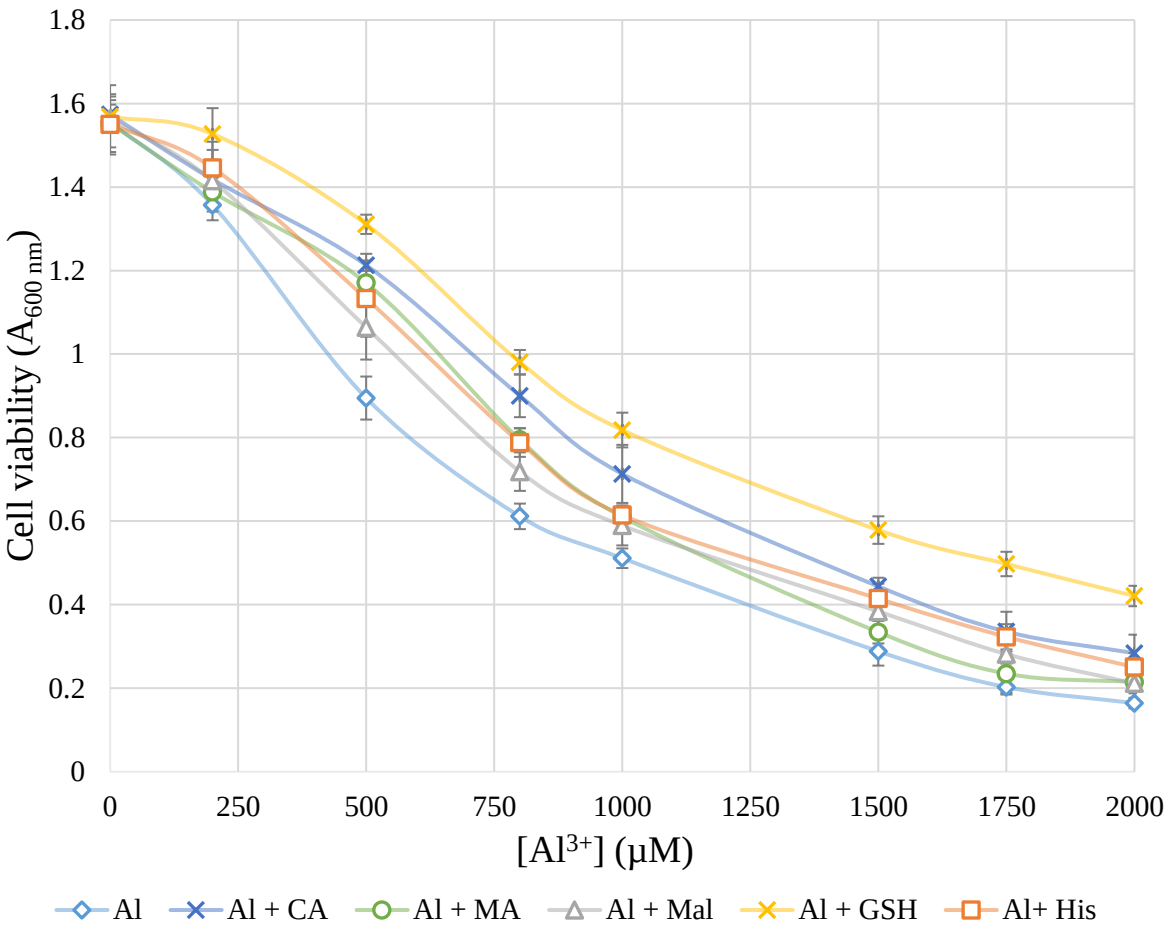

Figure 5.8 Comparative cytotoxic response curves of aluminium treated with ligands. The SH-SY5Y cells were exposed to increasing concentrations of Al^{3+} with each ligand including citric acid (2000 µM), malic acid (2000 µM), maltol (3000 µM), glutathione (2000 µM) or histidine (2000 µM), then incubated for 6 hr. The cell viability was determined by MTT assay. The values are the result of triplicate experiments and SD values are represented as error bars.

For Al^{3+}, the treatment of ligands protected SH-SY5Y cells against the Al^{3+} metal toxicity effect. As seen in Figure 5.8, GSH was the most effective in reducing metal toxicity and increasing the viability of the SH-SY5Y cells under physiological conditions. The marked increase of cell viability by GSH against Al^{3+}, is followed by citric acid, histidine, malic acid and maltol had the similar effect on Al^{3+} toxicity.

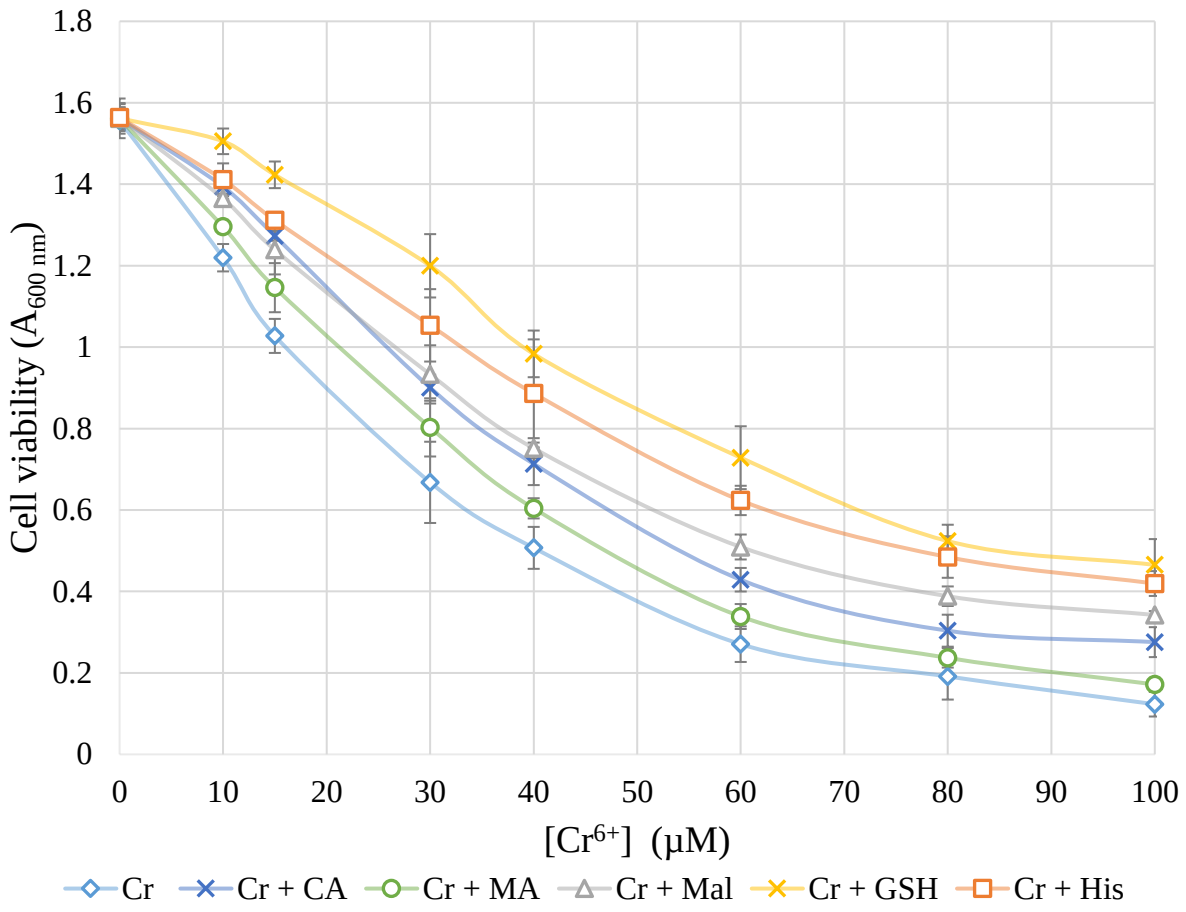

Figure 5.9 Comparative cytotoxic response curves chromium treated with ligands. The SH-SY5Y cells were exposed to increasing concentrations of CrO_3 with each ligand including citric acid (2000 µM), malic acid (2000 µM), maltol (3000 µM), glutathione (2000 µM) or histidine (2000 µM), then incubated for 6 hr. The cell viability was determined by MTT assay. The values are the result of triplicate experiments and SD values are represented as error bars.

The treatment of ligands significantly protected SH-SY5Y cells against the Cr^{6+} metal toxicity effect. As shown in Figure 5.9, GSH was the most effective in reducing metal toxicity and increasing the viability of the SH-SY5Y cells under physiological conditions. The marked increase of cell viability by GSH against Cr^{6+}, is followed by histidine, maltol, citric acid and then malic acid.

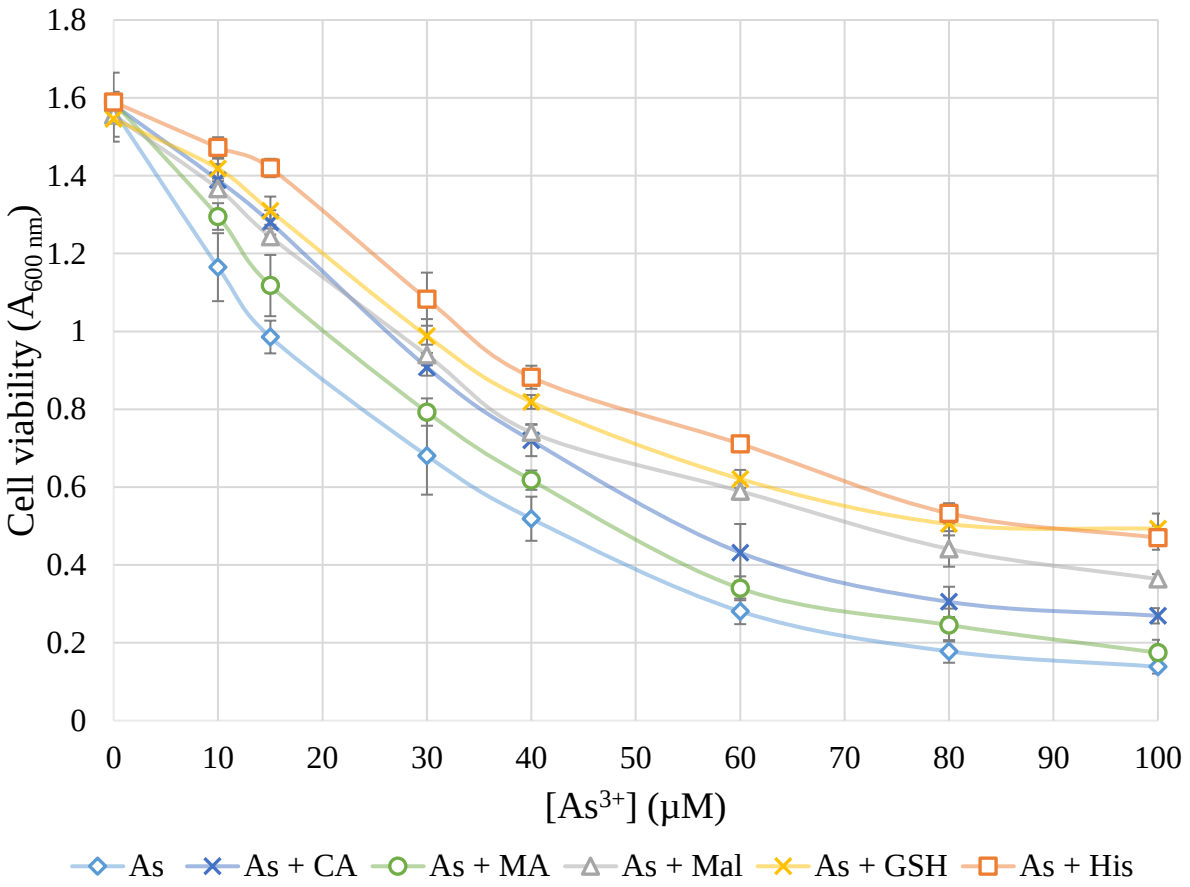

Figure 5.10 Comparative cytotoxic response curves of arsenic treated with ligands. The SH-SY5Y cells were exposed to increasing concentrations of $NaAsO_2$ with each ligand including citric acid (2000 µM), malic acid (2000 µM), maltol (3000 µM), glutathione (2000 µM) or histidine (2000 µM), then incubated for 6 hr. The cell viability was determined by MTT assay. The values are the result of triplicate experiments and SD values are represented as error bars.

For As^{3+}, the addition of ligands drastically improved the cell viability under As^{3+} exposure (Figure 5.10). Histidine and GSH are comparatively the most effective in increasing the cell viability. Additionally, the treatment of maltol, citric acid and malic acid also resulted in a marked increase of cell viability. Thus, demonstrating the ligands' ability to lower As^{3+} toxicity under the physiological condition for SH-SY5Y cells.

5.2.3 Gene expression of APP under metal ion exposure and the impact of chelating ligands

Accumulation of Aβ is thought to induce neuronal death in AD (Cherny et al., 2001; Walton and Wang, 2009; Pham et al., 2010). The over-production of Aβ is facilitated by the upregulation of APP gene expression (Walton and Wang, 2009). Therefore, I investigated the effect of metal ions on the expression of APP gene. To detect the effect of Al^{3+} and Zn^{2+} on the mRNA expression of APP using qRT-PCR, I firstly treated SH-SY5Y cells with the IC_{50} of Al^{3+} and Zn^{2+} respectively, then prepared the total RNA from the treated and untreated cells, followed by qRT-PCR quantification.

Relative expression of the APP gene was determined with reference to the expression of housekeeping gene GAPDH. A fold change of 1 indicates no change of the gene expression. Fold changes of >1 or <1 signifies the gene expression is increased or decreased, respectively.

Figure 5.11 demonstrates that the exposure of SH-SY5Y cells to Al^{3+} or Zn^{2+} led to the increase in the expression of APP gene (p <0.01 for Al^{3+}, p <0.05 for Zn^{2+}) by 22.9% and 19.7% respectively. Clearly, the presence of either Al^{3+} or Zn^{2+} resulted in significant upregulation of APP gene expression, albeit relative expression was slightly greater with Al^{3+} compared to Zn^{2+}.

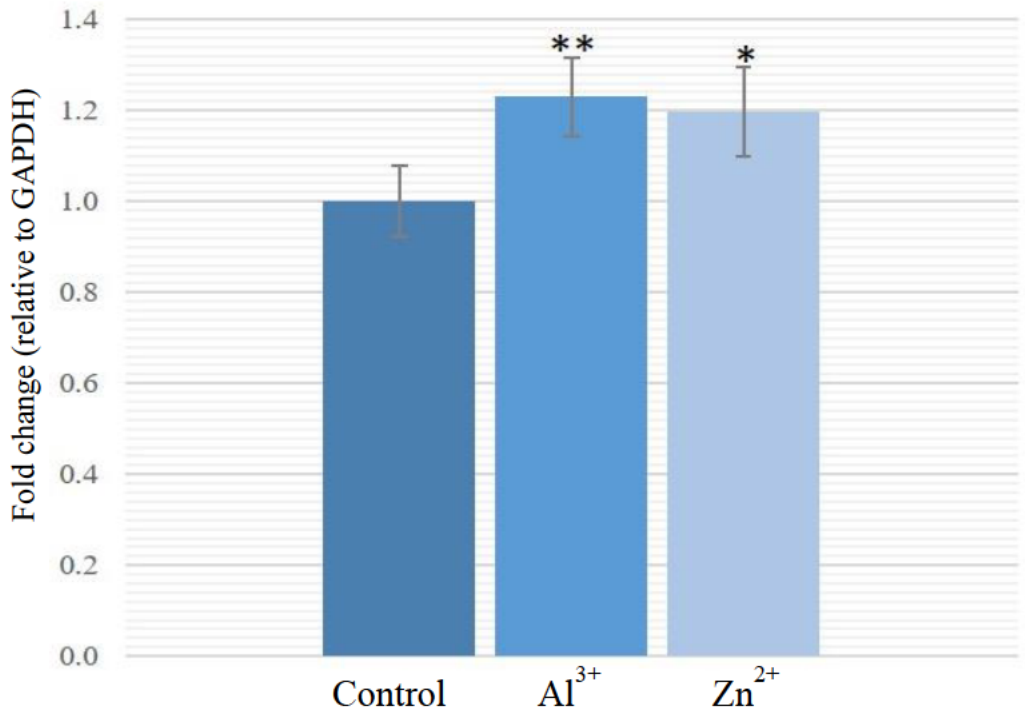

Figure 5.11 Relative expression of APP gene under aluminium or zinc exposure. SH-SY5Y cells at 80% confluency were treated with IC_{50} of $Al(mal)_3$ [1000 µM] and $ZnSO_4$ [180 µM]. Total RNA samples were harvested, prepared and reverse transcribed as described earlier in Chapter 2 after 6 hr incubation of the cells. Using TAQMAN® assays qRT-PCR was performed on cDNA. Relative expression was quantified against the house-keeping gene, GAPDH, using the $2^{-\Delta\Delta CT}$ method (Schmittgen & Livak, 2008). T-test compares the mean of fold change as relative expression of each treatment to the expression of the reference gene GAPDH. * $p < 0.05$, ** $p < 0.01$. Data represents the average of three independent experiments conducted in triplicate. Error bars represent SEM.

To determine whether chelating ligands could negate the effect of metal ions by decreasing the metal-induced expression of APP gene, qRT-PCR was performed to determine the expression of APP gene in SH-SY5Y cells in the presence and absence of ligands with Al^{3+}. The total RNA samples were prepared from the cells exposed to Al^{3+} then treated with and without the ligands, according to the procedure outlined in Chapter 2.10. The qRT-PCR analysis was then conducted according to Chapter 2.10.3.

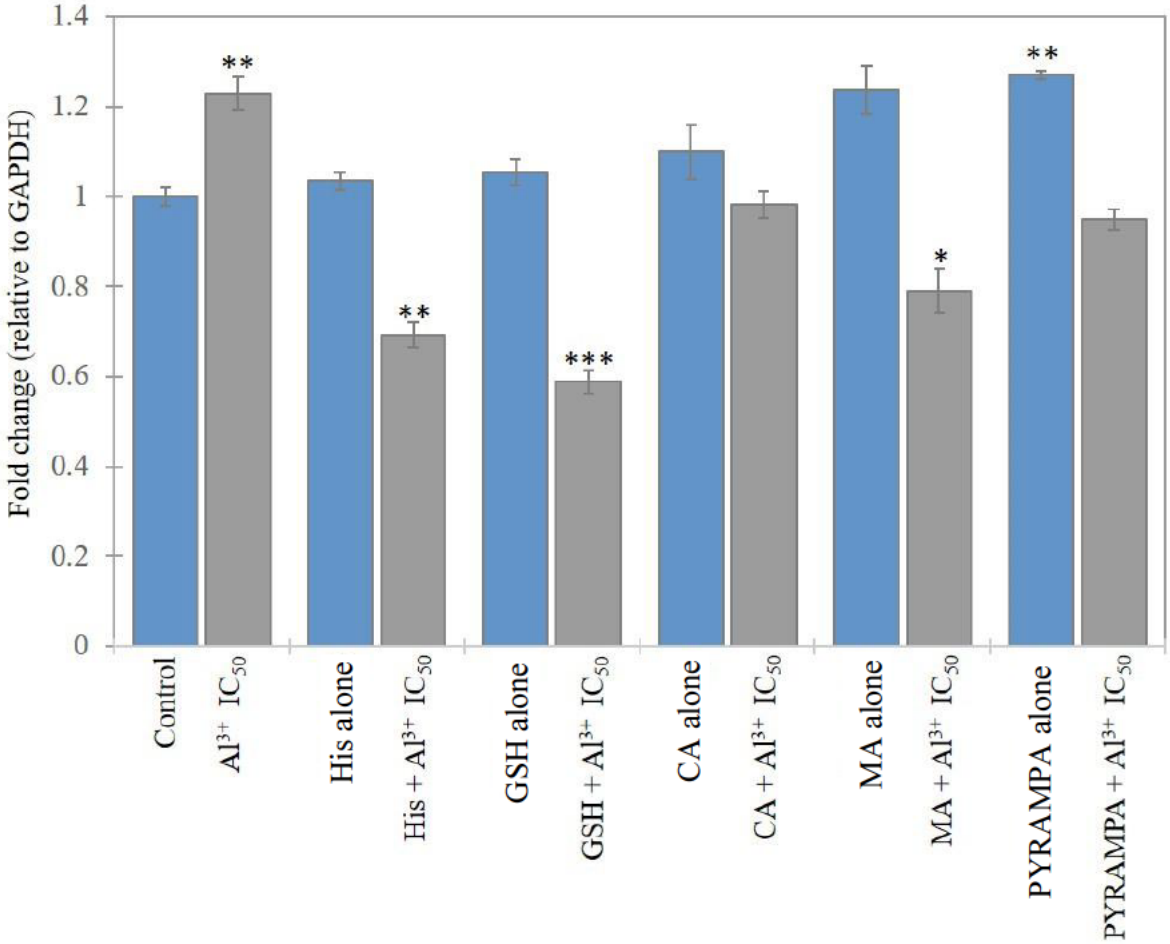

Figure 5.12 Relative expression of APP gene in cells treated by ligands with and without Al^{3+}. Once SH-SY5Y cells reached 80% confluency, they were pretreated with the respective ligands followed by exposure to the IC_{50} of $Al(mal)_3$ [1000 µM]. Total RNA samples were harvested, prepared and reverse transcribed as described earlier, after 6 hr incubation of the cells. Using TAQMAN® assays qRT-PCR was performed on cDNA. Relative expression was quantified relative to the house-keeping gene, GAPDH, using the $2^{-\Delta\Delta CT}$ method (Schmittgen & Livak, 2008). T-test compares the mean of fold change as relative expression of each treatment to the expression of the reference gene GAPDH. * $p < 0.05$, ** $p < 0.01$, *** $p < 0.001$. Data represents the average of three biological replicates and each biological replicate has two technical replicates. Error bars represent SEM.

The results demonstrated that SH-SY5Y cells under Al^{3+} treatment led to increase in the expression of APP gene (Figure 5.1). The expression of APP gene was significantly reduced by

the treatment of chelating ligands (Figure 5.12), particularly histidine (p <0.01) and GSH (p <0.001). Under Al^{3+} exposure, the treatment of citric acid, malic acid ($p < 0.05$) and PYRAMPA ($p < 0.05$) down regulated the APP gene, to a lesser extent compared to histidine and GSH. The APP gene expression was reduced by 38.9% for histidine, 47.4% for GSH and 10.6% for citric acid against the respective controls. Compared to their controls, malic acid and PYRAMPA down regulated the gene expression of APP by 40.5% and 28.1%, respectively. However, the ligand treatment caused the upregulation of APP gene expression by 17.7% for malic acid and 21.0% for PYRAMPA compared to the medium control.

5.3 Discussion

5.3.1 Ligands ameliorated the metal toxicity

The titration with $Al(mal)_3$, $CuSO_4$, $ZnSO_4$, CrO_3 and $NaAsO_2$ (Figures 5.1 - 5.5) demonstrated that these metal ions have distinct cellular cytotoxicity. However, the treatment of neuronal cells with chelating ligands protected against the deleterious effects of these metal ions (Figures 5.7 - 5.11).

The ligand, GSH, improved the cell viability by 60.1% for Al^{3+}, 73.5% for Cu^{2+}, 34.8% for Zn^{2+}, 79.6% for Cr^{6+} and 57.8% for As^{3+}, demonstrating its detoxifying ability. The molecular mechanisms preventing metal toxicity by GSH appear to follow two routes, namely its coordinating structure and its antioxidant activity. GSH is a proven antioxidant which can maintain the redox balance against biometals (Cu^{2+} and Zn^{2+}) and toxic metal/metalloid (Cr^{6+}, Al^{3+} and As^{3+}) (Forman et al., 2009; Wegmuller et al., 2014; Hernandez et al., 2015; Saporito-

Magriñá et al., 2018), and the thiol group in GSH can act as a key metal binding ligand (Hernandez et al., 2015). The effectiveness of GSH in metal detoxification signifies its therapeutic potential for metal dyshomeostasis of biometals as well as over-exposure of nonessential and toxic metals.

Likewise, the presence of histidine increased cell viability by 20.2% for Al^{3+}, 54.9% for Cu^{2+}, 4.4% for Zn^{2+}, 57.7% for Cr^{6+} and 70.1 % for As^{3+}. The underlying molecular mechanisms by which histidine exerts this protective function against metal ions is likely due to its coordinating property and its antioxidant activity. Histidine was demonstrated as the most effective hydroxyl radical scavenger out of several investigated amino acids (Zs.-Nagy and Floyd, 1984) and it is well established to be able to bind to excess divalent metal ions (e.g. Cu^{2+} and Zn^{2+}) (Van Campen and Gross, 1969; Sandstrom et al., 1985). Therapeutic use of histidine was explored by Matsui (2017), who found that the supplementation of histidine, at concentrations higher than 10 mM, can be effective in maintaining mitochondrial function by suppressing oxidative stress. Treatment of histidine increased both nitric oxide synthases (NOS) and total antioxidant capacity in neural tissue of rats (Milewski et al., 2015).

Maltol improved cell viability by 15.3% for Al^{3+}, 11.9% for Cu^{2+}, 39.7% for Cr^{6+} and 42.7% for As^{3+}. Intriguingly, it could not improve the cell viability under zinc treatment, rather exacerbating the cytotoxicity of Zn^{2+}, with a decrease of 13.4% cell viability compared to zinc alone control. As a membrane-permeable chelator, maltol was found to facilitate the uptake of Zn^{2+} in erythrocytes (Brand and Kleineke, 1996), which explains the above finding in this study. Further evidence demonstrates that maltol increases the accumulation of Zn^{2+} in the cells in comparison to zinc in the form of zinc acetate, zinc chloride or zinc sulphate (Hider et al., 1990). The decrease in cell viability caused by maltol under zinc treatment is likely due to the maltol

facilitating the zinc uptake and in turn increasing zinc toxicity. With maltol exacerbating effect in Zn^{2+} toxicity as well as its lower improvement in cell viability for Al^{3+} and Cu^{2+}, it is reasonable I believe to conclude that maltol might not be an ideal chelating agent for therapeutic purpose against Al^{3+}, Cu^{2+} and Zn^{2+}. However, the findings demonstrate that maltol is potentially useful against the toxic metal/metalloids, Cr^{6+} and As^{3+}. Thompson (2006) investigated maltol as a therapeutic agent for toxic metalloids. Maltol as well as its close analogues hydroxypyrones and hydroxypyridinones have many medicinal applications, from the ability to remove or supplement metal ion absorption (Barrand et al., 1987), to forming complexes in contrast agents used in magnetic resonance imaging (MRI), and chemotherapeutic agents (Santos, 2002). Maltol and the analogues were demonstrated to have high affinity with a range of metal ions (Santos, 2002; Yu et al., 2002; Kaneko et al., 2004).

Citric acid seemed to be effective in protecting cell against metal ion toxicity with an increase in cell viability of 39.5% for Al^{3+}, 24.9% for Cu^{2+}, 34.8% for Cr^{6+} and 38.8% for As^{3+}. It is known that citric acid can stimulate plant growth, and enhance phytoextraction of metal ions (Brand and Kleineke, 1996), it is a better alternative environmentally to synthetic chelator EDTA (Ethylenediaminetetraacetic acid) in the removal of heavy metals (Chaturvedi et al., 2015). It also acts as a superoxide anion scavenger (Van Den Berg et al., 2003) and in heavy metals contaminated sludge acts as a chemical extracting agent (Zhang et al., 2008). However, citric acid requires a low pH of 3 to be effective in extracting metal ions from the environment, which is not physiologically possible (del Dacera and Babel, 2006). In contrast, citric acid exacerbates Zn^{2+} toxicity by decreasing the cell viability (Figure 5.8). This might be explained by its ability to facilitate zinc uptake as citric acid is known to increase zinc absorption (Wegmuller et al., 2014). While citric acid was found to prevent Al^{3+} from binding to the serum transferrin protein in humans, its metal chelation required a substantial excess of citrate (Harris

et al., 2003). Also CD (circular dichroism) titration studies indicated citric acid could not reverse the β-pleated sheet conformation in Aβ aggregation caused by Al^{3+} (Samanta et al., 2018). Therefore, considering my findings together with the previous literature, citric acid may not be an effective agent for AD patient in reducing metal overload. However, as citric acid is a harmless natural compound, it should be beneficial no matter how infinitesimal such benefit is.

Malic acid increased the cell viability by 19.4% for Al^{3+}, 24.9% for Cu^{2+}, 34.8% for Cr^{6+}, 38.8% for As^{3+} and decreased the cell viability by 40.5% for Zn^{2+}. The increase in the toxicity of zinc by malic acid is due to the ability of malic acid to increase Zn^{2+} absorption (Saunders et al., 2013). Malic acid can readily reduce Cr^{6+} to Cr^{3+} (Zhong and Yang, 2012) and the acid exhibits higher affinity for trivalent metals (Jones, 1998). This notion is also supported by the relative increase of cell viability in As^{3+} and Cr^{6+} treated cells I have found.

5.3.2 The effect of Al^{3+} and Zn^{2+}on APP gene expression in SH-SY5Y cells

APP gene encodes amyloid precursor protein (APP) (Ghasemi-Fasaei, 2012). The finding (Figure 5.11) demonstrates the relative expression of APP gene is upregulated in the presence of Al^{3+}, which likely results in more amyloid precursor protein in neuronal cells. Walton and Wang (2009) also found similar results in animal models, which shows that Al^{3+} consistently derived from chronic oral ingestion resulted in upregulation of APP gene expression, and an increased APP deposition compared to the brains of the cognitively-intact controls. Therefore, the finding in this study adds further support to the role of Al^{3+} in the development of AD.

Yet while aluminium is the main metal of interest in this study, its involvement in AD remains controversial. Metals, Al^{3+}, Zn^{2+}, Cu^{2+} and $Fe^{2+/3+}$, have been found in AD brains (Exley et al.,

2012; House et al., 2012). In the brains of the cognitively-deteriorated rats, aluminium was accumulated in the cores of senile plaque of cortical neurons and astrocytes in the hippocampus (Walton and Wang, 2009). *In vitro* studies by Kawahara et al. (1994) found Al^{3+} readily promotes the aggregation of Aβ, which is supported by my findings in Chapter 3. Not only does Al^{3+} increase the relative expression of the APP gene, Zn^{2+} also elevates the expression of APP, albeit to a lesser degree than Al^{3+} (Figure 5.11). The increase of intracellular Zn^{2+} by genetic or pharmacological methods in different cellular and *in vivo* systems consistently affect the production of Aβ and APP (House et al., 2004; Lovell, 2009; Bolognin et al., 2011). Although Zn^{2+} may play a role in multiple pathways relevant to AD. It is significate that APP production is regulated by Zn-containing transcription factors (NF-κβ and sp1) and Zn^{2+} is essential for their activity (Zabel et al., 1991; Zeng et al., 1991). In addition to the effect of Zn^{2+} on APP expression, Zn^{2+} also elevates processing of the protein. Normal non-amyloidogenic processing of APP by cleavage in the Golgi complex, leads to formation of sAPPα, a neurotrophic factor (Wilquet and De Strooper, 2004). Zn^{2+} inhibits the α-secretase mediated sAPPα formation pathway and increase generation of $A\beta_{40}$ and $A\beta_{42}$ (Bush et al., 1994). Altogether, these cellular and physiological observations strongly indicate that Al^{3+} and Zn^{2+} play important roles in APP production, Aβ aggregation and AD pathology.

5.3.3 Chelating ligand treatment decreases metal-induced APP gene expression.

Finally, the effect of chelating ligands on metal-induced APP gene expression as I have reported was consequential, the ligands bring down the expression of the APP under Al^{3+} (Figure 5.12). GSH exhibited the greater decrease in relative expression of APP gene. This is in agreement with the study by Vinothkumar (2017) who found that the addition of GSH could lower $A\beta_{42}$

expression. Yet another important aspect of the potential therapeutic value for AD in addition to its ability to reduce metal toxicity.

Histidine treatment also lowers the expression of APP gene in Al^{3+} treated cells. Little is known about how histidine lowers APP gene expression. Based on the metal chelating and antioxidant ability of the amino acid previously discussed, it is likely it functions similarly to GSH. Histidine is yet another potential therapeutic ligand.

In regards to the organic acids, citric acid and malic acid, they did down regulate APP in Al^{3+} treated cells, compared to the respective control. However, they alone, while not statistically significant, upregulated APP expression compared to the control. Similarly, PYRAMPA alone significantly increased the expression of APP, compared to the control. While citric acid, malic acid and PYRAMPA can chelate metals and down-regulate APP gene expression, this study indicates they are not as effective as GSH and histidine. With a complex neurodegenerative disease such as AD, multiple causative factors are involved. We need to develop therapeutic agents which can target multiple causative factors. Based on this study, GSH and histidine demonstrate multiple beneficial effects in metal toxicity and APP gene expression. They should be further explored in future studies for their potential in treatment of AD.

5.4 Conclusion

The findings demonstrate that GSH and histidine significantly increased the cell viability in the presence of Cu^{2+}, Zn^{2+}, Al^{3+}, Cr^{6+} and As^{3+}. It is shown, for the first time, that Al^{3+} upregulates the expression of the APP gene in human neuronal cells, and that GSH and histidine can lower the gene expression of APP induced by Al^{3+} and Zn^{2+}. My results provide more evidence for the involvement of metal ions such as Al^{3+} and Zn^{2+} in AD development, as they can upregulate APP gene expression in addition to their direct binding to the Aβ peptide. Furthermore, the findings demonstrate that the ligands GSH and histidine are effective in detoxifying metal ions and negate the metal-induced APP gene expression, clearly shows their strong potential in combatting AD.

6 CONCLUDING DISCUSSION

Alzheimer's disease (AD) is a devastating neurodegenerative condition that poses major challenges to human health, with a prevalence of around 35 million patients worldwide (Atrián-Blasco et al., 2017). In order to better understand the roles of metal ion in Aβ aggregation and in APP expression, I have focused on the molecular interaction of metal ions with Aβ peptide, the interaction of ligands with metal ions, and the effect of metal ions on the expression of APP gene which encodes amyloid precursor protein. The main discoveries presented in this PhD analysis are:

1. the determination of the solution structure of synthetic $A\beta_{1-28}$ complexed with Al^{3+} by NMR spectroscopy,
2. the characterisation of the metal binding sites on $A\beta_{1-28}$,
3. the upregulation of the expression of APP gene by Al^{3+}, and
4. the presence of metal chelating ligands can lower the metal-induced APP gene expression, which should subsequently reduce the accumulation of Aβ.

6.1 Al^{3+} coordinates to Aβ triggering structural modifications and aggregation

Exposure to Al^{3+} results in Aβ aggregation and neurofibrillary degeneration (Langui et al., 1990; Bush, 2003; Exley, 2006) and increased Al^{3+} levels can lead to degenerating neurons in AD (Vasudevaraju et al., 2008; Exley and Vickers, 2014). Nevertheless, the role of Al^{3+} in AD continues to be controversial although accumulating evidence demonstrates that Al^{3+} is linked

to AD (Kawahara and Kato-Negishi, 2011). I have identified specific Al^{3+} binding sites within Aβ peptide, which provides further evidence for the association of Al^{3+} with AD.

The binding of Al^{3+} to Aβ is manifested by the exchange phenomena which are evident in the ^{1}H NMR and 2D NMR data in Chapter 3. Comprehensive information for Aβ coordination to Al^{3+} was presented in Figure 3.13, and further verified by Aβ analogues. The amino acid residues involved in the Al^{3+} coordination was deduced from the TOCSY NMR. As indicated by Figure 3.3, the $A\beta_{1\text{-}28}$ can coordinate to Al^{3+} via the imidazole NH group of His6, His13, His14 and the N-terminal amino group or Asp1. As demonstrated by the titration of Al^{3+} with $A\beta_{1\text{-}28}$, the CSP values of the αH Asp1 at 4.09ppm; His6 at 4.51ppm; His13 at 4.57ppm and His14 at 4.52 ppm were significant compared to other residues.

The use of the Aβ analogue, H6,13,14A (where the His residues at positions 6, 13 and 14 are replaced by alanine residues) demonstrated that only Asp1 αH in H6,13,14A was significantly affected by Al^{3+} addition. Titration of H6,13,14A produced a slow exchange, indicating potential secondary binding sites of Al^{3+} within Aβ. Previous studies also suggest additional residues may interact specifically with Al^{3+} such as Gly9, Tyr10 and Glu11 (Narayan et al., 2013). A computational simulation identified Glu3, Asp7, and Glu11 as likely site for Cu^{2+} and Zn^{2+} binding (Mujika et al., 2017). So, these negatively charged residues at physiological pH might also be able to bind Al^{3+}.

The stoichiometry of Al^{3+} to $A\beta_{1–28}$ was 1:1, resulting in the proposed structural mode of Al^{3+} coordination to $A\beta_{1–28}$, I presented in Figure 3.13. I found that Al^{3+} has a similar affinity to Aβ compared to Zn^{2+}. It is extensively known that Zn^{2+} is involved in Aβ aggregation (Arispe et al., 1996; Danielsson et al., 2007; Bolognin et al., 2011; Craddock et al., 2012). Zinc was expected to bind more strongly to Aβ. Intriguingly, the binding affinity (K_D) of 0.35 ± 0.03 mM

for Al^{3+} to $A\beta_{1-28}$ is very similar to the K_D of Zn^{2+}- $A\beta_{1-28}$ of 0.28 ± 0.03 mM (Alies et al., 2016). Dissociation constant value for Al^{3+} has been reported for the first time.

By using $A\beta_{1-28}$ and its analogues ($A\beta_{1-28}$ H6A, $A\beta_{1-28}$ H13A, $A\beta_{1-28}$ H14A and $A\beta_{1-28}$ H6,13,14A), the molecular details for the interaction of $A\beta_{1-28}$ and Al^{3+} via histidine have been delineated for the first time. As shown in Figure 3.13, the Al^{3+} ion is coordinated through the imidazole nitrogens of the three histidines, His6, His13, and His14. The N-terminal Asp1 and Gly25/Lys28. His13 and His14 coordinate in equilibrium for one binding position, His13 may be the preferred ligand in comparison to His14. These findings also suggest that His13 and His14 compete for one binding site due to their steric encumbrance (Faller and Hureau, 2009; Atrián-Blasco et al., 2017). The preference for His13 is supported by the finding that the methylation of His13 lowers the affinity for metal ions and thus depletes aggregation (Tickler et al., 2005; Smith et al., 2006). Interestingly naked mole-rats (*Heterocephalus glaber*) show greater homology to the human sequence, compared to the rat models (*Rattus norvegicus*), with only the arginine substitution for His13 (Andreeva et al., 2017). This subtle one residue variation, resulted in the interspecies difference in Aβ aggregation propensity and neurotoxicity (Smith et al., 2015). His13 is involved in the early formation of N-terminal β-sheet, found in amyloid plaques (Duff et al., 1996). With similar Aβ concentrations as the triple-transgenic mouse model (3xTg-AD), the naked mole-rats indicate no extracellular amyloid plaque formation or AD-like symptoms (Edrey et al., 2013). Therefore understandably from the importance of His13, this residue has even been targeted in AD therapeutic agents (Diaz et al., 2006).

The metal ion coordination with Aβ affects the secondary structure of Aβ. As indicated by calculating the CSI (Figure 3.9), the addition of Al^{3+} caused the structural transition of soluble

Aβ from a primarily random coil structure to a proto-filaments and β-sheet conformation which is the key structural feature in aggregated Aβ. Between Glu11 to Gln15 a β-sheet structure appears, supporting the notion that Al^{3+} facilitates this structural transition important for Aβ aggregation (Serpell, 2000). These findings together demonstrate that Al^{3+} is interacting with Aβ peptide and therefore is likely involved in AD pathogenesis.

Moving on to the effect of metal ions on Aβ at the gene level, I have asked whether metal ions can increase the expression of the APP gene. An upregulation of APP gene would most likely mean an increase of Aβ production in neuronal cells. The findings in Figure 5.11 demonstrate that the relative expression of APP gene is upregulated in the presence of Al^{3+} and Zn^{2+}, suggesting that these two metal ions likely induce higher level of amyloid precursor protein and consequently more Aβ. The upregulation of APP gene by metal ions is a novel finding for human neuronal cells, although similar result was found in animal models (Lin et al., 2008; Walton and Wang, 2009). Possible modulation of the production and metabolism of Aβ by means of Zn^{2+}-containing α-secretase was speculated in a previous review (Kepp, 2012), but no concrete evidence was provided. The presence of Cu^{2+} was also found to increase both the dimerization of APP and the extracellular release of Aβ (Noda et al., 2013). The current finding that Al^{3+} and Zn^{2+} upregulate the expression of APP gene in SH-SY5Y neuronal cells provides, for the first time, the experimental evidence for their potential role in regulating APP gene expression.

Taken together the findings of Chapter 3 and 5, as summarised above, demonstrate that metal ions are involved in the interaction with Aβ peptide and in the upregulation of APP gene, they therefore could play a role in Aβ accumulation and aggregation. My work thus supports the unification of the amyloid cascade and metal ion hypotheses for AD. The amyloid cascade

hypothesis suggests that aggregation of the Aβ peptide into soluble oligomers and senile plaques is the main driver of AD (Hardy and Higgins, 1992; Karran et al., 2011; Barage and Sonawane, 2015), while the metal ion hypothesis suggests that disruption of metal ion homeostasis promotes Aβ aggregation and onset of AD (Zatta et al., 2009; Tabner et al., 2011; Kepp, 2012). Here in this study, the collective findings demonstrate for the first time that metal ions are involved in both metal-Aβ interaction and upregulation of the APP gene expression which in turn may lead to higher Aβ production. These findings suggest that metal ions and Aβ are partners in crime for the pathogenesis of AD.

Whether Al^{3+} cause Aβ aggregation remains the subject of intense debate. However, I have shown that specific binding sites exist for Al^{3+}, and that Aβ undergoes primary and secondary structural changes in the presence of Al^{3+}. Finally, I have demonstrated the gene expression of APP is upregulated in the presence of Al^{3+} as well as Zn^{2+}. These findings support the very strong link between Al^{3+} and Aβ.

6.2 Metal chelating ligands antagonise the role of metal ions in APP gene expression

The aetiology of AD is complex. The ability of Al^{3+} to bind to Aβ as described in Chapter 3, as well as the previously established binding of Cu^{2+}, Zn^{2+} and $Fe^{2+/3+}$ to Aβ (Syme et al., 2004; Danielsson et al., 2007; Bousejra-El Garah et al., 2011), points to the involvement of metal ions in AD pathogenesis. This study also shows the presence of metal ions can cause conformational changes in the Aβ, which supports the notion that metal ions are linked to AD. Therefore, development of potential metal chelators for AD treatment is a vital approach in current and

future researches. With AD having complex and multi-causative factors, multiple approaches are likely the effective way forward in combating the disease. Therefore, I have investigated metal chelating ligands to see if they can antagonise metal ions in their cytotoxicity and in their role of upregulating APP gene expression.

The chelating ligands, GSH, histidine, maltol, citric acid and malic acid, did protect against the deleterious effects of metal ions. Histidine and GSH drastically increased cell viability in the metal induced cytotoxicity. GSH improving the cell viability by 60.1% for Al^{3+}, 73.5% for Cu^{2+}, 34.8% for Zn^{2+}, 79.6% for Cr^{6+} and 57.8% for As^{3+}. Histidine increased cell viability by 20.2% for Al^{3+}, 54.9% for Cu^{2+}, 4.4% for Zn^{2+}, 57.7% for Cr^{6+} and 70.1% for As^{3+}. The potential for histidine as a metal chelator to antagonise metal's binding to Aβ is ironically an epitome of fighting fire with fire, since it is mainly the histidine residues in Aβ that confer its metal binding. The protective activity of histidine and GSH are likely due to their coordination structure and antioxidant functionality, which incidentally addresses two causative AD factors, i.e. metal ions and oxidative stress. Histidine can bind to metals in a cellular environment with significantly less steric hindrance compared to Aβ. Histidine can also reduce oxidative stress and scavenge hydroxyl radicals (Zs.-Nagy and Floyd, 1984; Milewski et al., 2015). The structure of GSH contains donating atoms in the form of two carbonyls, an amide and thiol group. The number and diversity of coordination sites within GSH allow it to act as an efficient metal binding ligand. The antioxidant ability of GSH is well known (Forman et al., 2009; Wegmuller et al., 2014; Hernandez et al., 2015; Saporito-Magriñá et al., 2018). Therefore, these ligands can be used to combat Aβ aggregation and reduce reactive oxygen species. Of the tested ligands, histidine and GSH were the only molecules that did not increase the toxicity of Zn^{2+} (Figure 5.7). This suggests both histidine and GSH would not assist the transport of Zn^{2+} into the cell, in contrast to the other ligands such as maltol (Brand and Kleineke, 1996), citric acid

(Wegmuller et al., 2014) and malic acid (Saunders et al., 2013), which facilitate the metal uptake. The usefulness of histidine and GSH as the ideal metal ligands is further supported by their ability to reduce the expression of APP gene. Whilst the mechanism of histidine and GSH in reducing APP gene expression is not clear, the finding here demonstrates their potential for AD treatment. Future studies on this front is warranted.

6.3 The significance and prospective directions

Up until the present, the role of Aβ and metal ion in AD pathogenesis has been controversial. The findings I have reported demonstrate that Al^{3+} upregulates the expression of APP gene and binds to Aβ peptide. It also promotes the structural transition of soluble Aβ from a primarily random coil structure to the β-sheet conformation, a key feature of the aggregated Aβ. The data provide meaningful evidence for likely involvement of Al^{3+} in Aβ aggregation and AD development. Further studies on this front should be continued, at both molecular and clinical levels.

This thesis further characterised a panel of metal chelating ligands (GSH, histidine, maltol, citric acid and malic acid) which may be useful to combating AD and heavy metal toxicity. They mediate the drastic reduction of metal induced cytotoxicity. Specifically, GSH and histidine showed the highest protective ability. GSH and histidine also reduced the increase in APP gene expression caused by the presence of Al^{3+} and Zn^{2+}. This discovery has significance in the development of AD therapeutics. The underlying molecular mechanism for the role GSH and histidine play in reducing APP gene expression should be investigated in the future.

In conclusion, I have provided significant evidence for the interaction of metal ions with Aβ. The molecular details of Al^{3+} interaction with Aβ and its role in upregulating APP gene expression are novel. The findings related to the metal chelating ligands histidine and GSH are consequential, and their potential in AD treatment should be explored in future studies.

References

Adlard PA, Bush AI (2006) Metals and Alzheimer's disease. *The Journal of Alzheimer's Disease* **10:** 145-163

Aghav P, Dhage VN, Mane ML, Shengule D, Dorik R, Jadhav K (2011) Effect of aluminum substitution on the structural and magnetic properties of cobalt ferrite synthesized by sol–gel auto combustion process. *Physica B: Condensed Matter* **406:** 4350-4354

Akatsu H, Hori A, Yamamoto T, Yoshida M, Mimuro M, Hashizume Y, Tooyama I, Yezdimer EM (2012) Transition metal abnormalities in progressive dementias. *BioMetals* **25:** 337-350

Alfrey AC, LeGendre GR, Kaehny WD (1976) The dialysis encephalopathy syndrome: possible aluminum intoxication. *New England Journal of Medicine* **294:** 184-188

Alies B, Conte-Daban A, Sayen S, Collin F, Kieffer I, Guillon E, Faller P, Hureau C (2016) Zinc(II) Binding Site to the Amyloid-β Peptide: Insights from Spectroscopic Studies with a Wide Series of Modified Peptides. *Inorganic Chemistry* **55:** 10499-10509

Alies B, Renaglia E, Rózga M, Bal W, Faller P, Hureau C (2013) Cu(II) Affinity for the Alzheimer's Peptide: Tyrosine Fluorescence Studies Revisited. *Analytical Chemistry* **85:** 1501-1508

Allen DD, Orvig C, Yokel RA (1995) Evidence for energy-dependent transport of aluminum out of brain extracellular fluid. *Toxicology* **98:** 31-39

Anantharaman M, Tangpong J, Keller JN, Murphy MP, Markesbery WR, Kiningham KK, Clair DKS (2006) β-Amyloid mediated nitration of manganese superoxide dismutase: implication for oxidative stress in a APPNLH/NLH X PS-1P264L/P264L double knock-in mouse model of Alzheimer's disease. *The American Journal of Pathology* **168:** 1608-1618

Andersen O (2004) Chemical and biological considerations in the treatment of metal intoxications by chelating agents. *Mini-Reviews in Medicinal Chemistry* **4:** 11-21

Andreeva TV, Lukiw WJ, Rogaev EI (2017) Biological Basis for Amyloidogenesis in Alzheimer's Disease. *Biochemistry (Moscow)* **82:** 122-139

Antipova IA, Mukha SA, Medvedeva SA (2005) Al (III)–Maltol Complexes, Structure and Stability. *Chemistry for Sustainable Development* **13:** 377–381

Arispe N, Diaz J, Durell SR, Shafrir Y, Guy HR (2010) Polyhistidine peptide inhibitor of the Abeta calcium channel potently blocks the Abeta-induced calcium response in cells. Theoretical modeling suggests a cooperative binding process. *Biochemistry* **49:** 7847-7853

Arispe N, Diaz JC, Flora M (2008) Efficiency of histidine-associating compounds for blocking the alzheimer's Abeta channel activity and cytotoxicity. *Biophysical Journal* **95:** 4879-4889

Arispe N, Pollard HB, Rojas E (1996) Zn2+ interaction with Alzheimer amyloid beta protein calcium channels. *Proceedings of the National Academy of Sciences of the United States of America* **93:** 1710-1715

Arseniev AS, Wider G, Joubert FJ, Wüthrich K (1982) Assignment of the 1H nuclear magnetic resonance spectrum of the trypsin inhibitor E from Dendroaspis polylepis polylepis: Two-dimensional nuclear magnetic resonance at 500 MHz. *Journal of Molecular Biology* **159:** 323-351

Atrián-Blasco E, Conte-Daban A, Hureau C (2017) Mutual interference of Cu and Zn ions in Alzheimer's disease: perspectives at the molecular level. *Dalton Transactions* **46:** 12750-12759

Atwood CS, Moir RD, Huang X, Scarpa RC, Bacarra NME, Romano DM, Hartshorn MA, Tanzi RE, Bush AI (1998) Dramatic aggregation of Alzheimer Aβ by Cu (II) is induced by conditions representing physiological acidosis. *The Journal of Biological Chemistry* **273:** 12817-12826

B Pocernich C, LB Lange M, Sultana R, A Butterfield D (2011) Nutritional approaches to modulate oxidative stress in Alzheimer's disease. *Current Alzheimer Research* **8:** 452-469

Ballard C, Gauthier S, Corbett A, Brayne C, Aarsland D, Jones E (2011) Alzheimer's disease. *The Lancet* **377:** 1019-1031

Ballatori N, Krance SM, Marchan R, Hammond CL (2009) Plasma membrane glutathione transporters and their roles in cell physiology and pathophysiology. *Molecular Aspects of Medicine* **30:** 13-28

Barage SH, Sonawane KD (2015) Amyloid cascade hypothesis: Pathogenesis and therapeutic strategies in Alzheimer's disease. *Neuropeptides* **52:** 1-18

Barber RC (2012) The Genetics of Alzheimer's Disease. *Scientifica* **2012:** 246210

Barber VS, Griffiths HR (2003) Is glutathione an important neuroprotective effector molecule against amyloid beta toxicity? *Biofactors* **17:** 215-228

Barceloux DG (1999) Chromium. *The Journal of Clinical Toxicology* **37:** 173-194

Barrand MA, Callingham BA, Hider RC (1987) Effects of the pyrones, maltol and ethyl maltol, on iron absorption from the rat small intestine. *The Journal of Pharmacy and Pharmacology* **39:** 203-211

Beal MF (1995) Aging, energy, and oxidative stress in neurodegenerative diseases. *Annals of Neurology* **38:** 357-366

Beauchemin D, Kisilevsky R (1998) A method based on ICP-MS for the analysis of Alzheimer's amyloid plaques. *Analytical Chemistry* **70:** 1026-1029

Bernstein LR, Tanner T, Godfrey C, Noll B (2000) Chemistry and pharmacokinetics of gallium maltolate, a compound with high oral gallium bioavailability. *Metal based drugs* **7:** 33-47

Beyersmann D, Hartwig A (2008) Carcinogenic metal compounds: recent insight into molecular and cellular mechanisms. *Archives of Toxicology* **82:** 493

Bhat AH, Dar KB, Anees S, Zargar MA, Masood A, Sofi MA, Ganie SA (2015) Oxidative stress, mitochondrial dysfunction and neurodegenerative diseases; a mechanistic insight. *Biomedicine & Pharmacotherapy* **74:** 101-110

Bhattacharya S (2015) Reactive oxygen species and cellular defense system. *In* Free Radicals in Human Health and Disease. *Springer,* pp 17-29

Blessed G, Tomlinson BE, Roth M (1968) The association between quantitative measures of dementia and of senile change in the cerebral grey matter of elderly subjects. *The British Journal of Psychiatry* **114:** 797-811

Bolognin S, Messori L, Drago D, Gabbiani C, Cendron L, Zatta P (2011) Aluminum, copper, iron and zinc differentially alter amyloid-Abeta(1-42) aggregation and toxicity. *The International Journal of Biochemistry & Cell Biology* **43:** 877-885

Bolognin S, Messori L, Drago D, Gabbiani C, Cendron L, Zatta P (2011) Aluminum, copper, iron and zinc differentially alter amyloid-Aβ1–42 aggregation and toxicity. *The International Journal of Biochemistry & Cell Biology* **43:** 877-885

Bondy SC (2010) The neurotoxicity of environmental aluminum is still an issue. *Neurotoxicology* **31:** 575-581

Bousejra-El Garah F, Bijani C, Coppel Y, Faller P, Hureau C (2011) Iron(II) Binding to Amyloid-β, the Alzheimer's Peptide. *Inorganic Chemistry* **50:** 9024-9030

Boyd-Kimball D, Sultana R, Abdul HM, Butterfield DA (2005) γ-glutamylcysteine ethyl ester-induced up-regulation of glutathione protects neurons against Aβ (1–42)-mediated oxidative stress and neurotoxicity: Implications for Alzheimer's disease. *The Journal of Neuroscience* **79:** 700-706

Boyd-Kimball D, Sultana R, Poon HF, Mohmmad-Abdul H, Lynn BC, Klein JB, Butterfield DA (2005) γ-Glutamylcysteine ethyl ester protection of proteins from Aβ (1–42)-mediated oxidative stress in neuronal cell culture: A proteomics approach. *The Journal of Neuroscience* **79:** 707-713

Brajenović N, Tonković M (2003) The influence of malic acid, phosphate ion, and urea on the mobility of metal ions. *The Journal of Liquid Chromatography & Related Technologies* **26:** 1969-1976

Brand IA, Kleineke J (1996) Intracellular zinc movement and its effect on the carbohydrate metabolism of isolated rat hepatocytes. *The Journal of Biological Chemistry* **271:** 1941-1949

Breen KC, Bruce M, Anderton BH (1991) Beta amyloid precursor protein mediates neuronal cell-cell and cell-surface adhesion. *The Journal of Neuroscience* **28:** 90-100

Brown DR, Kozlowski H (2004) Biological inorganic and bioinorganic chemistry of neurodegeneration based on prion and Alzheimer diseases. *Dalton Transactions:* 1907-1917

Budimir A (2011) Metal ions, Alzheimer's disease and chelation therapy. *Acta Pharmaceutica Sinica B* **61:** 1-14

Buée L, Ding W, Delacourte A, Fillit H (1993) Binding of secreted human neuroblastoma proteoglycans to the Alzheimer's amyloid A4 peptide. *Brain Research* **601:** 154-163

Burnet FM (1981) A possible role of zinc in the pathology of dementia. *The Lancet* **1:** 186-188

Bush A, Tanzi R (2008) Therapeutics for Alzheimer's disease based on the metal hypothesis. *Neurotherapeutics* **5:** 421-432

Bush AI (2003) The metallobiology of Alzheimer's disease. *Trends in Neurosciences* **26:** 207-214

Bush AI, Masters CL (2001) Clioquinol's return: Cautions from Japan - Response. *Science* **292:** 2251-2252

Bush AI, Masters CL, Tanzi RE (2003) Copper, β-amyloid, and Alzheimer's disease: Tapping a sensitive connection. *Proceedings of the National Academy of Sciences of the United States of America* **100:** 11193-11194

Bush AI, Multhaup G, Moir RD, Williamson TG, Small DH, Rumble B, Pollwein P, Beyreuther K, Masters C (1993) A novel zinc (II) binding site modulates the function of the beta A4 amyloid protein precursor of Alzheimer's disease. *The Journal of Biological Chemistry* **268:** 16109-16112

Bush AI, Pettingell WH, Multhaup G, d Paradis M, Vonsattel JP, Gusella JF, Beyreuther K, Masters CL, Tanzi RE (1994) Rapid induction of Alzheimer A beta amyloid formation by zinc. *Science* **265:** 1464-1467

Butterfield DA (2002) Amyloid beta-peptide (1-42)-induced oxidative stress and neurotoxicity: implications for neurodegeneration in Alzheimer's disease brain. A review. *Free Radical Research* **36:** 1307-1313

Butterfield DA, Hensley K, Harris M, Mattson M, Carney J (1994) β-Amyloid Peptide Free Radical Fragments Initiate Synaptosomal Lipoperoxidation in a Sequence-Specific Fashion: Implications to Alzheimer′s Disease. *Biochemical and Biophysical Research Communications* **200:** 710-715

Butterfield DA, Poon HF, St Clair D, Keller JN, Pierce WM, Klein JB, Markesbery WR (2006) Redox proteomics identification of oxidatively modified hippocampal proteins in mild cognitive impairment: insights into the development of Alzheimer's disease. *Neurobiology of Disease* **22:** 223-232

Cahoon L (2009) The curious case of clioquinol. *Nature Medicine* **15:** 356-359

Cardenas-Aguayo Mdel C, Gomez-Virgilio L, DeRosa S, Meraz-Rios MA (2014) The role of tau oligomers in the onset of Alzheimer's disease neuropathology. *ACS Chemical Neuroscience* **5:** 1178-1191

Chaturvedi N, Dhal N, Patra H (2015) EDTA and citric acid-mediated phytoextraction of heavy metals from iron ore tailings using Andrographis paniculata: a comparative study. *International Journal of Mining, Reclamation and Environment* **29:** 33-46

Cheignon C, Tomas M, Bonnefont-Rousselot D, Faller P, Hureau C, Collin F (2018) Oxidative stress and the amyloid beta peptide in Alzheimer's disease. *Redox biology* **14:** 450-464

Chen P, Miah M, Aschner M (2016) Metals and neurodegeneration *F1000Research* **5**

Chen W-T, Liao Y-H, Yu H-M, Cheng IH, Chen Y-R (2011) Distinct effects of Zn2+, Cu2+, Fe3+, and Al3+ on amyloid-β stability, oligomerization, and aggregation amyloid-β destabilization promotes annular protofibril formation. *The Journal of Biological Chemistry* **286:** 9646-9656

Cherny RA, Atwood CS, Xilinas ME, Gray DN, Jones WD, McLean CA, Barnham KJ, Volitakis I, Fraser FW, Kim Y-S, Huang X, Goldstein LE, Moir RD, Lim JT, Beyreuther K, Zheng H, Tanzi RE, Masters CL, Bush AI (2001) Treatment with a Copper-Zinc Chelator Markedly and Rapidly Inhibits β-Amyloid Accumulation in Alzheimer's Disease Transgenic Mice. *Neuron* **30:** 665-676

Cherny RA, Legg JT, McLean CA, Fairlie DP, Huang X, Atwood CS, Beyreuther K, Tanzi RE, Masters CL, Bush AI (1999) Aqueous dissolution of Alzheimer's disease Aβ amyloid deposits by biometal depletion. *Journal of Biological Chemistry* **274:** 23223-23228

Cherny RA, Legg JT, McLean CA, Fairlie DP, Huang X, Atwood CS, Beyreuther K, Tanzi RE, Masters CL, Bush AI (1999) Aqueous dissolution of Alzheimer's disease Aβ amyloid deposits by biometal depletion. *The Journal of Biological Chemistry* **274:** 23223-23228

Chopra K, Misra S, Kuhad A (2011) Neurobiological aspects of Alzheimer's disease. *Expert Opinion on Therapeutic Targets* **15:** 535-555

Chow VW, Mattson MP, Wong PC, Gleichmann M (2010) An Overview of APP Processing Enzymes and Products. *NeuroMolecular Medicine* **12:** 1-12

Chua MS, Bernstein LR, Li R, So SK (2006) Gallium maltolate is a promising chemotherapeutic agent for the treatment of hepatocellular carcinoma. *Anticancer Research* **26:** 1739-1743

Craddock T, Tuszynski J, Chopra D, Casey N, Goldstein L, Hameroff S, Tanzi R (2012) The zinc dyshomeostasis hypothesis of Alzheimer's disease. *PLOS One* **7**

Crapper DR, Krishnan SS, Dalton AJ (1973) Brain Aluminum Distribution in Alzheimer's Disease and Experimental Neurofibrillary Degeneration. *Science* **180:** 511

D'Haese PC, De Broe ME (2001) Chapter 11 - Aluminium and Iron: Implications for Alzheimer's Disease. *In* C Exley, ed, Aluminium and Alzheimer's Disease. *Elsevier, Amsterdam,* pp 221-231

Danielsson J, Pierattelli R, Banci L, Gräslund A (2007) High-resolution NMR studies of the zinc-binding site of the Alzheimer's amyloid β-peptide. *The FASEB Journal* **274:** 46-59

Darbre PD, Bakir A, Iskakova E (2013) Effect of aluminium on migratory and invasive properties of MCF-7 human breast cancer cells in culture. *The Journal of Inorganic Biochemistry* **128:** 245-249

Davenward S, Bentham P, Wright J, Crome P, Job D, Polwart A, Exley C (2013) Silicon-rich mineral water as a non-invasive test of the 'aluminum hypothesis' in Alzheimer's disease. *The Journal of Alzheimer's Disease* **33:** 423-430

De Flora S (2000) Threshold mechanisms and site specificity in chromium(VI) carcinogenesis. *Carcinogenesis* **21:** 533-541

del Dacera DM, Babel S (2006) Use of citric acid for heavy metals extraction from contaminated sewage sludge for land application. *Water Science and Technology* **54:** 129-135

Delhaize E, Ryan PR, Randall PJ (1993) Aluminum tolerance in wheat (Triticum aestivum L.)(II. Aluminum-stimulated excretion of malic acid from root apices). *Plant physiology* **103:** 695-702

Deng Z, Coudray C, Gouzoux L, Mazur A, Rayssiguier Y, Pépin D (1998) Effect of oral aluminum and aluminum citrate on blood level and short-term tissue distribution of aluminum in the rat. *Biological Trace Element Research* **63:** 139-147

DeWeerdt S (2011) Activity is the best medicine. Nature **475:** S16

Dewji NN, Do C, Bayney RM (1995) Transcriptional activation of Alzheimer's β-amyloid precursor protein gene by stress. *Molecular Brain Research* **33:** 245-253

Diaz JC, Linnehan J, Pollard H, Arispe N (2006) Histidines 13 and 14 in the Abeta sequence are targets for inhibition of Alzheimer's disease Abeta ion channel and cytotoxicity. *Biological Research* **39:** 447-460

Ding Q, Keller JN (2003) Does proteasome inhibition play a role in mediating neuropathology and neuron death in Alzheimer's disease? *The Journal of Alzheimer's Disease* **5:** 241-245

Djurdjevic P, Cvijovic M, Pavelkic V, Zakrzewska J (2005) Spectrophotometric and 27-Al NMR Characterization of Aluminum (III) Complexes with l-Histidine. *Spectroscopy Letters* **38:** 617-634

Djurdjevic P, Jelic R, Dzajevic D, Cvijovic M (2001) Solution Equilibria between Aluminum (III) Ion and L-histidine or L-tyrosine. *Metal Based Drugs* **8:** 235-248

Dong J, Atwood CS, Anderson VE, Siedlak SL, Smith MA, Perry G, Carey PR (2003) Metal binding and oxidation of amyloid-beta within isolated senile plaque cores: Raman microscopic evidence. *Biochemistry* **42:** 2768-2773

Dong J, Atwood CS, Anderson VE, Siedlak SL, Smith MA, Perry G, Carey PR (2003) Metal binding and oxidation of amyloid-β within isolated senile plaque cores: Raman microscopic evidence. *Biochemistry* **42:** 2768-2773

Donnelly PS, Xiao Z, Wedd AG (2007) Copper and Alzheimer's disease. *Current Opinion in Chemical Biology* **11:** 128-133

Drago D, Bettella M, Bolognin S, Cendron L, Scancar J, Milacic R, Ricchelli F, Casini A, Messori L, Tognon G (2008) Potential pathogenic role of β-amyloid1–42–aluminum complex in Alzheimer's disease. *The International Journal of Biochemistry & Cell Biology* **40:** 731-746

Drago D, Bolognin S, Zatta P (2008) Role of Metal Ions in the A Oligomerization in Alzheimers Disease and in Other Neurological Disorders. *Current Alzheimer Research* **5:** 500-507

Dresler S, Hanaka A, Bednarek W, Maksymiec W (2014) Accumulation of low-molecular-weight organic acids in roots and leaf segments of Zea mays plants treated with cadmium and copper. *Acta Physiologiae Plantarum* **36:** 1565-1575

Drew SC (2017) The Case for Abandoning Therapeutic Chelation of Copper Ions in Alzheimer's Disease. *Frontiers in Neuroscience* **11:** 317

Dringen R (2000) Metabolism and functions of glutathione in brain. *Progress in Neurobiology* **62:** 649-671

Duce JA, Bush AI, Adlard PA (2011) Role of amyloid-β–metal interactions in Alzheimer's disease. *Future Neurology* **6:** 641-659

Duff K, Eckman C, Zehr C, Yu X, Prada C-M, Perez-Tur J, Hutton M, Buee L, Harigaya Y, Yager D (1996) Increased amyloid-β42 (43) in brains of mice expressing mutant presenilin 1. *Nature* **383:** 710

Dumont M, Beal MF (2011) Neuroprotective strategies involving ROS in Alzheimer disease. *Free Radical Biology and Medicine* **51:** 1014-1026

Ebert JC, Altman RB (2008) Robust recognition of zinc binding sites in proteins. *Protein Science* **17:** 54-65

Edrey YH, Medina DX, Gaczynska M, Osmulski PA, Oddo S, Caccamo A, Buffenstein R (2013) Amyloid beta and the longest-lived rodent: the naked mole-rat as a model for natural protection from Alzheimer's disease. *Neurobiology of Aging* **34:** 2352-2360

Evans P (1993) Free radicals in brain metabolism and pathology. *British Medical Bulletin* **49:** 577-587

Exley C (2004) The pro-oxidant activity of aluminum. *Free Radical Biology and Medicine* **36:** 380-387

Exley C (2006) Aluminium and iron, but neither copper nor zinc, are key to the precipitation of β-sheets of Aβ42 in senile plaque cores in Alzheimer's disease. *The Journal of Alzheimer's Disease* **10:** 173-177

Exley C (2014) What is the risk of aluminium as a neurotoxin? *Expert Review of Neurotherapeutics* **14:** 589-591

Exley C, House E, Polwart A, Esiri MM (2012) Brain burdens of aluminum, iron, and copper and their relationships with amyloid-beta pathology in 60 human brains. *The Journal of Alzheimer's Disease* **31:** 725-730

Exley C, Vickers T (2014) Elevated brain aluminium and early onset Alzheimer's disease in an individual occupationally exposed to aluminium: a case report. *Journal of Medical Case Reports* **8:** 41

Exley C, Vickers T (2014) Elevated brain aluminium and early onset Alzheimer's disease in an individual occupationally exposed to aluminium: a case report. *Journal of Medical Case Reports* **8:** 41

Faller P, Hureau C (2009) Bioinorganic chemistry of copper and zinc ions coordinated to amyloid-[small beta] peptide. *Dalton Transactions:* 1080-1094

Forloni G, Artuso V, La Vitola P, Balducci C (2016) Oligomeropathies and pathogenesis of Alzheimer and Parkinson's diseases. *Movement Disorders* **31:** 771-781

Forman HJ, Zhang H, Rinna A (2009) Glutathione: overview of its protective roles, measurement, and biosynthesis. *Molecular Aspects of Medicine* **30:** 1-12

Francis PT, Palmer AM, Snape M, Wilcock GK (1999) The cholinergic hypothesis of Alzheimer's disease: a review of progress. *The Journal of Neurology, Neurosurgery, and Psychiatry* **66:** 137-147

Frisardi V, Solfrizzi V, Capurso C, Kehoe PG, Imbimbo BP, Santamato A, Dellegrazie F, Seripa D, Pilotto A, Capurso A (2010) Aluminum in the diet and Alzheimer's disease: from current epidemiology to possible disease-modifying treatment. T*he Journal of Alzheimer's Disease* **20:** 17-30

Gaggelli E, Janicka-Klos A, Jankowska E, Kozlowski H, Migliorini C, Molteni E, Valensin D, Valensin G, Wieczerzak E (2007) NMR Studies of the Zn2+ Interactions with Rat and Human β-Amyloid (1−28) Peptides in Water-Micelle Environment. *The Journal of Physical Chemistry* B **112:** 100-109

Gaggelli E, Kozlowski H, Valensin D, Valensin G (2006) Copper homeostasis and neurodegenerative disorders (Alzheimer's, prion, and Parkinson's diseases and amyotrophic lateral sclerosis). *Chemical Reviews* **106:** 1995-2044

Genuis SJ, Birkholz D, Rodushkin I, Beesoon S (2011) Blood, urine, and sweat (BUS) study: monitoring and elimination of bioaccumulated toxic elements. *Archives of Environmental Contamination and Toxicology* **61:** 344-357

Ghasemi-Fasaei R (2012) Malic acid and phosphorus influences on nickel phytoremediation efficiency and metal nutrients relationships in a Ni-polluted calcareous soil. *The International Research Journal of Applied and Basic Sciences* **3:** 2805-2808

Giasson BI, Sampathu DM, Wilson CA, Vogelsberg-Ragaglia V, Mushynski WE, Lee VMY (2002) The environmental toxin arsenite induces Tau hyperphosphorylation. *Biochemistry* **41:** 15376-15387

Gill SC, Von Hippel PH (1989) Calculation of protein extinction coefficients from amino acid sequence data. *Analytical Biochemistry* **182:** 319-326

Gilman S, Koller M, Black RS, Jenkins L, Griffith SG, Fox NC, Eisner L, Kirby L, Rovira MB, Forette F, Orgogozo JM (2005) Clinical effects of Abeta immunization (AN1792) in patients with AD in an interrupted trial. *Neurology* **64:** 1553-1562

Glenner GG (1985) On causative theories in Alzheimer's disease. *Human Pathology* **16:** 433-435

Glenner GG, Wong CW (1984) Alzheimer's disease and Down's syndrome: Sharing of a unique cerebrovascular amyloid fibril protein. *Biochemical and Biophysical Research Communications* **122:** 1131-1135

Glenner GG, Wong CW (1984) Alzheimer's disease: initial report of the purification and characterization of a novel cerebrovascular amyloid protein. *Biochemical and Biophysical Research Communications* **120:** 885-890

Gong G, O'Bryant SE (2010) The arsenic exposure hypothesis for Alzheimer disease. *Alzheimer Disease & Associated Disorders* **24:** 311–316

Gramlich A, Tandy S, Frossard E, Eikenberg J, Schulin R (2013) Availability of Zinc and the Ligands Citrate and Histidine to Wheat: Does Uptake of Entire Complexes Play a Role? *The Journal of Agricultural and Food Chemistry* **61:** 10409-10417

Greger JL, Sutherland JE (1997) Aluminum exposure and metabolism. *Critical Reviews in Clinical Laboratory Sciences* **34:** 439-474

Guerinot ML, Meidl EJ, Plessner O (1990) Citrate as a siderophore in Bradyrhizobium japonicum. *The Journal of Bacteriology* **172:** 3298-3303

Gupta C (2014) Role of iron (Fe) in body. *Journal of Applied Chemistry (IOSR-JAC)* **7:** 38-46

Haass C, Schlossmacher MG, Hung AY, Vigo-Pelfrey C, Mellon A, Ostaszewski BL, Lieberburg I, Koo EH, Schenk D, Teplow DB, Selkoe DJ (1992) Amyloid β-peptide is produced by cultured cells during normal metabolism. *Nature* **359:** 322

Halverson K, Fraser PE, Kirschner DA, Lansbury PT (1990) Molecular determinants of amyloid deposition in Alzheimer's disease: conformational studies of synthetic beta-protein fragments. *Biochemistry* **29:** 2639-2944

Hammond CL, Lee TK, Ballatori N (2001) Novel roles for glutathione in gene expression, cell death, and membrane transport of organic solutes. *The Journal of Hepatology* **34:** 946-954

Hardy J (2006) A hundred years of Alzheimer's disease research. *Neuron* **52:** 3-13

Hardy J (2009) The amyloid hypothesis for Alzheimer's disease: a critical reappraisal. *The Journal of Neurochemistry* **110:** 1129-1134

Hardy J, Selkoe D (2002) The Amyloid Hypothesis of Alzheimer's Disease: Progress and Problems on the Road to Therapeutics. *Science* **297:** 353-356

Hardy JA, Higgins GA (1992) Alzheimer's disease: the amyloid cascade hypothesis. *Science* **256:** 184-185

Harris WR, Wang Z, Brook C, Yang B, Islam A (2003) Kinetics of metal ion exchange between citric acid and serum transferrin. *Inorganic chemistry* **42:** 5880-5889

Harris WR, Wang Z, Hamada YZ (2003) Competition between transferrin and the serum ligands citrate and phosphate for the binding of aluminum. *Inorganic Chemistry* **42:** 3262-3273

Hebert LE, Weuve J, Scherr PA, Evans DA (2013) Alzheimer disease in the United States (2010–2050) estimated using the 2010 census. *Neurology* **80:** 1778-1783

Hegde M, Bharathi P, Suram A, Venugopal C, Jagannathan R, Poddar P, Srinivas P, Sambamurti K, Rao K, Scancar J, Messori L, Zecca L, Zatta P (2009) Challenges associated with metal chelation therapy in Alzheimer's disease. *The Journal of Alzheimer's Disease* **17:** 457-468

Hem SL (2002) Elimination of aluminum adjuvants. *Vaccine* **20:** S40-S43

Hensley K, Hall N, Subramaniam R, Cole P, Harris M, Aksenov M, Aksenova M, Gabbita SP, Wu JF, Carney JM, et al. (1995) Brain regional correspondence between Alzheimer's disease histopathology and biomarkers of protein oxidation. *The Journal of Neurochemistry* **65:** 2146-2156

Hernandez LE, Sobrino-Plata J, Montero-Palmero MB, Carrasco-Gil S, Flores-Caceres ML, Ortega-Villasante C, Escobar C (2015) Contribution of glutathione to the control of cellular redox homeostasis under toxic metal and metalloid stress. *The Journal of Experimental Botany* **66:** 2901-2911

Hershfinkel M, Moran A, Grossman N, Sekler I (2001) A zinc-sensing receptor triggers the release of intracellular Ca^{2+} and regulates ion transport. *Proceedings of the National Academy of Sciences of the United States of America* **98:** 11749-11754

Hider RC, Ejim L, Taylor PD, Gale R, Huehns E, Porter JB (1990) Facilitated uptake of zinc into human erythrocytes: Relevance to the treatment of sickle-cell anaemia. *Biochemical Pharmacology* **39:** 1005-1012

Hilbich C, Kisters-Woike B, Reed J, Masters CL, Beyreuther K (1991) Aggregation and secondary structure of synthetic amyloid beta A4 peptides of Alzheimer's disease. *The Journal of Molecular Biology* **218:** 149-163

Hippius H, Neundörfer G (2003) The discovery of Alzheimer's disease. Dialogues in Clinical *Neuroscience* **5:** 101-108

Hochuli E, Bannwart W, Döbeli H, Gentz R, Stüber D (1988) Genetic approach to facilitate purification of recombinant proteins with a novel metal chelate adsorbent. *Nature Biotechnology* **6:** 1321–1325.

Holmes C, Boche D, Wilkinson D, Yadegarfar G, Hopkins V, Bayer A, Jones RW, Bullock R, Love S, Neal JW, Zotova E, Nicoll JA (2008) Long-term effects of Abeta42 immunisation in Alzheimer's disease: follow-up of a randomised, placebo-controlled phase I trial. *The Lancet* **372:** 216-223

Hong Enriquez RP, Do TN (2012) Bioavailability of metal ions and evolutionary adaptation. *Life (Basel, Switzerland)* **2:** 274-285

Hou L, Shao H, Zhang Y, Li H, Menon NK, Neuhaus EB, Brewer JM, Byeon IJL, Dale G, Vitek MP (2004) Solution NMR studies of the Aβ (1-40) and Aβ (1-42) peptides establish that the Met35 oxidation state affects the mechanism of amyloid formation. *The Journal of the American Chemical Society* **126:** 1992-2005

Hou L, Zagorski MG (2006) NMR Reveals Anomalous Copper(II) Binding to the Amyloid Aβ Peptide of Alzheimer's Disease. *The Journal of the American Chemical Society* **128:** 9260-9261

House E, Collingwood J, Khan A, Korchazkina O, Berthon G, Exley C (2004) Aluminium, iron, zinc and copper influence the in vitro formation of amyloid fibrils of Aβ 42 in a manner which may have consequences for metal chelation therapy in Alzheimer's disease. *The Journal of Alzheimer's Disease* **6:** 291-301

House E, Esiri M, Forster G, Ince PG, Exley C (2012) Aluminium, iron and copper in human brain tissues donated to the Medical Research Council's Cognitive Function and Ageing Study. *Metallomics* **4:** 56-65

Housecroft C, Sharpe AG (2008) Housecroft Inorganic Chemistry. Prentice Hal, New York

Hovatta O, Venäläinen E-R, Kuusimäki L, Heikkilä J, Hirvi T, Reima I (1998) Aluminium, lead and cadmium concentrations in seminal plasma and spermatozoa, and semen quality in Finnish men. *Human Reproduction* **13:** 115-119

Hsiao K, Chapman P, Nilsen S, Eckman C, Harigaya Y, Younkin S, Yang F, Cole G (1996) Correlative memory deficits, Abeta elevation, and amyloid plaques in transgenic mice. *Science* **274:** 99-102

Hu L, Liu X, Chervona Y, Yang F, Tang MS, Darzynkiewicz Z, Dai W (2011) Chromium induces chromosomal instability, which is partly due to deregulation of BubR1 and Emi1, two APC/C inhibitors. *Cell Cycle* **10:** 2373-2379

Huang J, Yao Y, Lin J, Ye YH, Sun WY, Tang Dagger WX (2004) The solution structure of rat Abeta-(1-28) and its interaction with zinc ion: insights into the scarcity of amyloid deposition in aged rat brain. *The Journal of Biological Inorganic Chemistry* **9:** 627-635

Huang WJ, Zhang X, Chen WW (2016) Role of oxidative stress in Alzheimer's disease. *Biomedical Reports* **4:** 519-522

Huang X, Atwood CS, Hartshorn MA, Multhaup G, Goldstein LE, Scarpa RC, Cuajungco MP, Gray DN, Lim J, Moir RD (1999) The Aβ peptide of Alzheimer's disease directly produces hydrogen peroxide through metal ion reduction. *Biochemistry* **38:** 7609-7616

Huang X, Atwood CS, Moir RD, Hartshorn MA, Tanzi RE, Bush AI (2004) Trace metal contamination initiates the apparent auto-aggregation, amyloidosis, and oligomerization of Alzheimer's Aβ peptides. *The Journal of Biological Inorganic Chemistry* **9:** 954-960

Huang X, Cuajungco M, Atwood C, Moir R, Tanzi R, Bush A (2000) Alzheimer's disease, beta-amyloid protein and zinc. *The Journal of Nutrition* **130:** 1488S-1492S

Huang X, Moir RD, Tanzi RE, Bush AI, Rogers JT (2004) Redox-active metals, oxidative stress, and Alzheimer's disease pathology. *The Annals of the New York Academy of Sciences* **1012:** 153-163

Huat TJ, Camats-Perna J, Newcombe EA, Valmas N, Kitazawa M, Medeiros R (2019) Metal toxicity links to Alzheimer's disease and neuroinflammation. *The Journal of Molecular Biology* **431:** 1843-1868

Hung LW, Ciccotosto GD, Giannakis E, Tew DJ, Perez K, Masters CL, Cappai R, Wade JD, Barnham KJ (2008) Amyloid-β Peptide (Aβ) Neurotoxicity Is Modulated by the Rate of Peptide Aggregation: Aβ Dimers and Trimers Correlate with Neurotoxicity. *The Journal of Neuroscience* **28:** 11950-11958

Hureau C (2012) Coordination of redox active metal ions to the amyloid precursor protein and to amyloid-β peptides involved in Alzheimer disease. Part 1: An overview. *Coordination Chemistry Reviews* **256:** 2164-2174

Irving H, Williams RJP (1948) Order of stability of metal complexes. Nature **162:** 746-747

Jacobsen NE (2007) NMR spectroscopy explained: simplified theory, applications and examples for organic chemistry and structural biology. John Wiley & Sons

Jarrett JT, Berger EP, Lansbury PT, Jr. (1993) The carboxy terminus of the beta amyloid protein is critical for the seeding of amyloid formation: implications for the pathogenesis of Alzheimer's disease. *Biochemistry* **32:** 4693-4697

Jennison D, Verdozzi C, Schultz P, Sears M (1999) Ab initio structural predictions for ultrathin aluminum oxide films on metallic substrates. *Physical Review B* **59:** R15605

Jomova K, Jenisova Z, Feszterova M, Baros S, Liska J, Hudecova D, Rhodes CJ, Valko M (2011) Arsenic: toxicity, oxidative stress and human disease. *The Journal of Applied Toxicology* ***31*:** 95-107

Jones DL (1998) Organic acids in the rhizosphere–a critical review. *Plant and soil* **205:** 25-44

Jones RE (1990) Hexavalent chrome: threshold concept for carcinogenicity. *Biomedical and Environmental Sciences* **3:** 20-34

Kamenetz F, Tomita T, Hsieh H, Seabrook G, Borchelt D, Iwatsubo T, Sisodia S, Malinow R (2003) APP Processing and Synaptic Function. *Neuron* **37:** 925-937

Kaneko N, Yasui H, Takada J, Suzuki K, Sakurai H (2004) Orally administrated aluminum-maltolate complex enhances oxidative stress in the organs of mice. *The Journal of Inorganic Biochemistry* **98:** 2022-2031

Kang J, Lemaire HG, Unterbeck A, Salbaum JM, Masters CL, Grzeschik KH, Multhaup G, Beyreuther K, Muller-Hill B (1987) The precursor of Alzheimer's disease amyloid A4 protein resembles a cell-surface receptor. *Nature* **325:** 733-736

Karran E, De Strooper B (2016) The amyloid cascade hypothesis: are we poised for success or failure? *The Journal of Neurochemistry* **139 Suppl 2:** 237-252

Karran E, Mercken M, Strooper BD (2011) The amyloid cascade hypothesis for Alzheimer's disease: an appraisal for the development of therapeutics. *Nature Reviews Drug Discovery* **10:** 698-712

Karran E, Mercken M, Strooper BD (2011) The amyloid cascade hypothesis for Alzheimer's disease: an appraisal for the development of therapeutics. *Nature Reviews Drug Discovery* **10:** 698

Kato N, Nakamura M, Uchiyama T (1999) 1H NMR studies of the reactions of copper(I) and copper(II) with D-penicillamine and glutathione. *The Journal of Inorganic Biochemistry* **75:** 117-121

Kawahara M, Kato-Negishi M (2011) Link between Aluminum and the Pathogenesis of Alzheimer's Disease: The Integration of the Aluminum and Amyloid Cascade Hypotheses. *International Journal of Alzheimer's Disease* **2011:** 276393-276393

Kawahara M, Mizuno D, Koyama H, Konoha K, Ohkawara S, Sadakane Y (2014) Disruption of zinc homeostasis and the pathogenesis of senile dementia. *Metallomics* **6:** 209-219

Kawahara M, Muramoto K, Kobayashi K, Mori H, Kuroda Y (1994) Aluminum Promotes the Aggregation of Alzheimer′s Amyloid β-Protein in Vitro. *Biochemical and Biophysical Research Communications* **198:** 531-535

Keeler J (2005) NMR and energy levels. Understanding NMR spectroscopy**:** 1-19

Keilin D, Mann T (1940) Carbonic anhydrase. Purification and nature of the enzyme. *The Biochemical Journal* **34:** 1163-1176

Kepp KP (2012) Bioinorganic chemistry of Alzheimer's disease. *Chemical Reviews* **112:** 5193-5239

Kern A, Behl C (2009) The unsolved relationship of brain aging and late-onset Alzheimer disease. *Biochimica et Biophysica Act*a **1790:** 1124-1232

Khan A, Dobson JP, Exley C (2006) Redox cycling of iron by Abeta42. *Free Radical Biology and Medicine* **40:** 557-569

Kim AC, Lim S, Kim YK (2018) Metal Ion Effects on Aβ and Tau Aggregation. *International Journal of Molecular Sciences* **19:** 128

Kim GH, Kim JE, Rhie SJ, Yoon S (2015) The Role of Oxidative Stress in Neurodegenerative Diseases. *Experimental Neurobiology* **24:** 325-340

Kim PR, Beaulé PE, Dunbar M, Lee JK, Birkett N, Turner MC, Yenugadhati N, Armstrong V, Krewski D (2011) Cobalt and chromium levels in blood and urine following hip resurfacing arthroplasty with the Conserve Plus implant. *Journal of Bone and Joint Surgery* **93:** 107-117

Klewpatinond M, Viles JH (2007) Fragment length influences affinity for Cu^{2+} and Ni^{2+} binding to His96 or His111 of the prion protein and spectroscopic evidence for a multiple histidine binding only at low pH. *The Biochemical Journal* **404:** 393-402

Korczyn A, Zeidman Y, Schweiger A, Vachapov V, Verchovsky R, Halperin I, Neuefeld M, Fried I, Andelman F (2008) RAVLT as an instrument for the early diagnosis of Alzheimer disease. *Neurology* **70:** A281-A281

Kowalik-Jankowska T, Ruta M, Wiśniewska K, Łankiewicz L (2003) Coordination abilities of the 1–16 and 1–28 fragments of β-amyloid peptide towards copper(II) ions: a combined potentiometric and spectroscopic study. *The Journal of Inorganic Biochemistr*y **95:** 270-282

Krezel A, Bal W (1999) Coordination chemistry of glutathione. *Acta Biochimica Polonica* **46:** 567-580

Kurganov B, Doh M, Arispe N (2004) Aggregation of liposomes induced by the toxic peptides Alzheimer's Abetas, human amylin and prion (106-126): facilitation by membrane-bound GM1 ganglioside. *Peptides* **25:** 217-232

Kuroda Y, Kawahara M (1994) Molecular Biology of 'Szheimer's Disease and Neuron's Death. *Neuropathology* **14:** 115-117

Lahiri DK, Maloney B (2010) Beyond the signaling effect role of amyloid-β42 on the processing of APP, and its clinical implications. *Experimental Neurology* **225:** 51-54

Laity JH, Lee BM, Wright PE (2001) Zinc finger proteins: new insights into structural and functional diversity. *Current Opinion in Structural Biology* **11:** 39-46

Lambrou A, Baccarelli A, Wright RO, Weisskopf M, Bollati V, Amarasiriwardena C, Vokonas P, Schwartz J (2012) Arsenic exposure and DNA methylation among elderly men. *Epidemiology (Cambridge, Mass.)* **23:** 668-676

Langui D, Probst A, Anderton B, Brion JP, Ulrich J (1990) Aluminium-induced tangles in cultured rat neurones. Enhanced effect of aluminium by addition of maltol. *Acta Neuropathologica* **80:** 649-655

Lanoiselée H-M, Nicolas G, Wallon D, Rovelet-Lecrux A, Lacour M, Rousseau S, Richard A-C, Pasquier F, Rollin-Sillaire A, Martinaud O, Quillard-Muraine M, de la Sayette V, Boutoleau-Bretonniere C, Etcharry-Bouyx F, Chauviré V, Sarazin M, le Ber I, Epelbaum S, Jonveaux T, Rouaud O, Ceccaldi M, Félician O, Godefroy O, Formaglio M, Croisile B, Auriacombe S, Chamard L, Vincent J-L, Sauvée M, Marelli-Tosi C, Gabelle A, Ozsancak C, Pariente J, Paquet C, Hannequin D, Campion D, collaborators of the CNRMAJp (2017) APP, PSEN1, and PSEN2 mutations in early-onset Alzheimer disease: A genetic screening study of familial and sporadic cases. *PLOS Medicine* **14:** e1002270

Lau LF, Schachter J, Seymour P, Sanner MA (2002) Tau Protein Phosphorylation as a Therapeutic Target in Alzheimer's Disease. *Current Topics in Medicinal Chemistry* **2:** 395-415

Lauderback CM, Hackett JM, Huang FF, Keller JN, Szweda LI, Markesbery WR, Butterfield DA (2001) The glial glutamate transporter, GLT-1, is oxidatively modified by 4-hydroxy-2-nonenal in the Alzheimer's disease brain: the role of Aβ1–42. *The Journal of Neurochemistry* **78:** 413-416

Lee HG, Zhu X, Castellani RJ, Nunomura A, Perry G, Smith MA (2007) Amyloid-beta in Alzheimer disease: the null versus the alternate hypotheses. *The Journal of Pharmacology and Experimental Therapeutics* **321:** 823-829

Lee M, Bard F, Johnson-Wood K, Lee C, Hu K, Griffith SG, Black RS, Schenk D, Seubert P (2005) Abeta42 immunization in Alzheimer's disease generates Abeta N-terminal antibodies. *Annals of Neurology* **58:** 430-435

Liboiron BD, Thompson KH, Hanson GR, Lam E, Aebischer N, Orvig C (2005) New insights into the interactions of serum proteins with bis(maltolato)oxovanadium(IV): transport and biotransformation of insulin-enhancing vanadium pharmaceuticals. *The Journal of the American Chemical Society* **127:** 5104-5115

Lin H-J, Sung T-I, Chen C-Y, Guo H-R (2013) Arsenic levels in drinking water and mortality of liver cancer in Taiwan. *The Journal of Hazardous Materials* **262:** 1132-1138

Lin R, Chen X, Li W, Han Y, Liu P, Pi R (2008) Exposure to metal ions regulates mRNA levels of APP and BACE1 in PC12 cells: Blockage by curcumin. *Neuroscience Letters* **440:** 344-347

Liu J, Liu H, Li Y, Wang H (2014) Probing the coordination properties of glutathione with transition metal ions (Cr^{2+}, Mn^{2+}, Fe^{2+}, Co^{2+}, Ni^{2+}, Cu^{2+}, Zn^{2+}, Cd^{2+}, Hg^{2+}) by density functional theory. *Journal of Biological Physics* **40:** 313-323

Liu R-M, Choi J (2000) Age-associated decline in γ-glutamylcysteine synthetase gene expression in rats. *Free Radical Biology and Medicine* **28:** 566-574

Liu ST, Howlett G, Barrow CJ (1999) Histidine-13 is a crucial residue in the zinc ion-induced aggregation of the A beta peptide of Alzheimer's disease. *Biochemistry* **38:** 9373-9378

Lorenzo A, Yankner BA (1994) Beta-amyloid neurotoxicity requires fibril formation and is inhibited by congo red. *Proceedings of the National Academy of Sciences of the United States of America* **91:** 12243-12247

Lovell M, Robertson J, Teesdale W, Campbell J, Markesbery W (1998) Copper, iron and zinc in Alzheimer's disease senile plaques. *The Journal of the Neurological Sciences* **158:** 47-52

Lovell MA (2009) A potential role for alterations of zinc and zinc transport proteins in the progression of Alzheimer's disease. *The Journal of Alzheimer's Disease* **16:** 471-483

Lovell MA, Robertson JD, Teesdale WJ, Campbell JL, Markesbery WR (1998) Copper, iron and zinc in Alzheimer's disease senile plaques. *The Journal of the Neurological Sciences* **158:** 47-52

Lu YM, Taverna FA, Tu R, Ackerley CA, Wang YT, Roder J (2000) Endogenous Zn2+ is required for the induction of long-term potentiation at rat hippocampal mossy fiber-CA3 synapses. *Synapse* **38:** 187-197

Lynch T, Cherny RA, Bush AI (2000) Oxidative processes in Alzheimer's disease: the role of Aβ-metal interactions. *Experimental Gerontology* **35:** 445-451

Ma JF (2000) Role of organic acids in detoxification of aluminum in higher plants. *Plant and Cell Physiology* **41:** 383-390

Macaulay L, O'Meara T (2011) Dementia and Alzheimer's disease. *In*, Vol 20th April 2012

Mahajan A, Sidhu SS (2019) In vitro corrosion and hemocompatibility evaluation of electrical discharge treated cobalt–chromium implant. *Journal of Materials Research* **34:** 1363-1370

Mancino AM, Hindo SS, Kochi A, Lim MH (2009) Effects of clioquinol on metal-triggered amyloid-beta aggregation revisited. *Inorganic Chemistry* **48:** 9596-9598

Mandal PK, Saharan S, Tripathi M, Murari G (2015) Brain glutathione levels–a novel biomarker for mild cognitive impairment and Alzheimer's disease. *Biological Psychiatry* **78:** 702-710

Mann DM, Esiri MM (1989) The pattern of acquisition of plaques and tangles in the brains of patients under 50 years of age with Down's syndrome. *The Journal of the Neurological Sciences* **89:** 169-179

Mantyh PW, Ghilardi JR, Rogers S, DeMaster E, Allen CJ, Stimson ER, Maggio JE (1993) Aluminum, Iron, and Zinc Ions Promote Aggregation of Physiological Concentrations of β-Amyloid Peptide. *The Journal of Neurochemistry* **61:** 1171-1174

Maret W (2001) Crosstalk of the group IIa and IIb metals calcium and zinc in cellular signaling. *Proceedings of the National Academy of Sciences of the United States of America* **98:** 12325-12327

Maret W (2012) New perspectives of zinc coordination environments in proteins. *The Journal of Inorganic Biochemistry* **111:** 110-116

Marino T, Russo N, Toscano M, Pavelka M (2010) On the metal ion (Zn2+, Cu2+) coordination with beta-amyloid peptide: DFT computational study. *Interdisciplinary Sciences: Computational Life Sciences* **2:** 57-69

Markesbery WR (1997) Oxidative Stress Hypothesis in Alzheimer's Disease. *Free Radical Biology and Medicine* **23:** 134-147

Markesbery WR, Carney JM (1999) Oxidative alterations in Alzheimer's disease. *Brain pathology* **9:** 133-146

Markovits G, Klotz P, Newman L (1972) Formation constants for the mixed-metal complexes between indium (III) and uranium (VI) with malic, citric, and tartaric acids. *Inorganic Chemistry* **11:** 2405-2408

Masaldan S, Bush AI, Devos D, Rolland AS, Moreau C (2018) Striking while the iron is hot: Iron metabolism and ferroptosis in neurodegeneration. *Free Radical Biology and Medicine* **133:** 221–233

Masters CL, Simms G, Weinman NA, Multhaup G, McDonald BL, Beyreuther K (1985) Amyloid plaque core protein in Alzheimer disease and Down syndrome. *Proceedings of the National Academy of Sciences of the United States of America* **82:** 4245-4249

Matsui T, Ichikawa H, Fujita T, Takagi T, Osada-Oka M, Minamiyama Y (2017) Histidine deficiency attenuates cell viability in rat intestinal epithelial cells by apoptosis via mitochondrial dysfunction. *The Journal of Nutrition & Intermediary Metabolism* **8:** 21-28

Matsuoka Y, Picciano M, La Francois J, Duff K (2001) Fibrillar β-amyloid evokes oxidative damage in a transgenic mouse model of Alzheimer's disease. *Neuroscience* **104:** 609-613

Mattson MP (2004) Pathways towards and away from Alzheimer's disease. *Nature* **430:** 631

McCafferty E (2003) Lewis acid/Lewis base effects in corrosion and polymer adhesion at aluminum surfaces. *The Journal of the Electrochemical Society* **150:** B342-B347

Medina S, Martínez M, Hernanz A (2002) Antioxidants inhibit the human cortical neuron apoptosis induced by hydrogen peroxide, tumor necrosis factor alpha, dopamine and beta-amyloid peptide 1-42. *Free Radical Research* **36:** 1179-1184

Meisl G, Yang X, Frohm B, Knowles TPJ, Linse S (2016) Quantitative analysis of intrinsic and extrinsic factors in the aggregation mechanism of Alzheimer-associated Aβ-peptide. *Scientific Reports* **6:** 18728

Mekmouche Y, Coppel Y, Hochgräfe K, Guilloreau L, Talmard C, Mazarguil H, Faller P (2005) Characterization of the ZnII Binding to the Peptide Amyloid-β1–16 linked to Alzheimer's Disease. *ChemBioChem* **6:** 1663-1671

Milewski K, Hilgier W, Albrecht J, Zielinska M (2015) The dimethylarginine (ADMA)/nitric oxide pathway in the brain and periphery of rats with thioacetamide-induced acute liver failure: Modulation by histidine. *Neurochemistry International* **88:** 26-31

Miller LM, Wang Q, Telivala TP, Smith RJ, Lanzirotti A, Miklossy J (2006) Synchrotron-based infrared and X-ray imaging shows focalized accumulation of Cu and Zn co-localized with β-amyloid deposits in Alzheimer's disease. *The Journal of Structural Biology* **155:** 30-37

Miller LM, Wang Q, Telivala TP, Smith RJ, Lanzirotti A, Miklossy J (2006) Synchrotron-based infrared and X-ray imaging shows focalized accumulation of Cu and Zn co-localized with β-amyloid deposits in Alzheimer's disease. *Journal of structural biology* **155:** 30-37

Mirza A, King A, Troakes C, Exley C (2017) Aluminium in brain tissue in familial Alzheimer's disease. *The Journal of Trace Elements in Medicine and Biology* **40:** 30-36

Mosmann T (1983) Rapid colorimetric assay for cellular growth and survival: Application to proliferation and cytotoxicity assays. *The Journal of Immunological Methods* **65:** 55-63

Mujika JI, Rodríguez-Guerra Pedregal J, Lopez X, Ugalde JM, Rodríguez-Santiago L, Sodupe M, Maréchal J-D (2017) Elucidating the 3D structures of Al(III)–Aβ complexes: a template free strategy based on the pre-organization hypothesis. *Chemical Science* **8:** 5041-5049

Mukha S, Antipova I, Medvedeva S, Saraev V, Larina L, Tsyrenzhapov A, Sukhov B (2007) Synthesis and properties of metal chelates based on natural γ-pyrone maltol. *Chemistry for Sustainable Development* **15:** 449-458

Multhaup G, Schlicksupp A, Hesse L, Beher D, Ruppert T, Colin L M, Beyreuther K (1996) The Amyloid Precursor Protein of Alzheimer's Disease in the Reduction of Copper(II) to Copper(I). *Science* **271:** 1406-1409

Murakami K, Murata N, Noda Y, Irie K, Shirasawa T, Shimizu T (2012) Stimulation of the amyloidogenic pathway by cytoplasmic superoxide radicals in an Alzheimer's disease mouse model. *Bioscience, Biotechnology, and Biochemistry* **76:** 1098-1103

Myers TW, Kazem N, Stoll S, Britt RD, Shanmugam M, Berben LA (2011) A Redox Series of Aluminum Complexes: Characterization of Four Oxidation States Including a Ligand Biradical State Stabilized via Exchange Coupling. *The Journal of the American Chemical Society* **133:** 8662-8672

Nair NG, Perry G, Smith MA, Reddy VP (2010) NMR studies of zinc, copper, and iron binding to histidine, the principal metal ion complexing site of amyloid-beta peptide. *The Journal of Alzheimer's Disease* **20:** 57-66

Nakamura M, Shishido N, Nunomura A, Smith MA, Perry G, Hayashi Y, Nakayama K, Hayashi T (2007) Three histidine residues of amyloid-beta peptide control the redox activity of copper and iron. *Biochemistry* **46:** 12737-12743

Nam E, Han J, Suh J-M, Yi Y, Lim MH (2018) Link of impaired metal ion homeostasis to mitochondrial dysfunction in neurons. C*urrent Opinion in Chemical Biolog*y **43:** 8-14

Narayan P, Krishnarjuna B, Vishwanathan V, Jagadeesh Kumar D, Babu S, Ramanathan KV, Easwaran KRK, Nagendra HG, Raghothama S (2013) Does Aluminium Bind to Histidine? An NMR Investigation of Amyloid β12 and Amyloid β16 Fragments. *Chemical Biology & Drug Design* **82:** 48-59

Narindrasorasak S, Lowery D, Gonzalez-DeWhitt P, Poorman RA, Greenberg B, Kisilevsky R (1991) High affinity interactions between the Alzheimer's beta-amyloid precursor proteins and the basement membrane form of heparan sulfate proteoglycan. *The Journal of Biological Chemistry* **266:** 12878-12883

Neri L, Hewitt D (1991) Aluminium, Alzheimer's disease, and drinking water. *The Lancet* **338:** 390

Neuhaus D, Williamson M (1989) The Nuclear Overhauser Effect in Structural and Conformational Analysis Verlag Chemie. *In*. Weinheim

Ngamchuea K, Batchelor-McAuley C, Compton RG (2016) The Copper(II)-Catalyzed Oxidation of Glutathione. *Chemistry – A European Journa*l **22:** 15937-15944

Nicoll JA, Wilkinson D, Holmes C, Steart P, Markham H, Weller RO (2003) Neuropathology of human Alzheimer disease after immunization with amyloid-beta peptide: a case report. *Nature Medicine* **9:** 448-452

Nigam A, Priya S, Bajpai P, Kumar S (2014) Cytogenomics of hexavalent chromium (Cr 6+) exposed cells: a comprehensive review. *Indian Journal of Medical Research* **139:** 349-370

Noda Y, Asada M, Kubota M, Maesako M, Watanabe K, Uemura M, Kihara T, Shimohama S, Takahashi R, Kinoshita A, Uemura K (2013) Copper enhances APP dimerization and promotes Aβ production. *Neuroscience Letters* **547:** 10-15

Okafor CD, Lanier KA, Petrov AS, Athavale SS, Bowman JC, Hud NV, Williams LD (2017) Iron mediates catalysis of nucleic acid processing enzymes: support for Fe(II) as a cofactor before the great oxidation event. *Nucleic Acids Research* **45:** 3634-3642

Olson MI, Shaw C-M (1969) Presenile Dementia and Alzheimer's Disease in Mongolism1. *Brain: A Journal of Neurology* **92:** 147-156

Opazo C, Barría MI, Ruiz FH, Inestrosa NC (2003) Copper reduction by copper binding proteins and its relation to neurodegenerative diseases. *BioMetals* **16:** 91-98

Oshiro S, Morioka MS, Kikuchi M (2011) Dysregulation of Iron Metabolism in Alzheimer's Disease, Parkinson's Disease, and Amyotrophic Lateral Sclerosis. *Advances in Pharmacological Sciences***:** 8

Park S-Y (2010) Potential therapeutic agents against Alzheimer's disease from natural sources. *Archives of Pharmacal Research* **33:** 1589-1609

Parkinson IS, Ward MK, Kerr DN (1981) Dialysis encephalopathy, bone disease and anaemia: the aluminum intoxication syndrome during regular haemodialysis. *The Journal of Clinical Pathology* **34:** 1285-1294

Pearson HA, Peers C (2006) Physiological roles for amyloid β peptides. *The Physiological Society* **575:** 5-10

Perl DP, Brody AR (1980) Alzheimer's disease: X-ray spectrometric evidence of aluminum accumulation in neurofibrillary tangle-bearing neurons. *Science* **208:** 297

Permenter MG, Lewis JA, Jackson DA (2011) Exposure to nickel, chromium, or cadmium causes distinct changes in the gene expression patterns of a rat liver derived cell line. *PLOS One* **6:** e27730-e27730

Perrone L, Sbai O, Nawroth PP, Bierhaus A (2012) The Complexity of Sporadic Alzheimer's Disease Pathogenesis: The Role of RAGE as Therapeutic Target to Promote Neuroprotection by Inhibiting Neurovascular Dysfunction. *International Journal of Alzheimer's Disease* **2012**

Pham E, Crews L, Ubhi K, Hansen L, Adame A, Cartier A, Salmon D, Galasko D, Michael S, Savas JN, Yates JR, Glabe C, Masliah E (2010) Progressive accumulation of amyloid-β oligomers in Alzheimer's disease and in amyloid precursor protein transgenic mice is accompanied by selective alterations in synaptic scaffold proteins. *The FEBS Journal* **277:** 3051-3067

Pierce JES, Trojanowski JQ, Graham DI, Smith DH, McIntosh TK (1996) Immunohistochemical characterization of alterations in the distribution of amyloid precursor proteins and beta-amyloid peptide after experimental brain injury in the rat. *The Journal of Neuroscience* **16:** 1083-1090

Pimplikar SW, Nixon RA, Robakis NK, Shen J, Tsai L-H (2010) Amyloid-independent mechanisms in Alzheimer's disease pathogenesis. *The Journal of Neuroscience* **30:** 14946-14954

Pocernich CB, Butterfield DA (2012) Elevation of glutathione as a therapeutic strategy in Alzheimer disease. *Biochimica et Biophysica Acta* **1822:** 625-630

Pollard HB, Arispe N, Rojas E (1995) Ion channel hypothesis for Alzheimer amyloid peptide neurotoxicity. *Cell Mol Neurobiol* **15:** 513-526

Portaro S, Naro A, Giorgianni R, Mazzon E, Calabrò RS (2019) Heavy metal intoxication and amyotrophic lateral sclerosis: causal or casual relationship? *Aging Clinical and Experimental Research* **32,** 351–352

Prasad KN, Hovland AR, Cole WC, Prasad KC, Nahreini P, Edwards-Prasad J, Andreatta CP (2000) Multiple Antioxidants in the Prevention and Treatment of Alzheimer Disease: Analysis of Biologic Rationale. *Clinical Neuropharmacology* **23:** 2-13

Radalla AM (2015) Potentiometric studies on ternary complexes involving some divalent transition metal ions, gallic acid and biologically abundant aliphatic dicarboxylic acids in aqueous solutions. Beni-Suef University *Journal of Basic and Applied Sciences* **4:** 174-182

Rae T, Schmidt P, Pufahl R, Culotta V, O'Halloran TV (1999) Undetectable intracellular free copper: the requirement of a copper chaperone for superoxide dismutase. *Science* **284:** 805-808

Ramanathan A, Nelson AR, Sagare AP, Zlokovic BV (2015) Impaired vascular-mediated clearance of brain amyloid beta in Alzheimer's disease: the role, regulation and restoration of LRP1. *Frontiers in Aging Neuroscience* **7:** 136

Raulin J (1869) Etudes chimiques sur la vegetation. Annales des Sciences Naturelles. *Botanique et Biologie Vegetale* **11:** 92-299

Reid DG, MacLachlan LK, Edwards AJ, Hubbard JA, Sweeney PJ (1997) Introduction to the NMR of Proteins. *In* DG Reid, ed, Protein NMR Techniques. Humana Press, Totowa, NJ, pp 1-28

Riordan JF (1977) The role of metals in enzyme activity. *Annals of Clinical & Laboratory* Science **7:** 119-129

Robinson SR, Bishop GM, Lee HG, Munch G (2004) Lessons from the AN 1792 Alzheimer vaccine: lest we forget. *Neurobiol Aging* **25:** 609-615

Roos PM, Vesterberg O, Syversen T, Flaten TP, Nordberg M (2013) Metal concentrations in cerebrospinal fluid and blood plasma from patients with amyotrophic lateral sclerosis. *Biological Trace Element Research* **151:** 159-170

Rubin AB (2017) Compendium of biophysics. John Wiley & Sons

Ruipérez F, Mujika JI, Ugalde JM, Exley C, Lopez X (2012) Pro-oxidant activity of aluminum: Promoting the Fenton reaction by reducing Fe(III) to Fe(II). *The Journal of Inorganic Biochemistry* **117:** 118-123

Rumble B, Retallack R, Hilbich C, Simms G, Multhaup G, Martins R, Hockey A, Montgomery P, Beyreuther K, Masters CL (1989) Amyloid A4 Protein and Its Precursor in Down's Syndrome and Alzheimer's Disease. *New England Journal of Medicine* **320:** 1446-1452

Salovaara S, Sandberg AS, Andlid T (2002) Organic acids influence iron uptake in the human epithelial cell line Caco-2. *The Journal of Agricultural and Food Chemistry* **50:** 6233-6238

Samanta B, Sengupta T, Pal S (2018) Specificity of Amino Acid–Aluminum Cluster Interaction and Subsequent Oxygen Activation by the above Complex. *The Journal of Physical Chemistry C* **122:** 28310-28323

Sandstrom B, Davidsson L, Cederblad A, Lonnerdal B (1985) Oral iron, dietary ligands and zinc absorption. *The Journal of Nutrition* **115:** 411-414

Santos MA (2002) Hydroxypyridinone complexes with aluminium. In vitro/vivo studies and perspectives, Vol 228

Santos MA, Gil M, Gano L, Chaves S (2005) Bifunctional 3-hydroxy-4-pyridinone derivatives as potential pharmaceuticals: synthesis, complexation with Fe(III), Al(III) and Ga(III) and in vivo evaluation with 67Ga. *The Journal of Biological Inorganic Chemistry* **10:** 564-580

Saporito-Magriñá CM, Musacco-Sebio RN, Andrieux G, Kook L, Orrego MT, Tuttolomondo MV, Desimone MF, Boerries M, Borner C, Repetto MG (2018) Copper-induced cell death and the protective role of glutathione: the implication of impaired protein folding rather than oxidative stress. *Metallomics* **10:** 1743-1754

Saunders AV, Craig WJ, Baines SK (2013) Zinc and vegetarian diets. *Medical Journal of Australia* **199:** S17-S21

Sayre LM, Moreira PI, Smith MA, Perry G (2005) Metal ions and oxidative protein modification in neurological disease. *The Annali dell'Istituto Superiore di Sanità* **41:** 143-164

Selkoe DJ (1991) The molecular pathology of Alzheimer's disease. *Neuron* **6:** 487-498

Senthil Raja D, Luo J-H, Chang T-G, Lo S-H, Wu C-Y, Lin C-H (2013) Synthesis, Crystal Structure, and Luminescence Properties of a New Calcium(II) Coordination Polymer Based on L-Malic Acid. J*ournal of Chemistry* **2013:** 7

Serpell LC (2000) Alzheimer's amyloid fibrils: structure and assembly. *Biochimica et Biophysica Acta (BBA) - Molecular Basis of Disease* **1502:** 16-30

Serrano-Pozo A, Mielke ML, Gómez-Isla T, Betensky RA, Growdon JH, Frosch MP, Hyman BT (2011) Reactive Glia not only Associates with Plaques but also Parallels Tangles in Alzheimer's Disease. *The American Journal of Pathology* **179:** 1373-1384

Sheykhansari S, Kozielski K, Bill J, Sitti M, Gemmati D, Zamboni P, Singh AV (2018) Redox metals homeostasis in multiple sclerosis and amyotrophic lateral sclerosis: a review. *Cell Death & Disease* **9:** 348

Shin B-k, Saxena S (2008) Direct evidence that all three histidine residues coordinate to Cu(II) in amyloid-β_{1-16}. *Biochemistry* **47:** 9117-9123

Silva AM, Kong X, Parkin MC, Cammack R, Hider RC (2009) Iron(III) citrate speciation in aqueous solution. *Dalton Transactions*: 8616-8625

Singh B, Das RS, Banerjee R, Mukhopadhyay S (2014) Uncatalyzed and copper(II) catalyzed oxidation of glutathione by Co(III) bound superoxide complex. *Inorganica Chimica Acta* **418:** 51-58

Singh I, Sagare AP, Coma M, Perlmutter D, Gelein R, Bell RD, Deane RJ, Zhong E, Parisi M, Ciszewski J, Kasper RT, Deane R (2013) Low levels of copper disrupt brain amyloid-β homeostasis by altering its production and clearance. *Proceedings of the National Academy of Sciences of the United States of America* **110:** 14771-14776

Slivarichova D, Mitrova E, Ursinyova M, Uhnakova I, Koscova S, Wsolova L (2011) Geographic accumulation of Creutzfeldt-Jakob disease in Slovakia--environmental metal imbalance as a possible cofactor. *Central European Journal of Public Health* **19:** 158-164

Small DH (2001) The role of presenilins in γ-secretase activity: catalyst or cofactor? *The Journal of Neurochemistry* **76:** 1612-1614

Smart TG, Hosie AM, Miller PS (2004) Zn^{2+} ions: modulators of excitatory and inhibitory synaptic activity. *The Neuroscientist* **10:** 432-442

Smith DP, Smith DG, Curtain CC, Boas JF, Pilbrow JR, Ciccotosto GD, Lau T-L, Tew DJ, Perez K, Wade JD (2006) Copper-mediated amyloid-β toxicity is associated with an intermolecular histidine bridge. *The Journal of Biological Chemistry* **281:** 15145-15154

Smith DP, Smith DG, Curtain CC, Boas JF, Pilbrow JR, Ciccotosto GD, Lau TL, Tew DJ, Perez K, Wade JD, Bush AI, Drew SC, Separovic F, Masters CL, Cappai R, Barnham KJ (2006) Copper-mediated amyloid-beta toxicity is associated with an intermolecular histidine bridge. The Journal of Biological Chemistry **281:** 15145-15154

Smith E, Schuhmacher LN, Husson Z (2015) The naked mole-rat as an animal model in biomedical research: current perspectives. *Open Access Animal Physiology*. **7**: 137-148

Smith MA, Harris PL, Sayre LM, Perry G (1997) Iron accumulation in Alzheimer disease is a source of redox-generated free radicals. *Proceedings of the National Academy of Sciences of the United States of America* **94:** 9866-9868

Sohn E (2014) Contamination: the toxic side of rice. Nature **514:** S62-S63.

Squitti R, Lupoi D, Pasqualetti P, Dal Forno G, Vernieri F, Chiovenda P, Rossi L, Cortesi M, Cassetta E, Rossini PM (2002) Elevation of serum copper levels in Alzheimer's disease. *Neurology* **59:** 1153-1161

Strange RW, Blackburn NJ, Knowles P, Hasnain SS (1987) X-ray absorption spectroscopy of metal-histidine coordination in metalloproteins. Exact simulation of the EXAFS of tetrabis (imidazole) copper (II) nitrate and other copper-imidazole complexes by the use of a multiple-scattering treatment. *The Journal of the American Chemical Society* **109:** 7157-7162

Streitz F, Mintmire J (1999) Energetics of aluminum vacancies in gamma alumina. *Physical Review B* **60:** 773

Streltsov V, Titmuss S, Epa V, Barnham K, Masters C, Varghese J (2008) The structure of the Amyloid-b peptide high-affinity copper II binding site in Alzheimer disease. *Biophysical Journal* **95:** 3447-3456

Strittmatter WJ, Weisgraber KH, Huang DY, Dong LM, Salvesen GS, Pericak-Vance M, Schmechel D, Saunders AM, Goldgaber D, Roses AD (1993) Binding of human apolipoprotein E to synthetic amyloid beta peptide: isoform-specific effects and implications for late-onset Alzheimer disease. *Proceedings of the National Academy of Sciences of the United States of America* **90:** 8098-8102

Subbarao KV, Richardson JS, Ang LC (1990) Autopsy samples of Alzheimer's cortex show increased peroxidation in vitro. *The Journal of Neurochemistry* **55:** 342-345

Syme C, Nadal R, Rigby S, Viles J (2004) Copper binding to the amyloid-β (Aβ) peptide associated with Alzheimer's Disease: folding, coordination geometry, ph dependence, stoichiometry, and affinity of Aβ-(1-28): insights from a range of complementary spectroscopic techniques. *The Journal of Biological Chemistry* **279:** 18169-18177

Syme CD, Nadal RC, Rigby SEJ, Viles JH (2004) Copper binding to the amyloid-beta (Abeta) peptide associated with Alzheimer's disease: folding, coordination geometry, pH dependence, stoichiometry, and affinity of Abeta-(1-28): insights from a range of complementary spectroscopic techniques. *The Journal of Biological Chemistry* **279:** 18169

Tabner BJ, Mayes J, Allsop D (2011) Hypothesis: soluble Aβ oligomers in association with redox-active metal ions are the optimal generators of reactive oxygen species in Alzheimer's disease. *International Journal of Alzheimer's Disease* **2011**

Talafous J, Marcinowski KJ, Klopman G, Zagorski MG (1994) Solution Structure of Residues 1-28 of the Amyloid .beta.-Peptide. *Biochemistry* **33:** 7788-7796

Talmard C, Yona RL, Faller P (2009) Mechanism of zinc (II)-promoted amyloid formation: zinc (II) binding facilitates the transition from the partially α-helical conformer to aggregates of amyloid β protein (1–28). *The Journal of Biological Inorganic Chemistry* **14:** 449-455

Tanzi RE, Kovacs DM, Kim T, Moir RD, Guenette SY, Wasco W (1996) The Gene Defects Responsible for Familial Alzheimer's Disease. *Neurobiology of Disease* **3:** 159-168

Taylor KM, Hiscox S, Nicholson RI, Hogstrand C, Kille P (2012) Protein kinase CK2 triggers cytosolic zinc signaling pathways by phosphorylation of zinc channel ZIP7. *Science Signaling* **5:** ra11

Tchounwou PB, Yedjou CG, Patlolla AK, Sutton DJ (2012) Heavy Metal Toxicity and the Environment. *In* A Luch, ed, Molecular, *Clinical and Environmental Toxicology: Volume 3: Environmental Toxicology. Springer Basel, Basel,* pp 133-164

Thompson KH, Barta CA, Orvig C (2006) Metal complexes of maltol and close analogues in medicinal inorganic chemistry. *Chemical Society Reviews* **35:** 545-556

Tickler AK, Smith DG, Ciccotosto GD, Tew DJ, Curtain CC, Carrington D, Masters CL, Bush AI, Cherny RA, Cappai R (2005) Methylation of the imidazole side chains of the Alzheimer disease amyloid-β peptide results in abolition of superoxide dismutase-like structures and inhibition of neurotoxicity. *The Journal of Biological Chemistry* **280:** 13355-13363

Tomljenovic L (2011) Aluminum and Alzheimer's disease: after a century of controversy, is there a plausible link? *Journal of Alzheimer's Disease* **23:** 567-598

Tomljenovic L (2011) Aluminum and Alzheimer's disease: after a century of controversy, is there a plausible link? *The Journal of Alzheimer's Disease* **23:** 567-598

Touchette JC, Williams LL, Ajit D, Gallazzi F, Nichols MR (2010) Probing the amyloid-$\beta_{(1–40)}$ fibril environment with substituted tryptophan residues. *Archives of Biochemistry and Biophysics* **494:** 192-197

Treiber C, Simons A, Strauss M, Hafner M, Cappai R, Bayer TA, Multhaup G (2004) Clioquinol mediates copper uptake and counteracts copper efflux activities of the amyloid precursor protein of Alzheimer's disease. *The Journal of Biological Chemistry* **279:** 51958-51964

Trist BG, Hare DJ, Double KL (2018) A Proposed Mechanism for Neurodegeneration in Movement Disorders Characterized by Metal Dyshomeostasis and Oxidative Stress. *Cell Chemical Biology* **25:** 807-816

Tschanz JT (2011) Senile Plaques. *In* JS Kreutzer, J DeLuca, B Caplan, eds, Encyclopedia of Clinical Neuropsychology. *Springer* New York, New York, NY, pp 2254-2255

Ueda K, Fukui Y, Kageyama H (1994) Amyloid β protein-induced neuronal cell death: neurotoxic properties of aggregated amyloid β protein. *Brain Research* **639:** 240-244

Urwin SJ, Rogers DM, Nichol GS, Cowley MJ (2016) Ligand coordination modulates reductive elimination from aluminium (III). *Dalton Transactions* **45:** 13695-13699

Van Campen D, Gross E (1969) Effect of histidine and certain other amino acids on the absorption of iron-59 by rats. *The Journal of Nutrition* **99:** 68-74

Van Den Berg A, Halkes S, Quarles van Ufford H, Hoekstra M, Beukelman C (2003) A novel formulation of metal ions and citric acid reduces reactive oxygen species in vitro. *Journal of Wound Care* **12:** 413-418

van Groen T, Puurunen K, Maki HM, Sivenius J, Jolkkonen J (2005) Transformation of diffuse beta-amyloid precursor protein and beta-amyloid deposits to plaques in the thalamus after transient occlusion of the middle cerebral artery in rats. *Stroke* **36:** 1551-1556

Vasudevaraju P, Govindaraju M, Palanisamy AP, Sambamurti K, Rao KS (2008) Molecular toxicity of aluminium in relation to neurodegeneration. *Indian Journal of Medical Research* **128:** 545-556

Vigo-Pelfrey C, Lee D, Keim P, Lieberburg I, Schenk DB (1993) Characterization of beta-amyloid peptide from human cerebrospinal fluid. *The Journal of Neurochemistry* **61:** 1965-1968

Vinothkumar G, Kedharnath C, Krishnakumar S, Sreedhar S, Preethikrishnan K, Dinesh S, Sundaram A, Balakrishnan D, Shivashekar G, Sureshkumar, Venkataraman P (2017) Abnormal amyloid β42 expression and increased oxidative stress in plasma of CKD patients with cognitive dysfunction: A small scale case control study comparison with Alzheimer's disease. *BBA Clinical* **8:** 20-27

Waggoner DJ, Bartnikas TB, Gitlin JD (1999) The role of copper in neurodegenerative disease. *Neurobiology of Disease* **6:** 221-230

Waldron KJ, Rutherford JC, Ford D, Robinson NJ (2009) Metalloproteins and metal sensing. *Nature* **460:** 823

Walton JR (2012) Aluminum disruption of calcium homeostasis and signal transduction resembles change that occurs in aging and Alzheimer's disease. *The Journal of Alzheimer's Disease* **29:** 255-273

Walton JR, Wang MX (2009) APP expression, distribution and accumulation are altered by aluminum in a rodent model for Alzheimer's disease. *The Journal of Inorganic Biochemistry* **103:** 1548-1554

Wang S, Shi X (2001) Molecular mechanisms of metal toxicity and carcinogenesis. *Molecular and Cellular Biochemistry* **222:** 3-9

Wang X, Li K, Yang XD, Wang LL, Shen RF (2009) Complexation of Al(III) with reduced glutathione in acidic aqueous solutions. *The Journal of Inorganic Biochemistry* **103:** 657-665

Wang Y, Cai Y, Cao Y, Liu J (2018) Aluminum-activated root malate and citrate exudation is independent of NIP1;2-facilitated root-cell-wall aluminum removal in Arabidopsis. *Plant Signaling & Behavior* **13:** e1422469

Watt NT, Whitehouse IJ, Hooper NM (2011) The Role of Zinc in Alzheimer's Disease. *International Journal of Alzheimer's Disease* **Article ID 971021:** 10

Wegmuller R, Tay F, Zeder C, Brnic M, Hurrell RF (2014) Zinc absorption by young adults from supplemental zinc citrate is comparable with that from zinc gluconate and higher than from zinc oxide. *The Journal of Nutrition* **144:** 132-136

Weinstock M (1995) The Pharmacotherapy of Alzheimer's Disease Based on the Cholinergic Hypothesis: an Update. *Neurodegeneration* **4:** 349-356

White AR, Barnham KJ, Bush AI (2006) Metal homeostasis in Alzheimer's disease. E*xpert Review of Neurotherapeutics* **6:** 711-722

Wiiliams RJP (2012) Zinc in evolution. *The Journal of Inorganic Biochemistry 1***11:** 104-109

Wilquet V, De Strooper B (2004) Amyloid-beta precursor protein processing in neurodegeneration. *Current Opinion in Neurobiology* **14:** 582-588

Wishart DS, Sykes BD, Richards FM (1992) The chemical shift index: a fast and simple method for the assignment of protein secondary structure through NMR spectroscopy. *Biochemistry* **31:** 1647-1651

Wüthrich K (1986) NMR with Proteins and Nucleic Acids. *Europhysics News* **17:** 11-13

Wyrzykowski D, Chmurzyński L (2010) Thermodynamics of citrate complexation with Mn^{2+}, Co^{2+}, Ni^{2+} and Zn^{2+} ions. *The Journal of Thermal Analysis and Calorimetry* **102:** 61-64

Xu ZC, Tang JP, Xu ZX, Melethil S (1992) Kinetics of aluminum in rats. IV: Blood and cerebrospinal fluid kinetics. *Toxicology Letters* **63:** 7-12

Yang D-S, McLaurin J, Qin K, Westaway D, Fraser PE (2000) Examining the zinc binding site of the amyloid-β peptide. *European Journal of Biochemistry* **267:** 6692-6698

Yao ZX, Papadopoulos V (2002) Function of beta-amyloid in cholesterol transport: a lead to neurotoxicity. *The FASEB Journal* **16:** 1677-1679

Yokel R (2012) The Pharmacokinetics and Toxicology of Aluminum in the Brain. *Current Inorganic Chemistry* **2:** 54-63

Yokel RA, Ackrill P, Burgess E, Day JP, Domingo JL, Flaten TP, Savory J (1996) Prevention and treatment of aluminum toxicity including chelation therapy: status and research needs. *The Journal of Toxicology and Environmental Health* **48:** 667-683

Yu P, Phillips BL, Olmstead MM, Casey WH (2002) Rates of solvent exchange in aqueous aluminium(iii)–maltolate complexes. *Dalton Transactions:* 2119-2125

Yumoto S, Kakimi S, Ohsaki A, Ishikawa A (2009) Demonstration of aluminum in amyloid fibers in the cores of senile plaques in the brains of patients with Alzheimer's disease. *The Journal of Inorganic Biochemistry* **103:** 1579-1584

Zabel U, Schreck R, Baeuerle P (1991) DNA binding of purified transcription factor NF-kappa B. Affinity, specificity, Zn^{2+} dependence, and differential half-site recognition. *The Journal of Biological Chemistry* **266:** 252-260

Zatta P, Drago D, Bolognin S, Sensi SL (2009) Alzheimer's disease, metal ions and metal homeostatic therapy. *Trends in Pharmacological Sciences* **30:** 346-355

Zeng J, Heuchel R, Schaffner W, Kägi JH (1991) Thionein (apometallothionein) can modulate DNA binding and transcription activation by zinc finger containing factor Spl. *FEBS Letters* **279:** 310-312

Zhang H, Zhu ZL, Zhang LH, Qiu YL, Zhao JF (2008) Extraction of heavy metals from sewage sludge using aspartic acid and citric acid. *Huan Jing Ke Xue* **29:** 733-737

Zhang Y-w, Thompson R, Zhang H, Xu H (2011) APP processing in Alzheimer's disease. *Molecular Brain* **4:** 3

Zheng H, Koo EH (2006) The amyloid precursor protein: beyond amyloid. *Molecular Neurodegeneration* **1:** 5

Zheng Z, White C, Lee J, Peterson TS, Bush AI, Sun GY, Weisman GA, Petris MJ (2010) Altered microglial copper homeostasis in a mouse model of Alzheimer's disease. *The Journal of Neurochemistry* **114:** 1630-1638

Zhitkovich A (2011) Chromium in drinking water: sources, metabolism, and cancer risks. *Chemical Research in Toxicology* **24:** 1617-1629

Zhong L, Yang J (2012) Reduction of Cr(VI) by malic acid in aqueous Fe-rich soil suspensions. *Chemosphere* **86:** 973-978

Zs.-Nagy I, Floyd RA (1984) Hydroxyl free radical reactions with amino acids and proteins studied by electron spin resonance spectroscopy and spin-trapping. *Biochimica et Biophysica Acta (BBA) - Protein Structure and Molecular Enzymology* **790:** 238-250

Appendices

Appendix A: HPLC chromatogram and MS analysis of Aβ$_{1–28}$ peptides and Aβ analogues

Aβ$_{1–28}$ peptide

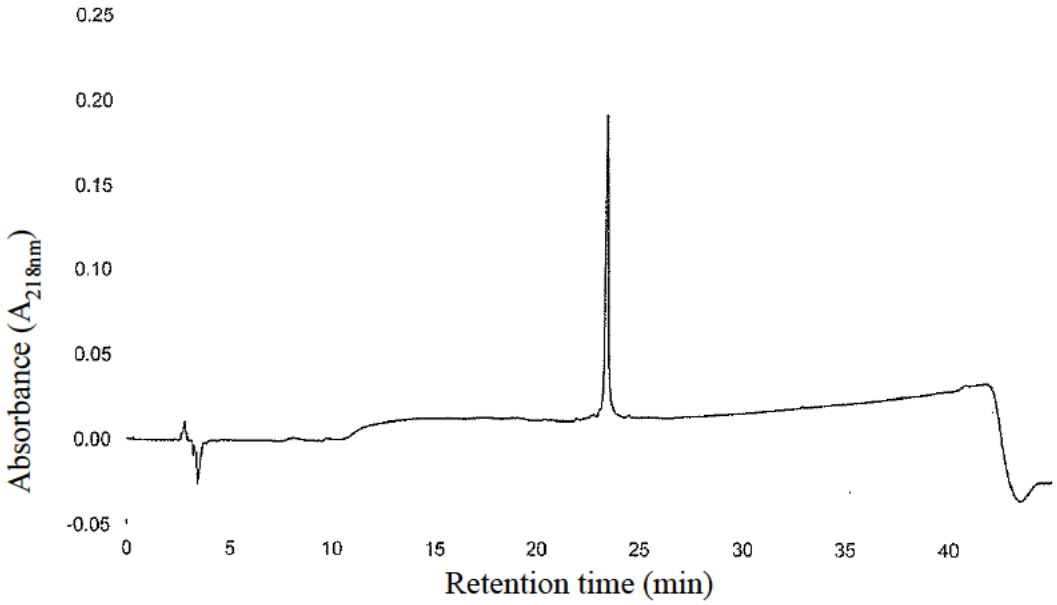

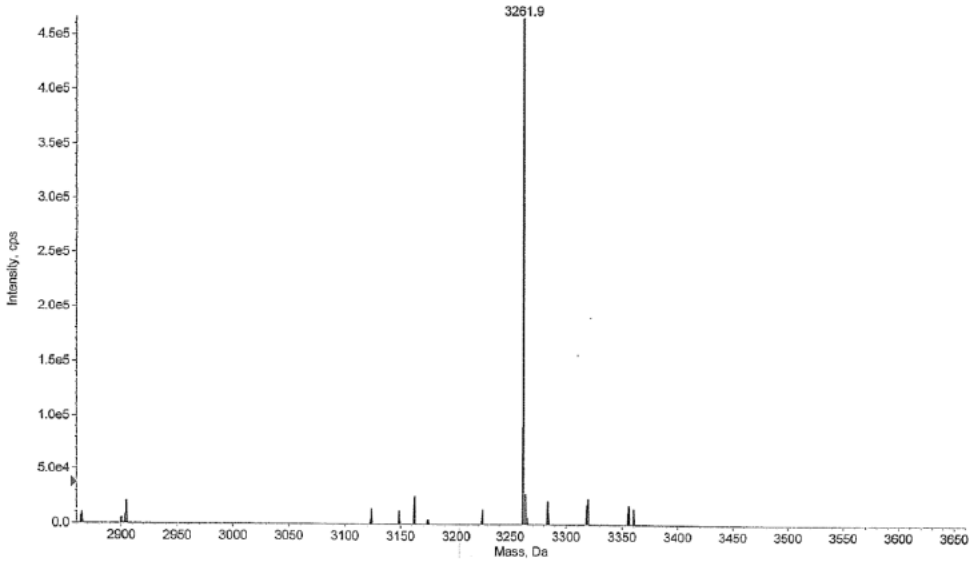

Aβ H6A analogue

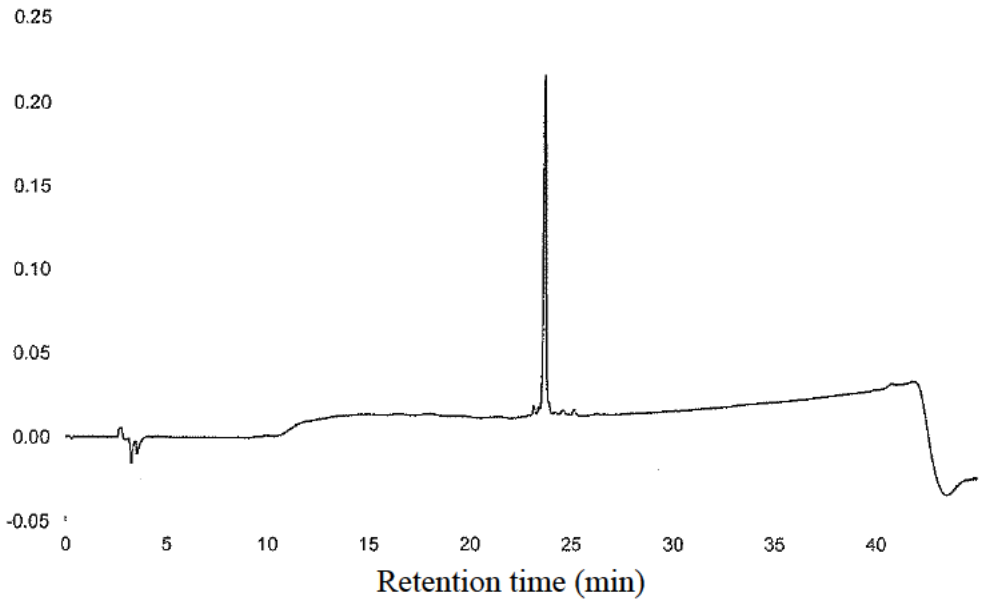

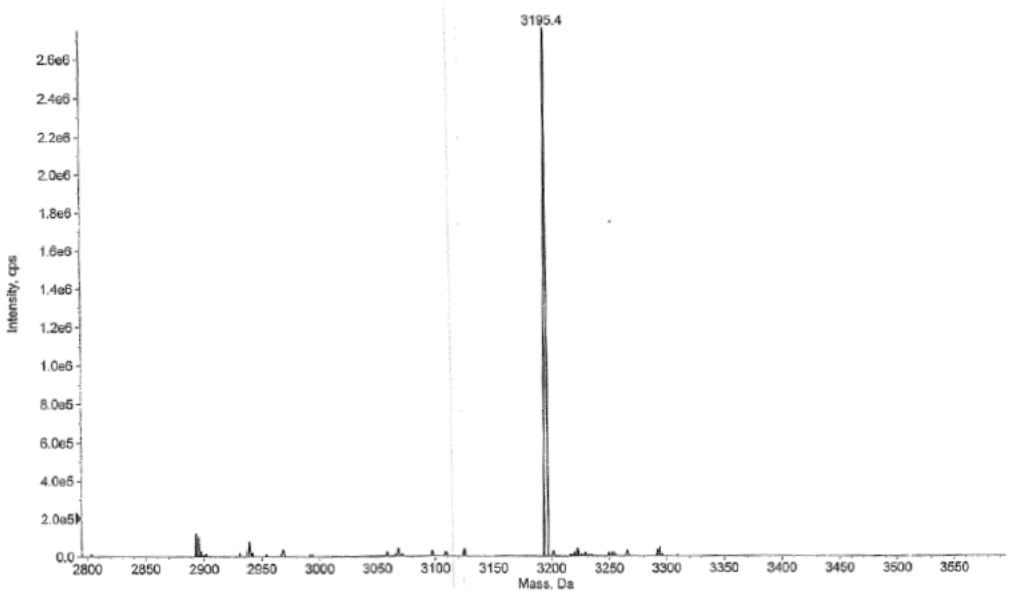

Aβ H13A analogue

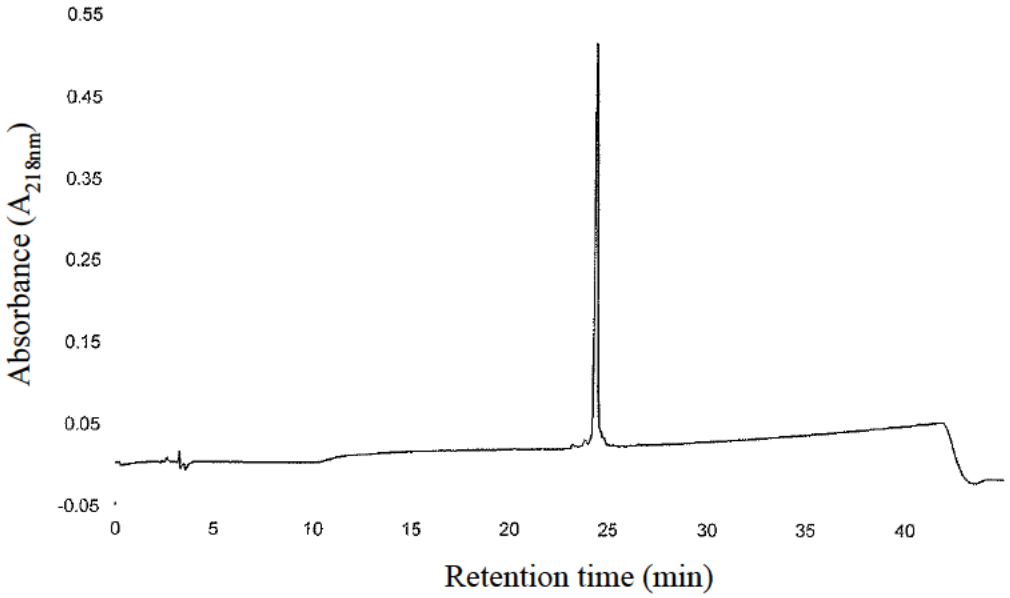

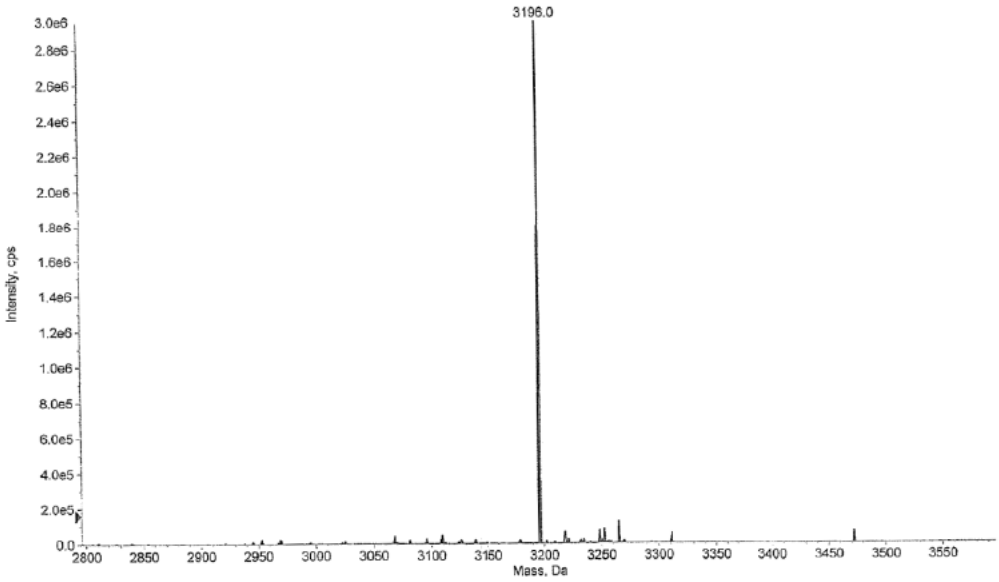

Aβ H14A analogue

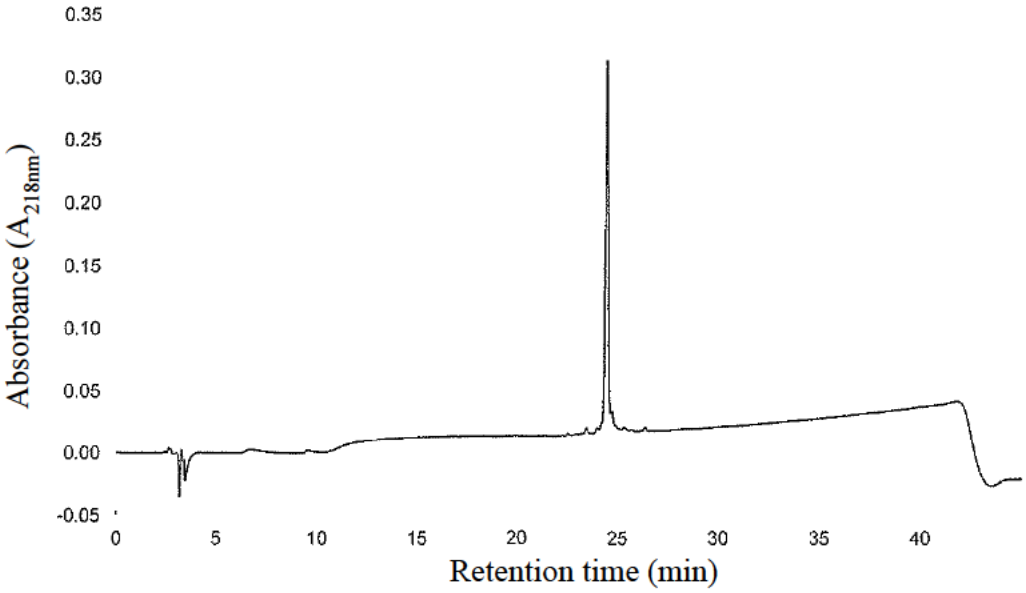

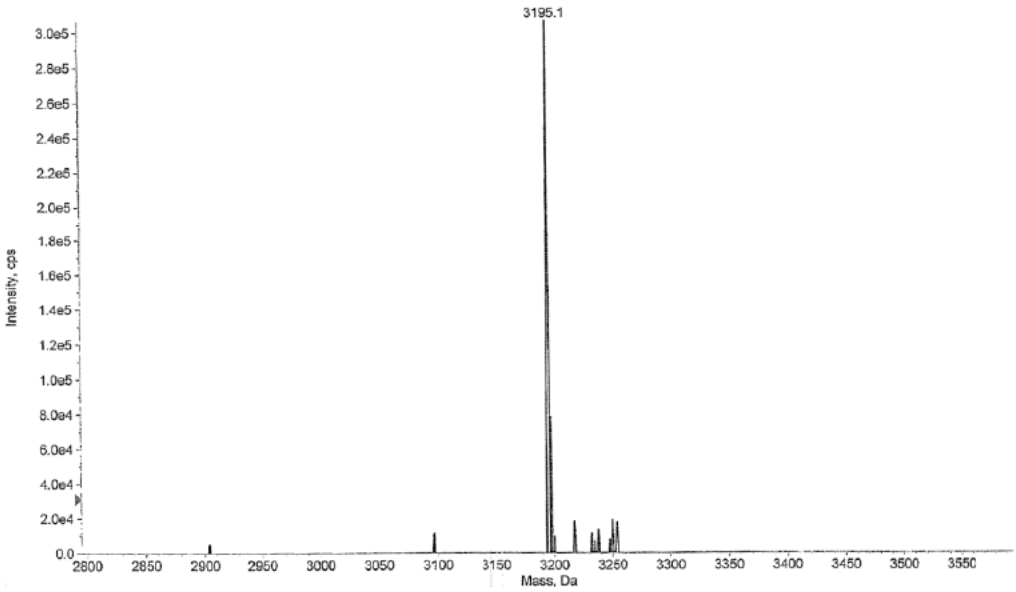

Aβ H6,13,14A analogue

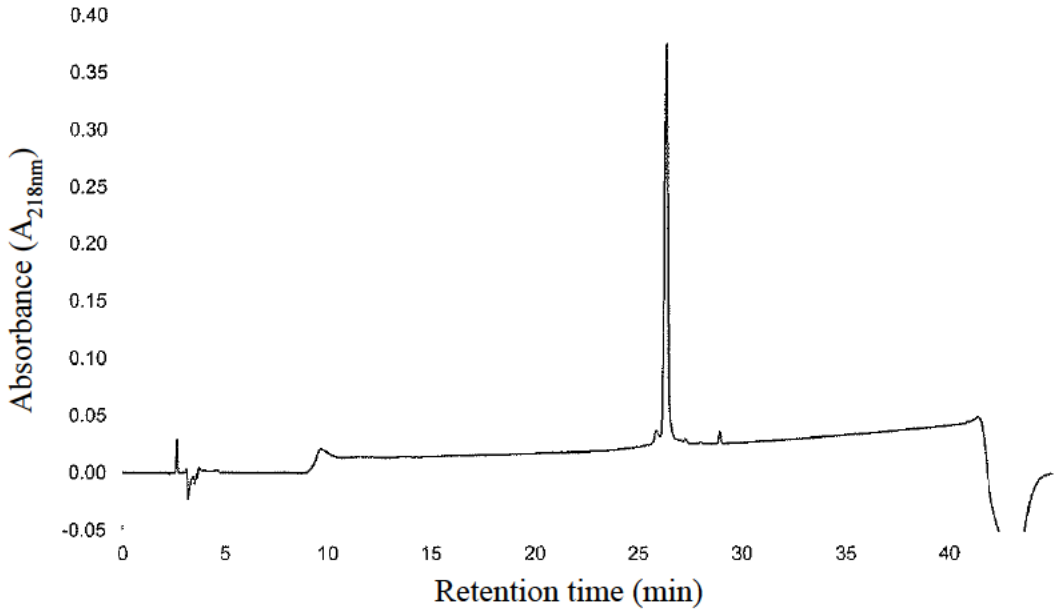

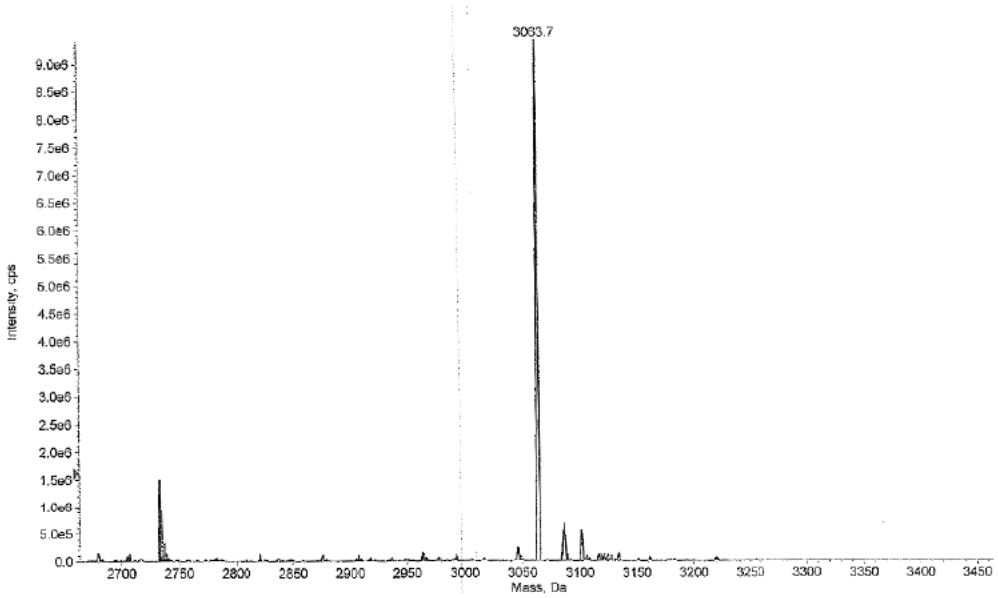

Appendix B: 2D NMR spectra for proton assignment of $A\beta_{1-28}$ peptide

NOESY spectrum (600 MHz) of $A\beta_{1-28}$ in 10 mM phosphate buffer in 10% H_2O:90% D_2O, pH 7.4 at 289 K.

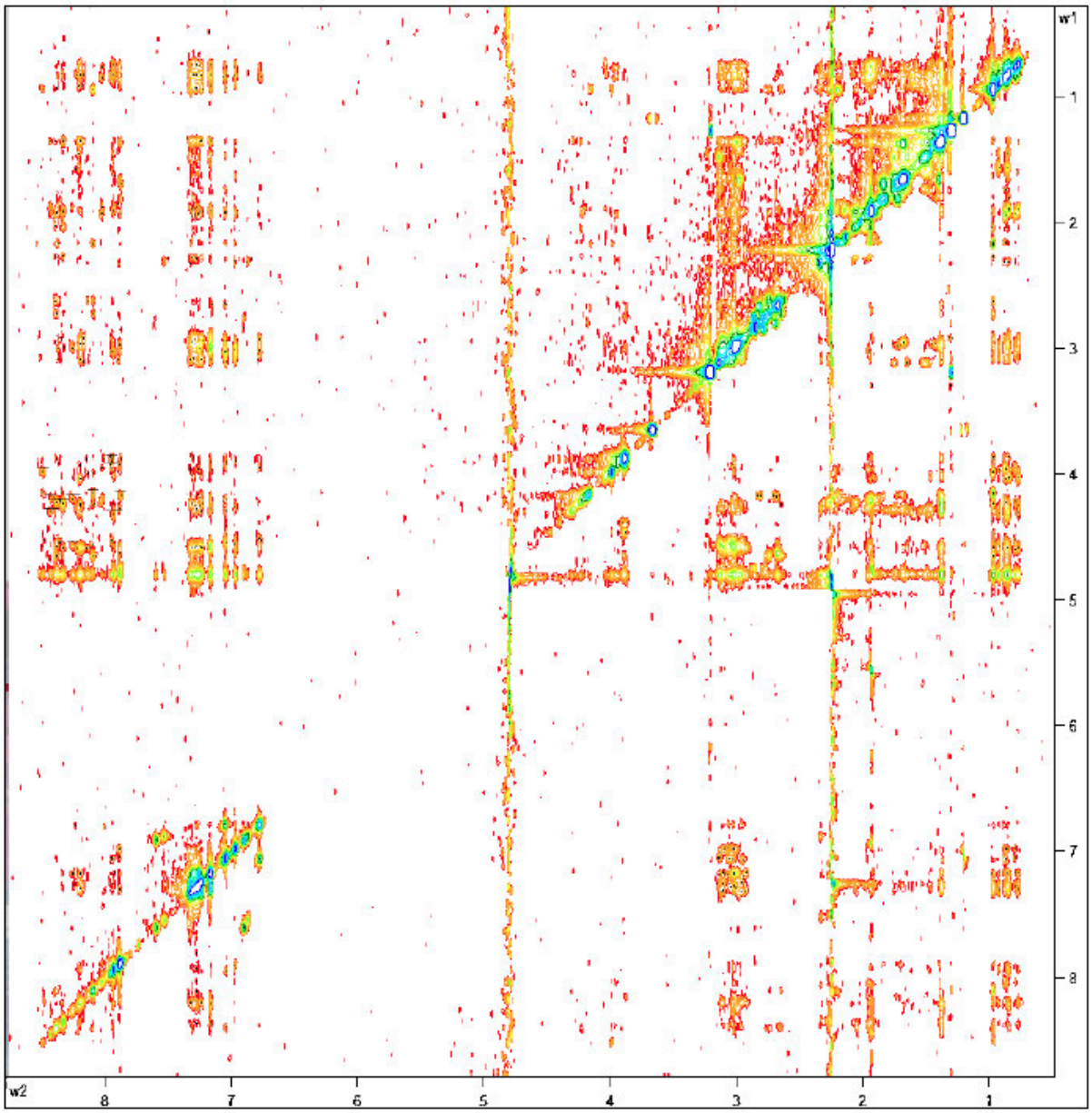

TOCSY spectrum (600 MHz) of $A\beta_{1-28}$ in 10 mM phosphate buffer in 10% H_2O:90% D_2O, pH 7.4 at 289 K.

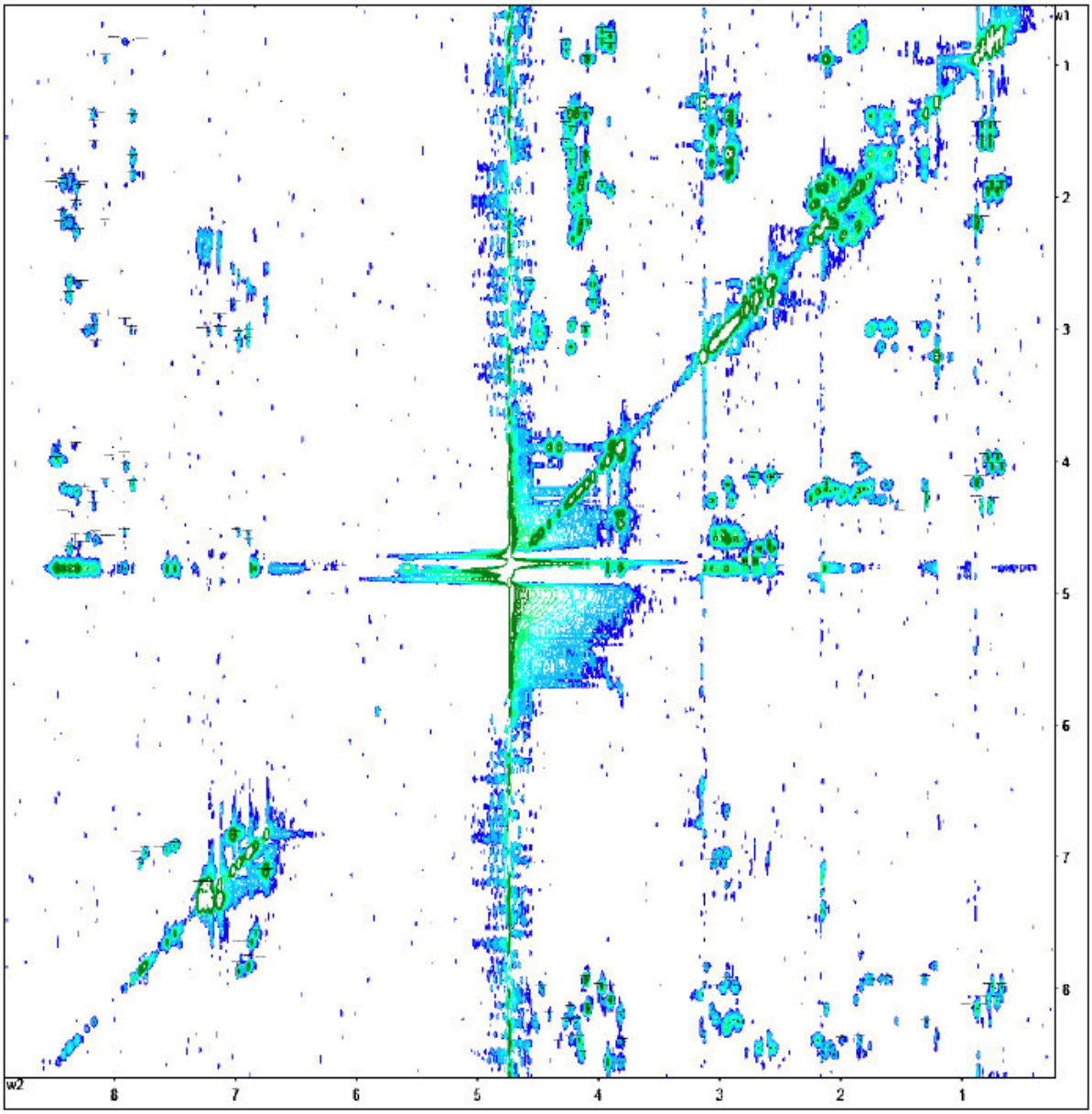

Appendix C: 2D NMR spectra for NMR titration of $A\beta_{1-28}$ against Al^{3+}

NOESY NMR spectrum (600 MHz) of Al^{3+} titrated wild-type $A\beta_{1-28}$. Wild-type $A\beta_{1-28}$ in 10% H_2O:90% D_2O pH 7.4 at 298 K, apo (black) and one equimolar Al^{3+} (blue).

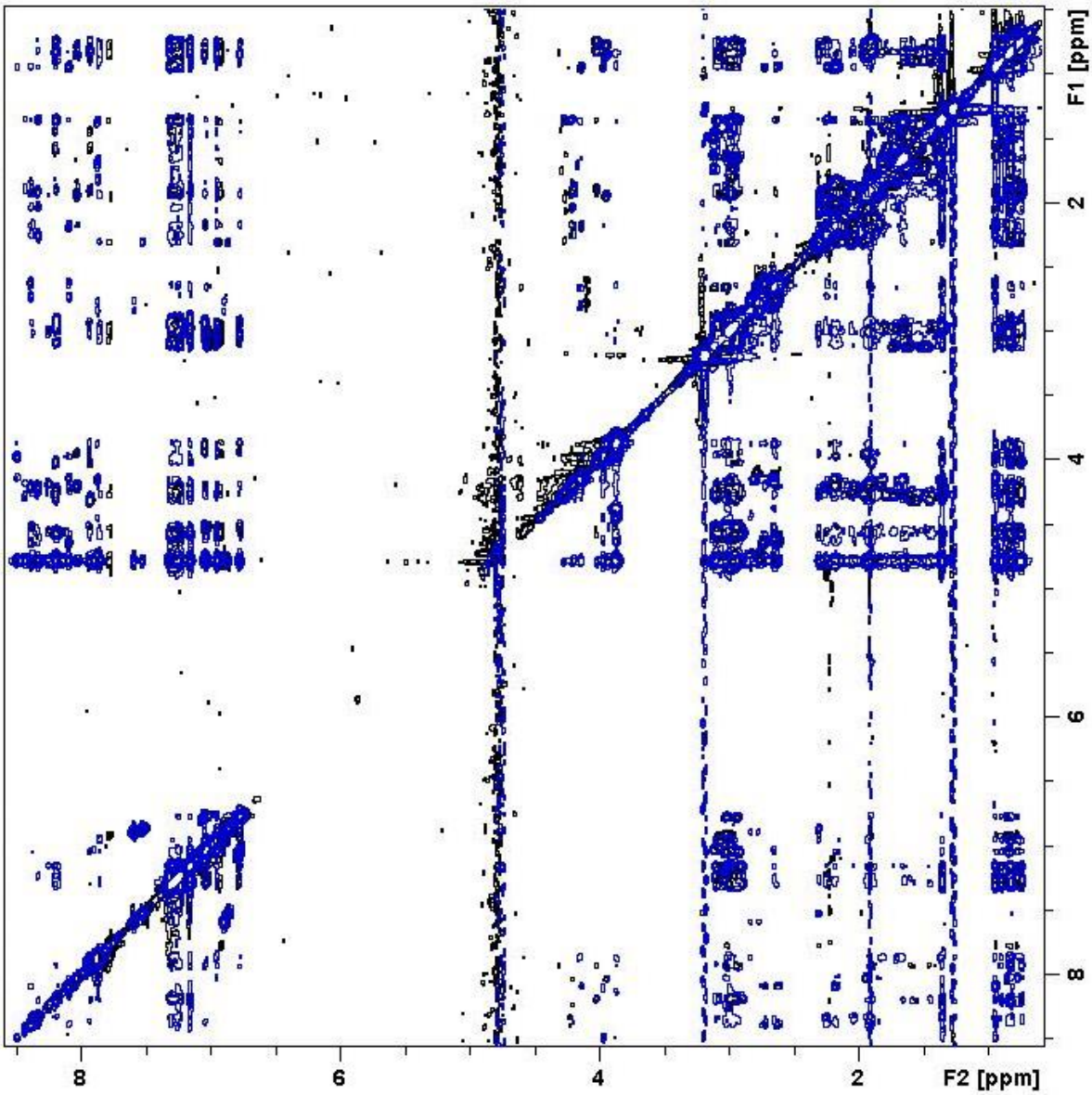

TOCSY NMR spectrum (600 MHz) of Al^{3+} titrated wild-type $A\beta_{1-28}$. Wild-type $A\beta_{1-28}$ in 10% H_2O:90% D_2O pH 7.4 at 298 K, apo (black) and one equimolar Al^{3+} (blue).

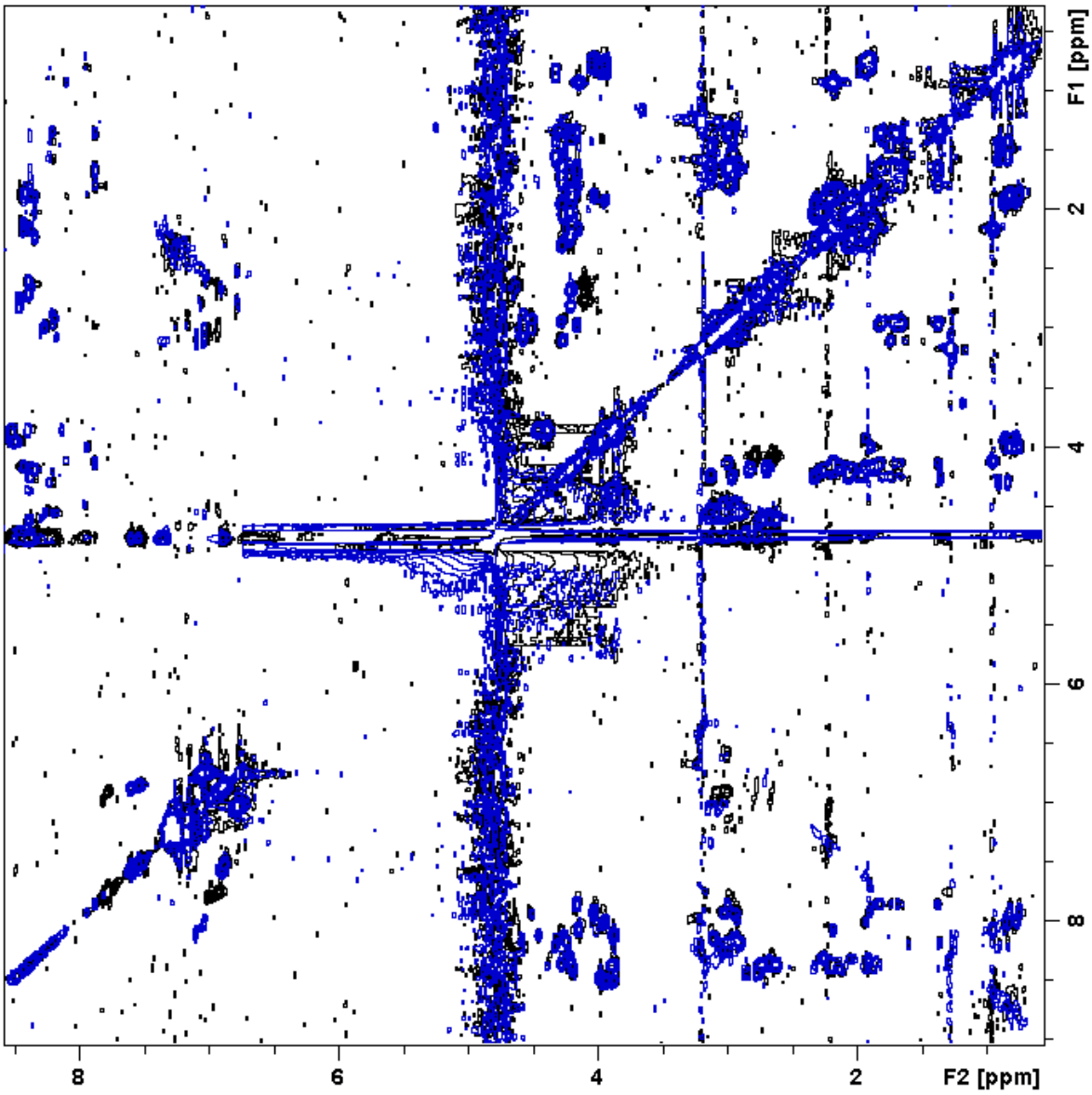

TOCSY NMR spectrum (600 MHz) of Al^{3+} titrated $A\beta_{1-28}$ H6,13,14A. $A\beta_{1-28}$ analogue H6,13,14A [1 mM] in 10% H_2O:90% D_2O pH 7.4 at 298 K, apo (black) and one equimolar Al^{3+} (blue).

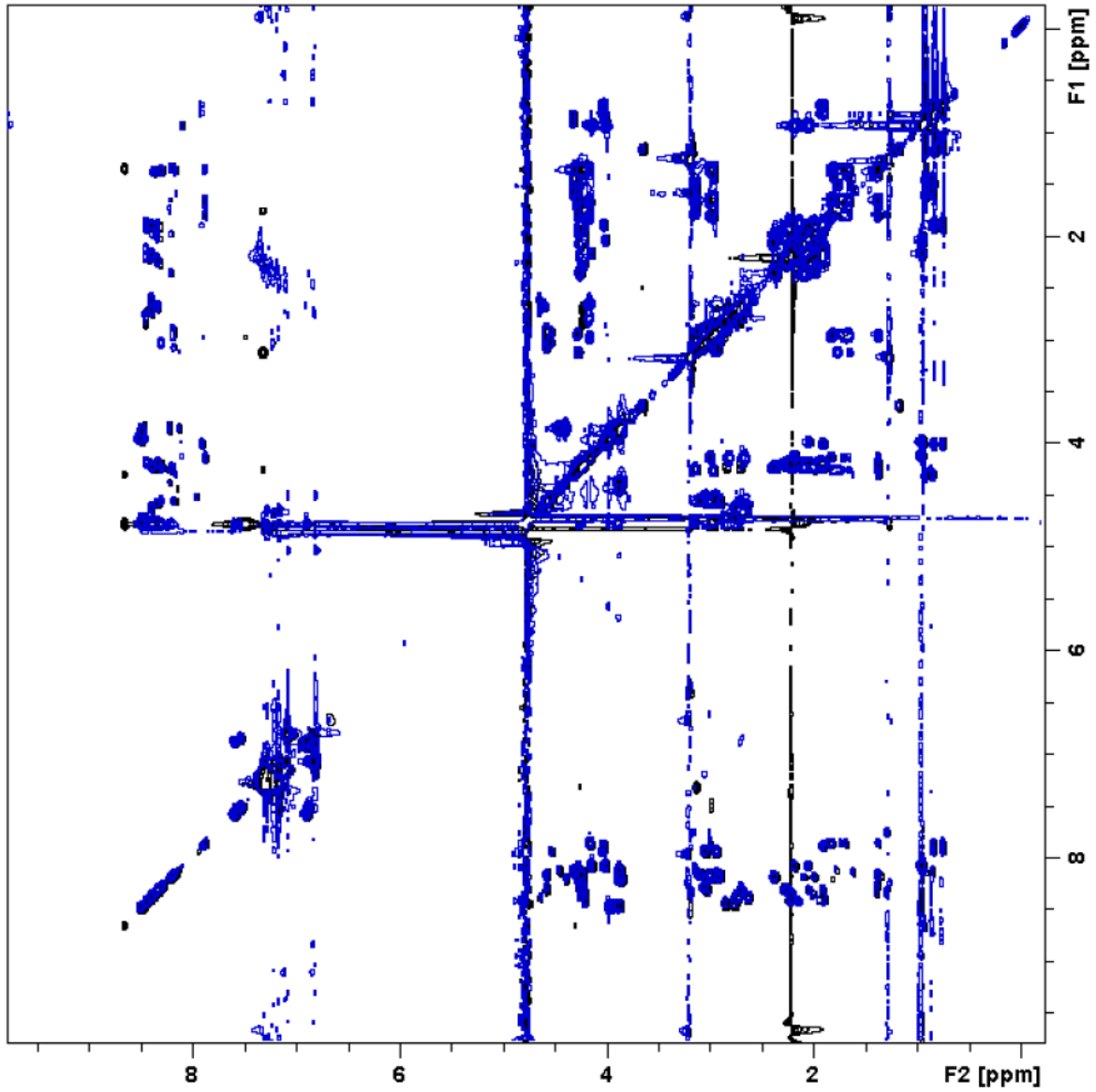

Appendix D: 1D NMR titration curve of α amino acid against Al^{3+} and Zn^{2+}

The different colour spectra indicate the different binding ratios where blue at the light base of the spectra is the control run (no metal), red, 0.2; dark green, 0.4; pink, 0.6; yellow, 0.8; orange, 1.0; light green, 1.4; black, 1.8; dark blue, 2.0.

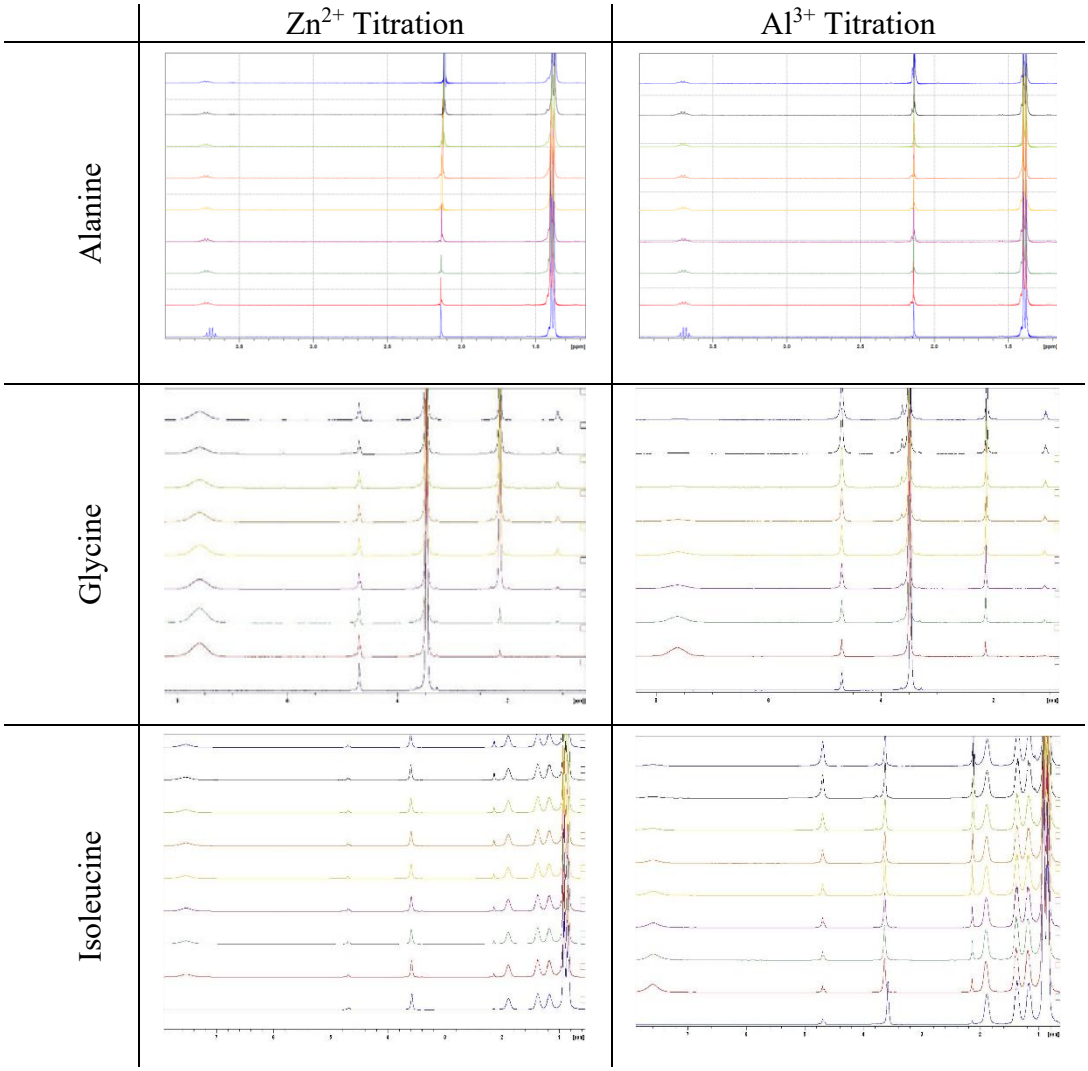

	Zn^{2+} Titration	Al^{3+} Titration
Leucine	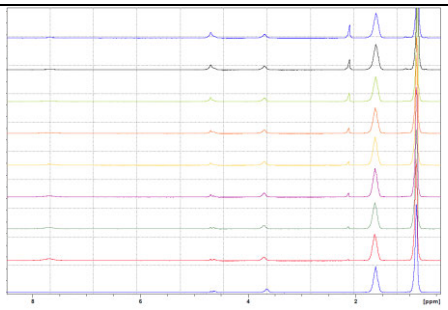	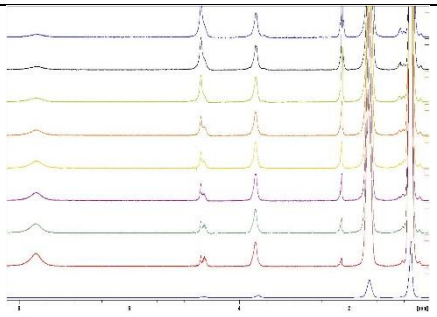
Proline	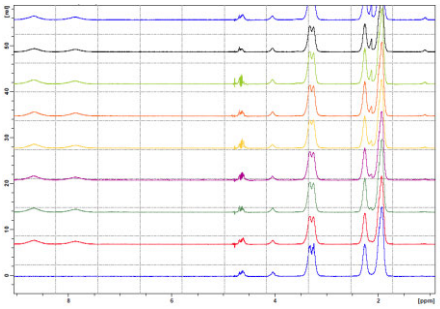	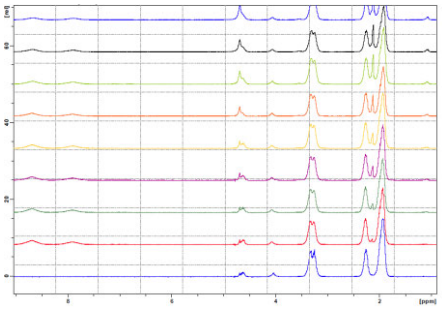
Valine	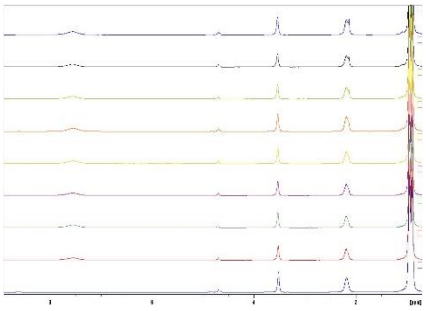	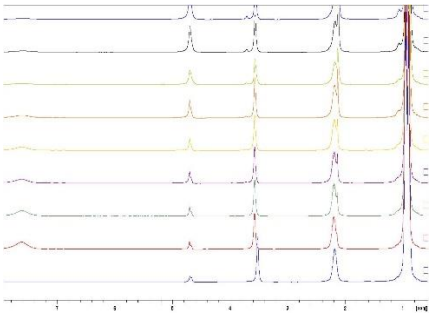
Phenylalanine	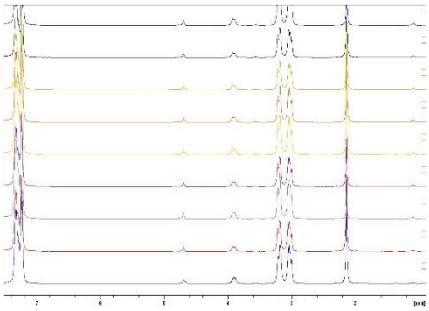	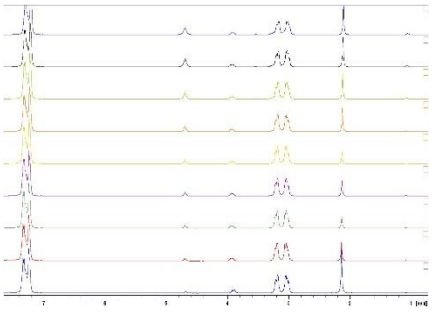
Tryptophan	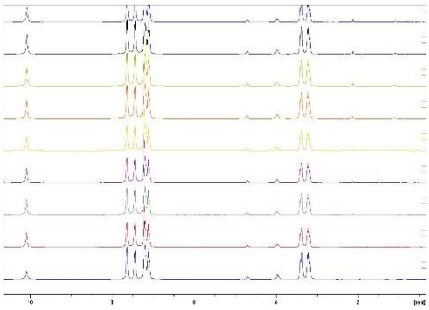	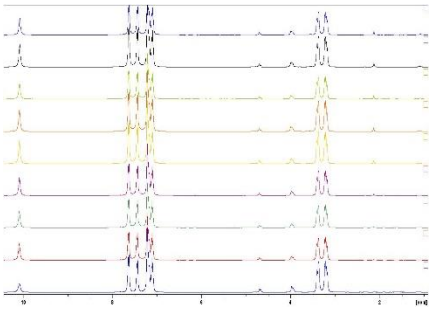

	Zn^{2+} Titration	Al^{3+} Titration
Tyrosine	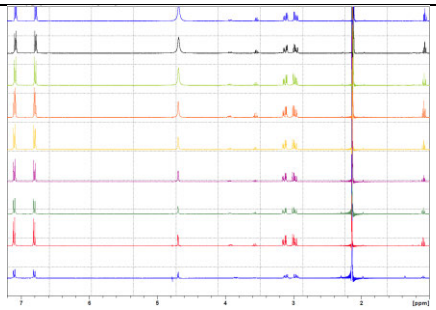	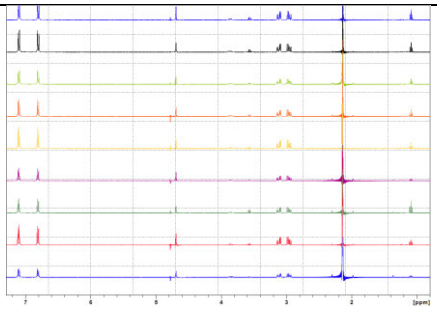
Aspartic Acid	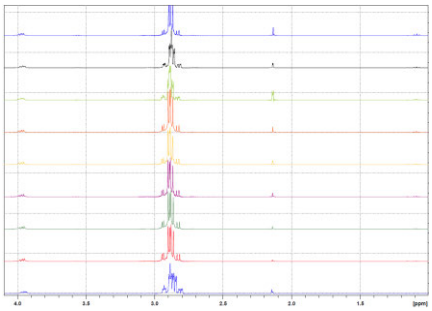	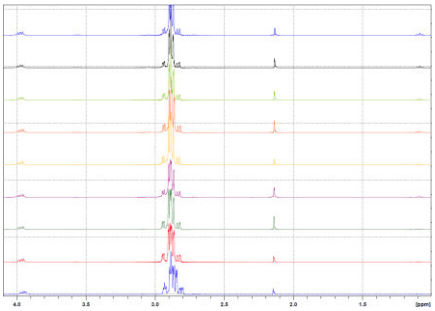
Glutamic Acid	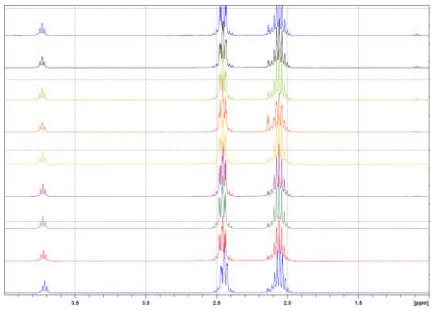	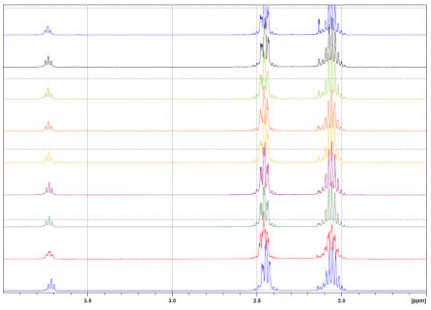
Arginine	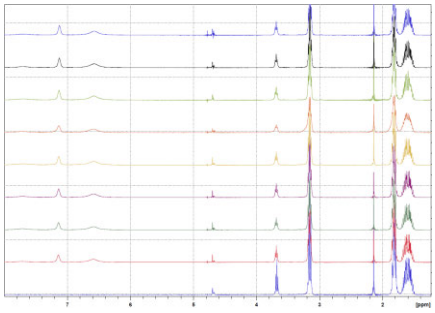	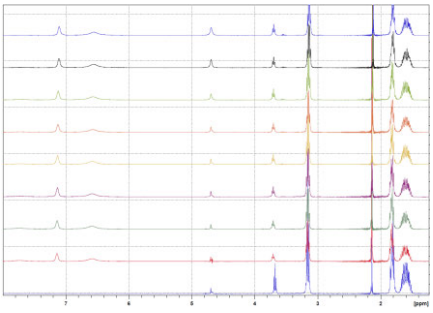
Histidine	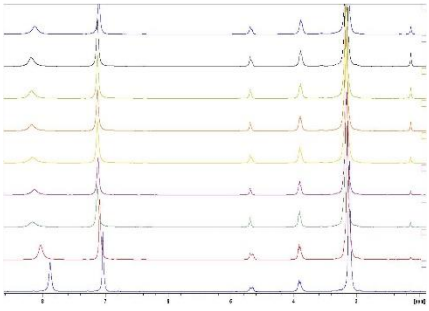	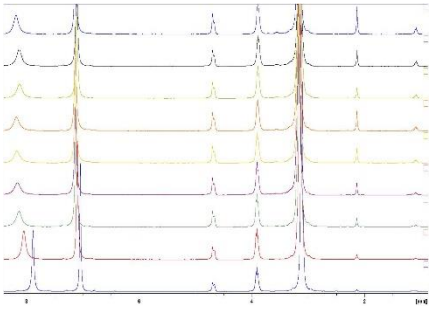

	Zn^{2+} Titration	Al^{3+} Titration
Lysine	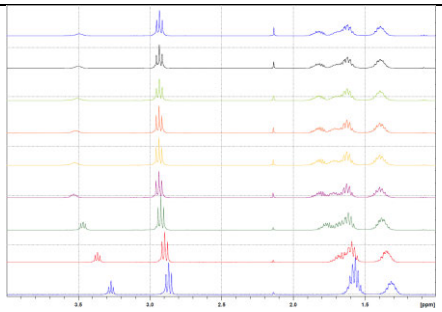	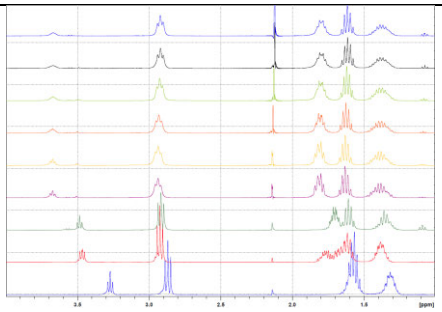
Serine	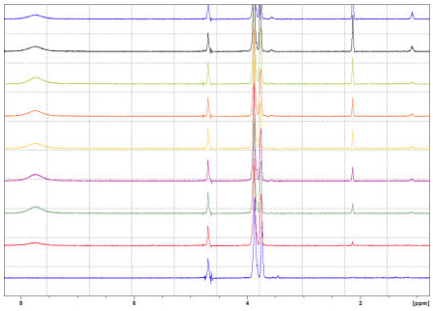	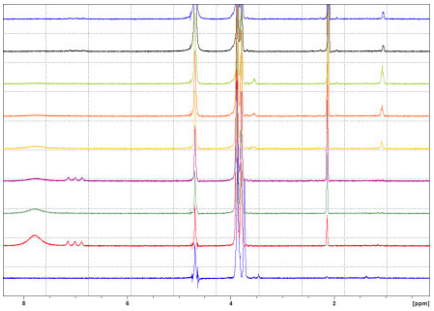
Threonine	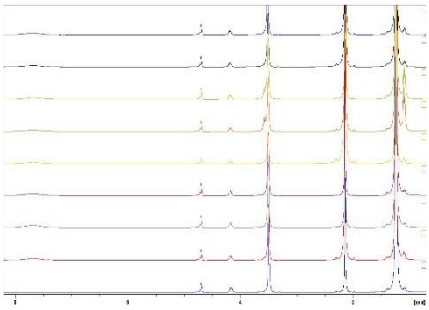	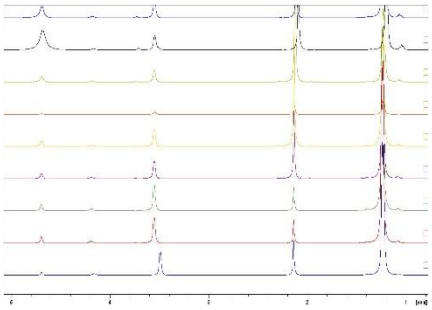
Cysteine	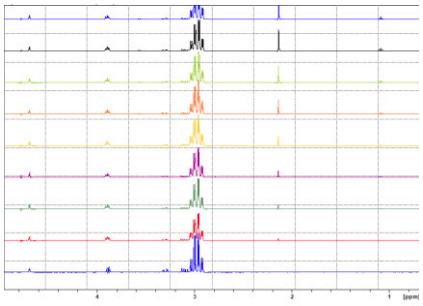	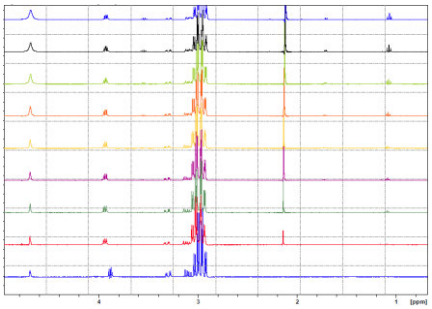
Methionine	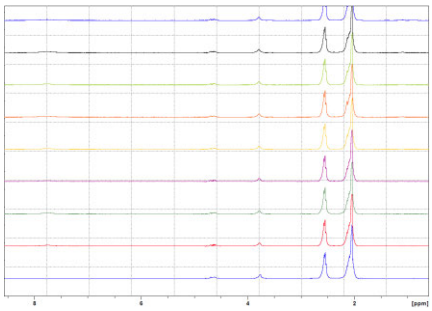	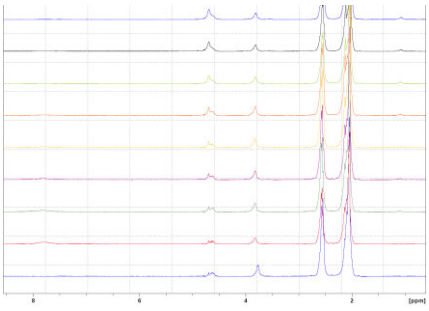

	Zn^{2+} Titration	Al^{3+} Titration
Asparagine	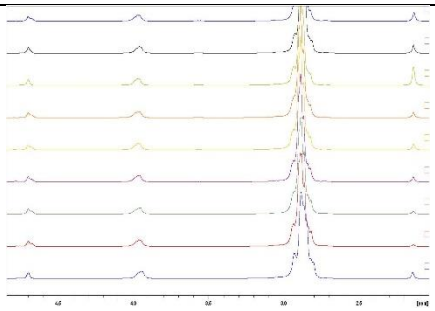	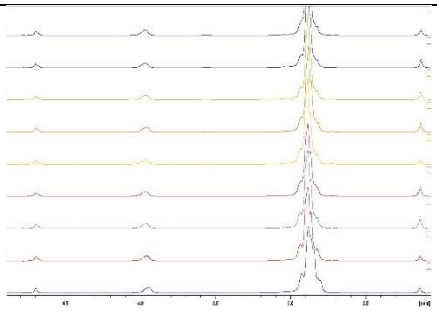
Glutamine